Studies on the Phospho-Aldol Reaction Catalysed by Aluminium Salcyan and Related Complexes

Nichola Elizabeth Cosgrove

Submitted in accordance with the requirements for the degree of Ph.D

The University of Leeds
School of Chemistry

July, 2011

The contribution of the candidate and the other authors to this work has been explicitly indicated below.

The chapter within this thesis which have been based on work from a jointly authored publication is Chapters 3. Information regarding the jointly authored publication is as follows:

Asymmetric general base catalysis of the phospho-aldol reaction *via* dimeric aluminium hydroxides. Alexandra C. Gledhill, Nichola E. Cosgrove, Tracy D. Nixon, Colin A. Kilner, Julie Fisher and Terence P. Kee, *Dalton Transactions*, **2010**, *39*, 9472-9475.

The work contained within this publication which is directly attributable to the candidate are the geometry optimisation calculations at the DFT level, including all associated images.

The work which is directly attributable to Alexandra C. Gledhill are the synthesis of {[(R,R)-salcyan-$^tPn_2$]Al(μ-OH)}$_2$, and its subsequent catalytic testing, the crossover experiments and the isotope change studies.

The work which is directly attributable to Tracey D. Nixon are the synthesis of {[(R,R)-salcyan]Al(μ-OH)}$_2$ and {[(R,R)-salcyan-$^tBu_2$]Al(μ-OH)}$_2$ and its subsequent catalytic testing.

Dr Julie Fisher was responsible for the diffusion-odered spectroscopy (DOSY) experiments.

Colin Kilner was responsible for the X-ray crystallographic data collected within this publication.

Dr Terence P. Kee was the lead supervisor for the work that was carried out in the publication.

The work described herein took place in laboratory 1.06 of the School of Chemistry, University of Leeds, under the supervision of Dr T. P. Kee between September 2006 and December 2010. All the work is my own unless otherwise stated and has not been presented for any other degree at this university or any other university.

Acknowledgements

I would like to dedicate this thesis to my parents, Michael and Pauline Cosgrove who are sadly no longer with us. Unfortunately my mum never knew that I was going to undertake a Ph.D, however I had the support of my dad for my first year and I'm sure he filled her in! Although both of their lives were taken at young ages I am proud to call them my parents and without their teachings, support and values I would not be the person that I am today. I hope by writing this thesis for them it goes some way to saying thank you for what they have given to me in such a short period of time.

I would like to say a very big thank you to my husband Davy Leroy who has helped me through all the bad times of the last 5 years. Without his support finishing this Ph.D would not have been possible. Alongside that I would like to thank our daughter Emelyne who's smiles motivated me to keep on writing.

Particular thanks go to my supervisor Dr. Terry Kee for giving me the opportunity to do this Ph.D and being understanding and supportive throughout, especially in the difficult moments. I just hope my upfront and sometimes blunt nature were not too hard to handle. I would also like to thank all the members, past and present of the Kee, Willans and McGowan groups, especially Katie Marriott and Chris Pask for the fun times in the office, pub and Chaston Chapman.

I must say thank you to all the technical staff who have been involved with the collection of data presented in this thesis, Mr. Simon Barrett, Ms. Tanya Marinko-Covell, Mr. Colin Kilner, Mr. Ian Blakely and Mr. Martin Huscroft for NMR, mass spectrometry, X-ray crystallography and microanalyses.

Finally I would like to say a special thanks to Friday cake day and everyone on the cake rota, without it Friday's would never be the same!!

Abstract

The phospho-aldol (PA) reaction is one of the most versatile reactions for the formation of phosphorus-carbon [P-C] bonds. The reaction is a base-catalysed addition reaction between a hydrogen-phosphonate ester and a carbonyl substrate, affording alpha-functionalised phosphonate esters. These PA products have found a wide-spread application in biomedical science.

Since the PA reaction is capable of affording products with new stereocentres, considerable effort has been devoted over the last few decades to developing asymmetric catalytic variants of the PA reaction. Through the manipulation of the substituent groups of the salcyan ligands there is the possibility of controlling the enantioselectivity and stereochemical outcome of the reaction.

This thesis describes previous work that has been carried out with regards to the PA reaction, how it works, Schiff base complexes and how aluminium can be incorporated in a Schiff base complex, ultimately resulting in the catalysis of the PA reaction. Discussed are the studies carried out towards the construction of chiral aluminium complexes based on the (R,R)- N_4-salcyan framework for application as catalyst precursors for the asymmetric phospho-aldol reaction.

A computational study focusing on the complex $\{[(R,R)\text{-salcyan}(^tBu)2]Al(\mu\text{-OH})\}_2$ as part of a validation study carried out on Gaussian 03 is outlined. The results were used to validate the original molecular modelling studies that used semi-empirical methods. In addition, geometry optimisation calculations were carried out on a selection of single crystal X-ray structures as a means of identifying the most basic site of the complex and therefore determine where deprotonation of DMHP could take place.

To conclude this thesis two relatively new areas for PA catalysis are discussed. One such area focuses on the incorporation of cyclams into the salcyen backbone, which could serve as a versatile framework for PA catalysts with the inclusion of a secondary basic functionality. The second area introduces phosphine oxide and phosphine substituted N_2O_2 salcyan compounds, which can provide a basic complex construction

with the added advantage of being able to introduce suitable co-factors, tuneable to a specific substrate. This approach would open up the chance of parallel processing and analysis.

Contents

Chapter 1

Introduction to the Phospho-Aldol (PA) Reaction and Catalysis

Chapter 2

N$_4$-Salcyan Ligand Frameworks. Syntheses, Characterisation and Structures

Chapter 3

Molecular Modelling of Aluminium Salcyan Complexes

Chapter 4

Multifunctional Ligands for PA Catalysis

Chapter 5

Overall Conclusions and Future Proposals

Chapter 6

Experimental Details

Appendicies

.

List of Figures

List of Schemes

Abbreviations

α	Alpha
$[\alpha]^D$	Optical rotation value
Å	Ångstrom
Ad	Adamantyl
ALB	Aluminium-lithium-BINOL complex
AM1	Austin model 1
aq.	Aqueous
ATP	Adenosine triphosphate
a.u.	Arbitrary unit
Ax	Axial
β	Beta
b	Broad
BINOL	1,1′-Bi(2-naphthol)
bs	Broad singlet
^{n}Bu	*neo*-Butyl
^{t}Bu	*tert*-Butyl
BuLi	Butyl lithium
ca	Circa, approximately
Cat	Catalyst
CCD	Charge coupled device
CPU	Central processing unit
cm^{-1}	Wavenumber
δ	Delta
2-D	2-Dimensional
d	Doublet
DCM	Dichloromethane
deg (°)	Degree

DEHP	Diethyl-*H*-phosphonate
DFT	Density functional theory
DMHP	Dimethyl-*H*-phosphonate
e.e.	Enantiomeric excess
eq.	Equivalent
Eq	Equatorial
et al	Et alia, and others
Et$_3$N	Triethylamine
EPSP	Excitatory postsynaptic potential
eV	Electron volt
F	Fluorine. Fluoro group
F$_2$Pmp	Phosphonodifluoromethyl phenylalanine
Fmoc	Fluorenylmethoxycarbonyl
γ	Gamma
g	Gram
GTO	Gaussian type orbital
h	Hour
H	Hydrogen
HF	Hartree Fock
HIV	Human immunodeficiency virus
HOMO	Highest occupied molecular orbital
HPLC	High performance liquid chromatography
Hz	Hertz
J	coupling constant
K	Kelvin
L	Ligand
LDA	Lithium diisopropylamide
LLB	Lanthanum-lithium-BINOL complex

LUMO	Lowest unoccuopied molecular orbital
m	Multiplet
M	moles per litre
Me	Methyl
Mes	Mesityl
MHz	Megahertz
Min	Minute
MINDO	Modified intermediate neglectof differential overlap
ml	Mililitre
μm	Micron
Mm+	Molecular mechanics
mmol	Milimole
mol	Mole
MOPAC	Molecular orbital package
m.p.	Melting point
MW	Molecular weight
m/z	Mass to charge ratio
NH_2	Amino group
nm	Nanometre
NMR	Nuclear magnetic resonance
o	Ortho
OH	Hydroxyl group
p	Para
PA	Phospho-aldol
Ph	Phenyl
pKa	Acid dissociation constant
PM3	Parameterised model number 3
Pmp	Phosphonomethyl phenylalanine

^{t}Pn	*tert*-Pentyl
ppm	Parts per million
^{i}Pr	*iso*-Propyl
PTK	Protein-tyrosine kinase
PTP	Protein-tyrosine phosphatase
q	Quartet
R/R′/R″	Functional group
RHF	Restricted Hartree Fock
r.t.	Room temperature
sec	Second
s	singlet
S_N2	Bimolecular nucleophilic substitution
STO	Slater type orbital
tert	Tertiary
THF	Tetrahydrofuran
TLC	Thin layer chromatography
TMS	Tetramethyl silane
TMSCN	Trimethylsilyl cyanide
T.O.F	Time of flight
v/v	Volume to volume

Chapter 1

Introduction to the Phospho-Aldol (PA) Reaction

ONLY A FOOL KNOWS EVERYTHING.

THE CHEMIST ANALYST, SEPTEMBER 1946

1.1 Phospho-transfer.

The transfer of a phospho group is one of the most important biochemical transformations that occur within cells. It is used to control functions such as cell membrane synthesis, signal transduction, energy conversion and skeletal construction.[1] The principal phospho-transfer processes are known as phosphorylation and de-phosphorylation whereby the formation and cleavage, respectively, of [P-O] linkages involving phosphate groups takes place, catalysed by specific enzymes (Scheme 1. 2), namely kinases and phosphatases. [1]
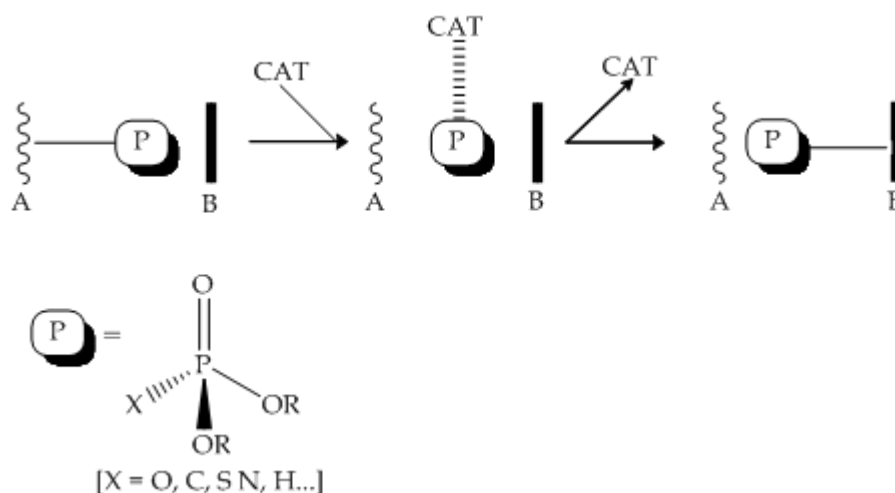
Scheme 1. 2 Catalyst-mediated phospho-transfer. A and B are different chemical sites. [2]

A variation on this concept is phosphonylation, where a phosphorus-carbon bond is formed. Various types of phosphorus-carbon bond-forming reactions are known, but one of the most versatile and valuable is the phospho-aldol (PA) reaction.[3] The specific process that we are interested in involves production of [P-C] linkages using a [P-H]-containing reagent. The original versions of this transformation were known as the Abramov (or phospho-Mukaiyama) reactions (Scheme 1. 3) involved heating an aldehyde with a trialkyl phosphite to yield a dialkyl-α-alkoxo-phosphonate. [4]
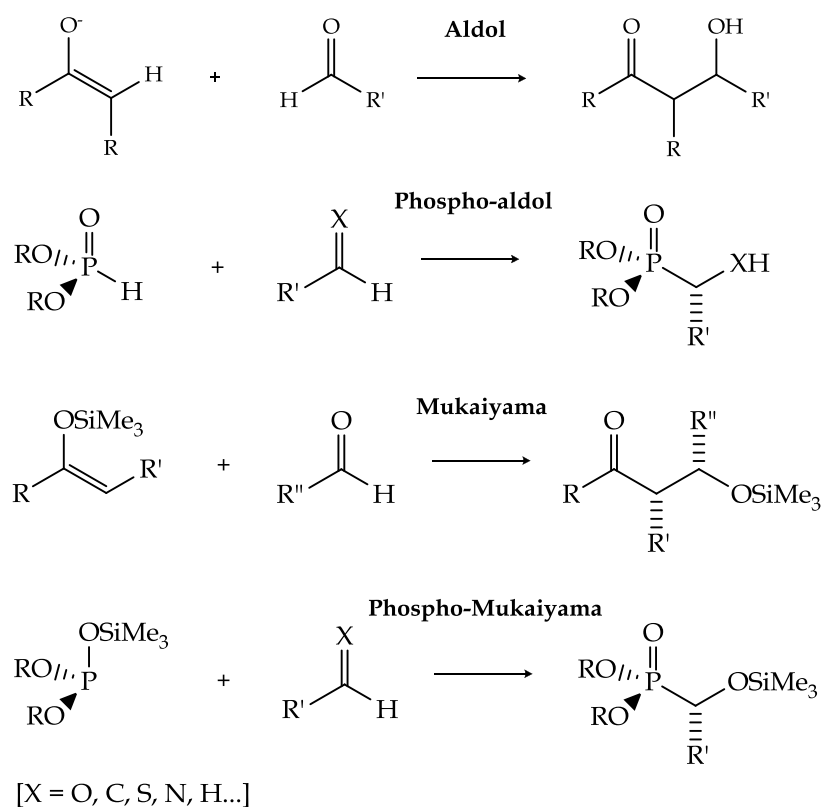
Scheme 1. 3 Comparisons between aldol, Mukaiyama aldol and their phospho-equivalents. [4]

1.2 What is the Phospho-aldol (PA) Reaction?

Before we can fully understand the phospho-aldol reaction, it is worth knowing what the aldol reaction is and how it relates to the phospho-aldol analogue.

The aldol reaction is a means of creating carbon-carbon bonds in organic chemistry, first discovered by Charles-Adolphe Wurtz and Alexander Porfyrevich Borodin in 1872. [5] The reactions combine's two carbonyl compounds to form a new β-hydroxy carbonyl compound (Scheme 1.).
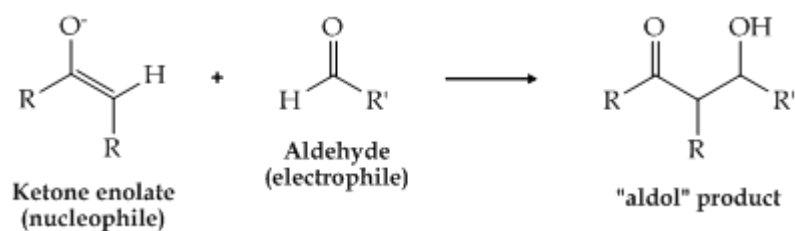
Scheme 1.4 A typical aldol reaction involving two carbonyl compounds. [5]

The aldol reaction may proceed *via* two different mechanisms. Firstly, carbonyl compounds, like aldehydes and ketones can be converted to enols or enol ethers. The nucleophilicity is centered on the α-carbon and so can attack reactive protonated carbonyls, like protonated aldehydes. This is called the "enol mechanism".
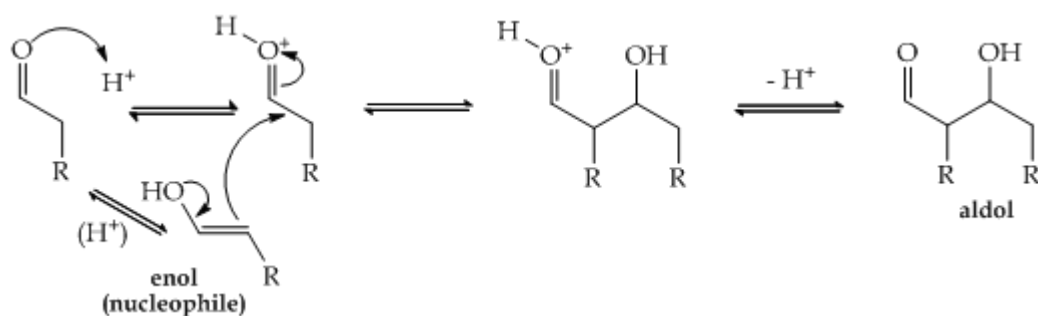
Scheme 1.5 Acid-catalysed aldol reaction, "enol mechanism".

Secondly, carbonyl compounds, such as carbonic acids can be deprotonated to form enolates, which are more nucleophilic than enols or enol ethers and can directly attach to electrophiles. This is called the "enolate mechanism".
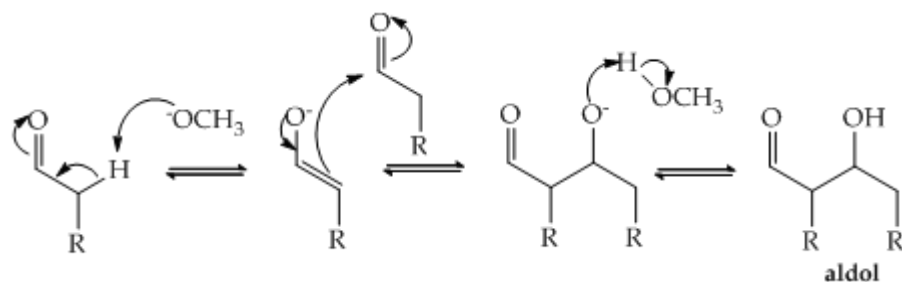
Scheme 1.6 Base-catalysed aldol reaction, "enolate mechanism".

The PA reaction is similar to the aldol reaction, in that it is a base-catalysed reaction and functions best when the catalyst combines both Lewis acidic and basic properties (Scheme 1.).   The PA reaction involves addition of a hydrogen-phosphonate ester to a carbonyl substrate, resulting in an alpha - (α) - functionalised phosphonate ester mediated by a basic catalyst.

R = alkyl, aryl, etc. CAT = Catalyst; X = O
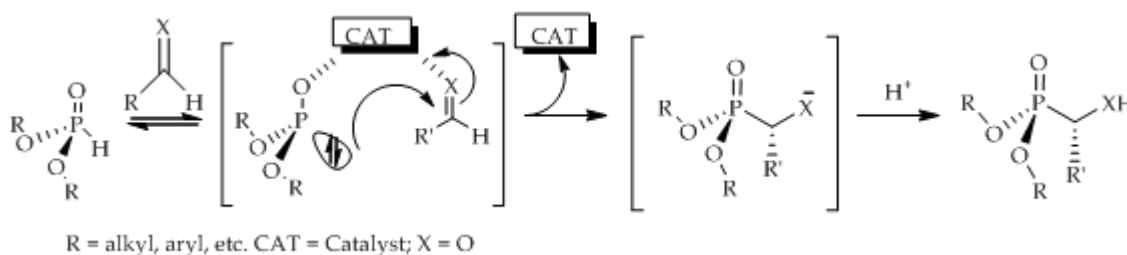
Scheme 1.7 The PA reaction. [6]

1.3 What is the Importance of the PA reaction?

As mentioned previously the phospho function plays an important role in many aspects of chemistry and biology. [1] Structurally the phosphonate group is similar to biological phosphates and for this reason they have the ability to act as structural mimics, phosphorus-carbon linkages replacing the phosphorus-oxygen linkages.[7] Consequently, phosphonates have found use in biochemistry as, for example, precursors to enzyme inhibitors such as rennin, thrombin, EPSP synthase, HIV protease and various classes of PTK and PTPs, phosphate analogues, antibiotics, and antiviral agents and also the nucleotide industry. [7], [8], [9], [10]

Because replacement of an oxygen atom by a carbon function can lead to alterations in the ion-binding, pK_a, metal binding capacity and hydrogen-bonding ability of phosphonates over phosphates for example, [7] this has led to the introduction of different functional groups at the α-carbon site, including fluoro (F), amino (NH_2) and hydroxy (OH) whereby ion-binding and H-bonding capabilities are re-introduced and the differences are overcome. [11] However, the introduction of an additional functional

group can also generate a stereogenic centre at the alpha-carbon (Figure 1.22) which would need to be controlled in order to affect a specific biological response, as often such responses are sensitive to molecular stereochemistry. [11]   This has led to significant interest in reactions to construct [P-C] bonds with control over attendant stereochemistry, one such variant being the enantioselective catalytic PA reaction.
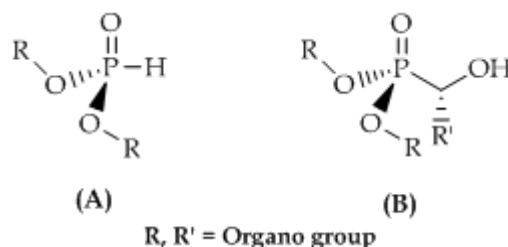
Figure 1.22 Phosphonate esters (A) and α-functionalised esters (B). [11]

1.4 Medicinal Properties of α-Functionalised Phosphonate Esters
1.4.1 PTPs – Protein Tyrosine Phosphatases

Protein tyrosine phosphatases are a family of signal transduction enzymes that are responsible for removing a phosphate group from phosphorylated tyrosine residues in proteins. They follow a reversible, dynamic equilibrium with protein tyrosine kinases (PTKs), which catalyse the transfer of a γ-phosphate moiety from ATP (**A**denosine **T**ri-**P**hosphate) to tyrosine residues. Their functions are extremely important in regulating the phosphorylation state of many important intracellular signalling transduction pathways triggered by extracellular effectors such as: [12]

- Hormones
- Mitogens
- Cytokines
- Nerve impulses that regulate metabolism
- Gene expression
- Cell division
- Differentiation, development, transport, locomotion, learning and memory

This diverse list indicates the crucial need for signal transduction in converting extracellular signals to biochemical responses by the cells. [13] The equilibrium between the two processes is an integral part of the mechanism through which cells communicate. Therefore an imbalance of the equilibrium between the two processes or a breakdown in the function of the PTKs and PTPs, could contribute to diseases such as cancer, diabetes and osteoporosis. [14], [15]

1.4.2 PTP Inhibition

As indicated in section 1.4.1 PTPs are an essential part of a successful pathway for cellular signalling. A prolonged disruption in these processes could have a profound effect on the system, as stated previously with the possible onset of diseases. However an ability to temporarily disrupt the signalling pathway could form the basis of disease control, for example in debilitating diseases like cancer. Burke and co-workers used PTP inhibitors to probe the various signal mechanisms and PTP active sites, in the hope that it could lead to possible solutions to some disease forms caused by PTP inhibition. [14], [16]
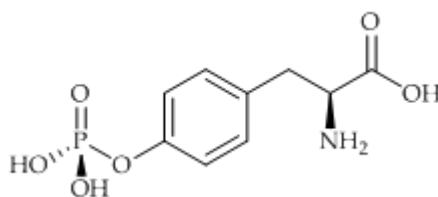
Figure 1.23 Phosphotyrosine.

Phosphotyrosine is a phosphorylated amino acid readily cleaved by PTPs along the [P-O] linkage. It is known that that the aberrant activity of PTPs and PTKs (**P**rotein **T**yrosine **K**inase) causes significant disruption to vital systems, that inhibition of the phosphatase or kinase activity could potentially prevent substantial damage. If one were able to introduce a mimic for phosphotyrosine, the usual substrate for the wild-type enzyme, which possesses much of the structural profile of the natural substrate, but a greater stability towards enzymatic cleavage, it may prove possible to inhibit

certain wild-type PTP/PTK systems. [17], [18] Thus hopefully by only changing a small part on phosphotyrosine, one should still be able to mimic its original activity and ultimately keeps its biological action without introducing potentially negative effects due to differences in charge profile and/or pH profiles. [17], [18]

1.4.3 Types of Inhibitors and their Medicinal Applications

The study of substrate-enzyme binding has provided great insight into the types of system that could potentially make useful PTP and PTK inhibitors. [14] There are many different types of inhibitors and also many ways of creating a new inhibitor, some of which are based on phosphorus compounds and others that are not phosphorus-based. In addition some systems contain metals. [14] Small molecules, such as nitric acid, have also been found to show inhibitory properties. [14] In addition, nature has its own way of inhibiting processes that could otherwise prove fatal if left to progress continuously (Figure 1.3). Such examples include PTPs as described in section 1.4.2, however the mechanism of action such compounds are rarely known as they are quite complex and so trying to design new systems which hopefully lead to improved inhibition is challenging. [14]
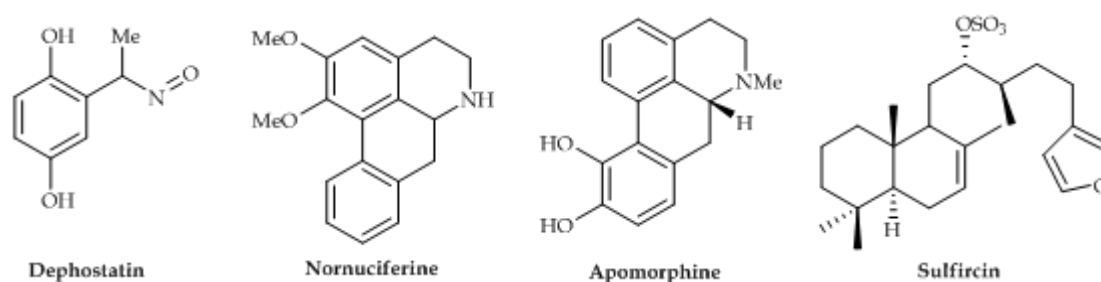
Figure 1.24 Examples of product inhibitors. [14]

(Phosphonomethyl)-phenylalanine (Pmp) is a non-hydrolysable phosphotyrosine mimetic, which upon protection could be incorporated into a peptide with potential as a PTP/PTK inhibitor. [17]
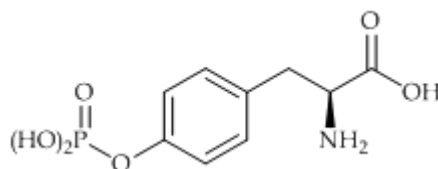
Figure 1.25 Pmp, (Phosphonomethyl)-phenylalanine.
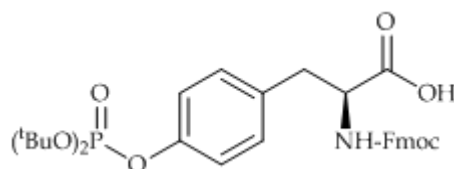
Figure 1.26 Protected Pmp (Fmoc = 9-fluorenylmethoxycarbonyl).

Although Pmp is a mimetic of phosphotyrosine, there are physical and chemical differences between the two. Pmp has a pK_{a2} value higher than the parent phosphotyrosyl-phosphate and its ability to form hydrogen bonds is diminished when the methylene group is introduced in place of the [P-O] bond.[19] To compensate for these physical differences, halogen groups have been introduced into the methylene group in order to lower the pK_{a2} value.[14], [19] Incorporating a fluorine atom still0 allows hydrogen bonding to take place, which has been found essential for interaction with the active site of the enzyme. [16], [17], [20]
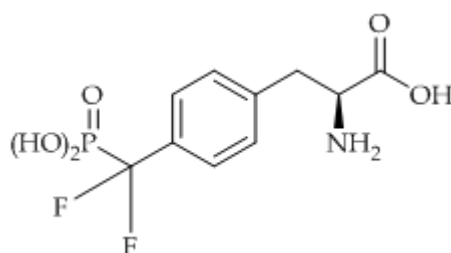
Figure 1.27 F2Pmp

The difluorophosphonate (F2Pmp) analogue of the peptide bound Pmp is a much superior PTP inhibitor. The only problem with using a phosphonate compound and incorporating it into a peptide is cleavage of the peptide bond and loss of activity.[14] Functionalised phosphonates remain a major molecular framework for PTP inhibitors despite the problems with poor cell permeability due to ionisation of the phosphonate

moiety. There is a need for new, selective synthetic pathways to create larger libraries of inhibitors with control over stereochemistry.

1.5 Mechanism of the PA Reaction

The phospho-aldol reaction as the name indicates is very similar to the well-known aldol-reaction (Scheme 1.), and is also a base-catalysed reaction as outlined in Scheme 1..

X = O,NH; R,R' = organo group
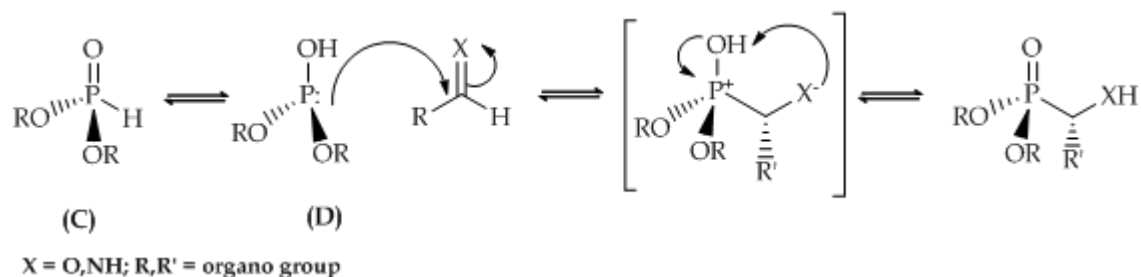
Scheme 1.8 Currently accepted mechanism of the phospho-aldol. [21]

Hydrogen phosphonates exist in two tautomeric forms, phosphonate $[(RO)_2P(O)H]$ and phosphite $[(RO)_2P(OH)]$ (Scheme 1.).[22] Under neutral conditions the equilibrium favours phosphonate ester tautomer **(C)**, the non-reactive form [22] and must therefore be forced toward phosphite tautomer **(D)** (Scheme 1.), where the lone pair of electrons on phosphorus facilitates nucleophilic attack on a carbonyl carbon.[22] Successful nucleophilic attack is aided by introduction of a catalyst; this forces the equilibrium towards the phosphite as well as the possibility of introducing stereoselectivity by bringing carbonyl substrate and phosphite together within an asymmetric environment such as that found within a chiral metal complex. [22]
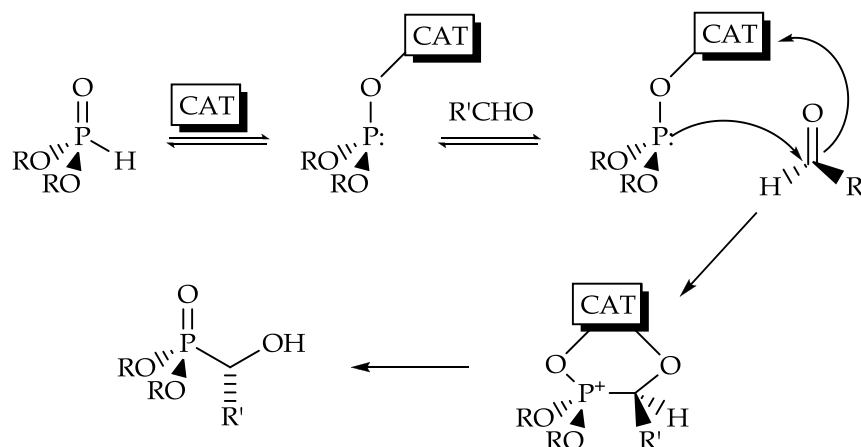
Scheme 1.9 Base-catalysed reaction mechanism of the phospho-aldol reaction. [22]

1.6 Catalysis of the PA Reaction
1.6.1 Catalysis and its Importance in the PA Reaction

The phospho-aldol (PA) reaction is an extremely important enantioselective reaction, although for the reaction to proceed, a catalyst with distinct Lewis basic characteristics is required. Indeed, the best catalyst systems to date appear to possess both Lewis acidic and basic components, but considerable challenges remain in developing catalysts which are: [11]

- Simple to prepare
- Inexpensive
- Tuneable
- Compatible with air and water
- Tolerant to substances without drying or special purification
- Reusable without reprocessing
- Highly stereoselective

Development of new and improved catalysts pays close attention to reaction efficiency; processes which minimise waste, side-reactions and allows products to be purified easily. Such processes are frequently termed 'green' processes. Currently there exist few catalysts for the PA reaction that meet all of the above criteria, and even

then only with varying degrees of success. High yields and stereoselectivity are extremely important and have to be considered as the chief goals when designing a catalyst for this transformation. Therefore, chiral complexes which possess both Lewis basic and acidic sites would be valuable targets for controlling the stereochemistry of PA processes. Research groups active in the field have developed new asymmetric catalytic systems based on two main classes; (i) non-metallic systems [6], [11] and (ii) metallic systems, in particular those based on lanthanum, [23] aluminium [24] and titanium. [25]

1.6.2 Asymmetric Catalysis of the PA Reaction by Non-Metallic Compounds

Some of the earliest catalysts used for the asymmetric phospho-aldol reaction were reported by the Wynberg group and utilised chiral nitrogen compounds based upon chinchona alkaloids such as quinine and quinidine, which were found to catalyse the reaction between *o*-nitrobenzaldehyde with dimethyl-*H*-phosphonate according to Scheme 1., to afford an α-hydroxyphosphonate ester in 28% e.e. [26], [27]
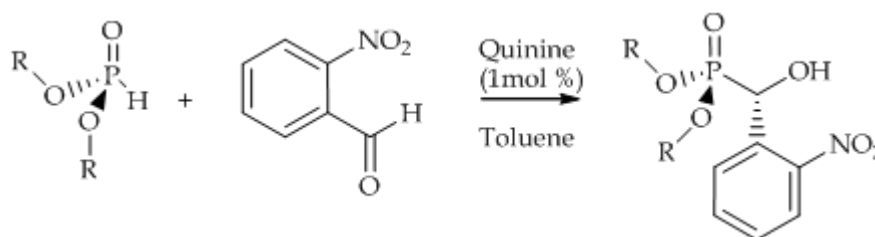
Scheme 1.10 The hydrophosphonylation reaction catalysed by a cinchona alkaloid, with the addition of DMHP. [26], [27]
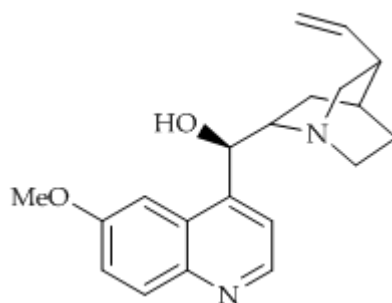
Figure 1.28 The structure of quinine.

The chirality of quinine and its ability to act as a hydrogen-bond donor and acceptor was proposed to facilitate reaction by bringing together the phosphite and carbonyl species within a chiral environment, (Figure 1.8). It was presumed that binding of the phosphate form by more than one type of interaction (in this case a combination of H-bonding and electrostatics) might allow transfer of stereochemical information. [22]
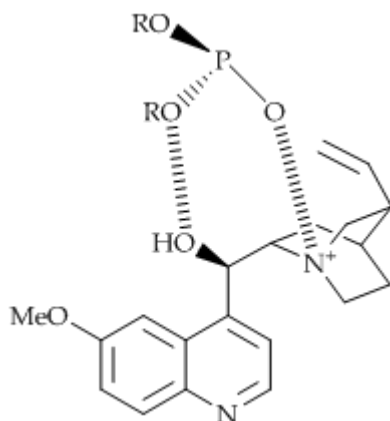
Figure 1.29 Binding of DMHP to quinine forming a chiral ammonium phosphito intermediate.

Enantioselectivities for the reaction between DMHP and benzaldehyde were low, however the yields were high. Selection of the R-function is also very important and played a role in increasing the enantiomeric excess from 28% e.e. when R = Me to 90% e.e. when R = tBu, the cause of which is down to a steric effect of the *tert*-butyl groups.[26], [27]

1.6.3 Asymmetric Catalysis of the PA Reaction by Metallic Compounds

The first salen complex was prepared in 1889 using copper. [28] A 'salen' is the resulting compound from the condensation reaction between salicylaldehyde and an amine and so is generically named a 'salen', where 'sal' refers to salicylaldehyde and 'en' to the imine bond. When these compounds are termed 'salan' it simply refers to the reduced variant of the imine bond. Over the years many such metal complexes have been synthesised as potential PA catalysts, including those of manganese, vanadium, titanium, tin and zinc salen complexes, [29] chromium and molybdenum salan complexes, [30] and cobalt, nickel and copper salen and salan complexes. [31] The most commonly used metals in PA catalysis to date have been aluminium, titanium and lanthanides and this report will review advances in each with respect to the PA reaction. Catalyst precursors for the PA reaction may, in general, be divided into two categories; those in which the Lewis acid and Lewis basic sites are directly connected **(Type A - monometallic)** and those where the two sites are remote from each other **(Type B - bimetallic),** Figure 1.9.
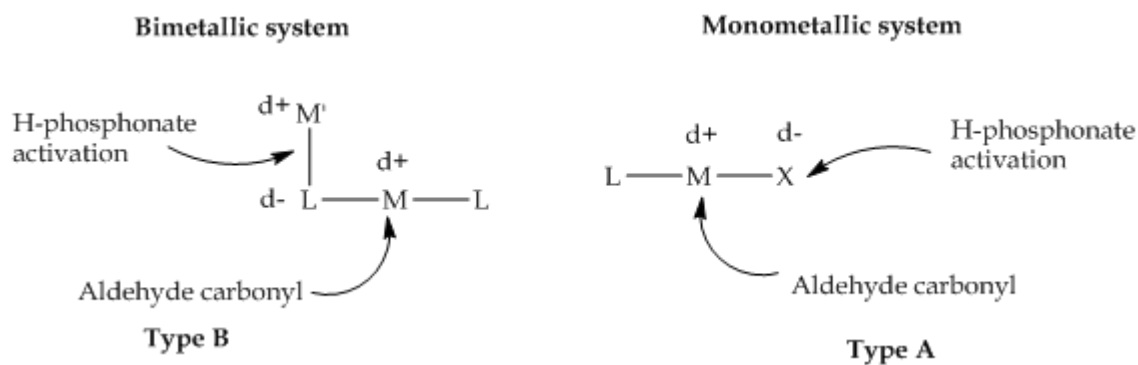
Figure 1.30 Bimetallic and monometallic systems **(Type B)** and **(Type A).** [22]

Catalysis *via* **Type A** complexes involves the Lewis basic site deprotonating the H-phosphonate and binding the resultant phosphite to the Lewis acidic metal centre [M], followed by activation and binding of the carbonyl function to the same metal centre. Proton transfer from the hydrogen phosphonate finally releases the desired product and allows for catalytic turnover (Scheme 1.).
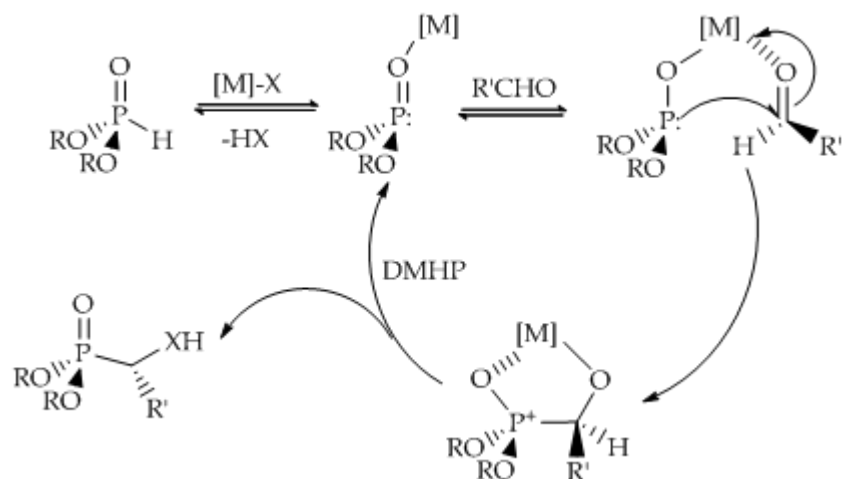
Scheme 1.11 Mechanistic overview of the catalysed phospho-aldol (PA) reaction *via* complexes of Type A. X = O, NH [22]

The mechanistic situation for **Type B** complexes is similar; the key difference being that carbonyl activation and H-phosphonate deprotonation occur at remote sites (Scheme 1.).

The potential advantage of this approach is that bimetallic systems can be designed to achieve optimum carbonyl binding and H-phosphonate activation independently of each other.
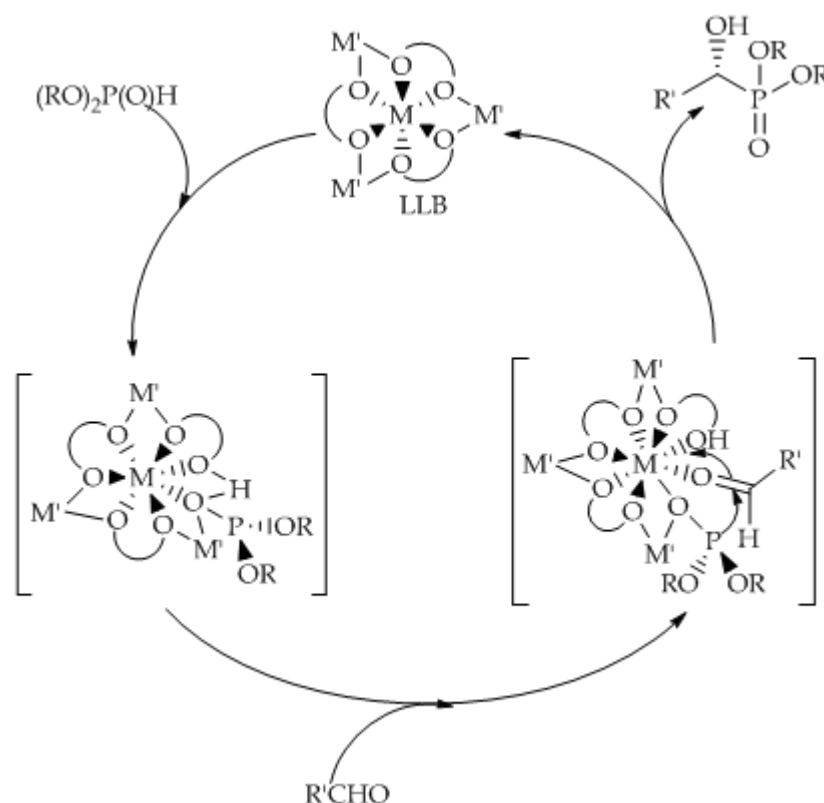
Scheme 1.12 Mechanistic overview of the catalysed phospho-aldol (PA) reaction *via* complexes of Type B. LLB = complex where M = La and M′ = Li (lanthanum lithium-binaphtholato). [22]

1.7 Titanium Complexes as Catalysts

The Shibuya group explored the asymmetric catalytic phospho-aldol reaction based on chiral titanium alkoxide frameworks (Scheme 1.). [32] The amphoteric nature of the complexes made them a good choice, with the ability to act as a Lewis acid and a Lewis base. It was expected that the Lewis basic alkoxy group would be sufficient to cause deprotonation of DEHP, with subsequent coordination of the phosphito group to the titanium centre. The chiral environment surrounding the metal, provided by the enantiopure tartrate esters was envisaged to induce enantiofacial selectivity, thus leading to asymmetric reaction products. [32]
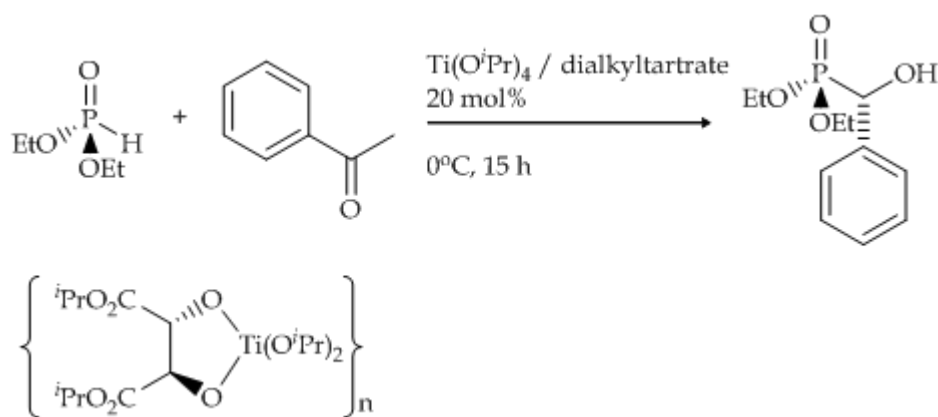
Scheme 1.13 Enantioselective addition of diethyl phosphite to aldehydes with the Sharpless catalyst. [32]

Shibuya also realised that by tuning the donor or acceptor ability of the reaction solvent, the Lewis acidity of the catalyst could be modified. A selection of reactions was undertaken with a catalyst loading of 20 mol% in a variety of solvents, of which the results are presented in Table 1.5.

Entry	Aldehyde	Solvent	Yield (%)	e.e. (%)
1	C_6H_5	Toluene	51	36
2	C_6H_5	DCM	12	0
3	C_6H_5	THF	61	51
4	C_6H_5	Et_2O	75	53
5	P-ClC_6H_4	Et_2O	76	52

Table 1.5 Summary of results for the enantioselective addition of a selection of aldehydes with DEHP in the presence of the $Ti(O^iPr)_4$/dialkyltartrate. [32]

The reaction was moderately successful with an enantiomeric excess of 53% achieved, but the system was found to be highly water and oxygen sensitive and required a high catalytic load (20 mol%). A significant variation in e.e. and yield was observed when the solvent was changed, indicating that the choice of solvent was an important factor in these reactions. Solvents with greater donor ability (THF and Et_2O) afforded higher yields and e.e.[32]

In 1996 North *et al.* reported the synthesis of salcyen complexes of titanium from titanium tetra*iso*propoxide and the Schiff base salcyen(*t*Bu)$_4$ (Scheme 1.14).[33]   A selection of aromatic, aliphatic and α, β-unsaturated aldehydes were treated with TMSCN in the presence of the Schiff base titanium complex resulting in □-siloxycyano compounds with enantioselectivities (e.e.s) between 40-80%. The resulting products are versatile and important synthetic intermediates, being readily converted into a wider range of homochiral products. [33]
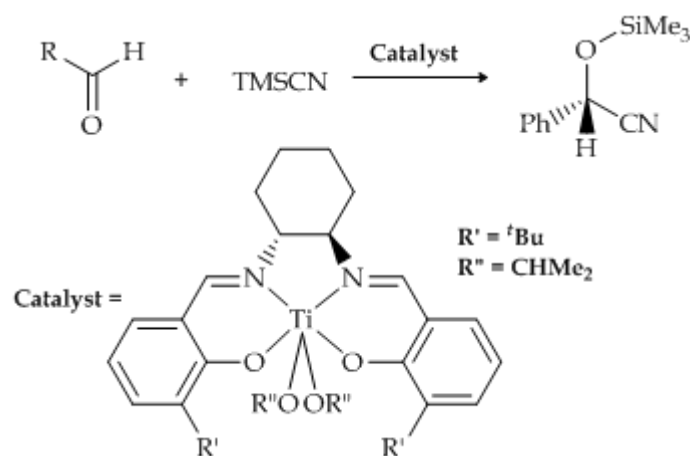
Scheme 1.14 Asymmetric silylcyanation of aldehydes catalysed by salcyen-(*t*Bu)$_4$Ti(IV)(OCHMe$_2$)$_2$. [33]

In 1998 Spilling and co-workers investigated further the use of chiral titanium alkoxo complexes initially first proposed by Shibuya in 1993.[34] By using a simpler synthetic approach and replacing the *iso*propyl and *iso*benzyl part of the titanium ligand with a *trans*-1,2-cyclohexane diol, the e.e. values in the addition of DMHP to cinnamaldehyde increased up to 70%. [35]

Further investigations were carried out using a variety of substituted aldehydes to better understand the effects these changes made on the yield and e.e., (Scheme 1. and Table 1.2).

The afforded yield was moderate to good however it is important to note the dominant stereoisomer of the product was *R*.
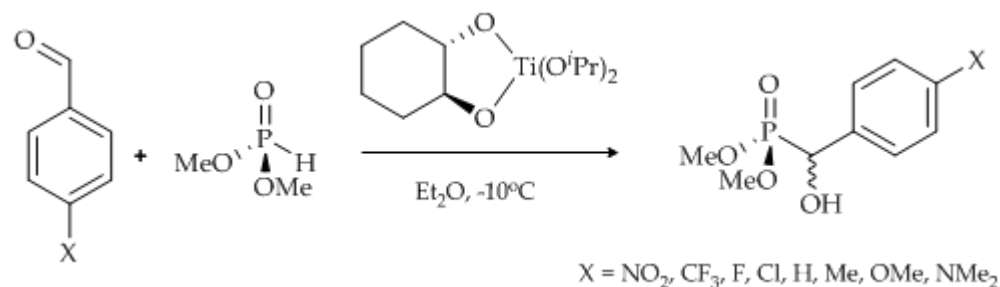
Scheme 1.15 Phosphonylation of aldehydes with dimethyl-*H*-phosphonate using (S, S)-*trans*-cyclohexanediol with Ti(O^{i}Pr)$_4$. [35]

Entry	X	Yield (%)	e.e. (%)	Configuration
1	NO$_2$	58	52	*R*
2	CF$_3$	73	55	*R*
3	F	44	62	*R*
4	Cl	66	53	*R*
5	H	51	64	*R*
6	Me	69	64	*R*
7	OMe	65	57	*R*
8	NMe$_2$	61	64	*R*

Table 1.6 Phosphonylation of aldehydes with DMHP using the catalyst generated from (S, S)-*trans*-cyclohexanediol and Ti(O^{i}Pr)$_4$.[35]

1.8 f-Block Complexes in PA catalysis

Accompanying their work on titanium complexes, Shibuya *et al*. reported the use of lanthanum-based complexes, previously prepared and exploited by Shibasaki in related aldol-type reactions; [23] however it was Shibuya's team that investigated their uses further by catalysing the phospho-aldol reaction between DEHP and a variety of *para*-substituted benzaldehydes. [34]

Binaphthol was used as the principal source of chirality and results showed that the levels of asymmetric induction were much higher than those observed from related titanium systems.[34]   Enantioselectivities also increased as the substituent X in *para*-benzaldehyde became more electron donating, providing evidence that the binding of the carbonyl substrate to the more basic lanthanum centre was crucial for producing a higher e.e. (Scheme 1.). [34]
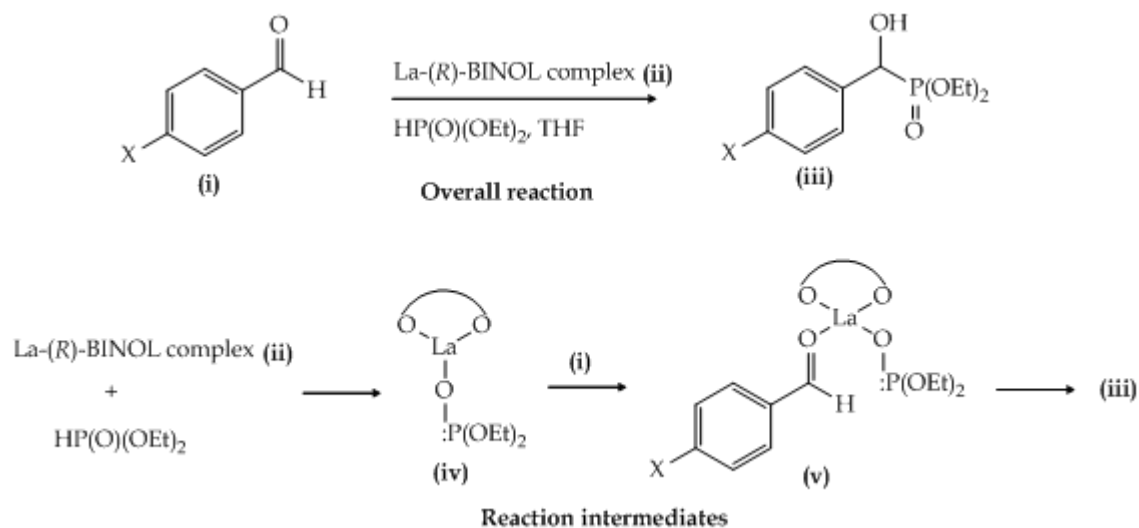
Scheme 1.16 **B**inding of a carbonyl to the lanthanum centre. [34]

The authors proposed a 2-step mechanism (Scheme 1.). In the first step DEHP was incorporated into the chiral lanthanum complex **(ii)** *via* its phosphite tautomer **(iv)**.[34] The coordination of an aldehyde **(i)** to the metal giving **(v)** is followed by the stereo-determining [P-C] bond forming step to give the final product **(iii,)** representing the second step.   It is difficult to know if there is a further step which results in the regeneration of the active complex, as this is not discussed in the paper.

Spilling also reported comparable catalytic results to those of Shibuya whilst using a lanthanum complex of binaphthol to catalyse the addition of DMHP to cinnamaldehyde. However the result was rather disappointing, in that after 7 h at -65 °C, with a catalyst loading of 10-20 mol%, an e.e. of only 33% was achieved. By comparison, Shibuya who used simple aromatic aldehydes, was able to achieve an e.e. of 79%. [34], [36]

Since these initial attempts the group of Shibasaki has pursued the use of lanthanum-based complexes and are now considered the most developed and potent catalyst for the phospho-aldol reaction. The key to these developments has been down to improving the synthetic route and introducing a heterobimetallic system.[37]

1.9 Aluminium Complexes as PA Catalysts

Systems based upon lanthanide metals have used binaphthol as a source of chirality.[38] The work of Shibasaki has extended this binaphthol-based heterobimetallic system to include aluminium, [39] in the form of an aluminium-lithium-binaphthol (ALB) composite. [22], [39]
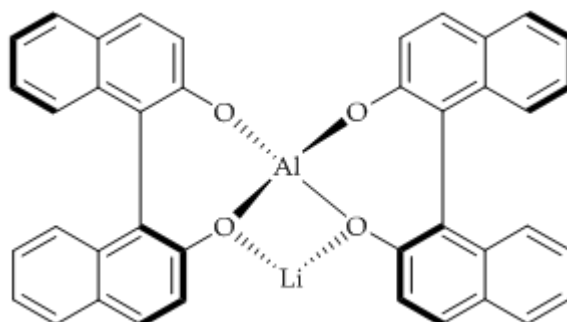
Figure 1.31 Aluminium-lithium-binaphthol (ALB) complex. [40]

The ALB system has proved to be as effective as its lanthanide counterparts although overall slightly less reactive. However, it was found to be very useful when used with electron-withdrawing carbonyl substrates, although less efficient for aliphatic and un-activated aldehydes than its lanthanide cousins. [40] The ALB complex is a bimetallic multifunctional catalyst of Type A where the aluminium atom is presumed to activate the carbonyl and the alkoxo moiety activates the H-phosphonate *via* phosphite formation. [41] Essentially the central aluminium metal centre is acting as a Lewis acid and the alkoxo moiety as a Brønsted base. [41] After carrying out a variety of catalytic tests it was found that ALB was not a good catalyst for aliphatic or un-activated

aldehydes as can be seen in Table 1.3 , entry number 10. However the ALB catalyst does show good activity with α,β-unsaturated systems and is more facile when activated carbonyls are used.

Entry	Aldehyde	Reaction time (h)	Yield (%)	e.e. (%)
1	PhCHO	51	95	90
2	$4\text{-}O_2NC_6H_4CHO$	40	85	71
3	$4\text{-}ClC_6H_4CHO$	38	80	83
4	$4\text{-}MeC_6H_4CHO$	92	82	86
5	$4\text{-}MeOC_6H_4CHO$	115	88	78
6	$4\text{-}(Me_2N)C_6H_4CHO$	-	-[a]	-
7	E-PhCH=CHCHO	83	85	82
8	E-PhCH=CMeCHO	61	47	56
9	$E\text{-}CH_3(CH_2)_2CH=CHCHO$	39	53	55
10	$CH_3(CH_2)_4CHO$	41	95	16

Table 1.7 Phospho-aldol reaction promoted by aluminium heterobimetallic systems based on ALB (10 mol % catalyst loading, -40 °C, THF). [a] No reaction. [42]

Optimum reaction conditions were found to be -40 °C in toluene, though the reactions occurred very slowly. Only aromatic aldehydes worked particularly well, especially those with electron withdrawing groups. The reaction of benzaldehyde and dimethyl-*H*-phosphonate catalysed by ALB (10 mol %) produced $(MeO)_2P(O)CHPh(OH)$ in 90% e.e. and a 95% yield in THF at -40 °C. [42]
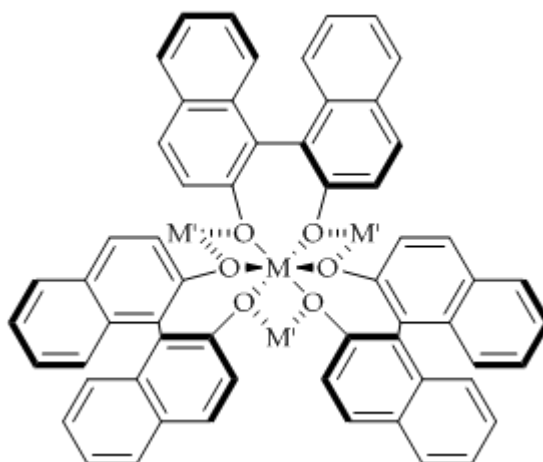
Figure 1.32 Lanthanoid lithium binol (LLB) complex where M = La and M' = Li. [42]

Although both ALB and LLB are bimetallic multifunctional catalysts, they have very different structures (compare Figure 1.10 and Figure 1.11). The reaction mechanism for the phospho-aldol transformation is thought to proceed with the activation of the carbonyl by aluminium and activation of *H*-phosphonate *via* phosphite formation with the lithium ion.
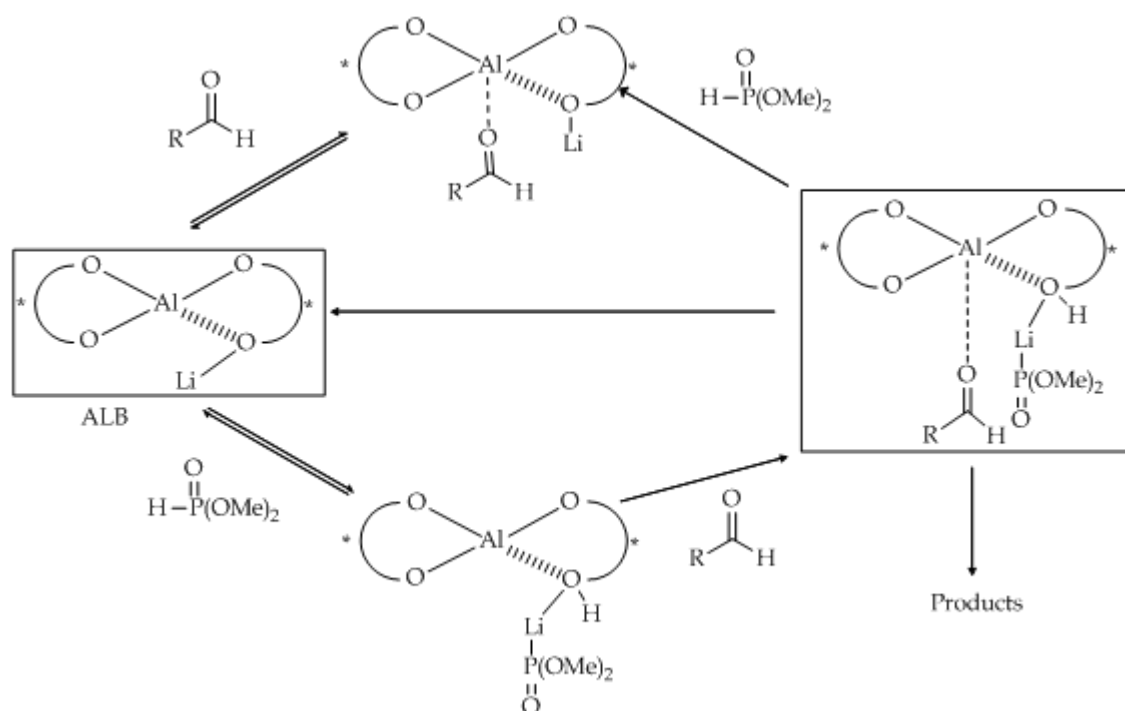
Scheme 1.17 ALB-catalysed phospho-aldol reaction. [41]

The catalytic reaction was enhanced when a combination of ALB and BuLi were used, giving a 58% yield and 98% e.e. Switching to NaO-*t*-Bu instead of BuLi resulted in a 64% yield and a 99% e.e. and the noted absence of a 1,2-adduct was reported.[41] Studies by Shibasaki have shown that the active catalytic species is likely to be complex **I** (Scheme 1. 18). [41]
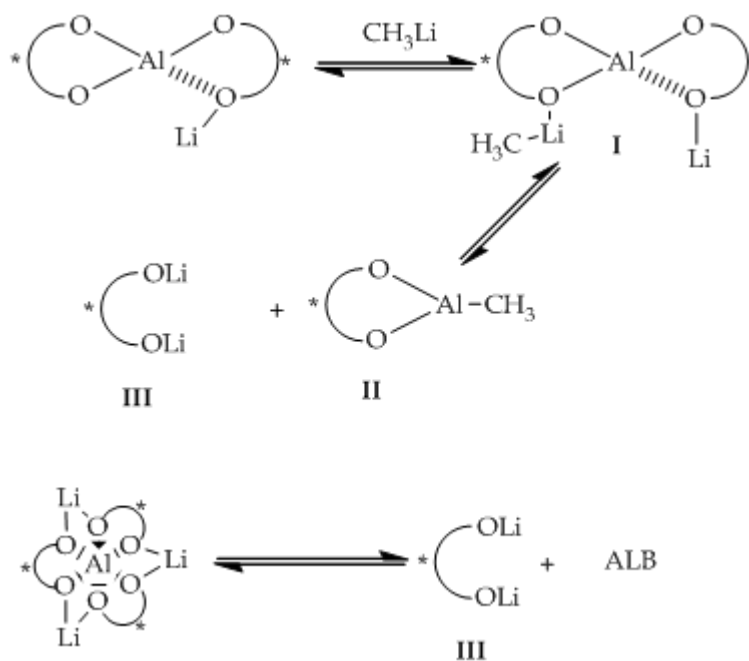
Scheme 1. 18 The role of a base with ALB. [41]

1.10 Catalysis of the PA reaction *via* Schiff Base Complexes

Schiff bases are substituted imines formed by reaction of a primary amine with a carbonyl substrate.[43] There are two main classes of Schiff bases; salens and hydrogenated salens or salans (Scheme 1.).
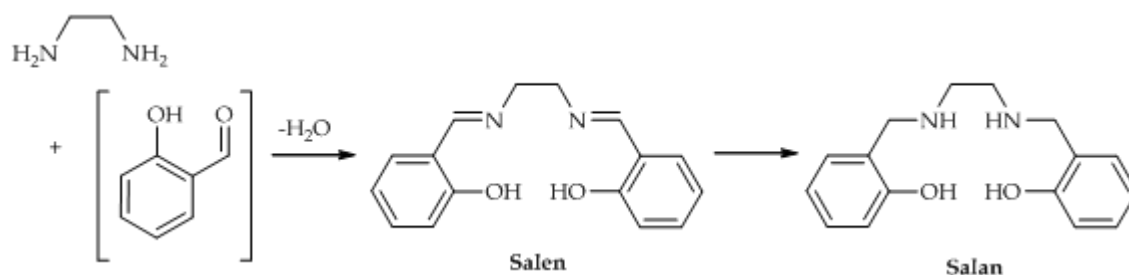
Scheme 1.19 Reaction of an aldehyde with a primary amine to afford Schiff bases. [11]

Schiff bases are synthesised through a condensation reaction between a salicylaldehyde and an amine, resulting in the formation of the generic name "salen" (or salenH$_2$). The "sal" refers to the salicylaldehyde and "en" refers to the use of an ethylene diamine backbone. The hydrogenated form of the salen is simply known as the "salan" (or salanH$_4$), where "an" refers to the formation of the new amine bond. There are additional variations to the nomenclature of Schiff bases corresponding to the nature of the amine, for instance when diaminocyclohexane condenses with salicylaldehyde the name changes to "salcyen". The reduced form of salcyen is known as "salcyan". (Figure 1.12)
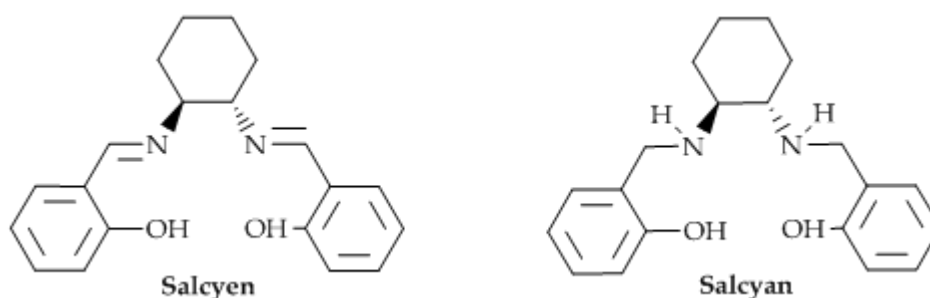
Figure 1.33 General structure of salcyen and salcyan complexes. [43]

Schiff bases are very useful because they can bind metals *via* covalent coordinate bonds through either the OH or NH groups (Figure 1.13). [44] When coordinating to a metal the hydroxy groups normally become deprotonated to form two covalent M-O bonds and the nitrogen atom donates its lone pair of electrons to form two dative coordinate bonds.
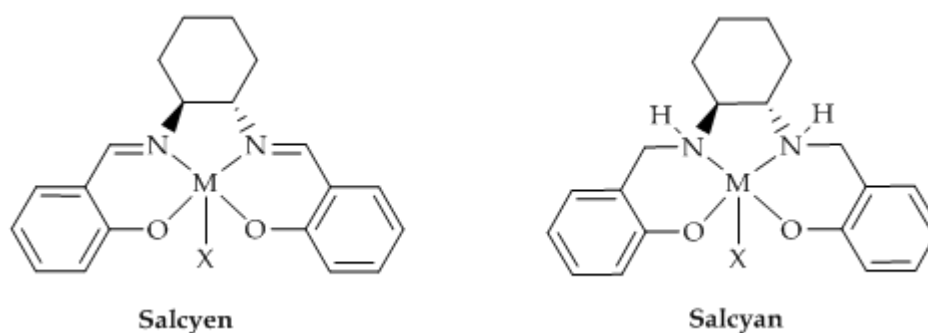
Salcyen   Salcyan

Figure 1.34 The bonding of a salcyen and salcyan ligand (L) to a metal atom (M), X = monoanionic group. [44]

The aromatic rings and diamine backbone can be substituted to afford Schiff base complexes with different properties, for example a ^{t}butyl group attached to the phenolic ring would make it a good NMR marker for characterisation as it has a distinctive chemical shift. With regards to the salcyen and salcyan systems, structural analyses have shown that the salcyen ligand tends to prefer meridional coordination geometry, however the salcyan ligand is conformationally more flexible and can more readily adopt twisted facial coordination geometries. [24] This increased conformational flexibility of salan over salen systems is the result of the presence of a sp^2-hybridised N=CHR function in salcyen compared to a more flexible sp^3-hybridised NHCH$_2$R in salcyan. [6] Although salcyen and salcyan ligands possess the same absolute configuration of backbone, their structural properties may in fact differ as a result of the changes in hybridisation. [6]

1.11 Aluminium Salcyen Complexes

Kee and co-workers have been exploring chiral complexes that facilitate PA catalysis under aerobic conditions.[22] They have moved away from binaphthol as a chiral ligand framework towards the salen class of Schiff bases, especially those derived from the *R,R-trans*-1,2-diaminocyclohexane backbone championed by Jacobsen and others, as they offer considerable scope for synthetic modification. [45] The Kee group first

prepared and screened a series of chiral aluminium salen complexes as potential PA catalyst precursors (Scheme 1.).
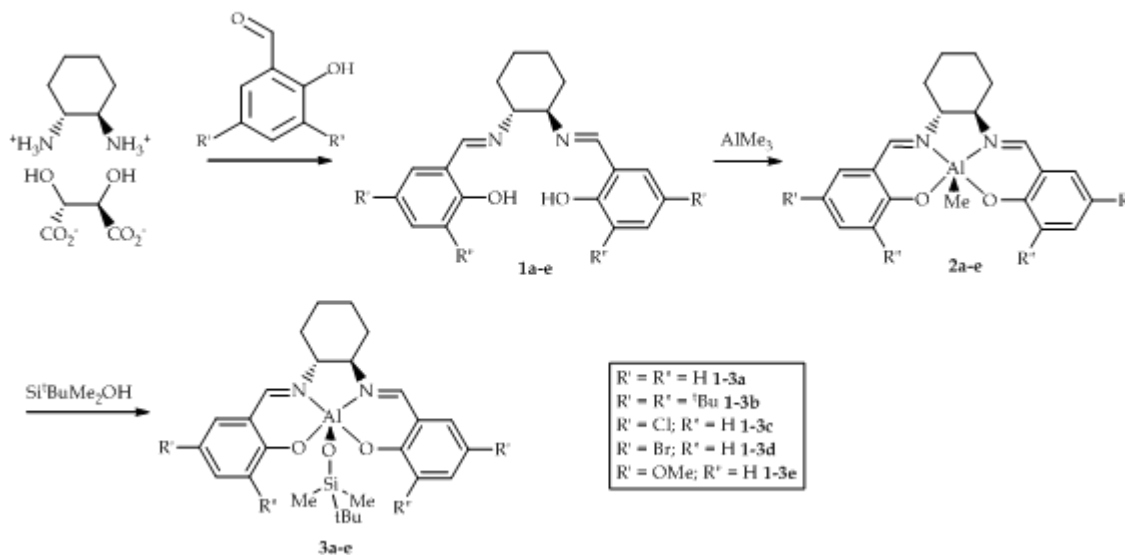
Scheme 1.20 A simple synthetic route to the synthesis of silyl salcyen aluminium complexes, established by the Kee group. [22]

Single crystal X-ray analyses of salcyen aluminium complexes indicated that the ligand backbone can distort from a meridional geometry. Figure 1.14 and Figure 1.15 clearly show the aluminium metal centre as a five-coordinate complex, with a structure that might be described as an intermediate between square pyramidal and trigonal bipyramidal. [11]   The twisting of the metal centre was presumed to promote asymmetric binding of the phosphito and carbonyl reagents before [P-C] bond formation. It is possible that sterically demanding R groups on the phenolic ring could cause the backbone to twist to allow the [P-C] bond formation to take place.
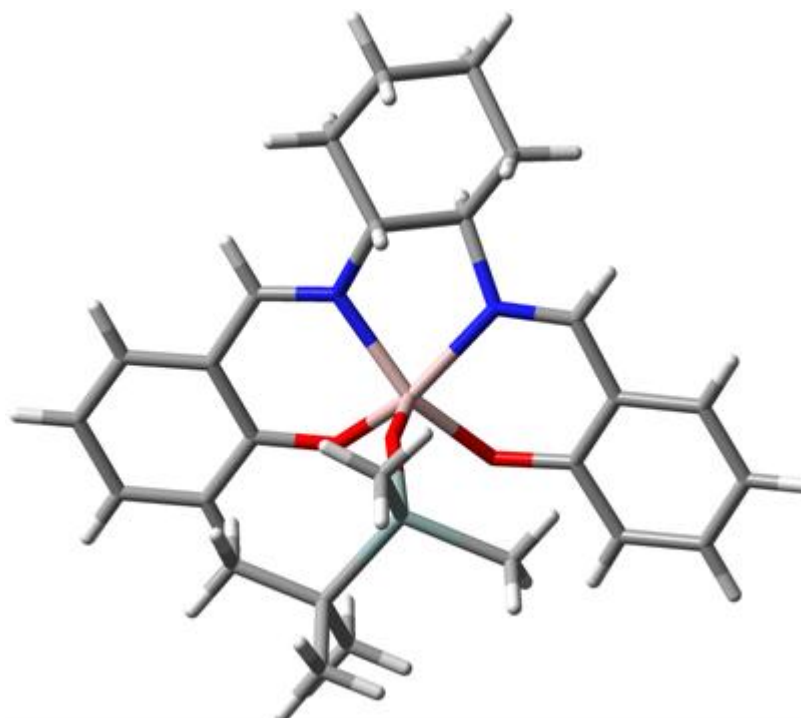
Figure 1.35 GaussView image of X-ray molecular structure of (*R,R*) [salcyen]AlOSiMe$_2{}^t$Bu (**3b** Scheme 1.)
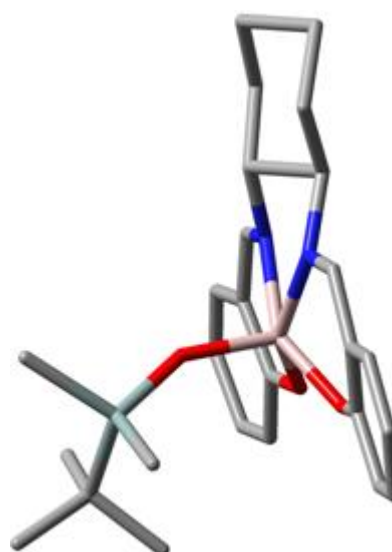
Figure 1.36 GaussView profile image of X-ray molecular structure of (*R,R*) [salcyen]AlOSiMe$_2{}^t$Bu, with hydrogen's removed for ease of viewing. Emphasis is on the significant twisting of the diaminocyclohexane backbone, (**3b** Scheme 1.).

Studies carried out in the Kee group on complexes **2a** (Scheme 1.) ((*R,R*) [salcyen] AlMe) and **2b** (Scheme 1., Figure 1.14 and Figure 1.15) demonstrated that both catalysed the phospho-aldol reaction at room temperature and under normal

atmospheric conditions (20 °C and 1 atmosphere pressure). [11], [46]   Reactions were performed in dry THF and analysed by ^{31}P-NMR spectroscopy after 3-6 hrs.[46]

Entry	Aldehyde	e.e. (%)[a]	e.e. (%)[b]	e.e. (%)[c]
1	PhCHO	37	41	45
2	$4\text{-}O_2NC_6H_4CHO$	15	10	-
3	$4\text{-}ClC_6H_4CHO$	30	19	-
4	$4\text{-}MeC_6H_4CHO$	44	49	46
5	$4\text{-}MeOC_6H_4CHO$	39	46	49
6	$4\text{-}BrC_6H_4CHO$	27	24	21
7	$2\text{-}ClC_6H_4CHO$	12	12	-
8	$2\text{-}MeC_6H_4CHO$	25	20	-
9	$2\text{-}MeOC_6H_4CHO$	20	27	-

Table 1.8 Results of the reaction of substituted aldehydes with ((*R,R*)[salcyen(*t*-Bu)$_4$]AlOSiMe$_2$*t*Bu).   [a] Reactions performed under dry, inert atmosphere conditions with **2a** (Scheme 1.) as catalyst at 5 mol% in THF. [b] Reactions performed under aerobic conditions with **2a** (Scheme 1.) as catalyst at 5 mol% in THF. [c] Reactions performed using **3a** (Scheme 1.) as catalyst at 5 mol% in THF. [46]

Substitution around the aryl group of the ligand framework with groups that would bring about a structural or steric change, were observed to affect the e.e. as can be seen in Table 1.4, entries 1-6. The e.e.s decrease as the *para* substituent on the benzaldehyde becomes more electron withdrawing. Benzaldehyde substitution in the *ortho* position (entries 7-9, Table 1.4) leads consistently to lower e.e.s than for *para* substitutions, presumably due to steric effects playing a more significant role. [11]

It was presumed that a lack of flexibility in the salcyen framework may have been the main reason for such modest enantiomeric excesses and hence the decision was made to move to a more asymmetrical environment at the metal centre; for this reason it was judged appropriate to switch attention from the unsaturated salcyen systems to those based on the tetrahydrogenated, or salcyen systems.

1.12 Aluminium Salcyan Complexes as PA Catalysts

Atwood and co-workers have reported extensively on the synthesis, characterisation and catalytic applications of salan complexes and procedures developed from Atwood's work [43] were used to prepare complexes such as [(R,R)-salcyan]Al(OH) **4** and [(R,R)-ᵗBu₄-salcyan]Al(OH) **5**. [24]
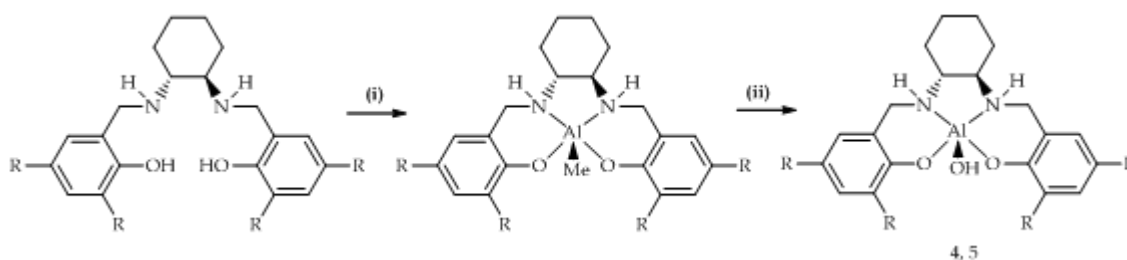
Scheme 1.21 Syntheses of **4** (R = H) and **5** (R = ᵗBu); (i) AlMe₃; (ii) H₂O. [24]

Results showed that complexes **4** and **5** were active catalysts for the PA reaction of dimethyl-*H*-phosphonate (DMHP) and benzaldehydes, but their catalytic behaviour was somewhat different to their salcyen counterparts. [44]

Catalysis of the PA reaction using salcyans, proved both enantioselective and more tolerant to water than the same process catalysed by salcyen complexes of aluminium.[7] Kee *et al.* subsequently prepared and analysed a variety of aluminium salcyan complexes with various R' groups (Figure 1.16). It was found that all derivatives catalysed the phospho-aldol reaction, with moderate enantioselectivities, e.e. <50% (Table 1.9).

R' = H (6), ^{t}Bu (7)
X = Me (a), OSiMe$_2$^{t}Bu (b)
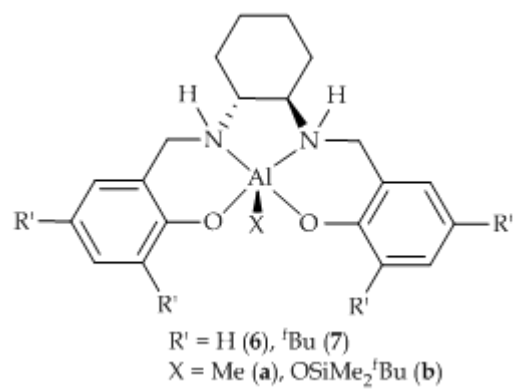
Figure 1.37 (*R,R*) [salcyan (R)$_4$] AlX. [22]

Entry	Catalyst loading (mol %)	4-XC$_6$H$_4$CHO	Solvent	Conv (%)[a]	e.e. (%)
1	45	X = H	THF	100	18
2	20	X = H	THF	100	26
3	10	X = H	THF	100	39
4	5	X = H	THF	100	48 [b]
5	1	X = H	THF	95	59
6	0.5	X = H	THF	74 [c]	58
7	0.2	X = H	THF	54 [d]	52
8	5	X = H	THF [e]	87	50
9	5	X = H	THF [f]	81	52
10	1	X = Br	THF	75	42
11	1	X = Br	THF	85	42
12	1	X = Me	THF	76	57
13	1	X = Me	THF [g]	88	53
14	1	X = OMe	THF	91	47
15	1	X = NO$_2$	THF	64	18
16	1	X = NMe$_2$	THF	45	22
17	1	X = Br	CH$_2$Cl$_2$	32	40
18	1	X = Me	CH$_2$Cl$_2$	8	53
19	1	X = H	C$_7$H$_8$	26	42
20	1	X = Br	C$_7$H$_8$	60	41
21	1	X = Me	C$_7$H$_8$	45	52

Table 1.9 Results of phospho-aldol catalysis *via* salan complex **7b**. All reactions were performed in air at 289 K unless otherwise specified. [a] Conversions (conv) obtained after 4 h. No product other than α-hydroxyphosphonate ester was observed. [b] Yield = 78% and e.e. = 53% (*S*) when reaction is performed at 273 K. [c] After 12 h. Al absolute configurations are (*S*). [d] After 21 h. [e] With 20 mol% water added. [f] 100 mol% water added. [g] In the presence of 4 Å molecular sieves. [22]

From the data presented in Table 1.5 it may be inferred that several factors have an effect on the phospho-aldol catalysis reaction. These include catalyst loading, substitution on the phenyl ring and solvent. Although one would expect a high

catalyst loading to give a high conversion rate, the e.e. on the other hand is considerably small. With a considerable decrease in the catalyst loading, a significant increase in the e.e. is observed, with consequent and expected diminution of conversion. Solvent also seems to effect the catalysis, with the most successful results being those conducted in THF. Finally the substitution of the aldehyde is also significant, with small organic functional groups being favoured over electron withdrawing groups.

1.13 Bifunctional Catalyst Systems

To date, the best catalyst systems for PA reactions appear to possess both Lewis basic and Lewis acidic character; they are bifunctional. Bifunctional salcyen catalyst systems have previously been employed in reactions such as alkylations of α-ketoesters, but not as yet in PA catalysis. [47], [48] DiMauro and Kozlowski demonstrated the stereoselective addition of diethylzinc to aldehydes using zinc salcyen complexes with basic groups incorporated into the ligand framework, rather than directly attached to the metal centre. [47], [48]
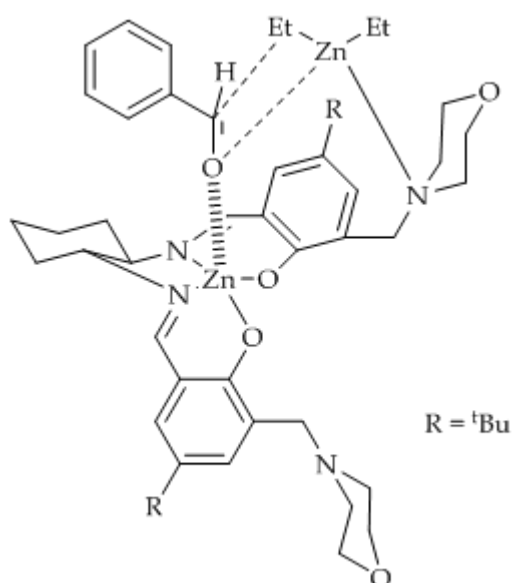
Figure 1.38 Proposed attachment of diethyl zinc to benzaldehyde as catalysed by [(*R*,*R*)-salcyen]Zn. [47], [48]

The pendant arms (*e.g.* methylmorpholine) are positioned on the phenyl ring of the ligand framework and are thought to be responsible for activating the nucleophilic diethyl zinc *via* dative bond formation, whilst the metal centre activates the carbonyl reagent (Figure 1.17). The complex had been tuned in order to incorporate different functions, such as Lewis acid and Lewis basic functions, allowing both reagents to be brought together in the same chiral environment, then activated and reacted. This concept of tuning may have distinct potential in the PA reaction.
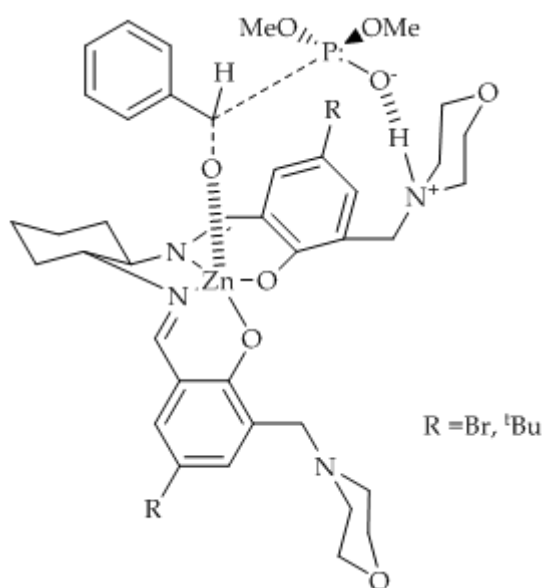
Figure 1.39 Proposed attachment of *H*-phosphonate (DMHP) to benzaldehyde for the PA reaction as catalysed by [(*R,R*)-salcyen]M. [49]

Similar systems of the type shown in (Figure 1.18) have previously been studied within the Kee group, with rather less than impressive results to date. Specifically, it was found that zinc salcyen complexes were not sufficiently stable in the PA reaction mixture and that racemic catalysis occurred presumably initiated *via* some as yet unidentified breakdown products. [49]

More recently You *et al.* developed a bifunctional catalyst by the metal-organic self-assembly of substituted BINOL's [39] and cinchona alkaloids [32] in combination with Ti(O*i*Pr)$_4$ [32] for the asymmetric hydrophosphonylation of aldehydes. [50] The cinchona

alkaloid acts as a Lewis base moiety, which coordinates to the central metal of the Lewis acid moiety (binol-Ti complex) to form a metal-organic molecule.
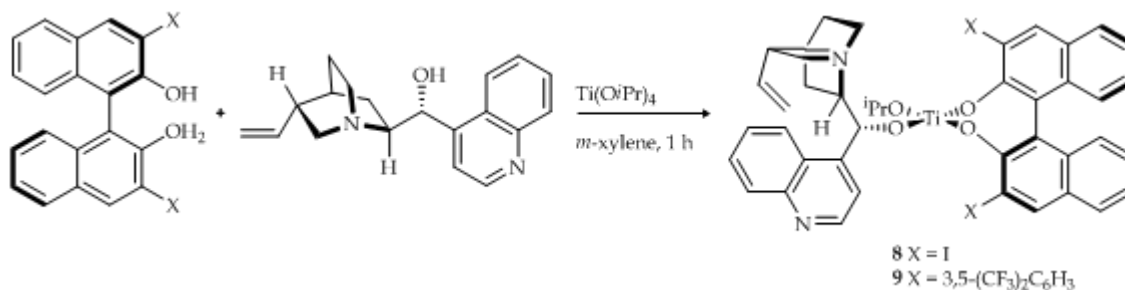
Scheme 1.22 Preparation of self-assembled cinchona-BINOL titanium complexes. [50]

It was thought that due to the highly modular nature of the catalytic systems there would be better matching of the chiral ligand, metal ion and substrate, therefore facilitating a more active and enantioselective catalytic performance.

The bifunctional catalyst (substituted BINOL, cinchona alkaloids with Ti(OiPr)$_4$) was tested against a variety of aliphatic and aromatic aldehydes at a catalyst loading of 10 mol %, achieving e.e.s ≤ 99%. You *et al.* also tested the catalyst at 2.5 mol%, reporting no notable loss of sensitivity or reactivity, albeit with a somewhat longer reaction time.

$$R^1CHO \quad + \quad HPO(OMe)_2 \quad \xrightarrow[\text{m-xylene, -20 °C, N}_2]{\textbf{8 or 9} \text{ / Ti(O}^i\text{Pr)}_4 \text{ (2.5 mol\%)}} \quad$$
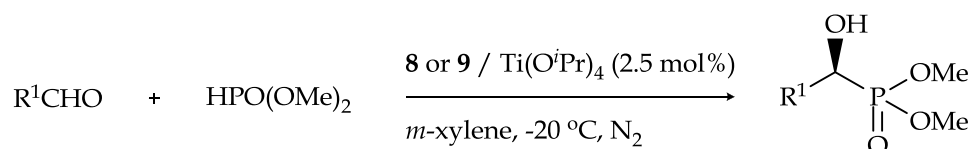
Entry	R¹	T (h)	Yield (%)[a]	e.e. (%)[b]
1	Ph	6	92	94
2	3-MeC6H4	8	90	95
3	4-MeC6H4	8	92	94
4	2-MeOC6H4	8	95 (82)[c]	96 (>99)[c]
5	2-ClC6H4	4	99	90
6	4-ClC6H4	8	87	90
7	4-NO2C6H4	4	99	90
8	1-naphthyl	6	97	>99
9	2-naphthyl	6	97	>99
10	PhCH2CH2	12	96	92
11	cyclohexyl	18	93	92[d]
12	nOct	12	98	94[d]
13	iPr	24	90	94[d]

Table 1.10 Summary of results from the hydrophosphonylation of aldehydes using **8** or **9** at 2.5 mol% under an inert atmosphere. [a] Yield of isolated product based on 1.0 mmol of aldehyde. [b] Enantiomeric ratio was determined by HPLC analysis on a chiral stationary phase. [c] After recrystallisation from n-hexane/iPrOH 4:1. [d] After conversion of the product into the corresponding benzoate. [50]

1.14 Hybrid-ligand systems

In the last few years there has been increasing interest in the hydrophosphonylation of aldehydes, incorporating salcyen, salalen and binaphthol frameworks. In 2005 Katsuki *et al.* first introduced the concept of a hybrid salen/salan (salalen) framework for the application of catalysing the hydrophosphonylation of aldehydes.[51]
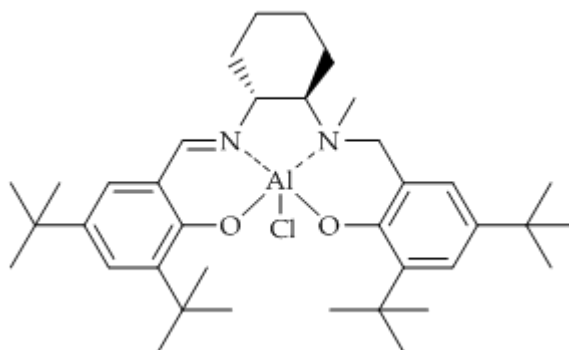
Figure 1.40 Aluminium salalen complex **10**. [51]

The X-ray diffraction analysis of Figure 1.19 showed that the complex had a unique structure, different to those seen in Al(salen) complexes.
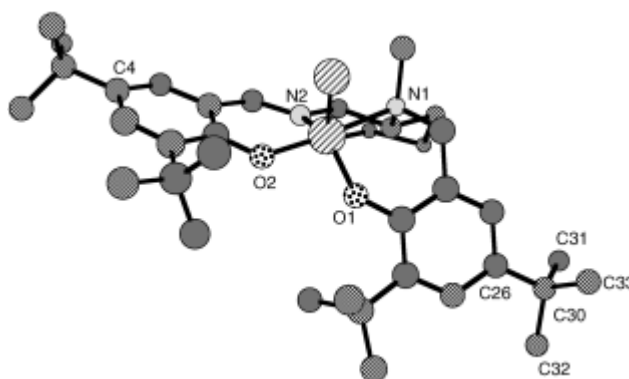
Figure 1.41 X-ray molecular structure of **10**. Hydrogen atoms have been omitted for clarity. [52]

The structure adopted a distorted trigonal-bipyramidal configuration and the absolute configuration of the coordinated tertiary amine was *S*.[52] The chiral ligand adopts a *cis-β*-like structure and the *N*-methyl group can be located in the middle of the ligand, *cis* to the chlorine atom, which under catalytic conditions would be replaced by a substrate (*e.g.* an aldehyde).[52]   Katsuki attributed the efficacy of complex **10** to its trigonal bipyramidal structure, thus creating a unique asymmetric reaction site which allows *cis* binding of reagents that leads to increased stereoselectivity.[51]

Katsuki investigated the asymmetric hydrophosphonylation of benzaldehyde with dimethyl-H-phosphonate at room temperature under various conditions (Table 1.11).[51]
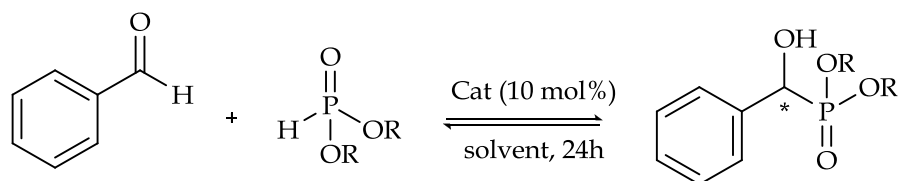
Entry	R	Solvent	T (°C)	Yield (%) [a]	e.e. (%) [b]	Config [c]
1	Me	THF	RT	92	73	S
2	Et	THF	RT	96	70	
3	Ph	THF	RT	87	17	
4	Me	Et$_2$O	RT	97	68	S
5	Me	iPr$_2$O	RT	94	79	S
6	Me	THF	0	91	87	S
7	Me	iPr$_2$O	0	94	89	S
8[d]	Me	THF	-15	87	90	S
9[d]	Me	iPr$_2$O	-15	80	81-90	S

Table 1.11 Asymmetric hydrophosphonylation of benzaldehyde. [a] Yield isolated product. [b] Determined by HPLC analysis using a chiral stationary phase column (Daicel Chiralpak AS-H; hexane/iPrOH 4:1). [c] Determined by chiroptical comparison. [d] The reaction was carried out for 48 h. Cat = Aluminium salalencomplex **10**. [52]

The asymmetric hydrophosphonylation of benzaldehyde reaction as shown in Table 1.11 afforded good yields and enantioselectivities with THF as solvent and a temperature of -15 °C being optimal. With this in mind, a variety of aromatic and aliphatic aldehydes were tested.
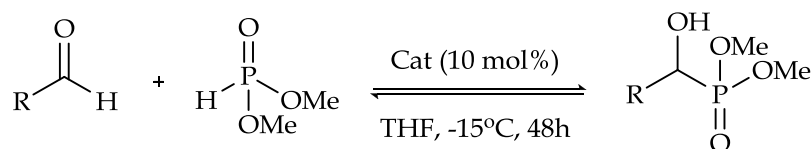
Entry	R	Yield (%)[a]	e.e. (%)	Config
1	p-O$_2$NC$_6$H$_4$	95	94[b]	S[c]
2	p-ClC$_6$H$_4$	88	88[b]	S[c]
3	p-MeOC$_6$H$_4$	87	81[b]	S[c]
4	o-ClC$_6$H$_4$	96	91[b]	-
5	(E)-PhCH=CH	77	83[b]	S[c]
6	PhCH$_2$CH$_2$	94	91[b]	-
7	(CH$_3$)$_2$CH	89	89[d]	-
8	CH$_3$CH$_2$	61	89[d]	S[e]

Table 1.12 Asymmetric hydrophosphonylation of various aldehydes. [a] Yield isolated product. [b] Determined by HPLC analysis using a chiral stationary phase column (Daicel Chiralpak AS-H; hexane/iPrOH 7:3). [c] Determined by chiroptical comparison. [d] Determined by HPLC analysis using a chiral stationary phase column (Daicel Chiralpak AS-H; hexane/iPrOH 9:1) after conversion of the product into the corresponding benzoate. [e] Determined by chiroptical comparison. Cat = Aluminium salalencomplex **10**. [52]

The results again afforded good yields and enantioselectivities for both aromatic and aliphatic aldehydes. By 2007 Katsuki *et al.* had moved onto exploiting and combining the excellence of a salcyen Schiff base framework, removing the cyclohexyl ring and combining it with a binaphthyl group as previously investigated by Shibuya [32] and Shibasaki [53], again forming a hybrid type aluminium binaphthyl Schiff base complex.

This new hybrid complex was screened as a catalyst for the PA reaction of DMHP with a range of substituted aldehydes as summarised in Table 1.13. Initial studies of the hydrophosphonylation of *p*-chlorobenzaldehyde with DMHP showed that by using a catalyst bearing a *tert*-butyl and bromo group (Figure 1.21) the reaction was catalysed more efficiently, achieving e.e.s of 84%. Bearing this in mind, Katsuki undertook a variety of reactions using this catalyst, Figure 1.21.
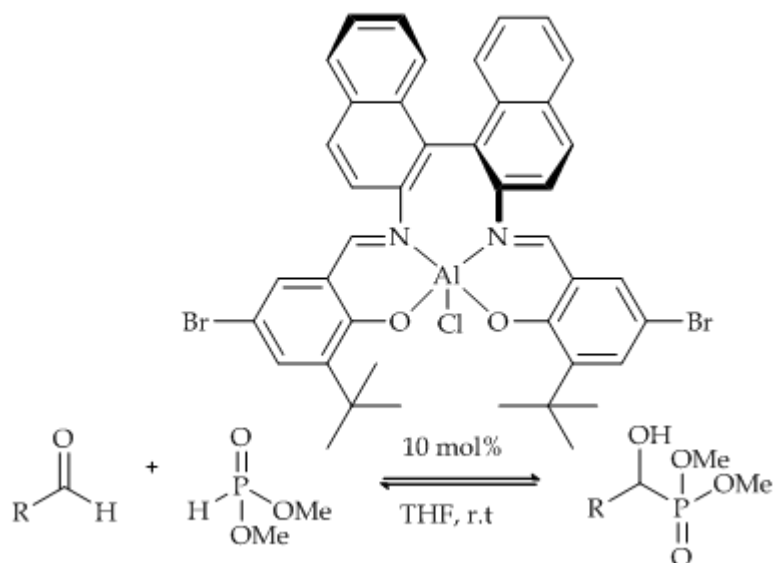
Figure 1.42 Asymmetric catalysis of the hydrophosphonylation of aldehydes using an aluminium binaphthyl Schiff base complex (11) as a catalyst.[54]

Entry	R in RCHO	Time (d)	Yield (%)	e.e. (%)	Config.[b]
1	Ph	5	62	79[c]	R
2	p-FC$_6$H$_4$	5	69	82[c]	
3	p-MeOC$_6$H$_4$	2	55	79[c]	
4	p-MeC$_6$H$_4$	2	82	80[c]	R
5	o-FC$_6$H$_4$	2	69	80[c]	R
6	o-MeC$_6$H$_4$	2	79	75[c]	
7	PhCH$_2$CH$_2$	1	71	83[c]	
8	c-Hex	1	86	86[d]	
9	n-Hex	2	79	86[d]	
10	(E)-PhCH=CH	2	82	64[c]	R

Table 1.13 Asymmetric catalysis of the hydrophosphonylation of aldehydes using an aluminium binaphthyl Schiff base complex **11** [a] All reactions were carried out at r.t. with a 1:1.1:0.1 molar ratio of aldehyde:dimethyl–H-phosphonate :complex. [b] Absolute configuration was determined by chiroptical comparison with the published value. [c] Determined by HPLC analysis using chiral stationary phase column (Daicel Chiralpak AS-H; hexane-i-PrOH = 4:1). [d] Determined by HPLC analysis using chiral stationary phase column (Daicel Chiralpak AS-H; hexane-i-PrOH = 9:1) after benzoylation of the product. [54]

These preliminary results are very promising and they show that catalysts of this type can catalyse the hydrophosphonylation of aromatic and aliphatic aldehydes.[55] Although the mechanism is unknown the authors suggest that the *tert*-butyl substituent is crucial for the regulation of the transition-state structure.[54]

Recently Feng *et al.* reported a new tridentate Schiff base (Figure 1.43), derived from L-vicinal and 3,5-*tert*-butylsalicylaldehyde and reacted *in situ* with various aluminium(III) reagents (Table 1.10) to form the complexes needed to catalyse the asymmetric hydrophosphonylation. [55]

11a: R^1 = ^tBu, R^2 = ^tBu
11b: R^1 = H, R^2 = H
11c: R^1 = H, R^2 = ^tBu
11d: R^1 = H, R^2 = NO_2
11e: R^1 = Ad, R^2 = ^tBu
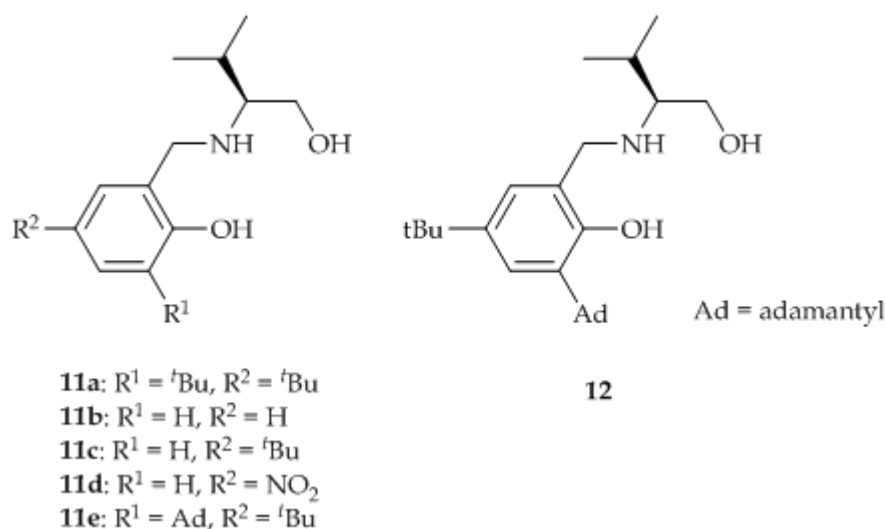
Figure 1.22 Typical chiral ligands used by Feng *et al*. [55]

A series of aromatic and aliphatic aldehydes were tested under optimised conditions, affording excellent yields and enantioselectivities of up to 97%. [55]
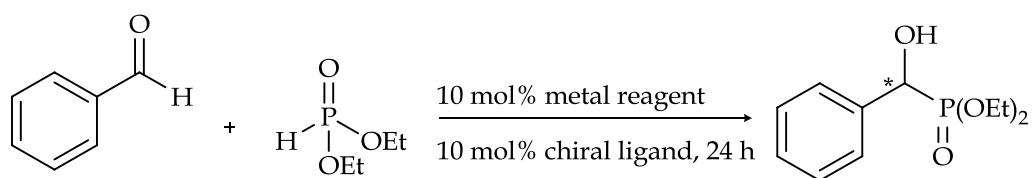
Entry [a]	Al source	L	Solvent	T (°C)	Yield (%) [b]	e.e. (%) [c]
1	Et$_2$AlCl	11a	THF	0	88	86 (S)
2	Al(OiPr)$_3$	11a	THF	0	50	30 (R)
3	AlEt$_3$	11a	THF	0	60	0
4	Et$_2$AlCl	11b	THF	0	68	60 (S)
5	Et$_2$AlCl	11c	THF	0	71	73 (S)
6	Et$_2$AlCl	11d	THF	0	48	43 (S)
7	Et$_2$AlCl	11e	THF	0	81	86 (S)
8	Et$_2$AlCl	12	THF	0	30	35 (R)
9	Et$_2$AlCl	11a	CH$_2$Cl$_2$	0	59	92 (S)
10	Et$_2$AlCl	11e	CH$_2$Cl$_2$	0	53	94 (S)
11	Et$_2$AlCl	11e	CH$_2$Cl$_2$	-20	36	97 (S)
12 [d]	Et$_2$AlCl	11e	CH$_2$Cl$_2$	-15	80	96 (S)[e]

Table 1.14 Summary of results for the asymmetric hydrophosphonylation of benzaldehyde with diethyl-H-phosphonate under the indicated condition. [a] All reactions carried out under nitrogen: diethyl-H-phosphonate (0.3 mmol), benzaldehyde (0.25 mmol) in 1.0 ml solvent. [b] Yield of isolated product. [c] Determined by HPLC analysis. [d] The catalyst was prepared in situ in 0.4 ml CH$_2$Cl$_2$. [e] The R product with the same e.e. value could be obtained by changing the absolute configuration of **11e** to R. [55]

Feng was also interested in the use of bifunctional chiral Al(III) complexes as a way of catalysing the asymmetric hydrophosphonylation of aldehydes. [56] Their ability to attach both electrophilic and nucleophilic substrates to the chiral catalyst makes them a good candidate for hydrophosphonylation. Feng developed a BINOL-based titanium (IV) complex for the asymmetric cyano-ethoxycarbonylation of aldehydes resulting in good yields and enantioselectivities. [56] With this success they developed a bifunctional chiral aluminium(III) complex of a BINOL derivative bearing a *tert*-amine group at the 3, 3′ positions of the BINOL moiety. [55]
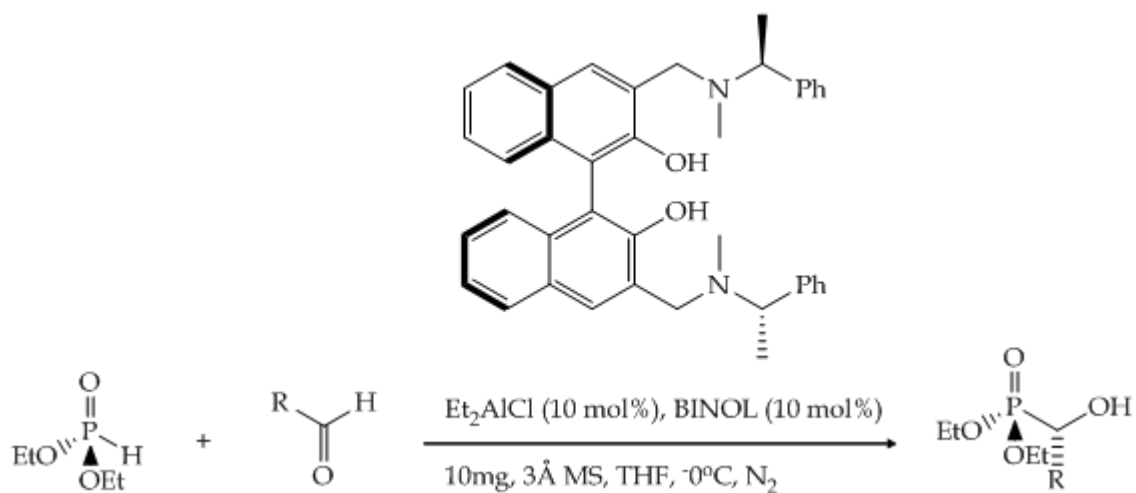
Scheme 1.23 Asymmetric hydrophosphonylation of aldehydes catalysed by Al(III) BINOL complex. [55]

Entry [a]	Aldehyde	Time (h)	Yield (%) [b]	e.e. (%) [c]
1	Benzaldehyde	24	88	75 (S)
2	4-Methoxybenzaldehyde	40	74	87 (R)
3	3-Methoxybenzaldehyde	40	71	81
4	Benzo[*d*][1,3]dioxole-5-carbaldehyde	24	73	83 [d]
5	4-Methylbenzaldehyde	40	91	83 (S)
6	4-Chlorobenzaldehyde	40	88	65 (S)
7	4-Fluorobenzaldehyde	40	87	62
8	4-Bitrobenzaldehyde	20	88	67
9	Biphenyl-4-carbaldehyde	40	85	82
10	1-Naphthaldehyde	20	90	78 (S) [e]
11	2-Naphthaldehyde	20	82	74
12	(*E*)-Cinnamaldehyde	20	86	63 (S)
13	Thiophene-2-carbaldehyde	30	75	45 (S)
14	3-Phenylpropanal	30	99	75
15	Pentanal	20	85	77 [f]

Table 1.15 Summary of results for the asymmetric hydrophosphonylation of aldehydes using Al(III) BINOL complex as catalyst. [a] The reactions were carried out under nitrogen, aldehyde (0.25 mmol), and diethyl-H-phosphonate (0.325 mmol) in 0.5 ml THF. [b] Isolated yield. [c] Unless indicated, the e.e. was determined by HPLC on Chiral AS-H column analysis, the absolute configuration of the major product was *S* compared with the reported value of optical rotation. [d] Determined by Chiral OD-H column analysis. [e] Determined by Chiral AD-H column analysis. [f] Determined by HPLC analysis after conversion of the product into the corresponding benzoate. [55]

The authors proposed that the reaction proceeded as shown in **Error! Reference source not found.**. The Al(III) centre of complex (**I**) acts as a Lewis acid, which serves to activate the aldehyde to afford species (**II**). Once the aldehyde is bound to the metal it is then held in place by a weaker, secondary interaction involving hydrogen bonding between the aldehyde hydrogen and the aluminium-bound chlorine atom. The *tert*-amine moiety of the complex acts as a Lewis base, activating DEHP through hydrogen

bonding. Nucleophilic addition of the phosphite to the aldehyde affords the desired α-hydroxyphosphonate and at the same time leads to regeneration of the catalyst. [57]
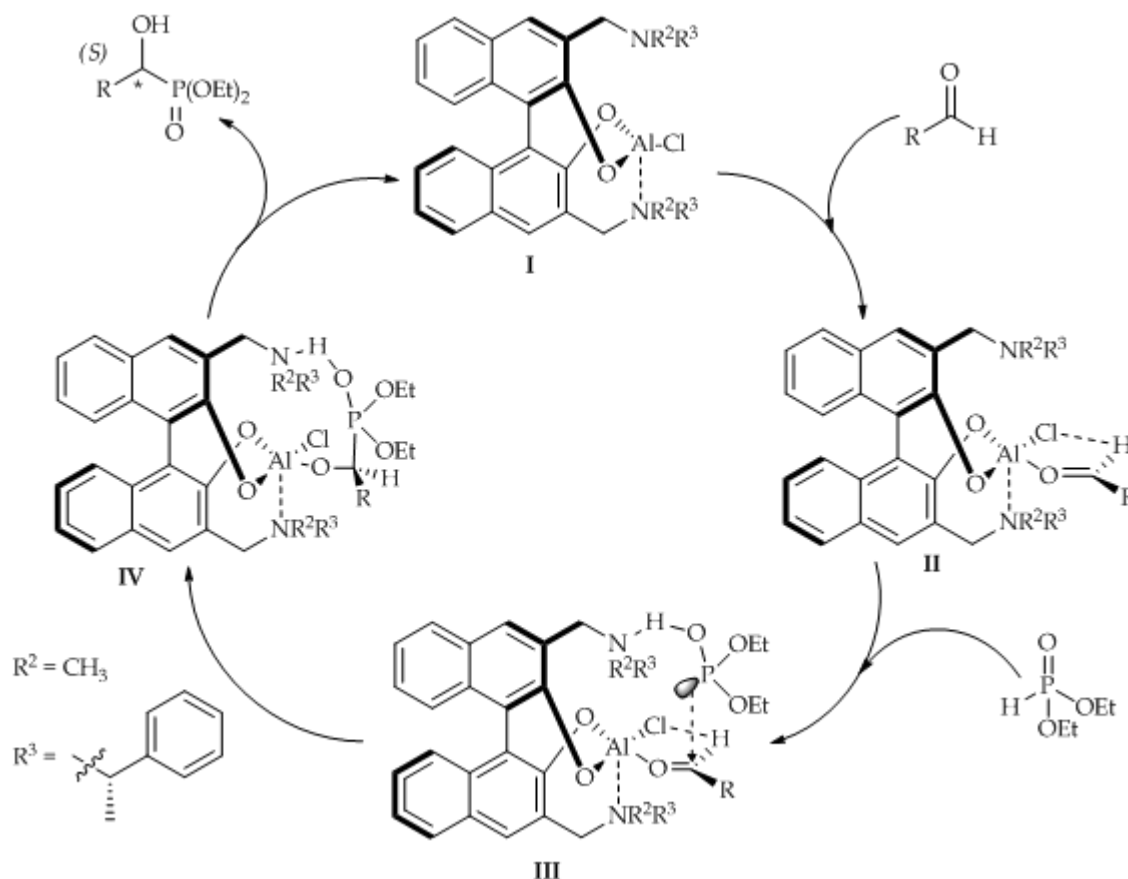
Scheme 1.24 Proposed catalytic cycle for the asymmetric hydrophosphonylation of aldehyde. [57]

1.15 Research Aims and Objectives

Over the last two decades there has been considerable interest in asymmetric, catalytic variants of the PA reaction. A number of systems thus far described show promising results, however, the described systems need high catalyst loadings, an inert atmosphere as well as low temperatures, which can greatly hinder the reaction time. From these previous studies it is possible to delineate the key features needed to build an efficient catalyst for the PA reaction. The most important features are the presence of Lewis acid and Lewis basic sites and a source of chirality. Of the systems already

discussed, the aluminium salcyan complexes have been of most interest as they can catalyse the PA reaction to high yields with moderate e.e.s and have shown themselves to be tuneable, re-usable and stable to air and water.

It is with this knowledge that this thesis seeks to progress by addressing two key issues concerning the phospho-aldol reaction:

(i)   To better understand the mechanism of the asymmetric PA reaction catalysed by salcyan complexes of aluminium using computational techniques such as HyperChem and Gaussian

(ii)   To use this information to prepare new salcyan and related complexes, which   should be better placed to deliver greater stereoselectivities in the asymmetric PA process.

Over the next five chapters is described work on the synthesis and characterisation of N_4-salcyan ligands with the aim of isolating new aluminium complexes for PA catalysis (Chapter 2) and two methods for the preparation of bifunctional salcyan complexes of aluminium for a similar objective (Chapters 4). The second half of this thesis is dedicated to computational modelling studies carried out on a library of X-ray crystallographic data (Chapter 3). The main aims of these computational studies are: (i) to bench-mark lower levels of modelling, specifically semi-empirical modelling using the Hyperchem 7.0 package, against higher electronic structure methods such as DFT. Given the large atom numbers involved in most of the systems of interest, being able to have confidence in semi-empirical analyses is very valuable in building a simple molecular modelling picture of potentially interesting systems to synthesise; and (ii) to better understand the reaction mechanism of the phospho-aldol reaction.

Appendices: All X-ray crystallographic data are included.

1.16 References

[1]   D. Gani, J. Wilkie, *Chem. Soc. Rev.*, **1995**, *24*, 55.

[2]   M. J. Cain, A. Cawley, V. Sum, D. Brown, M. Thornton-Pett, T. P. Kee, *Inorg. Chim. Acta.*, **2003**, *345*, 154.

[3]   M. Jiang, S. Dalgarno, C. A. Kilner, M. A. Halcrow, T. P. Kee, *Polyhedron*, **2001**, *20*, 2151.

[4]   (a) V. S. Abramov, *Doklady Akademii Nauk SSR.*, **1954**, *95*, 991.

(b) V. Sum, T. P. Kee, *J. Chem. Soc., Perkin Tans.* **1993**, *1*, 2701.

(c) N. Greene, T. P. Kee, *Synth, Commun.*, **1993**, *23*, 1651.

(d) I. F. Pickersgill, P. G. Devitt, T. P. Kee, *Synth. Commun.*, **1993**, *23*, 1643.

(e) P.G. Devitt, T. P. Kee, *J. Chem. Soc. Perkins Tans.*, **1994,** *1*, 3169.

(f) V. Sum, C. A. Baird, T. P. Kee, M. Thornton-Pett, *J. Chem. Soc, Perkins Trans.*, **1994**, *1*, 3183.

(g) M. J. Cain, C. A. Baird, T. P. Kee, *Tetrahedron Lett.*, **1994**, *35*, 8671.

(h) P. G. Devitt, T. P. Kee, *Tetrahedron Lett.*, **1995**, *51*, 10987.

[5]   (a) C. A. Wurtz, *Bull. Soc. Chim. Fr.*, **1872**, *17*, 436;

(b) C. A. Wurtz, J. Prakt, *Chemie.*, **1872**, *5*, 457.

(c) C. A. Wurtz, *Comp. Rend.*, **1872**, *74*, 361.

[6]   T. D. Nixon, S. Dalgarno, C. V. Ward, M. Jiang, M. A. Halcrow, C. Kilner, M. Thornton-Pett, T. P. Kee, *C. R. Chimie.*, **2004**, *7*, 809.

[7]   R. Engel, *Chem. Rev.*, **1977**, *77*, 349.

[8]   D. V. Patel, K. Reilly-Gauvin, D. E. Ryono, *Tet. Lett.*, **1990**, *31*, 5587.

[9]   B. Stowasser, K. H. Budt, L. Jian-Qi, A. Peyman, D. Ruppert, *Tetrahedron Lett.*, **1992**, *33*, 6625.

[10]   R. L. Hilderbrand, T. O. Henderson, T. Glonek, T. C. Myers, *Biochemistry.*, **1973**, *12*, 4756.

[11]   J. P. Duxbury, J. N. D. Wane, R. Mushtaq, C. Ward, M. Thornton-Pett, M. Jiang, R. Greatrex, T. P. Kee, *Organometallics.*, **2000**, *19*, 4445.

[12]   D. Barford, Z. Jia, N. K. Tonks, *Nature Structural Biology.*, **1995**, *2*, 1043.

[13]   Y-L. Zhang, Z-J. Yao, M. Sarmiento, L. Wu, T. R. Burke. Jr, *J. Biol. Chem.*, **2000**, *275*, 34205.

[14]   T. R. Burke. Jr, Z-Y. Zhang, *Biopolymers (peptide science).*, **1998**, *47*, 225.

[15]   T. R. Burke. Jr, B. Ye, X. Yan, S. Wang, Z. Jia, L. Chen, Z-Y. Zhang, D. Barford, *Biochem.*, **1996**, *35*, 15989.

[16]   F. A. Al-Obeidi, J. J. Wu, K. S. Lam, *Biopolymers (peptide science).*, **1998**, *47*, 197.

[17]   T. R. Burke. Jr, M. S. Smyth, M. Nomizu, A. Otaka, P. P. Roller, *J. Org. Chem.*, **1993**, *58*, 1336.

[18]   G. R. J. Thatcher, A. S Campbell, *J. Org. Chem.*, **1993**, *58*, 2272.

[19]   T. Yokomatsu, T. Yamagishi, K. Matsumoto, S. Shibuya, *Tet. Lett.,* **1996**, *52*, 11725.

[20]   Z. J. Yao, B. Ye, X. W. Wu, S. Wang, Z. Y. Zhang, T. R. Burke. Jr, *Bio. Med. Chem.*, **1998**, *6*, 1799.

[21]   J. Clayden, N. Greeves, S. Warren, P. Wothers, *Organic Chemistry.*, **2001**, *1st Ed*, p 689, Oxford.

[22]   T. P. Kee, T. D. Nixon, *Topics Curr. Chem.*, **2003**, *223*, 46.

[23]   M. Shibasaki, H. Sasai, T. Arai, *Angew. Chem. Int. Ed.,* **1997**, *36*, 1236.

[24]   C. V. Ward, M. Jiang, T. P. Kee, *Tet. Lett.,* **2000**, *41*, 6181.

[25]   M. D. Groaning, B. J. Rowe, C. D. Spilling, *Tet. Lett.,* **1992**, *33*, 4137.

[26]   H. Wynberg, A. A. Smaardijk, *Tetrahedron Lett.,* **1983**, *24*, 5899.

[27]   A. A. Smaardijk, S. Noorda, F. van Bolhuis, H. Wynberg, *Tet. Lett.*, **1985**, *26*, 493.

[28]   A. Combes, *C. R. I'Academie Science.*, Ser II Univers. **1889**, *108*, 1252.

[29]   W. Zhang, J. L. Loebach, S. R. Wilson, E. N. Jacobsen, *J. Am. Chem. Soc.*, **1990**, *112*, 2801.

[30]   G. Soto-Garrido, V. Salas-Reyes, *Transition Metal Chemistry.*, **2000**, *25*, 192.

[31]   R. Sanzenbacher, A. Böttcher, H. Elias, M. Hüber, W. Haase, J. Glerup, T. B. Jensen, M. Neuberger, M. Zehnder, J. Springborg, C. E. Olsen, *Inorg. Chem.*, **1996**, *35*, 7493.

[32] T. Yokomatsu, T. Yamagishi, S. Shibuya, *Tetrahedron: Asymm.*, **1993**, *4*, 1779.

[33]   Y. Belokon, N. Ikonnikov, M. Moscalenko, M. North, S. Orlova, V. Tararov, L. Yashkina, *Tet: Asymm.*, **1996**, *7*, 851.

[34]   T. Yokomatsu, T. Yamagishi, S. Shibuya, *Tetrahedron: Asymm.,* **1993**, *4*, 1783.

[35]   M. D. Groaning, B. J. Rowe, C. D. Spilling, *Tet. Letts.*, **1998**, *39*, 5483.

[36]   N. P. Rath, C. D. Spilling, *Tet. Lets.*, **1994**, *35*, 227.

[37]   H. Sasai, T. Suzuki, N. Itoh, K. Tanaka, T. Date, K. Okamura, M. Shibasaki, *J. Am. Chem. Soc.*, **1993**, *115*, 10372.

[38]   T. Morita, T. Arai, H. Sasai, M. Shibasaki, *Tetrahedron: Asymmetry.,* **1998**, *9*, 1445.

[39]   T. Arai, M. Bougauchi, H. Sasai, M. Shibasaki, *J. Org. Chem.*, **1996**, *61*, 2926.

[40]   A. Takayoshi, Y. M. A. Yamada, N. Yamamoto, H. Sasai, M. Shibasaki, *Chemistry a European Journal.,* **1996**, *2*, 1368.

[41]   H. Sasai, T. Arai, S. Wananbe, M. Shibasaki, *Catalysis Today.,* **2000**, *62*, 17.

[42]   H. Sasai, M. Bougauchi, T. Arai, M. Shibasaki, *Tet. Lett.,* **1997**, *38*, 2717.

[43]   D. A. Atwood, *Coord. Chem. Rev.,* **1997**, *165*, 267.

[44]   J. March *Advanced Organic Chemistry.*, **1992**, *4th Ed*, Wiley Interscience, p 897, Canada.

[45]   J. F. Larrow, E. N. Jacobsen, Y. Gao, Y. Hong, X. Nie, C. H. Zepp, *J. Org. Chem.*, **1994**, *59*, 1939.

[46]   J. P. Duxbury, A. Cawley. M. Thornton-Pett, L. Wantz, J. N. D. Warne, R. G. Greatrex, D. Brown, T. P. Kee, *Tet. Lett.,* **1999**, *40*, 4403.

[47]   E. F. DiMauro, M. C. Kozlowski, *Org. Letts.,* **2001**, *3*, 3053.

[48]   E. F. DiMauro, M. C. Kozlowski, *Org. Letts.,* **2002**, *4*, 3781.

[49]   A. V. Davies, *Ph.D.*, University of Leeds, **2005**.

[50]   F. Yang, D. Zhao, J. Lan, P. Xi, L. Yang, S. Xiang, J. You, *Angew. Chem. Int. Ed.,* **2008**, *47*, 5646.

[51]   B. Saito, T. Katsuki, *Angew. Chemie. Int. Ed.,* **2005,** *44*, 4600.

[52]   B. Saito, H. Egami, T. Katsuki, *J. Am. Chem. Soc.,* **2007**, *129*, 1978.

[53]   T. Arai, M. Bougauchi, S. Sasai, M. Shibasaki, *J. Org. Chem.,* **1996,** *61*, 2926.

[54]   K. Ito, H, Tsutsumi, M. Setoyama, B. Saito, T. Katsuki, *Synlett*., **2007**, *12*, 1960.

[55]   X. Zhou, X. Liu, X. Yang, D. Shang, J. Xin, X. Feng, *Angew. Chem. Int. Ed.,* **2008**, *47*, 392.

[56]   S. Gou, X. Liu, X. X. Zhou, X. Feng, *Terahedron.,* **2007**, *63*, 7935.

[57]   S. Gou, X. Zhou, J. Wang, X Liu, X. Feng, *Tetrahedron.,* **2008**, *64*, 2864.

Chapter 2

N4-Salcyan ligand frameworks. Syntheses,

characterisation and structures

2.1 Introduction

In this chapter are described the syntheses of ligand frameworks based on salcyen and salcyan compounds containing *trans*-1,2-diaminocyclohexane backbones, with an N$_4$ instead of an N$_2$O$_2$ binding motif. Phenolic N$_2$O$_2$ type salcyen and salcyan ligands may not be able to provide steric hindrance close to the metal centre as substitution of the ligand is remote. Replacing the oxygen with a hetero-atom that has the ability to bind to more groups will allow the addition of steric pressure in closer proximity to the metal centre, which could potentially cause stereo induction in the phospho-aldol reaction.

2.2 Current literature about N$_4$-derivatives

The search for new ligands for asymmetric catalysis is of continuous interest. The ligands should be easy to prepare from simple and accessible starting materials. [1] Reports have shown that the use of nitrogen-containing ligands is suited to many types of homogeneous catalysis. [2], [3]

bis(Sulfonamide)-based ligands derived from (1*R*,2*R*)-*trans*-cyclohexanediamine have successfully been applied as catalysts for many asymmetric transformations, such as the Simmons-Smith reaction [4] and the addition of organozinc reagents to carbonyl compounds. [5], [6]
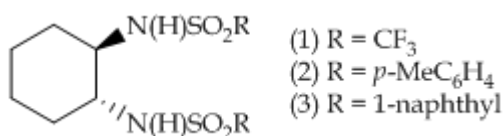
Figure 2.16 (1*R*,2*R*)-*trans*-cyclohexanediamine used as a derivative for bis(sulfonamide)-based ligands. [4], [5], [6]

The N_4-type salen ligands of the type mentioned in Figure 2.1 have been used with some degree of success in the asymmetric addition of diethylzinc to aldehydes as reported by König in 2003.[7] Schiff bases were synthesised in good yield from the condensation of (1R,2R)-*trans*-cyclohexanediamine and respective aldehydes in ethanol.

R = (a) p-MeC$_6$H$_4$, (b) C$_6$H$_5$, (c) p-MeOC$_6$H$_4$, (d) p-NO$_2$C$_6$H$_4$, (e) p-ClC$_6$H$_4$, (f) 2,4,6-Cl$_3$C$_6$H$_4$
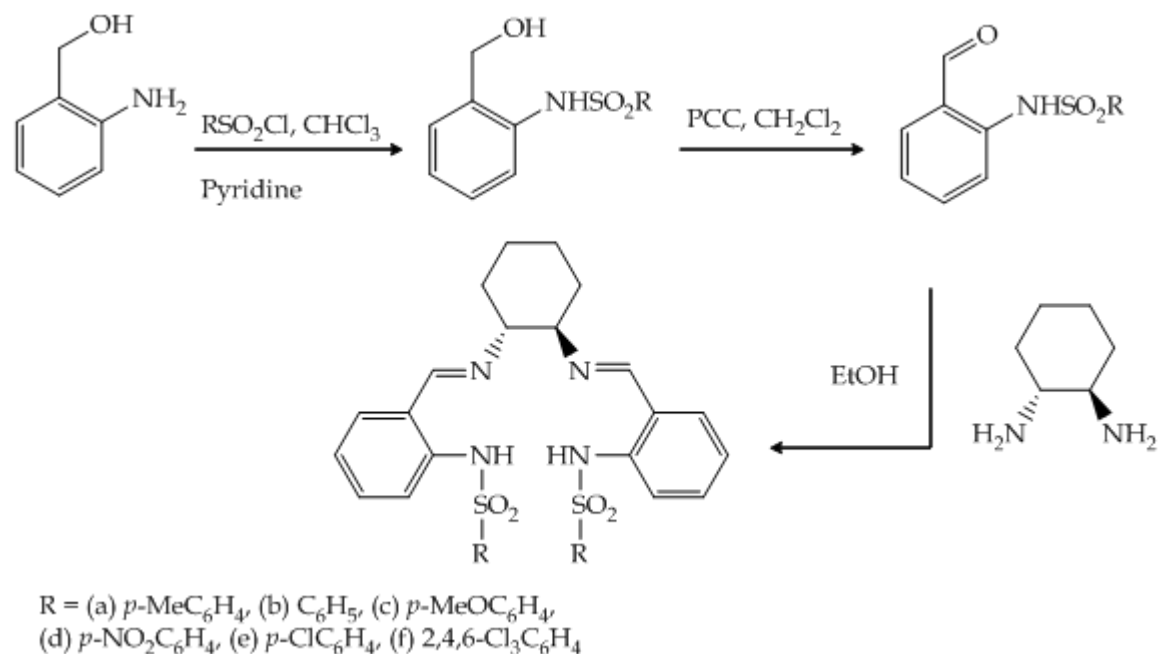
Scheme 2.20 General procedure for the synthesis of sulfonamide Schiff bases derived from (1R,2R)-*trans*-cyclohexanediamine. [7]

The sulfonamide derivatives (5 mol %) (Scheme 2.1) were screened in the asymmetric alkylation of benzaldehyde with diethylzinc (2.5 equivalents) at room temperature over 24 h. [7] A 100% conversion and e.e. of 74% were achieved. [7]
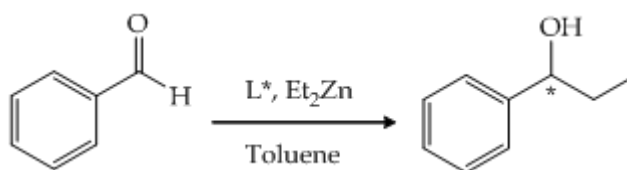
Scheme 2.21 Asymmetric alkylation of benzaldehyde with diethylzinc. [7]

In 2004 Lemaire designed a new series of N$_4$-Schiff bases containing amine or sulfonamide functionalities. Coupled with ruthenium catalysts the Schiff bases produced some interesting results in the asymmetric hydrogenation of acetophenone. [8] The Schiff bases are derived from *C$_2$*-symmetric dithioureas and diamines and complexed to rhodium, iridium and ruthenium. [8] An iridium diamine complex gave 1-phenylethanol in 63% e.e. when used in the asymmetric reduction of acetophenone. [9]
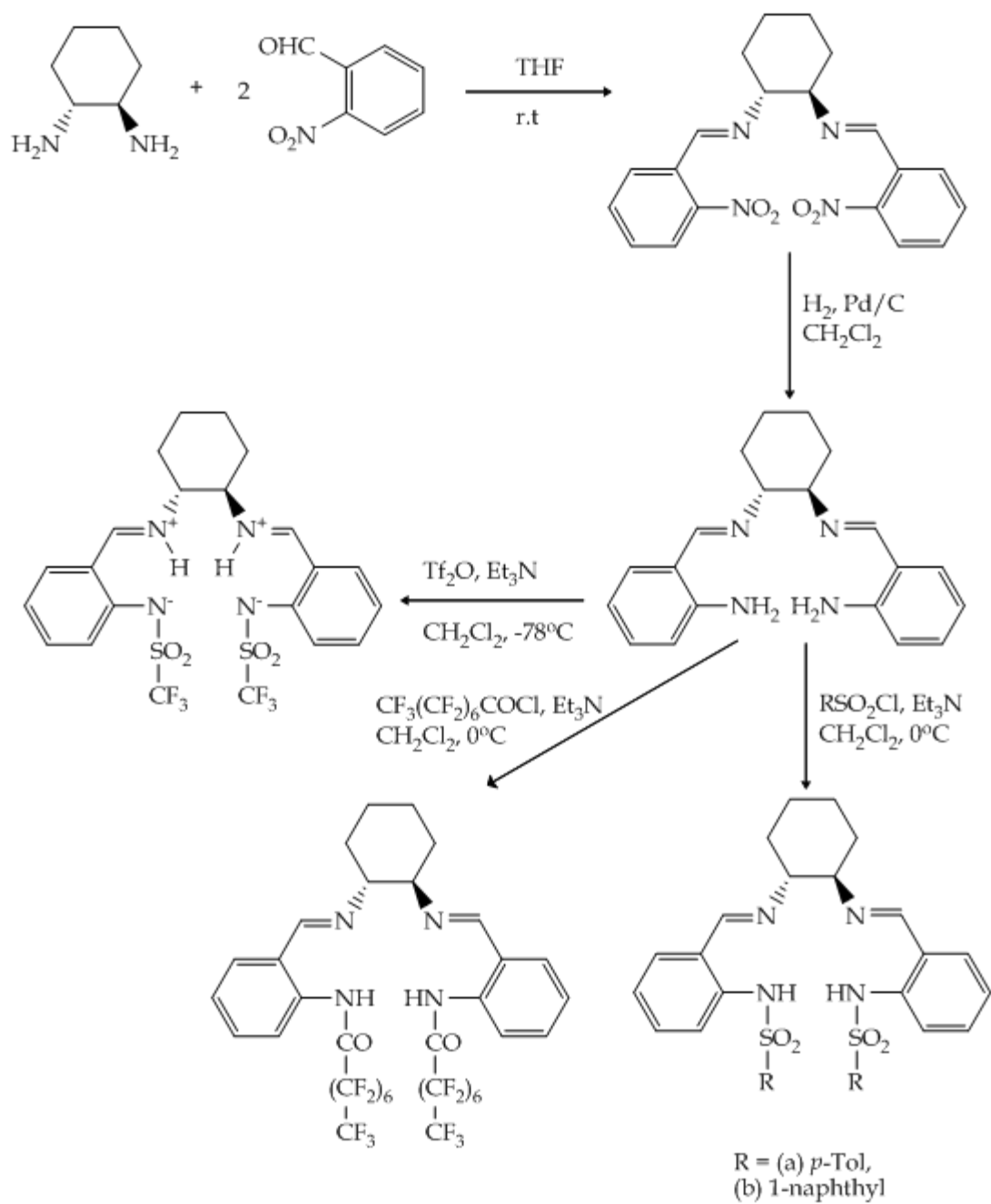
Scheme 2.22 Synthesis of N$_4$-Schiff bases. [9]

The interest in the synthesis of macrocyclic metal compounds with N$_4$ and N$_2$O$_2$ donor ligands is growing rapidly due to their unique structural properties and biological activities. [10]

More recently in 2009 Ho and Ravinder synthesised a series of N$_4$ donor macrocycles from *o*-phthaladehyde by a non-template route. [11]
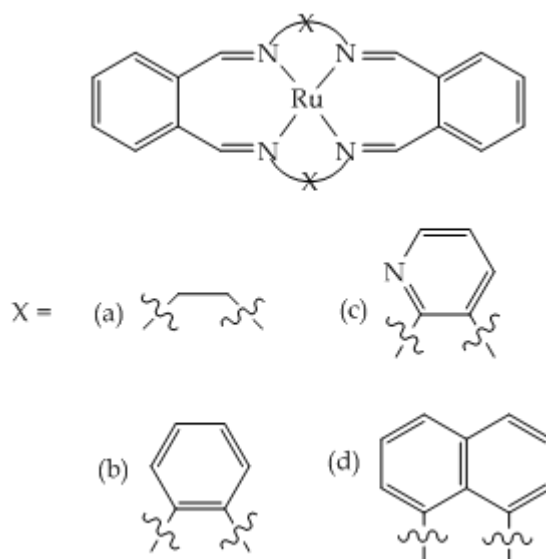
Figure 2.17 Structures of macrocyclic Ru(II) compounds. [11]

The N$_4$ donor macrocycles were then treated with [RuCl$_2$(DMSO)$_4$] to give neutral complexes of the type [RuCl$_2$(L)], where L is the tetradentate macrocyclic ligand. All of the compounds were screened for their antibacterial and antifungal activity. [11]

Reviewing the current literature on N$_4$ ligands it is clear to see that major studies have been carried out over the last decade with respect to their use as catalysts for asymmetric reactions. The literature thus described is by far no means exclusive, but it does however

pave the way for future investigations. However, with regards to N₄-Schiff bases being used as potential catalysts for the phospho-aldol reaction very little is known.

The remainder of this of this chapter will include a discussion of the synthetic pathways, characterisations and data comparisons for all N₄ compounds, starting with the resolution of the diamine, synthesis of the ligand substituents, followed by the building of the salcyen and resulting reduction to the salcyan frameworks and finishing with the attempts made to achieve aluminium bound N₄ complexes.

2.3 Resolution of *(R, R)-trans* -1, 2-diaminocyclohexane (1) [12]

The purpose of this report is to prepare salcyen and salcyan complexes of metals such as aluminium, and investigate their potential as catalysts for the PA reaction. With this background knowledge the first piece of synthetic chemistry on the project, resolution of a chiral diamine *via* the Jacobsen procedure was completed successfully. [12] The diamine product (**1**) has two chiral centres of which the stereochemistry is maintained throughout all manipulations.

(1)
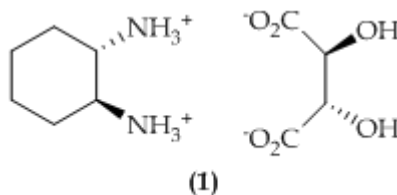
Figure 2.18 (R, R)–*trans*-1,2-diaminocyclohexane tartrate salt.

A mixture of *cis/trans*-1,2-diaminocyclohexane is added to a stirred mixture of L-(+)-tartaric acid in water, along with glacial acetic acid and the temperature allowed to reach

70 °C. A white precipitate forms which is collected after a series of vigorous stirring and cooling cycles, the final precipitate filtered, washed with water and methanol and vacuum dried. The tartrate salt was subsequently recrystallised from hot water (70 °C), to afford the product **(1)** in 53% yield, optical purity $[\alpha]_D$ = +12.5 (c = 4 g/dl H$_2$O); (Literature value; $[\alpha]_D$ = +12.5). [13]
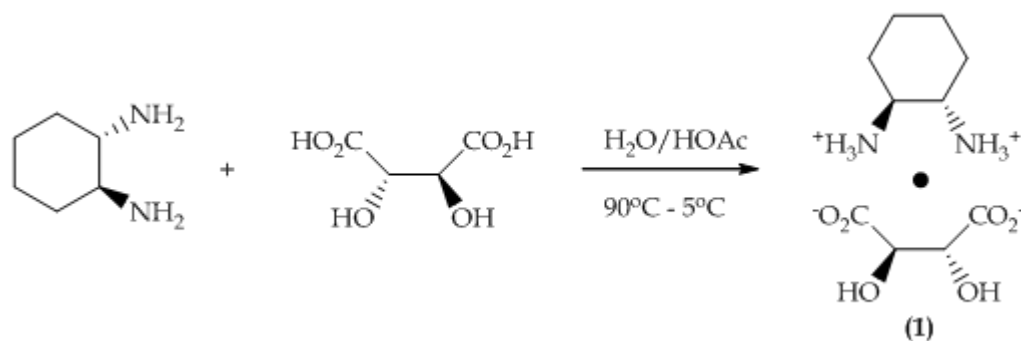
Scheme 2.23 Resolution of (R,R) – *trans*-1,2-diaminocyclohexane tartrate salt. [12]

Subsequently, four complexes were targeted for synthesis **(9-12)**.
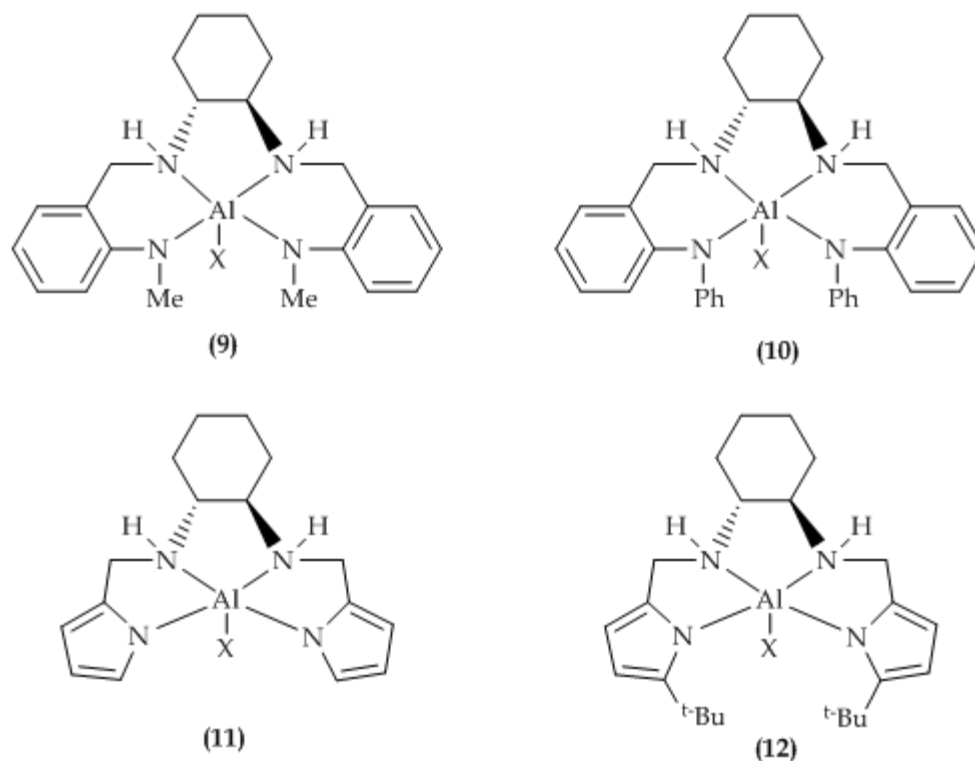
Figure 2.19 Four targeted salcyan aluminium complexes, (9-12) X = OH, Me or Cl.

2.4 Preparation of aldehydes

2.4.1 General synthesis of *N*-organo-aminobenzaldehyde (13-14) [3]
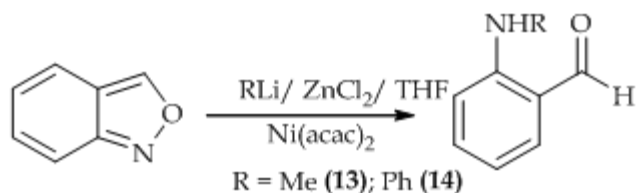
Scheme 2.24 General synthesis of N-organo-aminobenzaldehyde **(13)** and **(14)**. [3]

The organolithium starting material (methyl-lithium or phenyl-lithium) was added to a chilled slurry of zinc chloride in tetrahydrofuran followed by warming to room temperature with anthranil and the addition of a nickel catalyst. Following the addition of HCl, the crude products were purified by flash column chromatography with diethyl

ether: hexane (1:3 v/v) to afford either a yellow-orange oil **(13)** (59%) or bright yellow needle crystals **(14)** (74%).

The mechanism of this reaction has yet to be fully delineated however the consensus is that it proceeds in two stages. [3] Initial preparation of the organozinc chloride reagent followed by catalytic cleavage of the anthranil [N-O] bond and addition of an R-group onto the nitrogen atom. [4]

Microanalysis and mass spectrometric analysis of **(13)** and **(14)** were consistent with the desired product formation. Characteristic NMR resonances were observed for both **(13)** and **(14)**. A singlet resonance at δ^1H 9.86 ppm **(13)** and 9.95 ppm **(14)** can be assigned to the carbonyl hydrogens (Figure 2.5 and Figure 2.6) and a singlet resonance at δ^{13}C {^{1}H} 194.3 ppm **(13)** and 194.0 ppm **(14)** for the carbonyl carbon nuclei. Broad singlet resonances at δ^1H 8.28 ppm **(13)** and 10.05 ppm **(14)** are consistent with amine-bound hydrogen nuclei, with the higher chemical shift attributed to greater conjunction in **(14)** (Figure 2.6). In the aromatic region between δ^1H 6.73 to 7.49 ppm for compound **(13)**, the resonances observed were two doublets and two doublet of doublets (Figure 2.5). The aromatic region of compound **(14)** is rather more complex due to the presence of two aromatic rings (Figure 2.6).
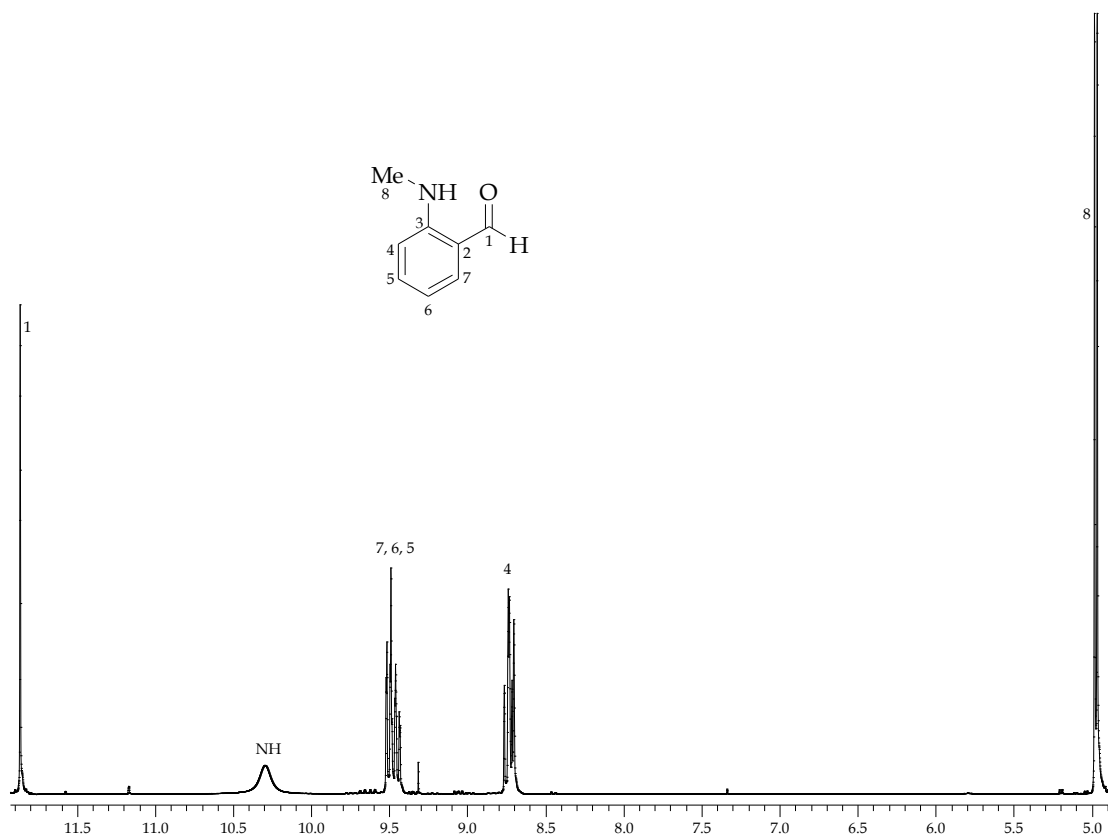
Figure 2.20 ^{1}H NMR of 2-methylamino benzaldehyde **(13)** CDCl$_3$, 298K, 300 MHz.
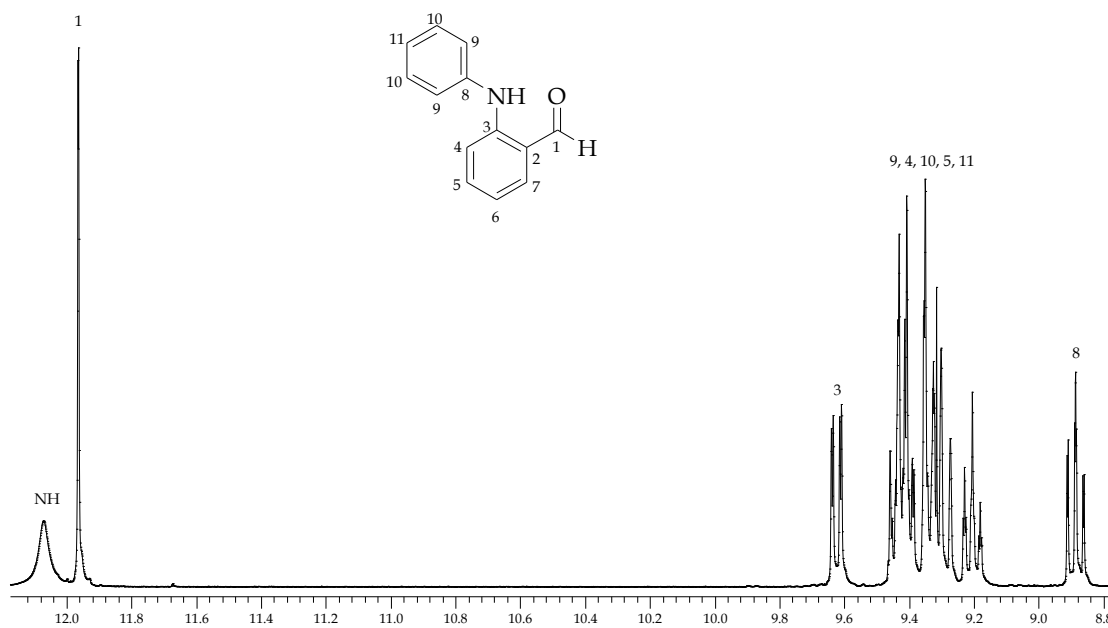
Figure 2.21 ^{1}H NMR of 2-phenylamino benzaldehyde **(14)** CDCl3, 298K, 300 MHz.

60

2.4.2 Single crystal X-ray analysis

2.4.2.1 Single crystal X-ray analysis of 2-phenylaminobenzaldehyde (14)
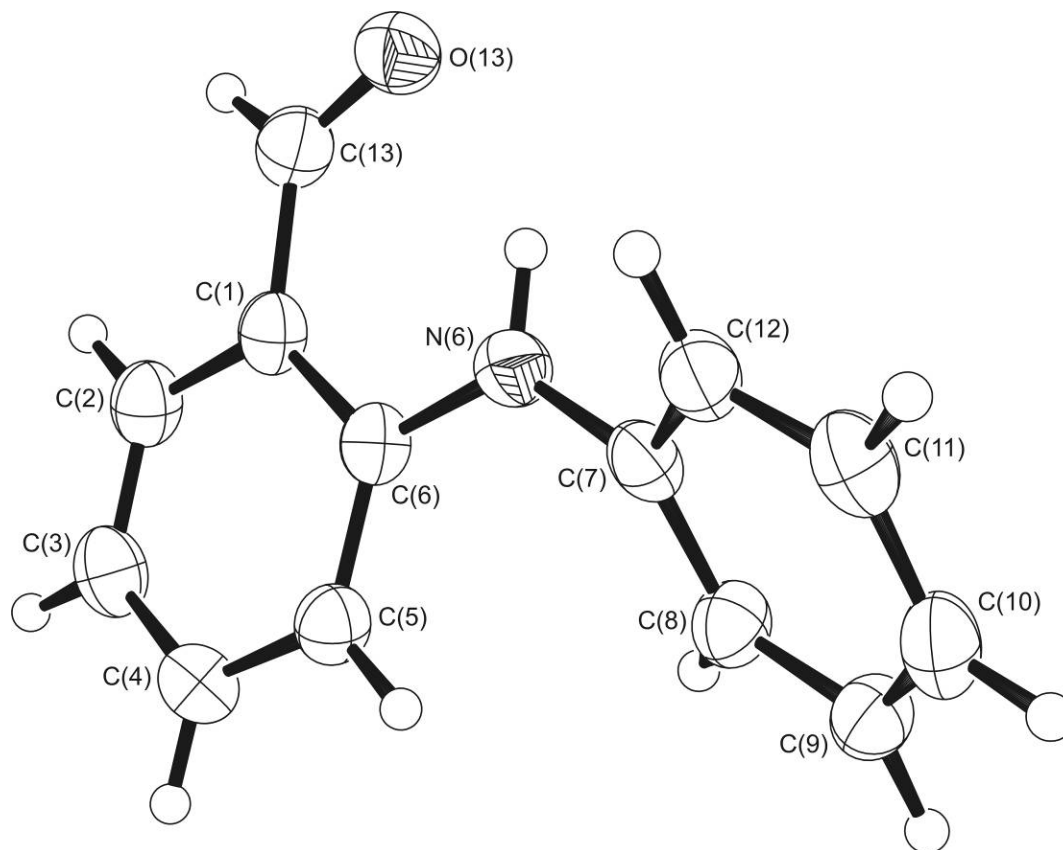
Figure 2.22 ORTEP plot of the crystallographically determined molecular structure of 2-phenylaminobenzaldehyde **(14).**

Slow recrystallisation from pentane afforded yellow prisms suitable for X-ray diffraction examination with full crystallographic data provided in the Appendix.   Angle measurements taken around N6 indicate that its geometry is trigonal planar, as shown in Table 2.7.

Interatomic Vectors	Angle / °
C(6)-N(6)-H	116.22
C(6)-N(6)-C(7)	127.63
C(7)-N(6)-H	116.15

Table 2.7 Selected interatomic vectors for 2-phenylaminobenzaldehyde **(14)**.

2.4.3 General synthesis of (*R,R*)-N,N'-bis-(2-R-amino-benzylidene)-*trans*-1,2-diaminocyclohexane (15-16)
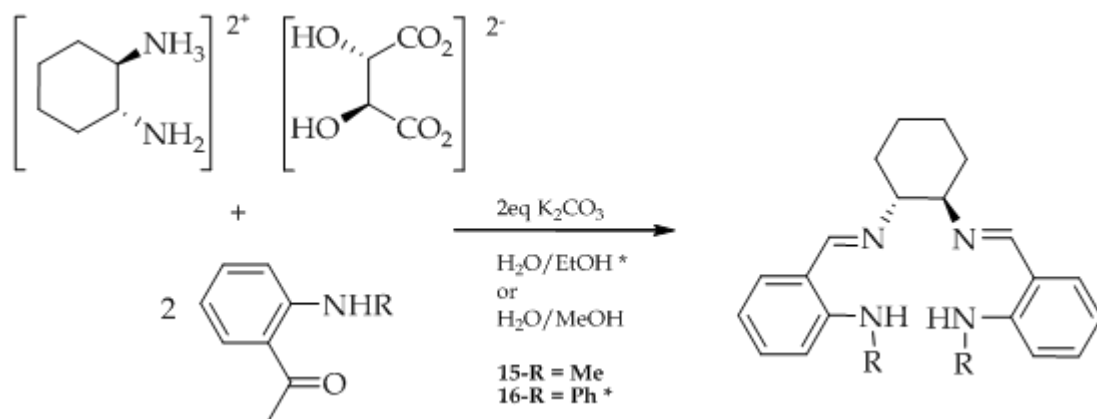
Scheme 2.25 General synthesis of N₄-type salcyen compounds **(15)** and **(16)**.

A modified procedure to that presented by Tommasino was used to synthesise the amino-benzaldehyde ligands. [9]   Tartrate salt **(1)** undergoes condensation with N-substituted aminobenzaldehydes in the presence of potassium carbonate in refluxing ethanol or methanol and water, as shown in Scheme 2.25.   Filtration of the cooled reaction slurry produces a yellow product that was washed with water to remove any impurities.   Crude **(15)** and **(16)** were recrystallised from either pentane or dichloromethane to afford either a yellow powder **(15)** (49%) or yellow crystals **(16)** (40%).   The mechanism by which this reaction takes place is thought to be the same as that for the formation of N₂O₂ salcyen compounds. [9]
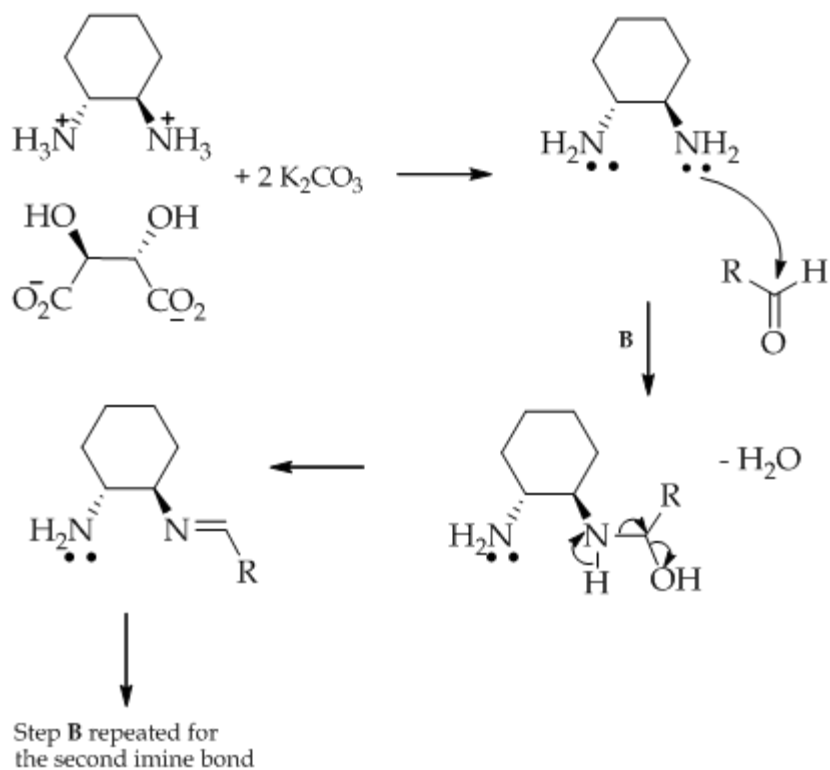
Scheme 2.26 The general mechanism for the synthesis of salcyen compounds.

Observed in the NMR spectra (Figure 2.8 and Figure 2.9) are broad resonances for the secondary amine units with chemical shifts of δ^1H 8.90 ppm **(15)** and 11.21 ppm **(16)**, the higher chemical shift of **(16)** being consistent with a greater degree of conjugation in this derivative. The imine functions gave characteristic singlet resonances of δ^1H 8.29 ppm **(15)** and 8.26 ppm **(16)**.
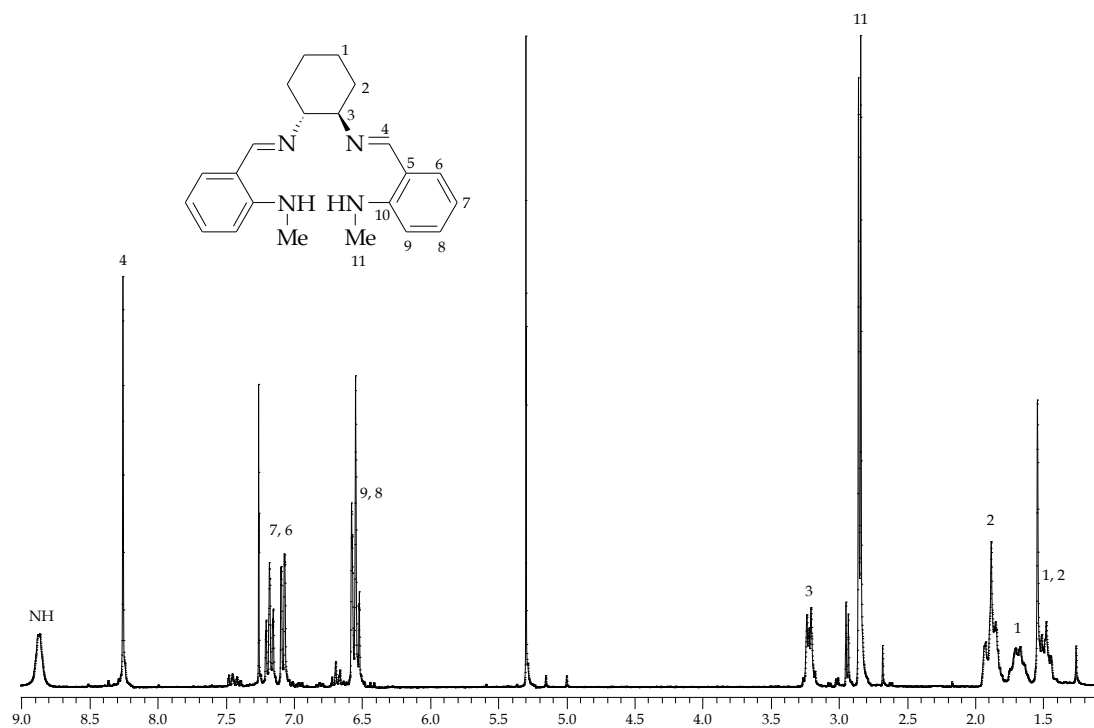
Figure 2.23 ¹H NMR of (*R*,*R*)-N,N'-bis-(2-methylamino-benzylidene)-*trans*-1,2-diaminocyclohexane **(15)** CDCl₃, 298K, 300 MHz.
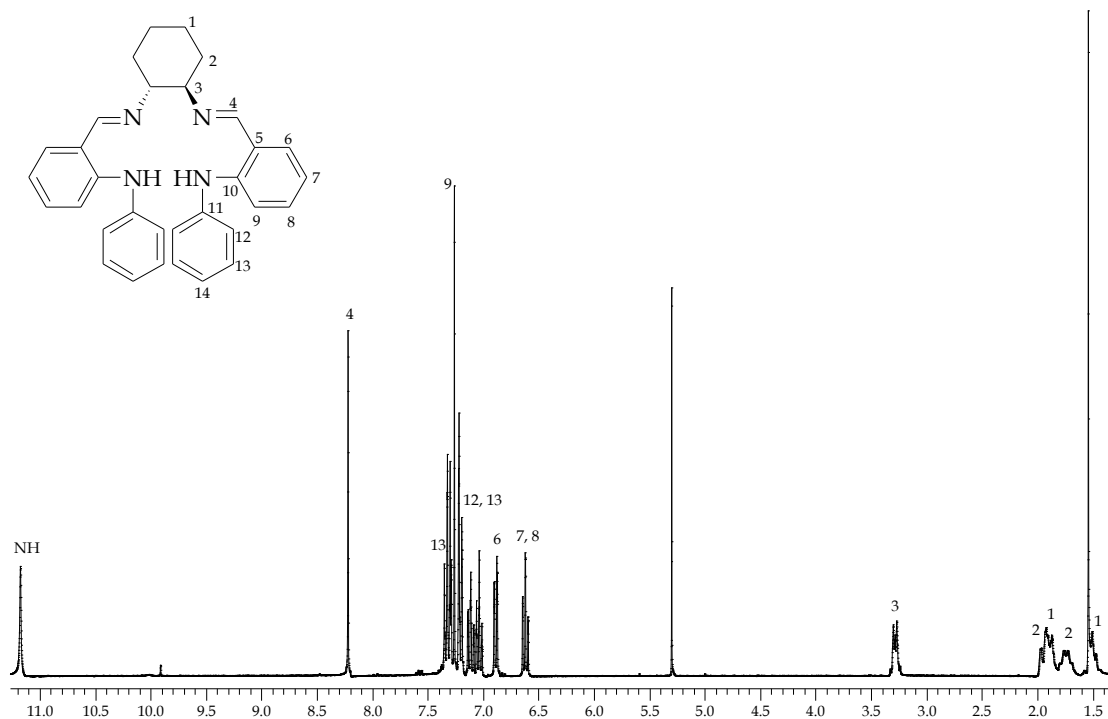
Figure 2. 24 ¹H NMR of (*R*,*R*)-N,N'-bis-(2-phenylamino-benzylidene)-*trans*-1,2-diaminocyclohexane **(16)** CDCl₃, 298K, 300 MHz.

It is clear to see that the N4 salcyen compounds **(15-16)** have strong similarities in their NMR spectra and therefore similar structures. The 3-position cyclohexyl chair proton is observed to be a multiplet in the ^1H NMR spectra for both salcyen ligands, δ^1H at C_3H 3.27 to 3.30 ppm. As there is no ring substitution for compounds **(15-16)** the four aromatic proton resonances are higher for **(16)** then for **(15)**, which could be due to greater conjugation in addition to the presence of the phenyl ring substituent on the nitrogen atoms. Similar trends are observed in the $^{13}C\{^1H\}$ NMR spectra.

2.4.4 General synthesis of (*R*,*R*)-N,N′-bis-(2-R-amino-benzyl)-*trans*-1,2-diaminocyclohexane (17-18)

17 - R = Me, 18 - R = Ph   **(17-18)**
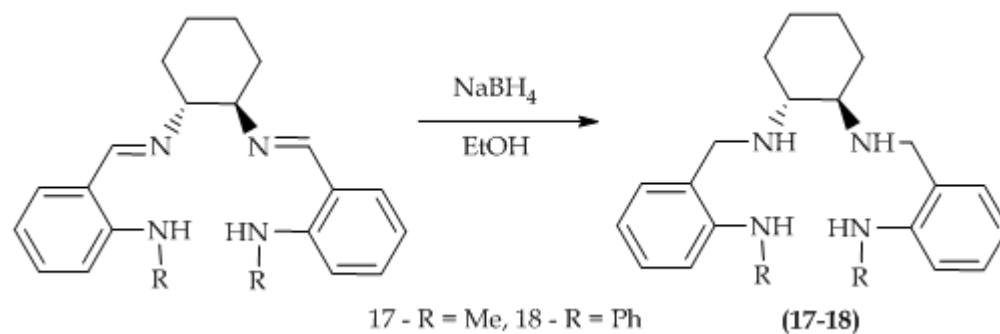
Scheme 2.27 General synthesis of N4-type salcyan compounds **(17)** and **(18).**

The N4 salcyen imine bond was reduced with sodium borohydride in ethanol following the procedure taken from Atwood's 1997 paper. [4] The products were collected as white solids by reduced pressure filtration following cooling and quenching with water. The resulting white solids were purified by recrystallisation from pentane **(17)** (61%) and dichloromethane **(18)** (78%). Broad singlet resonances are observed (Figure 2.10 and Figure 2.11) for the secondary amine NH units in the ^1H-NMR spectra with chemical shifts of δ^1H 5.30 ppm **(17)** and 8.09 ppm **(18)**, with the higher chemical shift attributed to greater conjugation as observed in the salcyen precursors. The characteristic AB pattern

resonances composed of two doublets for the methylene protons (C₄H) of the amine backbone are observed in the NMR spectra. The presence of four aromatic proton resonances for compounds **(17-18)** are due to the lack substitution on the aromatic ring. The aromatic proton resonances for compound **(18)** appear at a higher value than for compound **(17)**, due to a greater conjugation with the addition of the phenyl ring nitrogen substituent as observed in the salcyen precursors **(15-16)**.
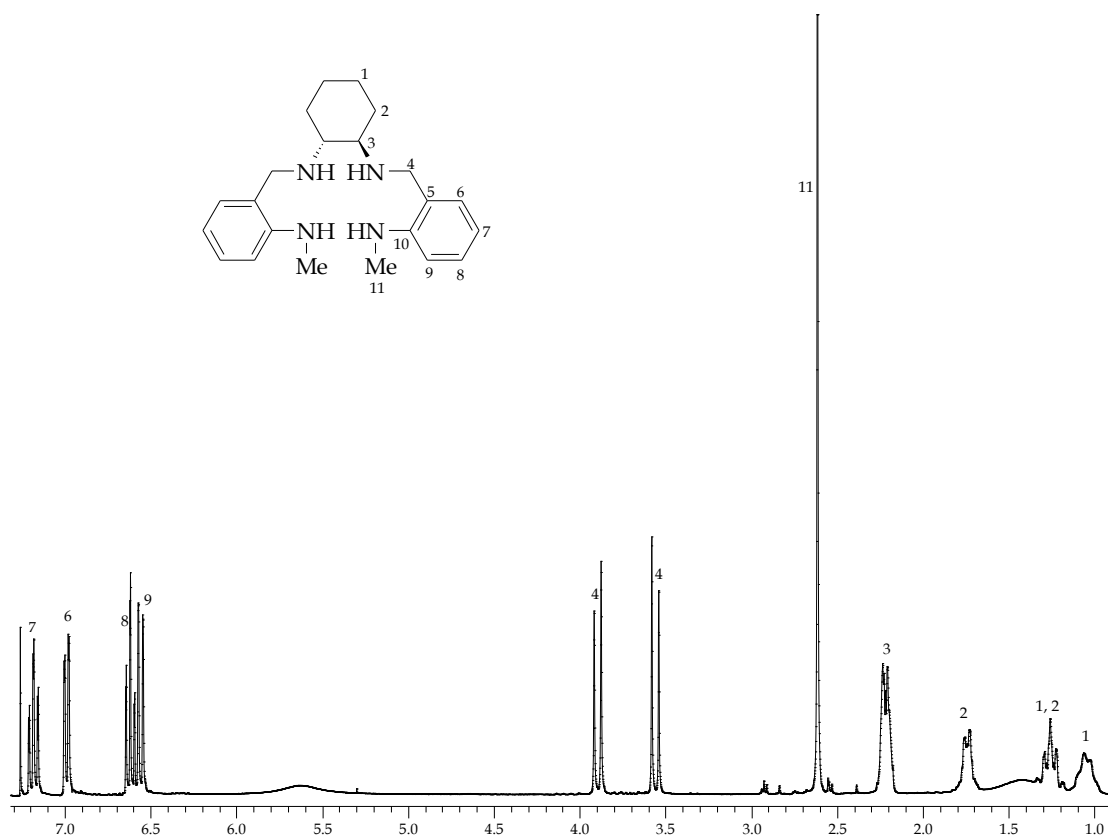
Figure 2.25 ¹H NMR of (*R,R*)-N,N′-bis-(2-methylamino-benzyl)-*trans*-1,2 diaminocyclohexane **(17)** CDCl₃, 298 K, 300 MHz.
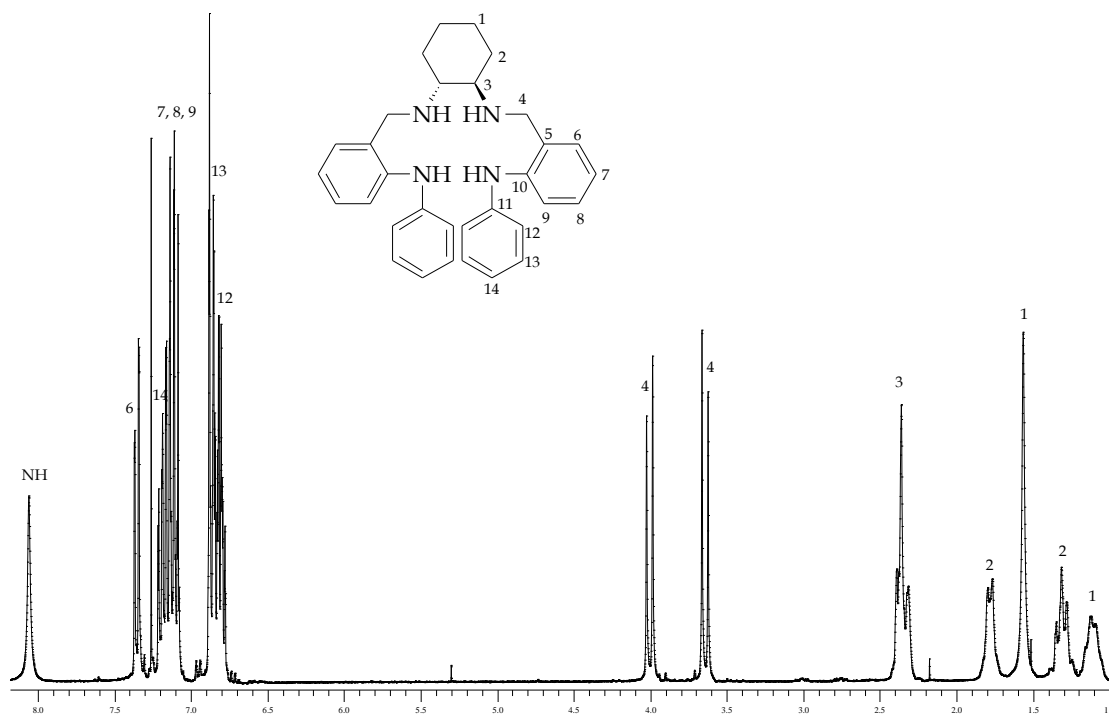
Figure 2.26 ¹H NMR of (*R,R*)-N,N′-bis-(2-phenylamino-benzyl)-*trans*-1,2-diaminocyclohexane **(18)** CDCl₃, 298 K, 300 MHz.

2.4.5 Single crystal X-ray structure of (R,R)-N,N′-bis-(2-phenylamino-benzyl)-trans-1,2-diaminocyclohexane (18)
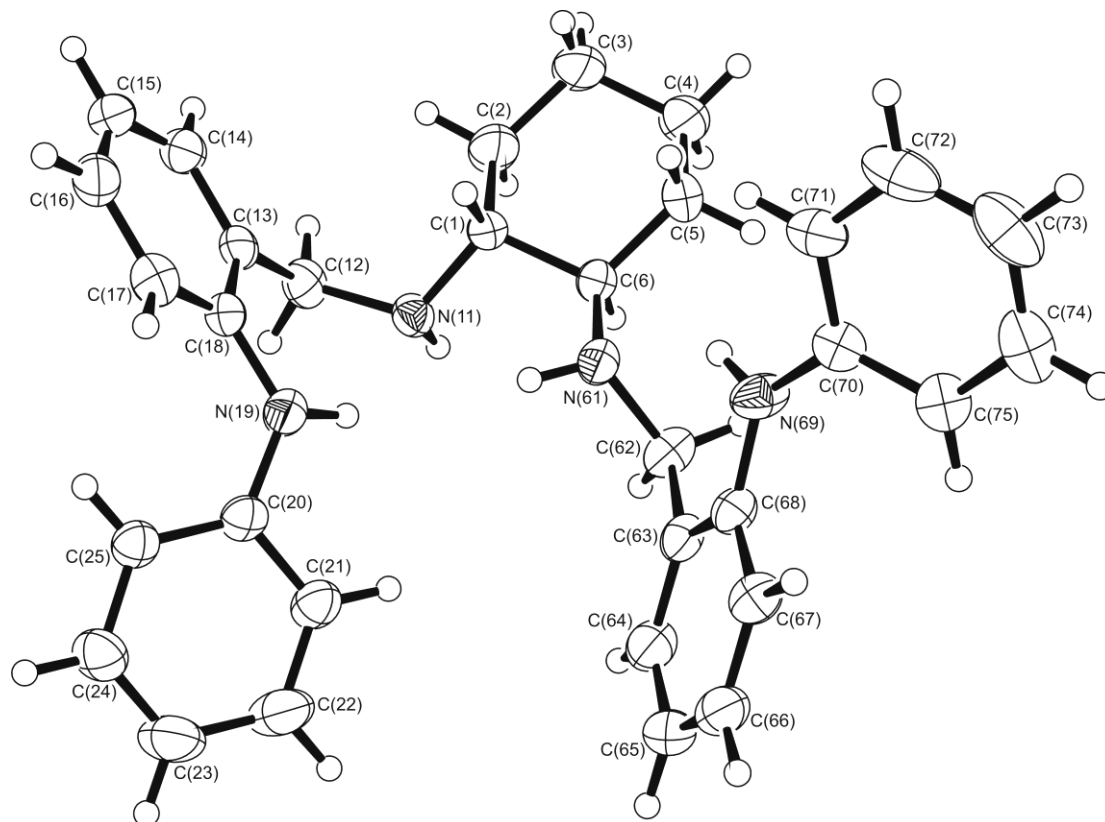
Figure 2.27 ORTEP plot of the crystallographically determined molecular structure of (*R*,*R*)-N,N′-bis-(2-phenylamino-benzyl)-*trans*-1,2-diaminocyclohexane **(18).**

Slow recrystallisation from pentane afforded **(18)** as yellow prisms suitable for X-ray diffraction examination (full crystallographic data was provided in Appendix (ii)). The molecular structure of (*R*,*R*)-N,N′-bis-(2-phenylamino-benzyl)-*trans*-1,2-diaminocyclohexane **(18)** shows, as expected, evidence that the cyclohexane rings adopts a chair conformation, with the nitrogen's occupying the equatorial positions. Intermolecular hydrogen bonding is evident between N(19)H to N(11) and N(69)H to N(61) with a distance of 2.85Å and 2.91Å respectively, forming a six-membered ring.

C(1)-N(11)	1.4828(18)	C(1)-C(6)	1.5452(19)
C(1)-C(2)	1.548(2)	C(2)-C(3)	1.536(3)
C(3)-C(4)	1.530(3)	C(4)-C(5)	1.534(3)
C(5)-C(6)	1.537(2)	C(6)-N(61)	1.4874(19)
N(11)-C(12)	1.4905(19)	C(12)-C(13)	1.525(2)
C(13)-C(14)	1.398(2)	C(13)-C(18)	1.419(2)
C(14)-C(15)	1.395(3)	C(15)-C(16)	1.391(3)
C(16)-C(17)	1.394(2)	C(17)-C(18)	1.404(2)
C(18)-N(19)	1.4106(19)	N(19)-C(20)	1.405(2)
C(20)-C(25)	1.404(2)	C(20)-C(21)	1.414(2)
C(21)-C(22)	1.390(3)	C(22)-C(23)	1.405(3)
C(23)-C(24)	1.382(3)	C(24)-C(25)	1.399(2)
N(61)-C(62)	1.4837(19)	C(62)-C(63)	1.517(2)
C(63)-C(64)	1.392(2)	C(63)-C(68)	1.4207(19)
C(64)-C(65)	1.397(3)	C(65)-C(66)	1.390(3)
C(66)-C(67)	1.401(2)	C(67)-C(68)	1.408(2)
C(68)-N(69)	1.4050(19)	N(69)-C(70)	1.4065(19)
N(69)-H(69)	0.84(2)	C(70)-C(71)	1.399(2)
C(70)-C(75)	1.407(2)	C(71)-C(72)	1.408(3)
C(72)-C(73)	1.398(3)	C(73)-C(74)	1.383(3)
C(74)-C(75)	1.393(2)		

Table 2.8 Interatomic distances (Å) with s.u.s in parentheses.

N(11)-C(1)-C(6)	107.41(12)	N(11)-C(1)-C(2)	113.32(13)
C(6)-C(1)-C(2)	109.97(12)	C(3)-C(2)-C(1)	112.90(18)
C(4)-C(3)-C(2)	111.11(16)	C(3)-C(4)-C(5)	110.41(17)
C(4)-C(5)-C(6)	111.32(17)	N(61)-C(6)-C(5)	109.77(14)
N(61)-C(6)-C(1)	112.40(11)	C(5)-C(6)-C(1)	111.47(12)
C(1)-N(11)-C(12)	116.51(12)	N(11)-C(12)-C(13)	113.56(12)
C(14)-C(13)-C(18)	118.80(14)	C(14)-C(13)-C(12)	120.12(14)
C(18)-C(13)-C(12)	120.95(13)	C(15)-C(14)-C(13)	121.67(16)
C(16)-C(15)-C(14)	119.19(15)	C(15)-C(16)-C(17)	120.49(16)
C(16)-C(17)-C(18)	120.59(15)	C(17)-C(18)-N(19)	122.75(14)
C(17)-C(18)-C(13)	119.23(14)	N(19)-C(18)-C(13)	117.98(14)
C(20)-N(19)-C(18)	126.99(12)	C(25)-C(20)-N(19)	124.97(13)
C(25)-C(20)-C(21)	118.40(14)	N(19)-C(20)-C(21)	116.60(14)
C(22)-C(21)-C(20)	120.67(16)	C(21)-C(22)-C(23)	120.30(16)
C(24)-C(23)-C(22)	119.25(16)	C(23)-C(24)-C(25)	121.08(16)
C(24)-C(25)-C(20)	120.22(14)	C(62)-N(61)-C(6)	111.43(11)
N(61)-C(62)-C(63)	113.01(12)	C(64)-C(63)-C(68)	119.03(14)
C(64)-C(63)-C(62)	121.23(13)	C(68)-C(63)-C(62)	119.62(13)
C(63)-C(64)-C(65)	122.06(15)	C(66)-C(65)-C(64)	118.70(15)
C(65)-C(66)-C(67)	120.88(15)	C(66)-C(67)-C(68)	120.28(14)
N(69)-C(68)-C(67)	124.01(13)	N(69)-C(68)-C(63)	116.93(12)
C(67)-C(68)-C(63)	119.03(13)	C(68)-N(69)-C(70)	128.26(13)
C(68)-N(69)-H(69)	114.2(14)	C(70)-N(69)-H(69)	117.2(14)
C(71)-C(70)-N(69)	118.17(14)	C(71)-C(70)-C(75)	119.35(14)
N(69)-C(70)-C(75)	122.44(14)	C(70)-C(71)-C(72)	119.75(17)
C(73)-C(72)-C(71)	120.43(18)	C(74)-C(73)-C(72)	119.40(17)
C(73)-C(74)-C(75)	121.05(18)	C(74)-C(75)-C(70)	120.03(16)

Table 2.9 Angles between interatomic vectors (°) with s.u.s in parentheses.

2.5 Reactions of N₄ salcyan systems with aluminium compounds

In this section are described attempts to prepare aluminium salcyan complexes of the N₄ framework. A discussion of the attempted synthetic pathways, characterisation methods and comparisons are also included.

2.5.1 Reaction of N₄-Salcyans (17) & (18) with AlMe₃
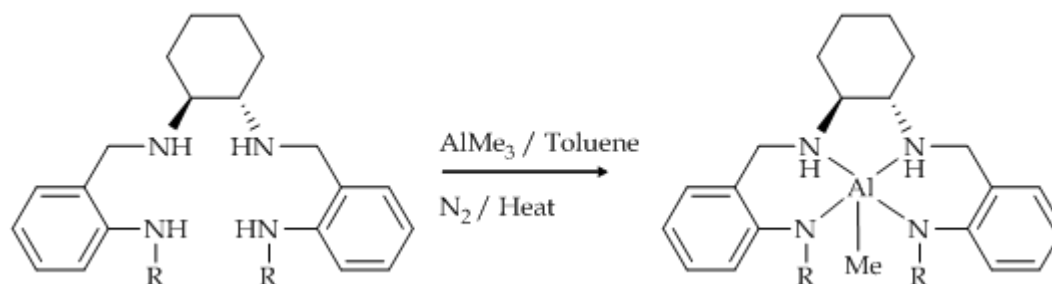
Scheme 2.28 Attempted syntheses of (R,R)-[salcyan(R-amino)₂]AlMe₂ **(42- 43)** complexes.

The purpose of this reaction was to use the procedure taken from Skell and Bean's 1962 paper, which has already been adopted in the Kee group for N₂O₂ complex syntheses and adapt it for the new N₄ derivatives. [16]

Vacuum dried salcyan **(17-18)**, dissolved in dry toluene, was treated with trimethylaluminium solution under a dry dinitrogen atmosphere. To compensate for trace amounts of water remaining in the salcyan **(17-18)**, a slight excess of the trimethylaluminium was employed. The solution was heated for 72 h then cooled to room temperature. Usually with N₂O₂-salcyan systems using the same reaction conditions, a precipitate is observed at this stage. However, none was observed in either of the N₄-systems. Subsequently all volatile components were removed under reduced pressure

leaving a yellow orange material. Recrystallisation of **(42)** and **(43)** was not successful. ^{1}H NMR of **(42)** and **(43)** indicated the presence of uncomplexed ligand and a clear absence of an aluminium-methyl peak, typically seen in the δ^1H –0.9 and –0.7 ppm region.

In a modified synthetic procedure using aluminium isopropoxide and LDA in the presence of the N$_4$-salcyan **(17)**, a toluene solution of these components was heated for a total of 24 h before being cooled and volatiles removed under reduced pressure resulting in a yellow orange solid. ^{1}H NMR indicated again the presence of uncomplexed ligand and a clear absence of an aluminium-methyl resonance, typically seen in the δ^1H –0.9 and –0.7 ppm region.
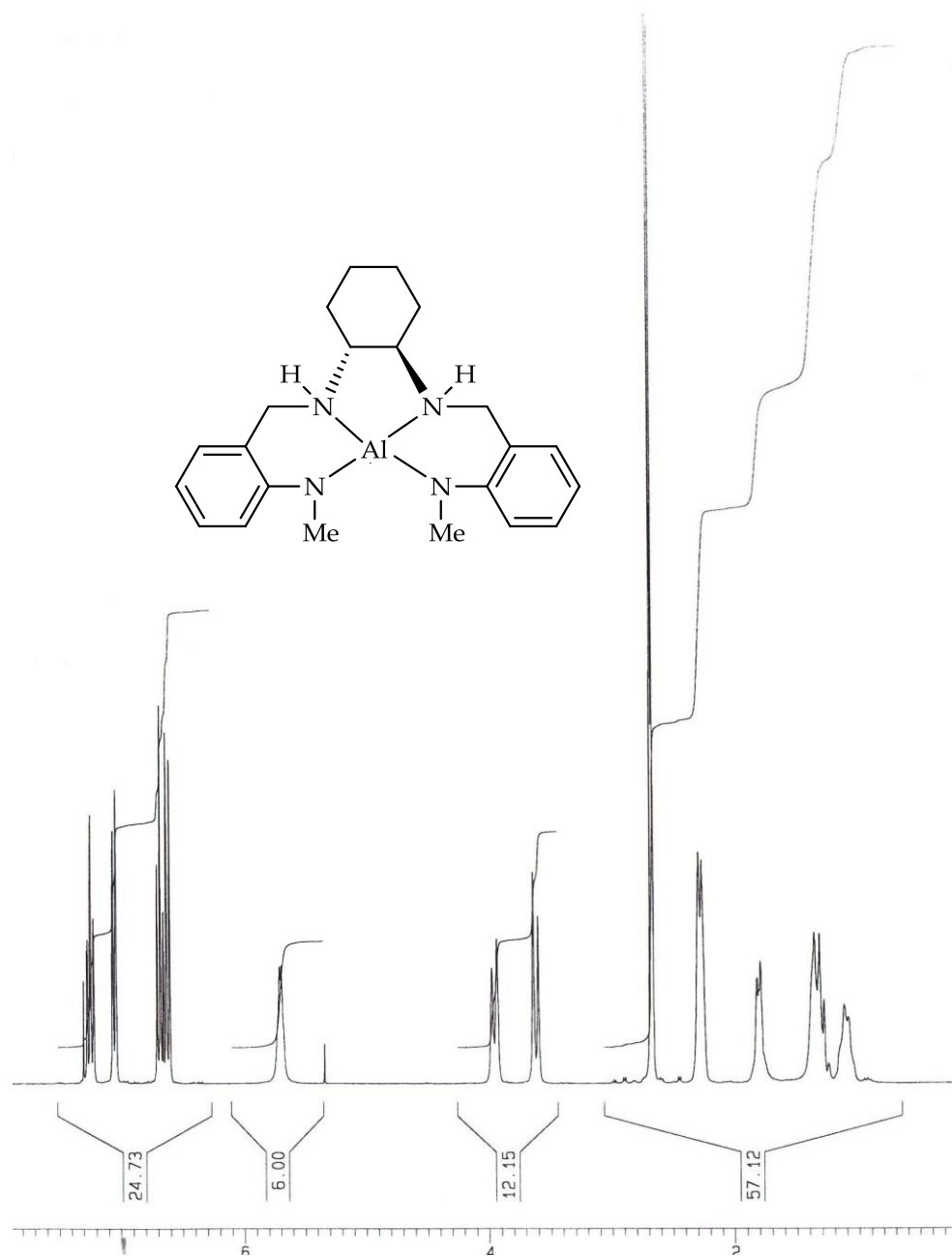
Figure 2.28 ¹H NMR of attempted synthesis of [(*R,R*)-N,N′-bis-(2-methylamino-benzyl)-*trans*-1,2-diaminocyclohexane]AlCl **(42)** CDCl₃, 298 K, 300 MHz.

2.5.2 Reaction of N$_4$-Salcyan (18) with R$_x$AlCl$_x$
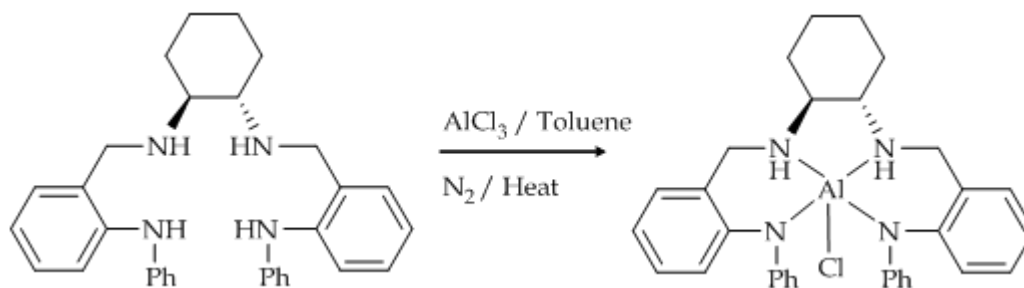
Scheme 2.29 Synthesis of (*R*,*R*)-[salcyan(phenylamino)$_2$]AlCl **(49)** complex.

Reactions conditions were taken from Gou's 2008 paper as an alternative way to synthesising an aluminium N$_4$-salcyan complex. [17] Vacuum dried salcyan **(18)**, dissolved in dry toluene, was treated with aluminium trichloride under dry dinitrogen as shown in Table 2.10. To compensate for trace amounts of water remaining in the salcyan **(18)**, a slight excess of the aluminium chloride proved to be advantageous. After 72 h the solutions were cooled and all volatile components removed under reduced pressure to afford a yellow orange material. Recrystallisation from hot methanol was not successful. ^{1}H NMR indicated the presence of the starting material only.

Reaction	Reagent(s)	Condition(s)	Solvent	Result
1	AlCl$_3$, ^{t}-BuLi	Room temp	Toluene	No complex
2	AlCl$_3$, NEt$_3$	Reflux	Toluene	No complex

Table 2.10 Complexation methods tested using (*R*,*R*)-N,N'-bis-(2-phenylamino-benzyl)-*trans*-1,2-diaminocyclohexane **(18).**

After the disappointing results obtained using aluminium chloride it was decided that resorting to an alternative chloride reagent would be beneficial, hence

dimethylaluminium chloride and ethylaluminium dichloride were used. To the dimethylaluminium chloride was added the salcyan **(18)** under two different conditions, as shown in Table 2.5.

Reaction	Reagent(s)	Condition(s)	Solvent
3	(CH$_3$)$_2$AlCl	-78°C - Room temp	Toluene
4	(CH$_3$)$_2$AlCl	-78°C - Room temp - 80°C	Toluene

Table 2.11 Complexation methods tested using (*R,R*)-N,N'-bis-(2-phenylamino-benzyl)-*trans*-1,2-diaminocyclohexane **(18)**. [17]

The dimethylaluminium chloride and salcyan solution was stirred for a total of 72 hours and cooled before all volatile components were removed under reduced pressure, leaving a pale yellow solid. Recrystallisation from hot methanol was successful resulting in yellow crystals of X-ray quality. However, the X-ray data indicated the presence of un-complexed ligand as shown in the NMR, Figure 2.14.
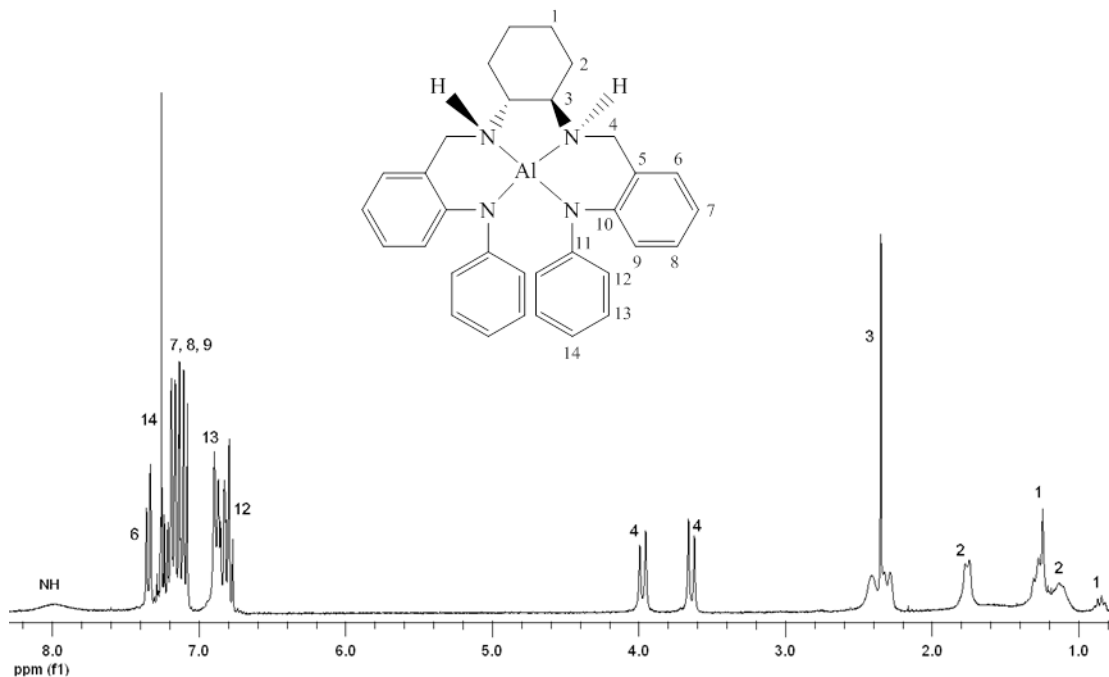
Figure 2.29 ^{1}H NMR of attempted synthesis of [(*R*,*R*)-N,N'-bis-(2-phenylamino-benzyl)-*trans*-1,2-diaminocyclohexane]AlCl **(49)** CDCl$_3$, 298 K, 300 MHz. Data indicates presence of free-ligand only.

2.5.3 Reaction of N$_4$-Salcyan (18) with EtAlCl$_2$
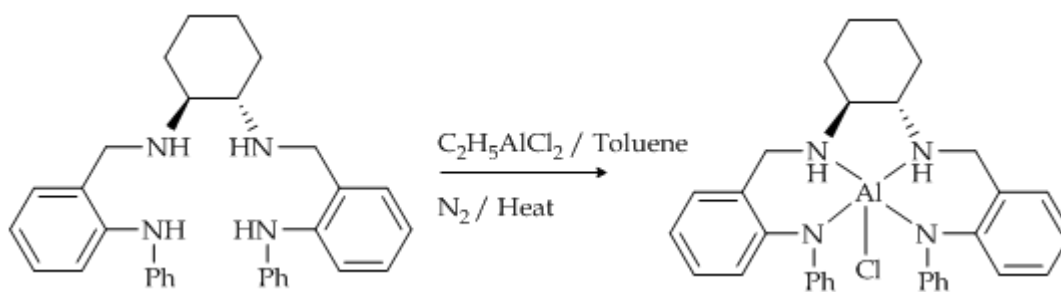
Scheme 2.30 Synthesis of (*R*,*R*)-[salcyan(phenylamino)$_2$]AlCl **(50)** complex.

Salcyan **(18)**, dissolved in dry toluene was treated with varied amounts of ethylaluminium dichloride under dry atmosphere of dinitrogen under 2 different conditions, as shown in Table 2.6.

Reaction	Reagent(s)	Condition(s)	Solvent
5	C$_2$H$_5$AlCl$_2$	-78°C - Room temp	Toluene
6	C$_2$H$_5$AlCl$_3$	-78°C - Room temp - 80°C	Toluene

Table 2.12 Complexation methods tested using (*R,R*)-N,N'-bis-(2-phenylamino-benzyl)-*trans*-1,2-diaminocyclohexane **(18)**.

To compensate for trace amounts of water remaining in the salcyan **(18)**, a slight excess of the ethylaluminium dichloride was used. The solution was heated for a total of 72 h cooled to ambient temperature and volatile components removed under reduced pressure to afford a yellow compound. Recrystallisation was successful from hot methanol producing long yellow needle crystals, suitable for X-ray. However, as with the synthesis using dimethylaluminium chloride, the crystals were of the uncomplexed ligand only. Analysis *via* ^{1}H NMR (Figure 2.15) showed no distinctive changes in the AB splitting pattern normally seen for the two doublets of the methylene protons (C$_4$H of Scheme 2.10 and Scheme 2.11), indicating no change in structure.
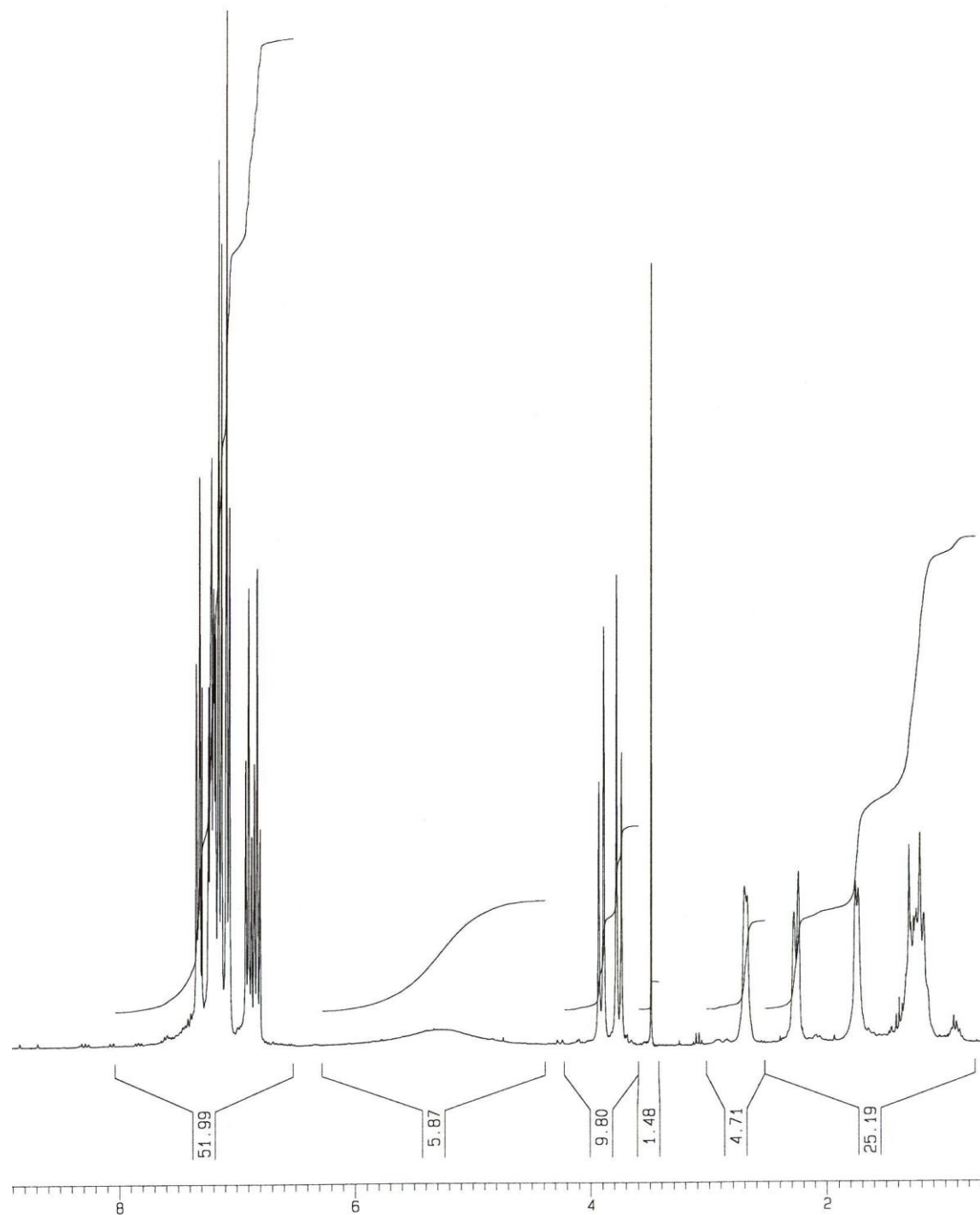
Figure 2.30 ^{1}H NMR of attempted synthesis of [(*R,R*)-N,N'-bis-(2-phenylamino-benzyl)-*trans*-1,2-diaminocyclohexane]AlCl$_2$ **(50)** CDCl$_3$, 298 K, 300 MHz.

The reactions using dimethylaluminium chloride and ethylaluminium dichloride were repeated under strict dry conditions, with the emphasis on eliminating all sources of water and oxygen. The work-up procedure also included a 'washing' stage with pentane which we know to dissolve free-ligand, making it easy to remove any unreacted ligand and hopefully leave the desired complex, however this procedure was not successful and due to time constraints further investigations were not carried out.

2.6 Preparation of pyrrole ligands [16]

The pyrrole N$_4$ systems were chosen in addition to the aniline-based N$_4$ systems because of their similarity in pKa values as shown below:

1 Phenol – pKa = 9.9 [6]

2 Aniline – pKa = 30.6 [7], [8]

3 Pyrrole – pKa = 23.0 [21]

The lower acidity of aniline-based systems compared to the phenolic and pyrrolic analogues are envisaged to make complex formation *via* reaction with either metal alkyls or alkoxides, less facile.

The first step in the ligand synthesis was to prepare a substituted pyrrole precursor. This process was found to be more challenging than initially expected. Described below are two methods used in the attempt to obtain an alkylated pyrrole.

2.6.1 Method 1: Alkylation of pyrrylmagnesium bromide
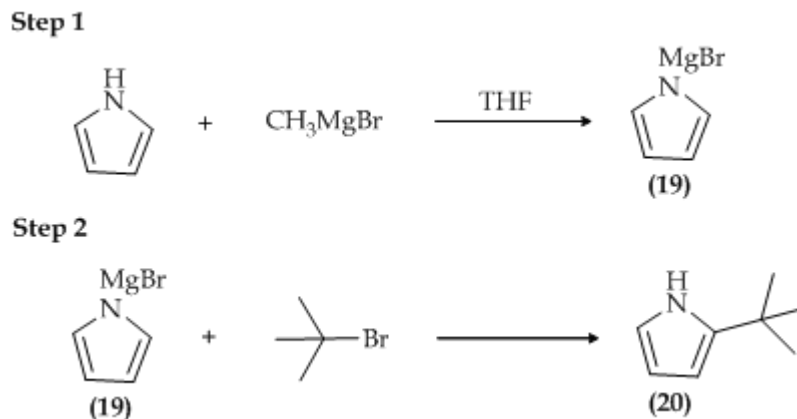
Scheme 2.31 Attempted synthesis of *tert*-butyl pyrrole.

General reaction conditions were taken from Gou's 2008 paper whereby a Grignard was prepared by slowly adding pyrrole **(Step 1,** Scheme 2.9**)** to a solution of methyl magnesium bromide in tetrahydrofuran. [17] When the evolution of gas (methane) ceased, the reaction was left to stir under reflux for 30 min. The end product was a light-brown solution with a slight green tint. Due to the sensitive nature of the pyrrylmagnesium bromide **Step 2** (Scheme 2.12) was performed immediately (see experimental for further details). Difficulties arose when purifying the crude product. The crude mixture was analysed by TLC (dichloromethane: methanol; 9:1 v/v) which gave clear separation between what could be the product and impurities (namely starting material), however upon running the flash column chromatography, a clean separation was not so apparent. The small amount of crude product was analysed by ¹H NMR suggesting that some *tert*-butyl pyrrole had formed, although in a very small quantity and not pure. The result was hopeful and indicated that further work was needed. The next obstacle was synthesising a pyrrole carboxaldehyde. One of the best methods for synthesising substituted salicylaldehyde derivatives is a hydroformylation protocol using magnesium (II) chloride in the presence of triethylamine as the catalyst and acetonitrile.
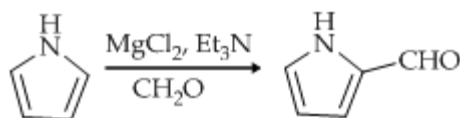
Scheme 2.32 Hydroformylation of pyrrole to create pyrrole carboxaldehyde. (22)

This reaction (Scheme 2.13) proved unsuccessful when used with pyrrole, with no reaction occurring. After another unsuccessful attempt it was decided that an alternative method would be needed.

2.6.2 Method 2: Variation on the Paal Knorr pyrrole synthesis [22]

The Paal Knorr pyrrole synthesis is a way of producing substituted pyrroles *via* the condensation of a 1,4-dicarbonyl compound with an excess of a primary amine or ammonia.
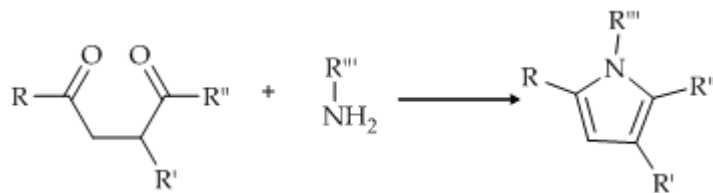
Scheme 2.33 The Paal Knorr pyrroles synthesis. [22]

This reaction did not provide the solution to making a pyrrole carboxaldehyde, however a literature search resulted in a procedure using acetylene, nitrile and a titanium reagent being discovered. [23]
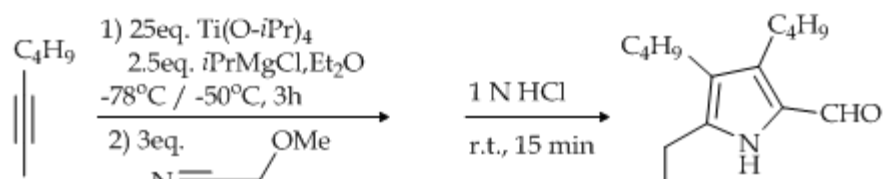
Scheme 2.34 Synthesis of substituted methoxy-pyrrole carboxaldehydes. [22]

The reaction involves titanium-mediated coupling of functionalised acetylenes to a nitrile substrate to generate an azatitanacyclopentadiene.
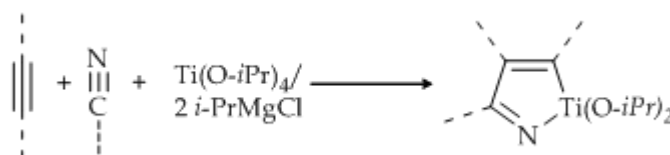
Scheme 2.35 Coupling of the titanium reagent to the nitrile and acetylene compounds. [22]

When excess nitrile was added, subsequent reaction with the acetylene-titanium complex should lead to a pyrrolecarboxaldehyde after acidic workup (Scheme 2.17). [22]
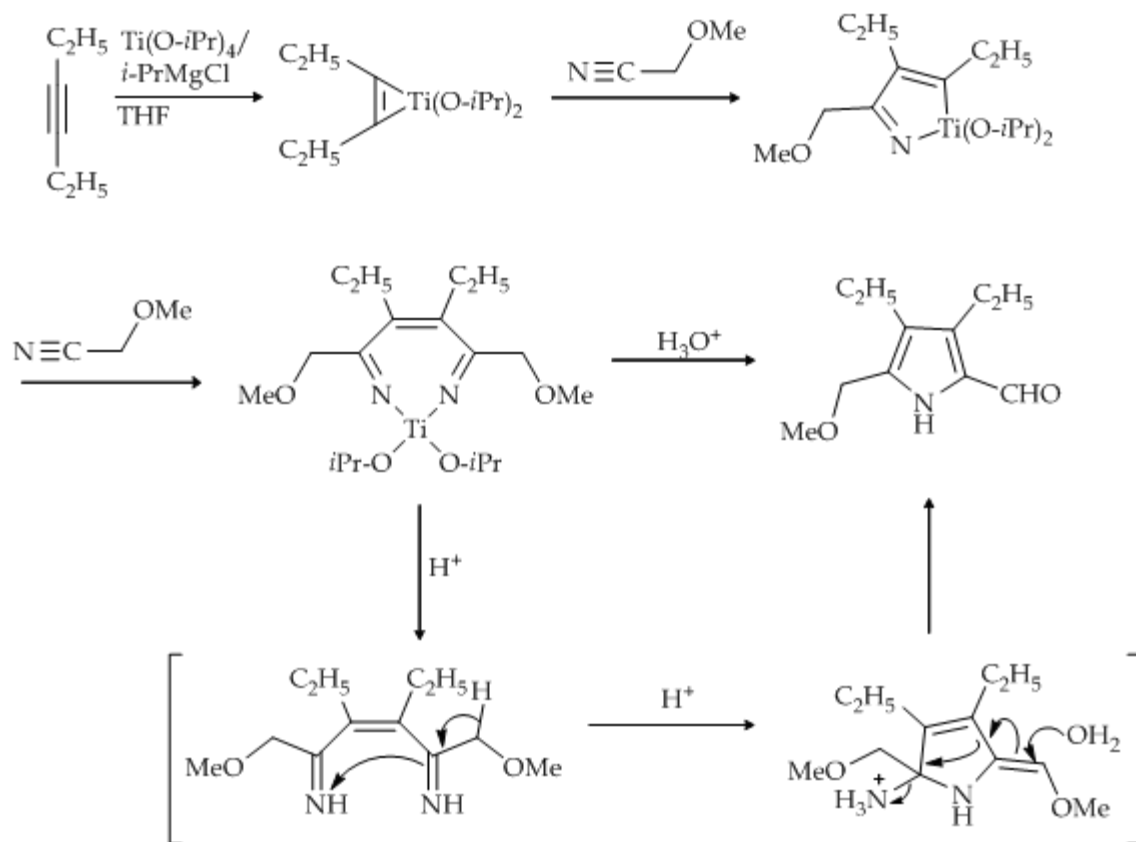
Scheme 2.36 Preparation and reaction mechanism of pyrrolecarboxaldehyde from acetylene and nitrile. [22]

To a stirred solution of 3-hexyne and titanium isopropoxide in THF, isopropylmagnesium chloride was added at -78 °C under nitrogen to give a bright yellow homogenous solution. The solution was warmed to -50 °C over a period of 30 min, to which the colour turned yellow-brown. Methoxyacetonitrile was added after stirring for 3 h at -50 °C and left to stir for a further 3 h. Following warming to room temperature, quenching with 1*N* HCl (15 mL), it was observed that the pyrrolecarboxaldehyde may have been formed, but not without significant impurities, which were apparent in the ^{1}H NMR. The product proved extremely difficult to separate *via* silica column chromatography and so this method was not pursued any further.

2.6.3 Method 3: Reaction of pyrrole-2-carboxaldehyde with (*R,R*)-1,2-diaminocyclohexane

A decision was made to build a salcyen framework with an unsubstituted pyrrole. A literature reference reported an excellent yield (90%) for *N,N'*-bis-(1H-pyrrol-2-ylmethylene)-cyclohexane-1*R*,2*R*-diamine. [23] However, diaminocyclohexane was used in the free form rather than the usual tartrate salt. In the first instance, a variant of our earlier salcyen synthesis was attempted (Scheme 2.15).
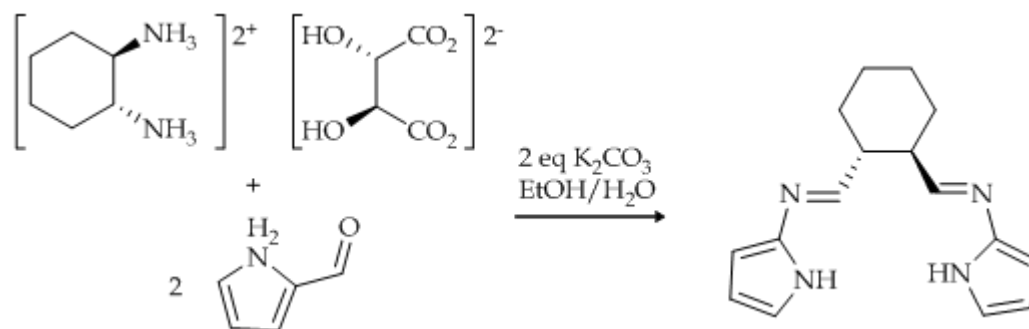
Scheme 2.37 General synthesis of (*R,R*)-N,N'-bis-(1H-pyrrol-2-ylmethylene-cyclohexane 1*R*, 2*R*-diamine).

Unfortunately, only starting materials were recovered from this reaction with no evidence for the formation of a pyrrole salcyen compound being evident by ¹H-NMR spectroscopy.
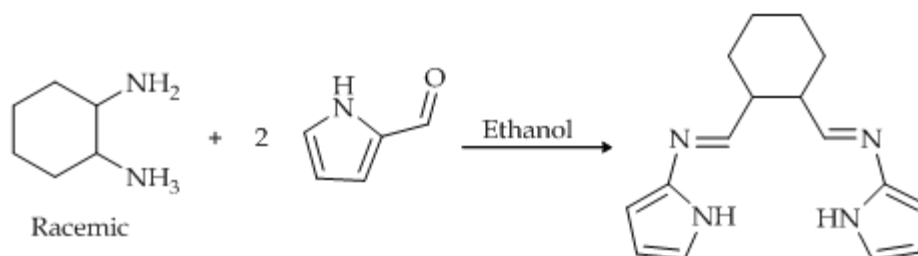
Scheme 2. 38 Synthesis of (*R,R*)-N,N'-bis-(1H-pyrrol-2-ylmethylene-cyclohexane *1R, 2R*-diamine) using racemic 1,2-diaminocyclohexane.

Moving instead to a trial reaction involving the diaminocyclohexane base in racemic form (Scheme 2.19) confirmed that this reaction worked, as verified by ^{1}H NMR spectroscopic analysis of the crude product. This does show a promising side to the N$_4$-pyrrole systems and one which could form the basis of a future reaction protocol. However due to time constraints, this work was unable to be completed as part of this thesis.

2.7 Conclusion

Successful syntheses of (*R,R*)-[N$_4$-salcyen (NMe)$_2$] and (*R,R*)-[N$_4$-salcyen (NPh)$_2$] were accomplished, which were reduced to their salcyan cousins and further reacted with AlMe$_3$ to form the aluminium complexes. Crystals of 2-phenylamino benzaldehyde were obtained and single crystal X-ray analysis was successful (see appendix A for full crystallographic data). Attempts at synthesising a metal complex of the N$_4$-aniline systems proved unsuccessful.

The synthesis of the target pyrrole complex appears to be far from simple. However, a new synthetic route has been identified from the tartrate-free diaminocyclohexane base,

which could be pursued with some degree of confidence now that model reactions have shown that success is likely.

2.8 References

[1]   F. Adrián, M. I. Burguete, J. M. Fraile, J. I. Garciá, J. Garciá, E. Garciá-España, S. V. Luis, J. A. Mayoral, A. J. Royo, M. C. Sánchez, *Eur. J. Inorg. Chem.*, **1999,** *00*, 2347.

[2]   H. U. Blaser, H. P. Jalett, J. Wiehl, *J. Mol. Catal*, **1991**, *68*, 215.

[3]   F. Fache, B. Dunjic, P. Gamez, M. Lemarie, *Top. Catal.*, **1997**, *4*, 201.

[4]   (a) H. Takahashi, M. Yoshioka, M. Shibasaki, M. Ohno, N. Imai, S. Kobayashi, *Tetrahedron*, **1995**, *51*, 1203.

(b) S. E. Denmark, B. L. Christenson, D. M. Coe, S. P. O'Connor, *Tetrahedron Lett.*, **1995**, *36*, 2215.

[5]   (a) H. Takahashi, T. Kawakita, M. Yoshioka, S. Kobayashi, M. Ohno, *Tetrahedron Lett.*, **1989**, *30*, 7095.

(b) H. Takahashi, T. Kawakita, M. Ohno, M. Yoshioka, S. Kobayashi, *Tetrahedron.*, **1992**, *48*, 5691.

(c) M. Yoshioka, T. Kawakita, M. Ohno, *Tetrahedron Lett.*, **1989**, *30*, 1657.

[6]   (a) P. Knochel, *Chemtr. Org. Chem.*, **1995**, *8*, 205.

(b) F. Langer, L. Schwink, A. Devasagayaraj, P. Y. Chavant, P. Knochel, *J. Org. Chem.*, **1996**, *61*, 8229.

(c) C. Lutz, P. Knochel, *J. Org. Chem.*, **1997**, *62*, 7895.

(d) S. Nowotny, S. Vettel, P. Knochel, *Tetrahedron Lett.*, **1994**, *35*, 4539.

(e) R. Ostwald, P. Y. Chavant, H. Stadtmuller, P. Knochel, *J. Org. Chem*, **1994**, *59*, 4143.

[7]   M. Hechavarria Fonseca, E. Eibler, M. Zabel, B. Konig, *Tetrahedron: Asymm.*, **2003**, *14*, 1989.

[8]   I. Karame, M. Jahjah, A. Messaoudi, M. Lorraine Toammasino, M. Lemaire, *Tetrahderon: Asymm*, **2004**, *15*, 1569.

[9]   (a) A. Ferrand, M. Bruno, M. L. Tommasino, M. Lemaire, *Tetrahedron: Asymm.*, **2002**, 1379.

(b) M. L. Tommasino, C. Thomazeau, F. Touchard, M. Lemaire, *Tetrahedron: Asymm.*, **1999**, *10*, 1813.

(c) M. L. Tommasino, M. Casalta, J. A. J. Breuzard, M. Lemaire, *Tetrahedron: Asymm.*, **2000**, *11*, 4835.

[10]   S. Chandra, L. K. Gupta, *Spectrochim. Acta. A.*, **2006**, *62*, 307.

[11]   K. Shankar, R. Rohini, V. Ravinder, P. Muralidhar Reddy, Y-P. Ho, *Spectrochim. Acta. A.*, **2009**, *73*, 205.

[12]   J. F. Larrow, E. N. Jacobsen, Y. Gao, Y Hong, X. Nie, C. H. Zepp, *J. Org. Chem.*, **1994**, *54*, 1939.

[13]   *Aldrich Handbook of Fine Chemicals*. **2007-2008**, 836.

[14]   J. S. Baum, M. E. Condon, D. A. Shook, *J. Org. Chem*. **1987**, *52*, 2983.

[15]   D. A. Atwood, *Coord. Chem. Revs*. **1997**, *165*, 267.

[16]   P.S. Skell, G. P. Bean, *J. Am. Chem. Soc*. **1962**, *84*, 4655.

[17]   S. Gou, X. Zhou, J. Wang, X. Liu, X. Feng, *Tetrahedron.*, **2008**, *64*, 2864.

[18]   F. G. Bordwell, R. J. McCallum, W. N. Olmstead *J. Org. Chem*, **1984**, *49*, 1424.

[19]   F. G. Bordwell, D. J. Algrim, N. R. Vanier, *J. Org. Chem*, **1977**, *42*, 1817.

[20]   F. G. Bordwell, D. J. Algrim, *J. Am. Chem. Soc*, **1988**, *110*, 2964.

[21]   B. F. G. Bordwell, G. E. Drucker, H. E. Fried, *J. Org. Chem*, **1981**, *46*, 632.

[22]   D. Suzuki, Y. Nobe, Y. Watai, R. Tanaka, Y. Takayama, F. Sato, H. Urabe, *J. Am. Chem. Soc*. **2005**, *127*, 7474.

[23]   M. H. Fonseca, E. Eibler, M. Zabel, B. König, *Inorg. Chim. Acta*. **2003**, *352*, 136.

Chapter 3

Molecular Modelling of Aluminium Salcyan Complexes

WE DON'T KNOW ONE MILLIONTH OF ONE PERCENT ABOUT ANYTHING.
T. A. EDISON.

3.1 Overview of Computational Chemistry

All chemists use models of some kind, the most commonly used amongst chemistry undergraduates are arguably plastic, ball-and-stick models. Researchers on the other hand use chemical drawing programs (such as ChemDraw, Chem3D etc…) to similar effect. Computational chemists employ computers to solve chemical problems utilising theoretical chemistry to calculate the structures and properties of molecules and solids. [1] The information gathered can be used to either explain pre-determined experimental data or used to predict properties of species yet to be prepared experimentally in the design of new drugs and materials. Chemical programs simulate chemical structures and/or reactions numerically based on the fundamental laws of physics. There are methods available that allow one to model stable and unstable intermediates and transition states. [1] In this way one can gain information about molecules and reactions which are otherwise challenging or impossible to obtain through observation.

Within computational chemistry there are two broad areas that are devoted entirely to the structure and reactivity of molecules: molecular mechanics and electronic structure theory, both of which perform the same basic types of calculation: [1]

- Spatial arrangement of the atoms, nuclei and electrons by computing the energy of the structure.
- Geometry optimisation: locating the lowest energy molecular structure as close to the starting structure as possible.
- Vibrational frequencies: as a result of the interatomic motion within the molecule. Although frequency calculations are not possible or practical for all computational chemistry methods.

3.2 Molecular Mechanics

Simulations using molecular mechanics are based on the laws of classical physics (Newtonian mechanics) to predict the structures and properties of a molecule. [1] It is a useful method for studying small molecules, large biological systems or material assemblies that can be upwards of millions of atoms in size, making them an inexpensive computational method. The potential energy of all systems in molecular mechanics is calculated using force fields. A force field has the following components:

- A set of equations defining the potential energy of a molecule as it varies with the locations of the atoms.

- A series of atom types defining the characteristics of an element within a specific chemical context. Different atom types stipulate different characteristics and behaviour, depending upon its environment. Hybridisation, charge and locally bonded atoms all play a part in defining the atom type.

- Parameter sets which fit the equations and atom types to the experimental data. They also define force constants which are the values used in the equations to relate atomic characteristics to energy components and structural data such as bond lengths and angles.

The basic methodologies behind molecular mechanics means that the calculations performed are based on interactions among nuclei and do not explicitly treat the electrons in a system. [1] This means that the method does have certain limitations:

- There is no single force field that can be generally used for all molecular systems of interest.

- Molecular systems dominated by electronic effects are not well treated due to the electrons being neglected. Therefore one cannot use this method to describe processes involved in bond making and bond breaking.

3.3 Electronic Structure Theory

Electronic structure methods use the laws of quantum mechanics rather than classical physics as adopted in molecular mechanics. Quantum mechanics states that the energy and other related properties of a molecule can be obtained by solving the Schrödinger equation for that system: [2]

$$H\Psi = E\Psi$$

Equation 3.1 Schrödinger equation, H = Hamiltonian operator, ψ = wave function, E = total energy. [2]

The majority of molecular systems, unless they are small, are not computationally practical and hence their Schrodinger equations cannot be solved exactly so simplifications are normally made.

There are two major classes of electronic structure methods: [1]

- Semi-empirical methods
- *Ab initio* methods

3.3.1 Semi-Empirical Methods

There are a number of different semi-empirical methods executed in software programs such as MOPAC, AMPAC, HyperChem and Gaussian. These include;

- AM1
- MINDO/3
- PM3

Each of the above mentioned methods aim to solve an approximate form of the Schrödinger equation that depends on having appropriate parameters available for the type of chemical system being investigated. [1]

Parameterised Model number 3 (PM3) is a semi-empirical method for the quantum calculation of molecular electronic structure in computational chemistry. [1] It is based on the Neglect of Differential Diatomic Overlap integral approximation. The PM3 method uses the same formalism and equations as the AM1 (Austin Method 1), the differences being that PM3 uses two Gaussian functions [also known as Gaussian Type Orbitals (GTO)] for the core repulsion function (core-electron repulsion and attraction effects), instead of the variable number used in AM1 (1-4 per element). [3]

The methodological processes during parameterisation also differ in the sense that AM1 uses some parameter values from spectroscopic data, whereas PM3 treats them as optimisable values. [3] Originally parameters were only established for elements: H, C, N, O, F, Al, Si, P, S, Cl, Br and I. Subsequently many more elements have been parameterised, metals mostly. [3]

3.3.2 *Ab Initio* Methods

The term *ab initio* refers to the calculation being from first principles and uses no empirical or semi-empirical data in the computations, being derived from theoretical principles, excluding all experimental data. [1] The calculations are based on the laws of quantum mechanics as well as a number of physical constants, such as speed of light, masses and charges of electrons and nuclei and Plancks constant: [1]

As with previous methods the *ab initio* method computes solutions to the Schrödinger equation associated with the Hamiltonian using a series of mathematical approximations, two of which are outlined below. [1]

3.3.2.1 Hartree-Fock (HF) Method of *Ab Initio* Calculation

The simplest type of *ab initio* method is the Hartree-Fock calculation, closely correlated to molecular orbital theory whereby the electron-electron repulsion is not specifically taken into account, only an average effect being included. [4], [5] This method is only approximate for the determination of ground-state wavefunctions and ground-state energies of many-body systems. Most calculations start with the Hartree-Fock method in the form of a geometry optimisation, a way of locating minima on the potential energy surface leading to predicting the equilibrium structures of molecular systems. In essence, optimisations can be called minimisations. [4], [5]

The main differences between semi-empirical and *ab initio* methods come down to how much computational time one is prepared to spend and also how accurate the results need to be. [1] Semi-empirical methods are relatively cheap, swift calculations that may provide acceptable, qualitative descriptions of molecular systems as well as providing acceptable quantitative predictions of energies and structures with good parameterisation. [1] In contrast, *ab initio* electronic structure calculations provide high quality quantitative predictions for a broad range of systems. [1] Obviously with the increase in quality there is a downside, mainly the expense and time needed to produce such accurate predictions. However with continually evolving computer technology and a consequently greater capacity to run larger molecular systems, what was once seen as a problem is becoming increasingly less troublesome.

3.3.2.2 Density Functional Theory (DFT)

Just like the Hartree Fock method, DFT is a quantum mechanical theory used to investigate the electronic structure of many-body systems using spatially dependent electron density functions. It is one of the most popular and versatile methods available in computational chemistry. They are an attractive computational method as they include electron correlation, the fact that electrons in a molecular system react to

one another's motions by repulsion or attraction. [1]   The fundamental difference between DFT and MO theory is that DFT optimises an electron density while MO theory optimises a wave function. [1]   For example, in order to determine a particular molecular property using DFT, one must know how that property depends on the electron density, whilst determining the same property using wave functions, requires one to know the correct quantum mechanical operator. [1]

3.4 Defining Model Chemistries
3.4.1 Basis Sets

The concept of basis sets is a complex topic comprising several factors.   A basic understanding of atomic and molecular orbitals is essential.

A basis set is a set of mathematical functions used to represent molecular orbitals. Usually these functions are atomic orbitals when they are centred on the atomic nuclei, however, in other instances they can be centred on bonds or lone pairs. Quantum chemical calculations are performed within a finite set of basis functions, due to limited computational resources. [6] In order to perform the calculation it is necessary to represent an orbital as a wavefunction, which can be written under its mathematical form as a vector.   The operators within the quantum chemical calculations are represented by a function which in mathematical terms is called a matrix. [6] Previously when carrying out a molecular calculation it was common to use a basis set composed of a finite number of atomic orbitals, which as stated above are centred on the atomic nucleus within a molecule. These atomic orbitals were called Slater orbitals (also called Slater-type orbitals, STOs), named after John C. Slater who introduced them in 1930. [7]   These Slater orbitals represented a set of functions which decayed exponentially with increasing distance from the nuclei. It was later realised that the Slater orbitals could be approximated to linear combinations of Gaussian orbitals instead. Gaussian orbitals (also called Gaussian-type orbitals, GTOs) are functions used as atomic orbitals for the computation of electron orbitals in molecules. [6]

The mathematical form for a STO is:

$$R(\mathbf{r}) = N \times \mathbf{r}^{\,n-1} \times e^{-\zeta r}$$

and for a GTO is:

$$R(\mathbf{r}) = N \times \mathbf{r}^{\,(2n-2-l)} \times e^{-\zeta r^2}$$

Equation 3. 2 Mathematical form for a Gaussian Type Orbital, where N is the normalisation constant, n and l are quantum numbers, r is the distance from the nucleus and ζ is a constant. [6]

Currently there are hundreds of basis sets comprised of GTOs. The smallest of which are called *minimal basis sets*. They are typically composed of the minimum number of basis functions needed to represent all of the electrons in each atom. For example, each atom in the second row of the periodic table (Li-Ne) would have a basis set of five functions (two s functions and three p functions). [8]

The polarised versions of minimal basis sets are denoted by an asterisk (*), or two asterisks (**) indicating that the polarisation function has been added to the light atoms (hydrogen and helium). Polarisation functions are functions with a higher angular momentum (*l*) e.g. *d*-functions for a carbon atom and *p*-functions for a hydrogen atom. Polarisation functions lower the energy of the wavefunction because the MOs have more flexibility to relax if they can use the space of the polarisation function. [6]

3.4.2 Polarised Sets

In the standard minimal basis sets atomic orbitals are treated as existing as 's', 'p', 'd', 'f' etc. Using these assumptions can give good approximations but it is necessary to take into account that some orbitals show shared qualities of 's' and 'p' or 'p' and 'd'. When atoms, and consequently their charges, are brought together the distribution causes a polarisation effect resulting in the atomic orbitals becoming distorted.   By

incorporating the asterisk signs(*) one can account for this polarisation effect by adding p, d, or f-type functions to a basis set.

3.5 Molecular Modelling

Within the Kee group there has been a substantial amount of molecular modelling of ligand precursors, ligand framework and our final complexes for use as catalyst precursors in the phospho-aldol reaction. [9] All have been energy minimised at both the MM+ level of molecular mechanics and at PM3 semi-empirical level using the HyperChem 7.0 software. [10]   As mentioned at the beginning of this chapter, computational calculations on large structures such as ours, can take many hours of CPU time. The advantage of using lower-level molecular modelling *via* packages such as HyperChem is that results are relatively quick to obtain using the processing power of one PC. The results we obtained from the PM3 molecular modelling studies provided valuable information with respect to the effect of steric influences around a complex metal centre. However the main disadvantage with using only PM3 data has been that we had not previously been able to validate our data against higher computational methods to ascertain whether or not these lower-level methods have some worthwhile predictive capability. One thing though is quite clear, we are using semi-empirical PM3 methods *via* HyperChem as molecular models only and *not* as the basis for electronic structure calculations or investigations of electronic structure. Such studies require more specialised treatments such as DFT.

Therefore, since a substantial amount of my research has focused on molecular modelling and computational methods on salcyan complexes of aluminium of the general form shown in Figure 3.16. It was necessary first to perform a validation analysis of the simple semi-empirical PM3 method against higher level models from HF, DFT using single-crystal X-ray diffraction data as the foundation for data input in each case. Ultimately, the objective of this section of my work is to understand how closely each modelling method approaches the interatomic parameters (bond distances and angles) found experimentally through X-ray diffraction and hence provide some confidence in the ability of simple semi-empirical models to predicting spatial arrangements around potential reaction sites in aluminium salcyan-type complexes.

3.5.1 Modelling Studies of {[(*R,R*)-R₂-Salcyan]Al(OR)}₂

The starting point for all our computational modelling studies was to input data from single crystal X-ray solutions of substituted aluminium salcyan complexes. The base complex that we have worked with is {[(*R,R*)-*t*Bu-Salcyan]Al(OH)}₂. [11] Single crystal X-ray data were inputted into the HyperChem 7.0 software as either a .pdb or .mol file and geometry optimised at the PM3 semi-empirical level (Algorithm Polak-Ribiere (conjugate gradient)). In addition, the same X-ray data, in the form of a .cif file of atomic coordinates, was used as input to the programme GaussView 4.1.2 graphical user interface, from which calculations at the HF and DFT levels of theory could be performed, (Figure 3.16 and Figure 4.2). [12]
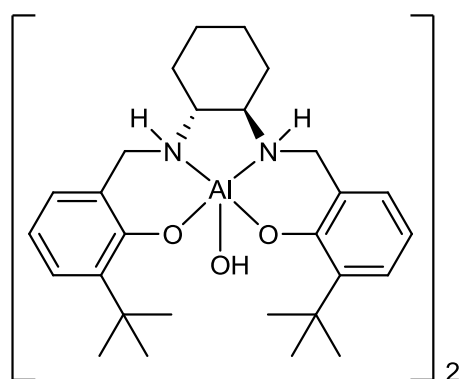
Figure 3.16 ChemDraw representation of {[(*R,R*)-*t*Bu-Salcyan]Al(OH)}₂ used as the basis of Gaussian DFT calculations.

GaussView 4.1.2 was used to set up the DFT calculation parameters which would subsequently be carried out using Gaussian 03 *via* the White Rose Grid and/or Gaussian 09 *via* the National Service for Computational Chemistry Software at Imperial College London. GaussView 4.1.2 is used as a pre- and post-processor and could also be used to run Gaussian calculations; however one needs a considerable amount of memory and processing power for calculations such as these on systems with 70+ atoms.

As with all computational software packages geometry optimisation is always carried out on a molecule before conducting advanced calculations. In the case of {[(*R,R*)-*t*Bu-

Salcyan]Al(OH)}₂ this was no exception, an energy minimisation calculation using RHF 6-31G(*) was obtained followed by a geometry optimisation using DFT B31LYP/6-31G(*). Once optimisation was complete the results were viewed and the angles and bond distances measured and compared to those from the original X-ray data.

3.5.2 {(*R*,*R*)-[Salcyan(ᵗBu)₂]Al(μ-OH)}₂

(a)

(b)

(c)

(d)

(e)
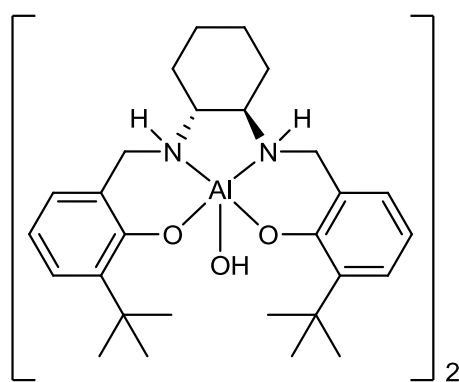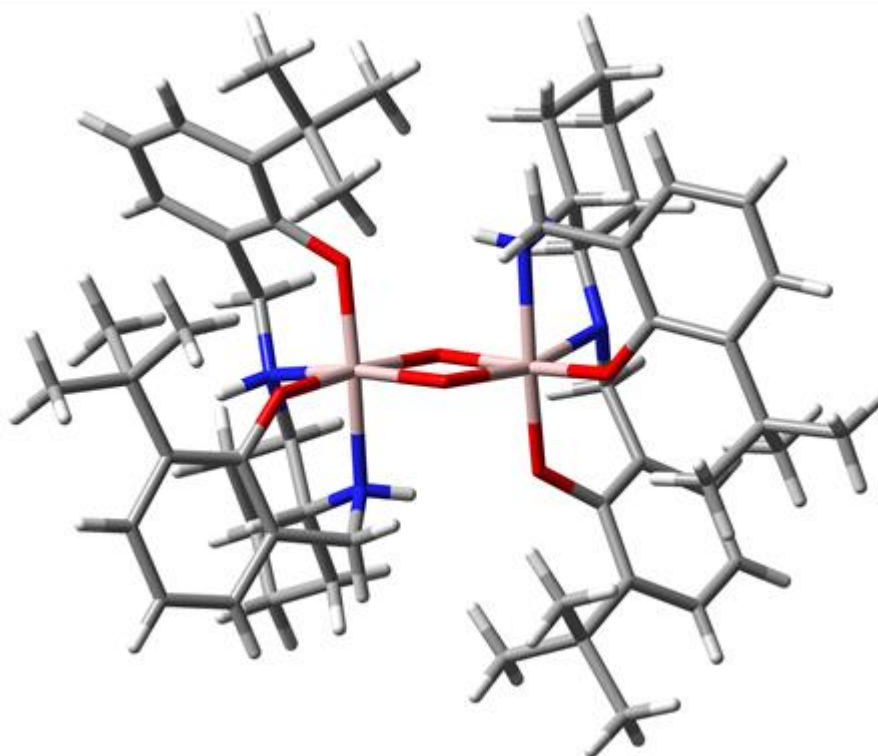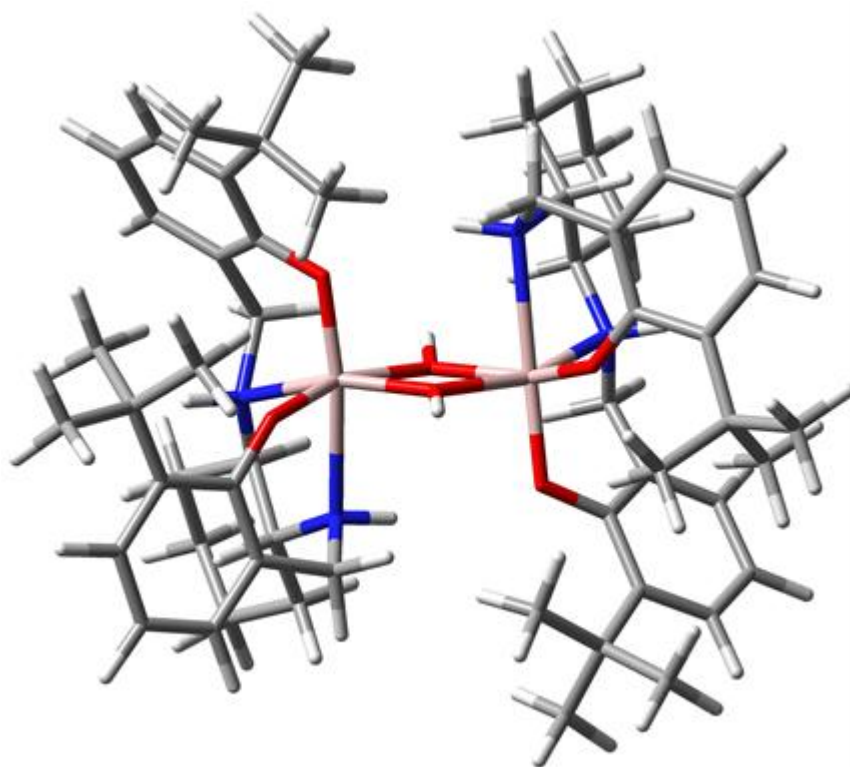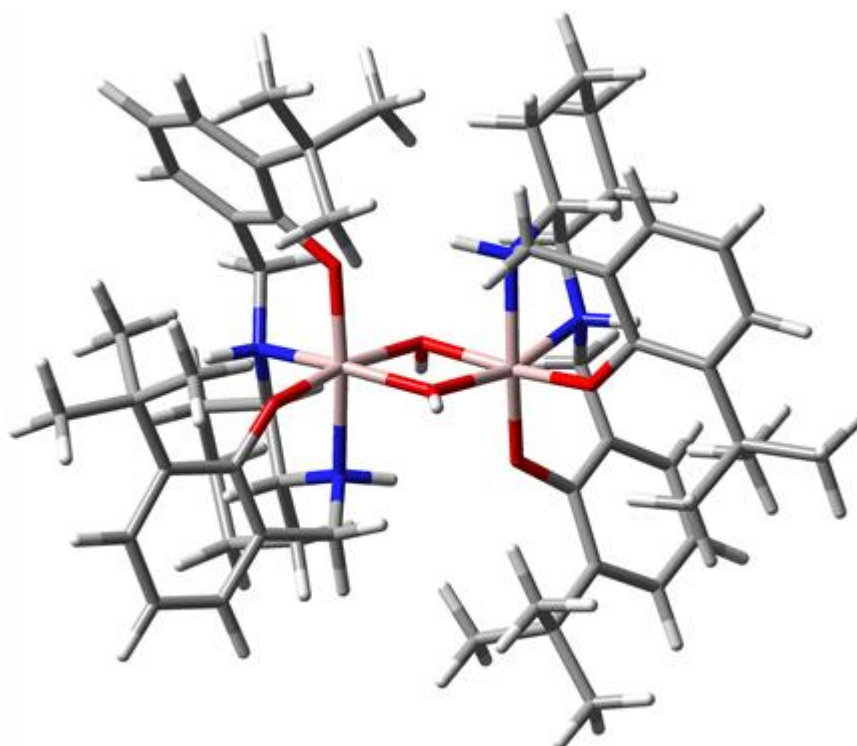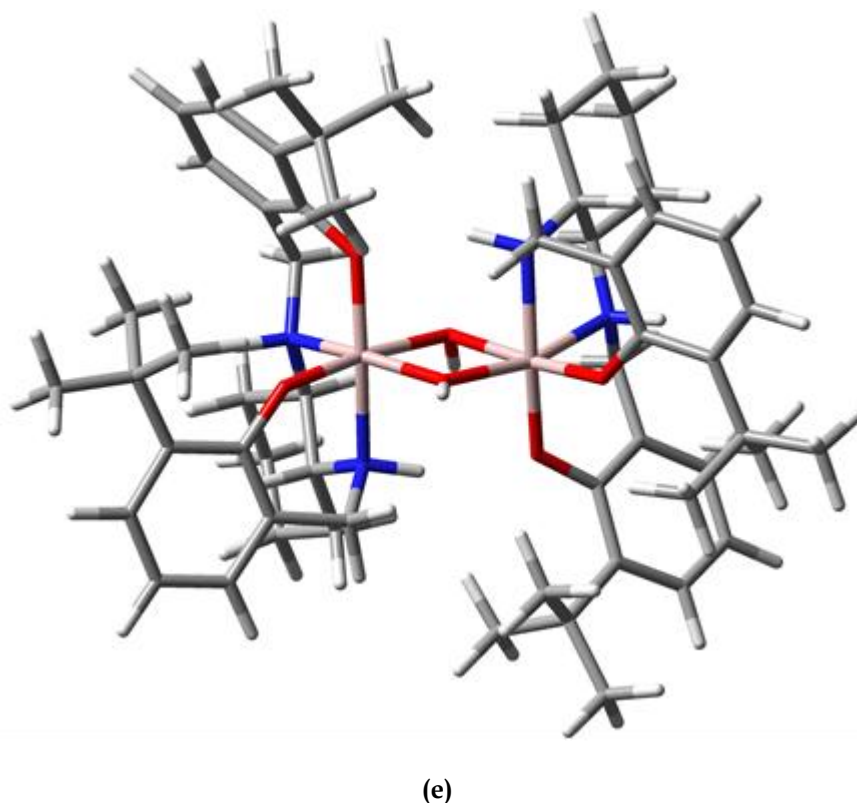
Figure 3.17 (a) ChemDraw schematic of {(*R,R*)-[salcyan(ᵗBu)₂]Al(μ-OH)}₂, (b) original X-ray structure, (c) structure of complex calculated at semi-empirical PM3 level, (d) structure of complex calculated with geometry optimisation at RHF 6-31G* and (e) structure of complex calculated to a geometry optimised at the DFT B31LYP/6-31G* level.

The original X-ray structure Figure 4.2 **(b)** reveals a dimer containing two octahedral six-coordinate aluminium centres.   Each metal centre is surrounded by one tetradentate salcyan ligand and bridged by two hydroxyl fragments. Only one of the *tert*-butyl groups per ligand lies over the metal coordination site, in the 3′ (proximal) position of the phenolic ring. The *tert*-butyl groups on each ligand do not interact with each other.
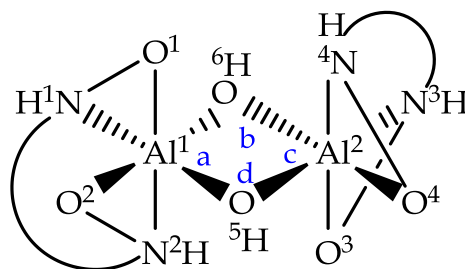
Figure 3.18 Atom numbering for {(R,R)-[salcyan(tBu)$_2$]Al(μ-OH)}$_{2.=}$

Interatomic Distances	X-Ray Structure **(b)** Interatomic Distance Å	PM3 Structure **(c)** Interatomic Distance Å	HF Structure **(d)** Interatomic Distance Å	DFT Structure **(e)** Interatomic Distance Å
Al$_1$ - O$_5$ *trans* N$_1$	1.87	1.87	1.87	1.89
Al$_1$ - O$_6$ trans O$_2$	1.94	1.96	1.95	1.99
Al$_2$ - O$_5$ *trans* N$_3$	1.85	1.87	1.88	1.91
Al$_2$ - O$_6$ trans O$_4$	1.93	1.93	1.93	1.97
Al$_1$ - O$_1$	1.84	1.84	1.85	1.88
Al$_1$ - N$_1$	2.08	2.08	2.09	2.12
Al$_1$ - O$_2$	1.85	1.85	1.82	1.85
Al$_1$ - N$_2$	2.08	2.08	2.08	2.14
Al$_2$ - N$_4$	2.08	2.08	2.09	2.11
Al$_2$ - N$_3$	2.10	2.10	2.10	2.13
Al$_2$ - O$_4$	1.84	1.84	1.83	1.85
Al$_2$ - O$_3$	1.85	1.85	1.85	1.89

Table 3.1 Data for the interatomic bond lengths (Å) for the metal to ligand coordination of {(R,R)-[salcyan(tBu)$_2$]Al(μ-OH)}$_2$.

Interatomic Distances	X-Ray (b) Bond Angles (deg)	PM3 (b) Bond Angles (deg)	HF (b) Bond Angles (deg)	DFT (b) Bond Angles (deg)
Ax O1-N2	170.46	167.35	168.36	170.04
Ax O3-N4	169.14	175.71	166.18	167.27
Eq N1-O5	163.49	158.04	164.38	162.84
Eq O2-O6	175.34	159.24	173.19	172.70
Eq N3-O5	163.89	161.08	164.98	163.94
Eq O4-O6	173.63	153.08	171.99	172.45
N1-O2	94.72	92.55	94.12	93.22
N3-N4	79.34	76.98	78.87	79.97
a	76.53	64.03	74.94	75.85
b	100.94	114.66	101.88	100.98
c	76.45	63.19	75.37	76.19
d	106.08	118.09	107.82	106.97

Table 3.2 Data for the interatomic bond angles (°) for the metal to ligand coordination of {(*R,R*)-[salcyan(^{t}Bu)$_2$]Al(μ-OH)}$_2$.

3.6 Conclusions of the Validation Study

A large amount of data has been collected on {(*R,R*)-[salcyan(^{t}Bu)$_2$]Al(μ-OH)}$_2$, which can be seen in Table 3.1 and Table 3.2. These data have been collected in order to validate our original molecular modelling studies. The original modelling studies were carried out using HyperChem 7.0 software using calculations at the molecular mechanics (Mm+) and semi-empirical (PM3) levels. These simple calculations provided us with a quick and simple way of creating and editing a library of salcyan ligands and complexes. However, one must be confident that these lower level modelling studies have value by bench-marking them against high level geometry optimisation methods (DFT).

With these issues in mind three different molecular modelling methods on the complex {(*R,R*)-[salcyan(ᵗBu)$_2$]Al(μ-OH)}$_2$. Once the three computational methods had finished, a variety of interatomic properties (bond distances and bond angles) were analysed and compared with those obtained from the original single-crystal X-ray data.

Even bearing in mind the fact that the same input set has been used in each case, the single crystal X-ray data, it is interesting just how similar the overall structures remain post-modelling and how comparable each set of data is to each other, in particular the interatomic bond distances. With regards to interatomic bond angles there are slight differences between each computational method. It is clear to see from Table 3.1 that the interatomic bond distances of the X-ray data and those of the PM3 calculation are extremely similar. This is also true for the HF and DFT calculations, however it isn't until the angles were that small differences were identified between each data set, especially around the hydroxy bridge. This shows that not only is it important to compare bond distances, it is also necessary to compare the bond angles. Indeed looking at the images (Figure 4.2) one can see that as you go from X-ray to PM3 to RHF and finally to DFT it is difficult to see any major changes in the structures. The only apparent change is the bending of the hydrogen of the hydroxy bridge.

For future computational work it is possible to conclude that HyperChem semi-empirical calculations make a good comparison with the original X-ray data and can be used with some reasonable sense of confidence as a quick study to screen complexes as potential precursors in phospho-aldol catalysis. In particular, the core structure should be reasonably well modelled by semi-empirical methods which should allow distal ligand substituent modifications to be made and modelled by semi-empirical methods, again with some confidence that they may represent a reasonable picture of the steric field surrounding the metal centres. However for more accurate information, for example regarding electronic data, Gaussian HF or DFT are better methods.

The one foreseeable problem in using X-ray data as an input file to the computational programmes, performing calculations on it and then comparing the output data with the original X-ray data, is that one might expect the output to be broadly similar to the X-ray data because the two (X-ray and calculation) are not independent. In order to be fully confident in these validation results it would be necessary to manually input the same salcyan complex as those of the single crystal X-ray data and perform the same level of calculations (PM3, HF and DFT). This process was attempted but the stereochemical complexity made the process too difficult and imprecise.

3.7 Computational studies towards understanding the mechanism of the PA reaction

As discussed so far in this chapter the validation study showed that using semi-empirical methods could provide a quick way of screening complexes as potential precursors for the phospho-aldol reaction. With these results in mind the next stage in computational calculations was regarding the theory on the catalytic mechanism of the PA reaction with respect to the library of complexes thus far collected.

As discussed previously in Chapter 1 the currently accepted working hypothesis for the mechanism of the PA reaction *via* complexes of the form {(R,R)-[salcyan(R)$_2$]Al(μ-OH)}$_2$ involves cleavage of at least one of the hydroxyl functions with the resulting formation of a phosphito intermediate (Scheme 3.3). This phosphito complex is then envisaged to coordinate a carbonyl substrate so that the key [P-C] bond forming step is able to occur within a single metal coordination sphere.
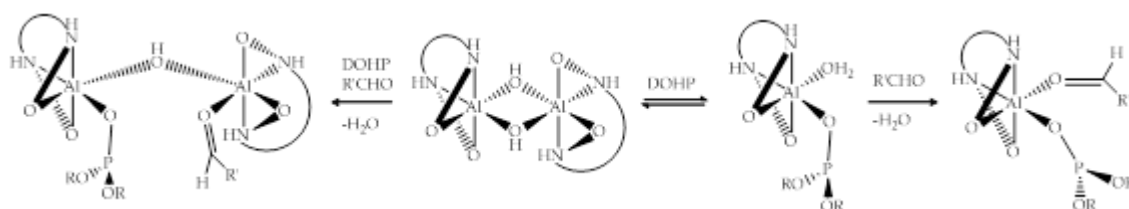
Scheme 3.3 Suggested role of {(R,R)-[salcyan(R)$_2$]Al(μ-OH)}$_2$ in phospho-aldol catalysis. [13]

H/D exchange studies [9] demonstrate that deprotonation of DMHP is an important step of the reaction and our initial hypothesis was that it is the bridging OH that is responsible, however what proceeds will indicate to a different hypothesis.

3.7.1 Experimental evidence towards the mechanism of the PA reaction

Within the Kee group it was established that aluminium salcyan complexes remain in their dimeric form in both the solid state (X-ray) and in solution phase, by NMR spectroscopy. Further probing as to whether any form of dissociation took place when in solution, was also undertaken. 2-D Diffusion ordered spectroscopy studies were carried out on the complex of $\{(R,R)$-[salcyan(^{t}Pn)$_2$]Al(μ-OH)$\}_2$, using $\{(R,R)$-[salcyan(^{t}Bu)$_2$]Al(μ-OSiMe$_3$)$\}$ a known monomeric compound as the reference compound, in order to confirm whether $\{(R,R)$-[salcyan(^{t}Pn)$_2$]Al(μ-OH)$\}_2$ was dimeric or monomeric in solution. [9] The calculated and observed diffusion coefficients for the reference compound were found to be in close agreement and observed diffusion coefficients for $\{(R,R)$-[salcyan(^{t}Pn)$_2$]Al(μ-OH)$\}_2$, were clearly compatible with a dimeric formulation. [9]

Solid state analyses were performed on a selection of single crystal X-ray structures to better understand their framework and thus build upon the mechanistic theory.

An underlying question that needed investigating was if there was something within the crystal structures that could give us an insight into the mechanism of the reaction?

Upon examination of the single crystal structures of a number of complexes of the form $\{(R,R)$-[salcyan(R)$_2$]Al(μ-OH)$\}_2$ (R = ^{t}Bu, ^{t}Pn, SiMe2Ph, mes), it was clear to see that the aluminium dimers possessed an 'open' face and a 'closed' face. Hydrogen bond interactions between the hydroxyl bridge and solvent were observed at the open face, whilst the closed face remained unchanged (Figure 3.19). [9]
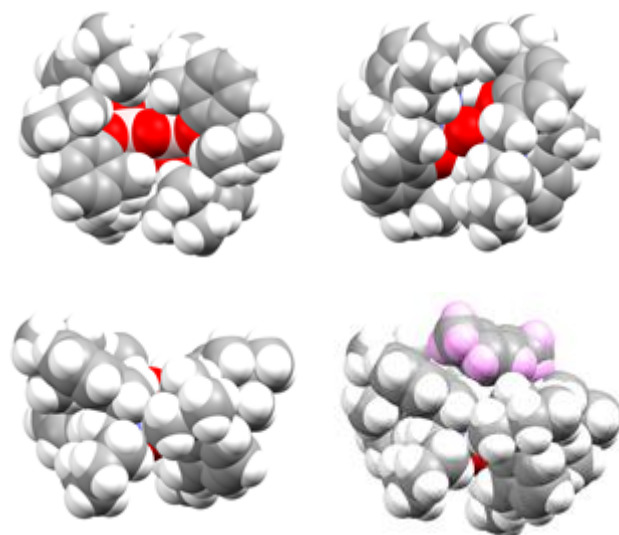
Figure 3.19 Four space filling views emphasising the more open (*top left*) and closed (*top right*) cavities surrounding the Al_2O_2 bridge region of $\{(R,R)\text{-[salcyan(}^tBu)_2]Al(\mu\text{-OH})\}_2$. A side-view (*bottom left*) of $\{(R,R)\text{-[salcyan(}^tBu)_2]Al(\mu\text{-OH})\}_2$ emphasises the rather shallow nature of the open cavity whilst a similar view of $\{(R,R)\text{-[salcyan(}^tPn)_2]Al(\mu\text{-OH})\}_2$ (*bottom right*) reveals that this open cavity is capable of hosting small molecules, in this case a disordered toluene molecule (whose hydrogen atoms are outlined in pink for emphasis). [9]

Interestingly in the case of $\{(R,R)\text{-[salcyan(SiMe}_2Ph)_2]Al(\mu\text{-OH})\}_2$ both sides of the molecule appeared to be equally accessible and thus resulted in hydrogen bonding being observed between the hydroxyl groups and THF at both sides of the complex. [14]
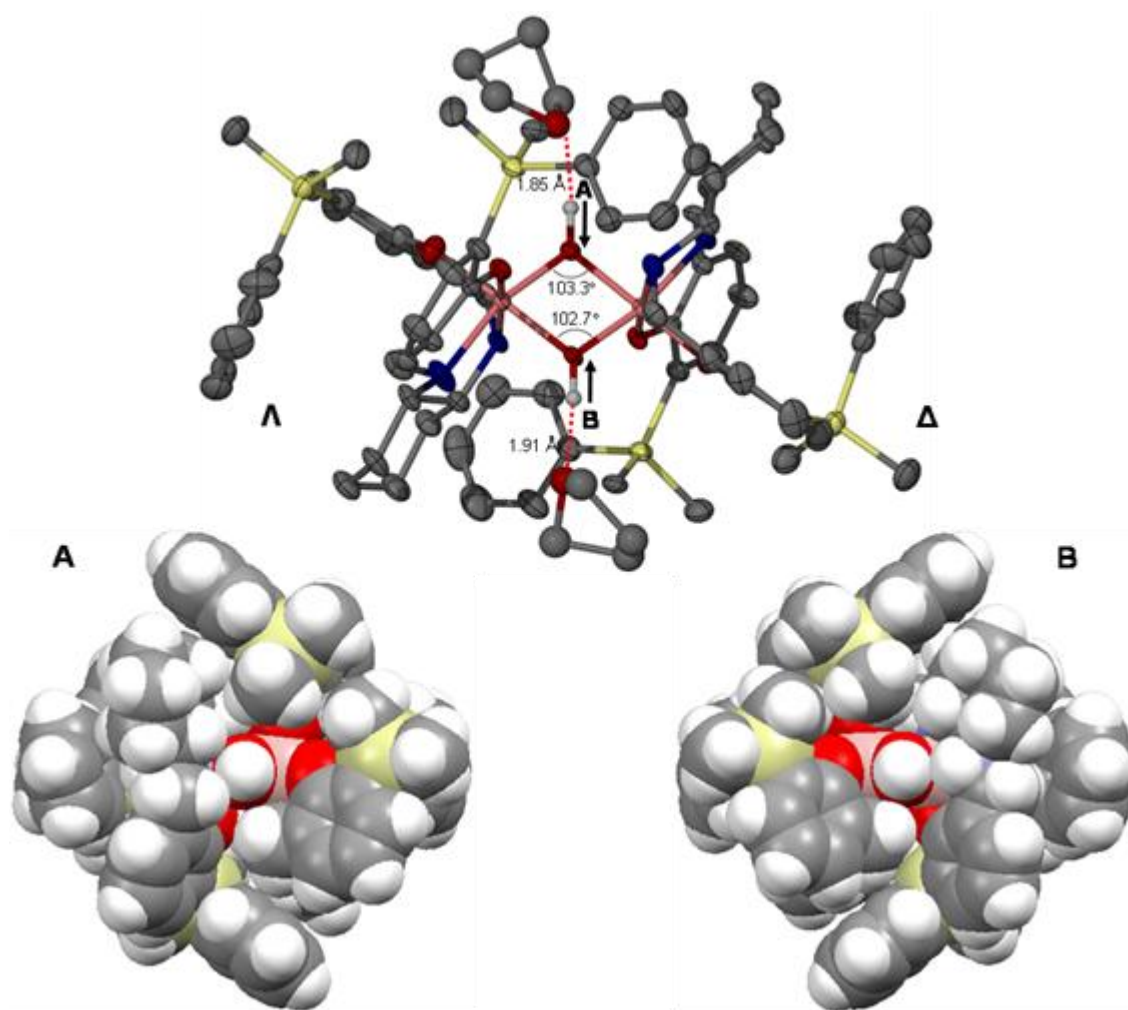
Figure 3.20 Space filling views of {(*R*,*R*)-[salcyan(SiMe₂Ph)₂]Al(*μ*-OH)}₂ obtained from THF showing opposite faces. [14]

With this evidence in mind it was now necessary to determine which site in the complex was the most basic and would act as a base in the mechanistic scheme. The most obvious site that comes to mind is the hydroxyl bridging group occupying the open face of the molecule. Is this true? Computational studies have been carried out to determine that most basic site of the complex and will be discussed further.

3.8 Geometry optimisation calculations

Geometry optimisation calculations were carried out on a selection of single crystal X-ray data of aluminium salcyan complexes of the forms $\{(R,R)\text{-[salcyan(R)}_2]Al(\mu\text{-OH})\}_2$ and $\{(R,R)\text{-[salcyan(R)}_2]Al(\mu\text{-OMe})\}_2$ (R = ^{t}Bu, ^{t}Pn, SiMe2Ph, mes). The calculations were carried out with the Gaussian 03, revision C.02 [12] program using restricted Hartree Fock (RHF) with a 6-31G* basis set.

The purpose of the study was to delineate the molecular orbitals of the system, specifically the highest occupied molecular orbital (HOMO) of each of the selected complexes. By knowing the distribution of electron density over the HOMO we will hopefully be able to suggest the most likely identity of the most basic site of the complex and conclude where deprotonation of DMHP could take place.

3.8.1 Molecular orbitals and electron density

For each selected aluminium salcyan complex the molecular orbital energies were collected and are presented in summary
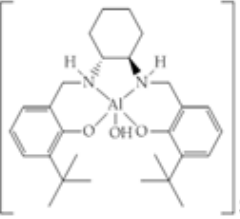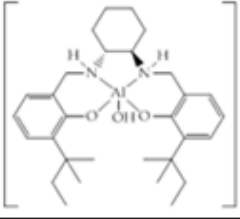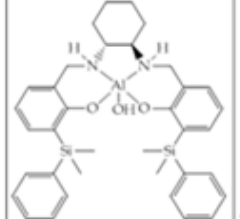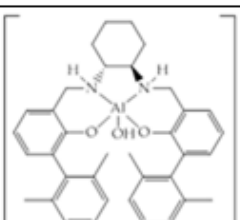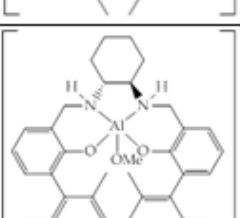
Structure	Molecular Orbital	Eigenvalue (a.u.)	Electron Volts (eV)	Energy (kcal mol^{-1})	Difference (kcal mol^{-1})	
	261	0.03809	1.0365	23.902	-196.17	L
	260	-0.27452	-7.4702	-172.264	0	H
	259	-0.27593	-7.5086	-173.149	0.88	H-1
	277	0.03911	1.064	24.542	-194.02	L
	276	-0.27008	-7.349	-169.478	0	H
	275	-0.27034	-7.356	-169.641	-0.163	H-1
	341	0.04707	1.281	29.537	-200.326	L
	340	-0.27217	-7.406	-170.789	0	H
	339	-0.27409	-7.459	-171.994	-1.205	H-1
	325	0.03777	1.028	23.701	-196.712	L
	324	-0.27571	-7.503	-173.011	0	H
	323	-0.27616	-7.515	-173.293	-0.282	H-1
	333	0.04968	1.352	31.175	-198.017	L
	332	-0.26588	-7.235	-166.842	0	H
	331	-0.26985	-7.343	-169.334	-2.491	H-1

Table 3.3. The data corresponding to the LUMO, HOMO and HOMO-1 of each complex are the most interesting and it is these results that will be the main focus of the rest of this chapter.

The full set of data tables containing a wider selection of energy values for each aluminium salcyan complex can be viewed in appendices (vi) to (x).
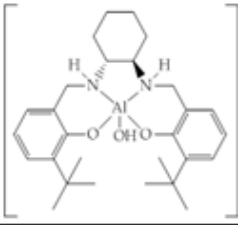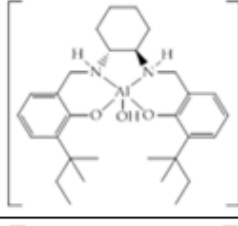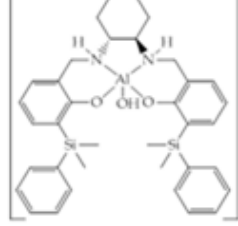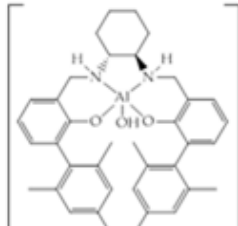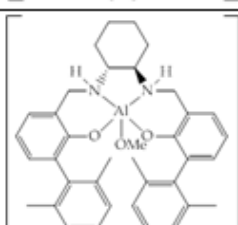
Structure	Molecular Orbital	Eigenvalue (a.u.)	Electron Volts (eV)	Energy (kcal mol^{-1})	Difference (kcal mol^{-1})	
	261	0.03809	1.0365	23.902	-196.17	L
	260	-0.27452	-7.4702	-172.264	0	H
	259	-0.27593	-7.5086	-173.149	0.88	H-1
	277	0.03911	1.064	24.542	-194.02	L
	276	-0.27008	-7.349	-169.478	0	H
	275	-0.27034	-7.356	-169.641	-0.163	H-1
	341	0.04707	1.281	29.537	-200.326	L
	340	-0.27217	-7.406	-170.789	0	H
	339	-0.27409	-7.459	-171.994	-1.205	H-1
	325	0.03777	1.028	23.701	-196.712	L
	324	-0.27571	-7.503	-173.011	0	H
	323	-0.27616	-7.515	-173.293	-0.282	H-1
	333	0.04968	1.352	31.175	-198.017	L
	332	-0.26588	-7.235	-166.842	0	H
	331	-0.26985	-7.343	-169.334	-2.491	H-1

Table 3.3 Summary table of molecular orbital data of the five aluminium salcyan complexes of the forms {(*R,R*)-[salcyan(R)$_2$]Al(μ-OH)}$_2$ and {(*R,R*)-[salcyan(R)$_2$]Al(μ-OMe)}$_2$ (R = *t*Bu,

^{t}Pn, SiMe2Ph, mes), collected from optimisation calculations carried out to RHF level using 6-31G* as a basis set. L = LUMO, H = HOMO and H-1 = HOMO-1.

One of the most important questions that have been answered by these calculations is regarding the location of the most basic site of the complex. When looking at the GaussView representations of the HOMO molecular orbital of each complex, it is clear to see that the HOMO lies on the ring of the O-Ar unit, rather than on the bridging hydroxyl oxygen atoms as first theorised.
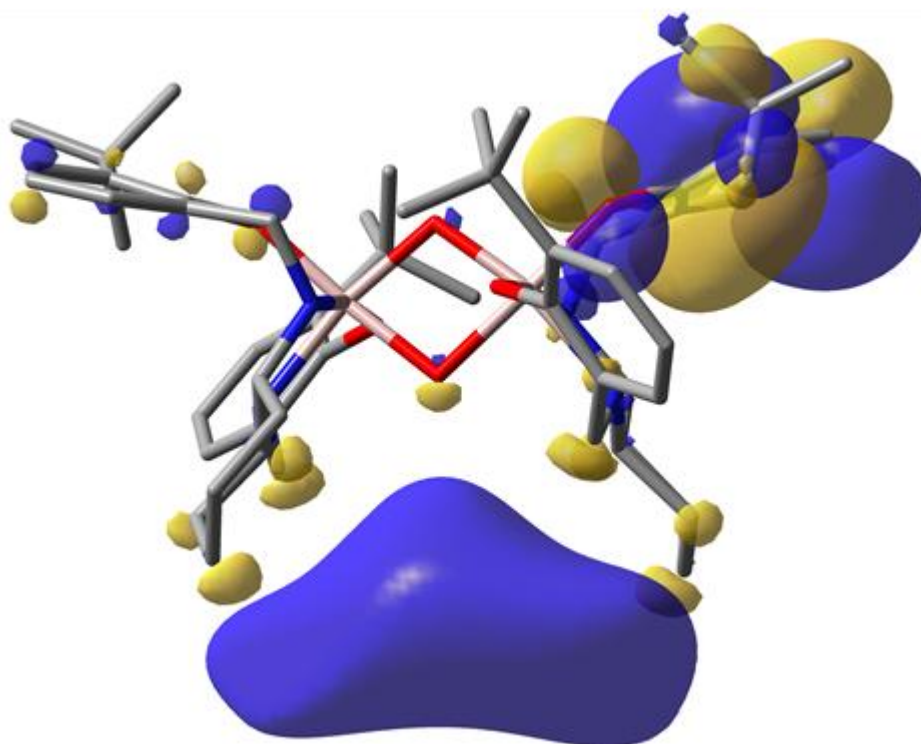
Figure 3.21 GaussView representation of MO-260 (HOMO) and MO-261 (LUMO) of {[(*R,R*)-^{t}Bu-salcyan]Al(μ-OH)}$_2$.
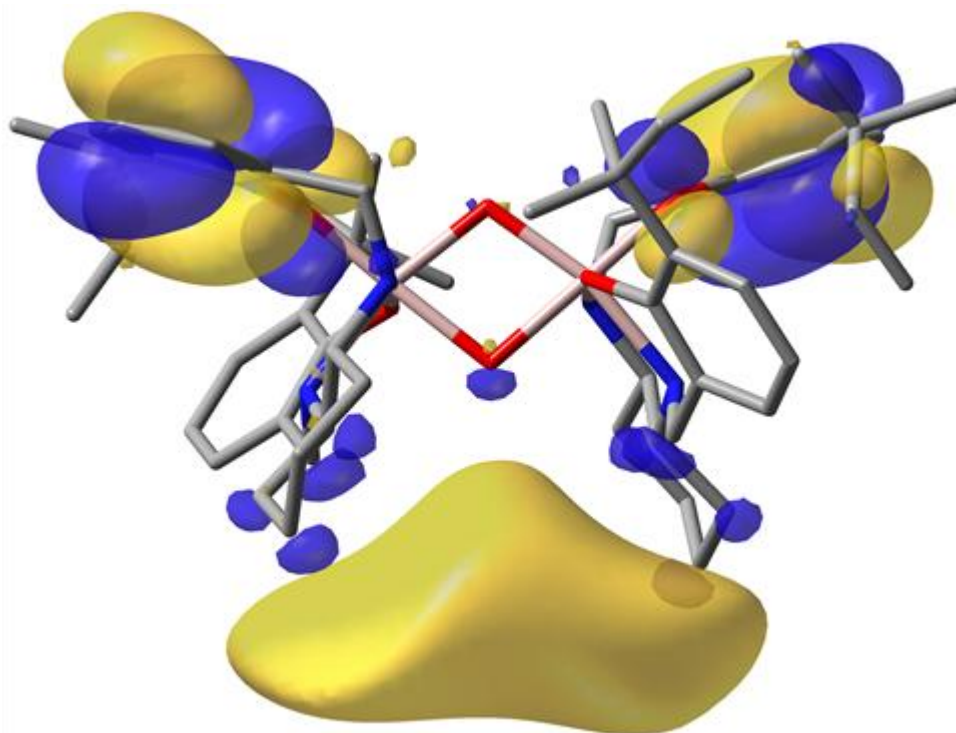
Figure 3.22 GaussView representation of MO-276 (HOMO) and MO-277 (LUMO) of {[(*R*,*R*)-*t*Pn-salcyan]Al(*μ*-OH)}₂.
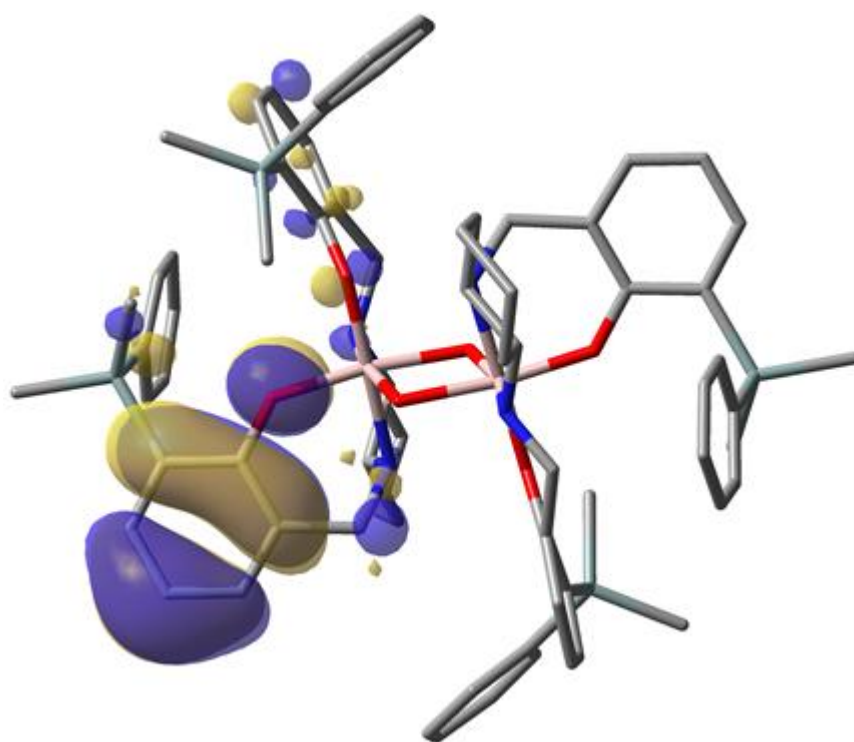
Figure 3.23 GaussView representation of MO-340 (HOMO) of {[(R,R)-SiMe2Ph-salcyan]Al(μ-OH)}2.
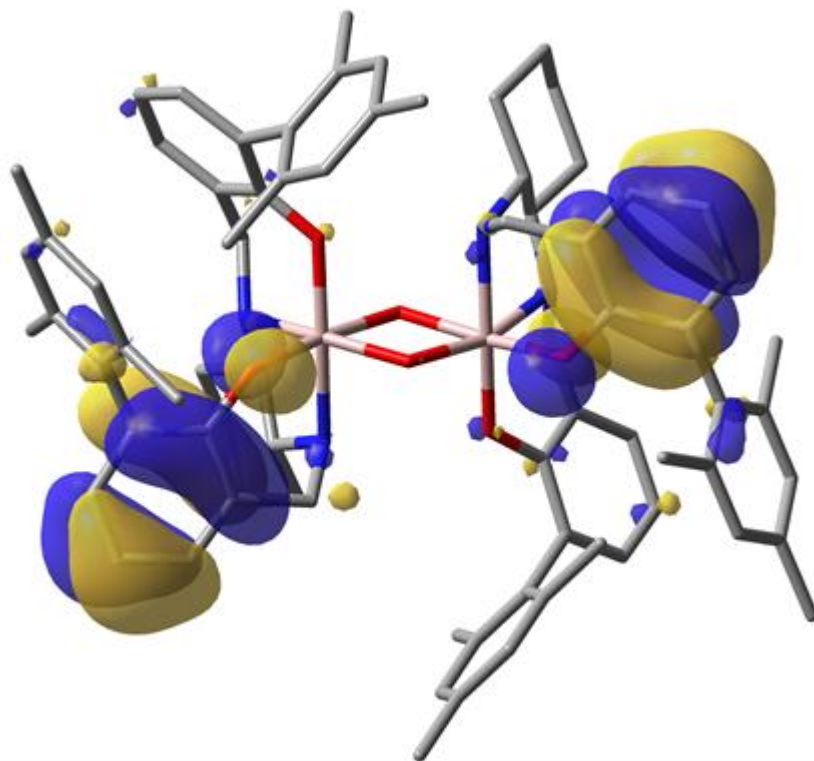
Figure 3.24 GaussView representation of MO-324 (HOMO) of {[(R,R)-mes-salcyan]Al(μ-OH)}2.
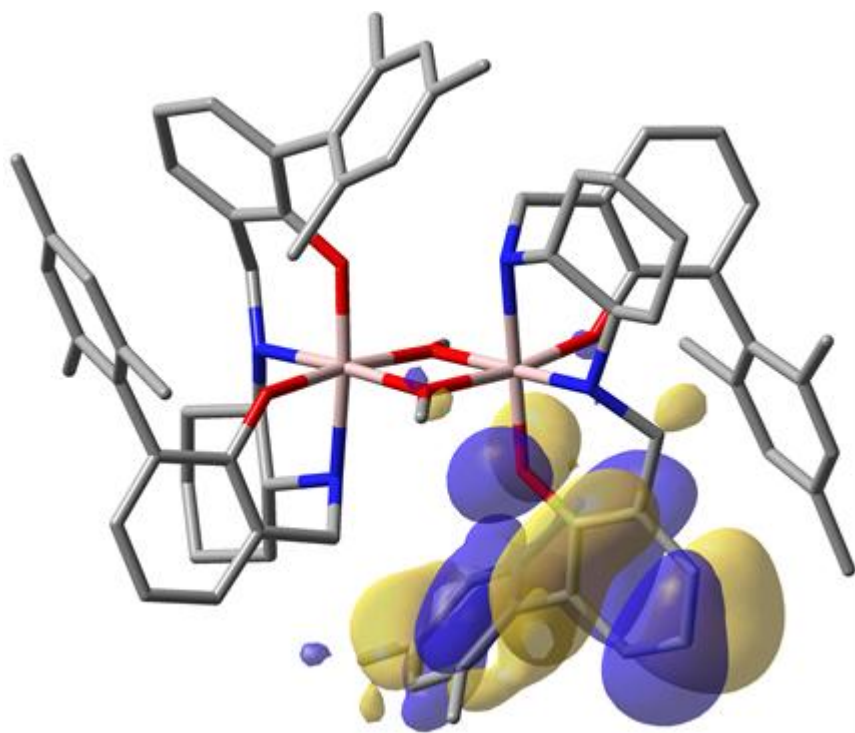
Figure 3.25 GaussView representation of MO-332 (HOMO) of {[(R,R)-mes-salcyan]Al(μ-OMe)}2.

In light of all the experimental (H/D exchange, solid state NMR analysis and 2D-diffusion ordered spectroscopy studies) and computational evidence the picture for PA catalysis can now be modified, as shown in Scheme 3.4.
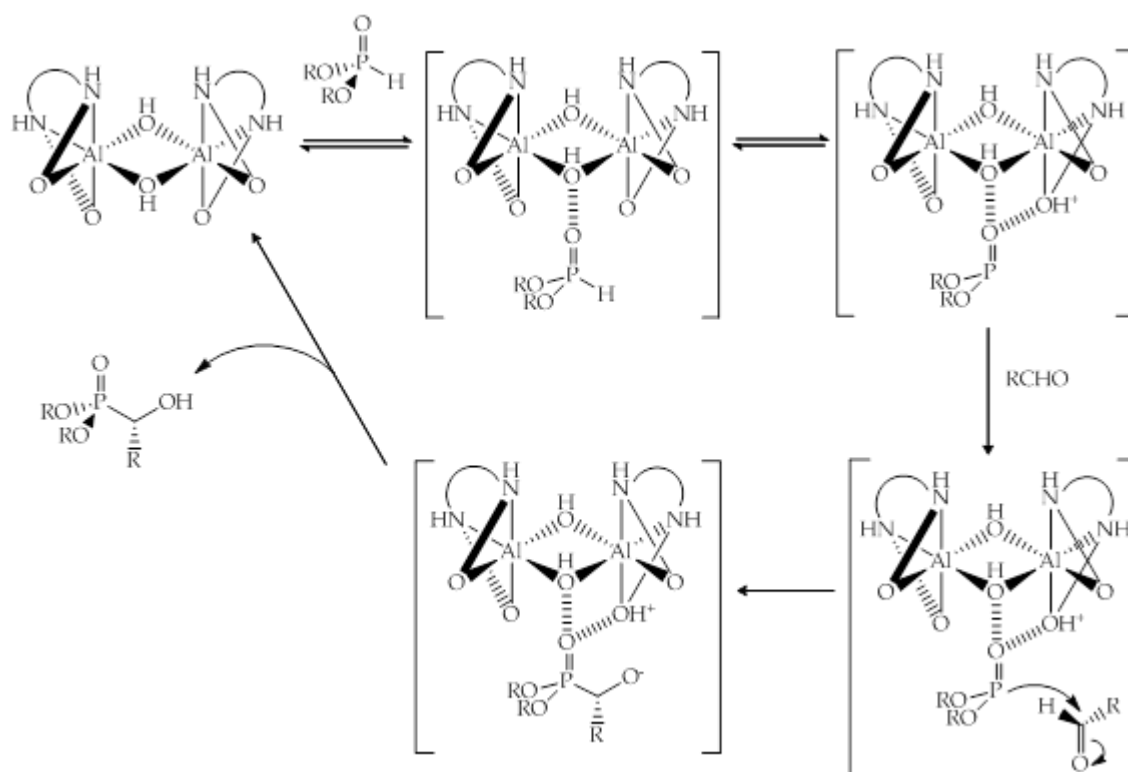
Scheme 3.4 Modified mechanistic outline for PA catalysis *via* dimeric aluminium salcyan complexes. [9]

The mechanism can be described as the initial approach of diorgano-H-phosphonate to the aluminium dimer in solution affording an H-bonded stabilised adduct at the open face of the dimer. [9] We envisage that benzaldehyde may act similarly towards H-bonding at this open face, but such binding would be expected to be reversible. The adduct subsequently undergoes a degree of proton transfer at the open cavity of the aluminium dimer to afford either a salt or strongly charged separated complex, bound *via* H-bonding and/or electrostratic interactions within the cavity, releasing significant electron density at the phosphorus centre. [15] Subsequent [P-C] bond formation followed by proton transfer and release of the phosphonate ester product completes the cycle. [9]

In addition to locating the most basic site of the complex it was also possible to better understand the structure of each aluminium salcyan complex. Solid state NMR studies have already pointed out a few interesting aspects of the structures, the main point of interest being the appearance of 'open' and 'closed' faces. Whilst analysing the molecular orbital data through electron density maps it was possible to see clearly C_2 symmetry in some of the complexes, namely $\{[(R,R)\text{-}^tBu\text{-salcyan}]Al(\mu\text{-OH})\}_2$ (Figure 3. 26), $\{[(R,R)\text{-}^tPn\text{-salcyan}]Al(\mu\text{-OH})\}_2$ (Figure 3.27) and $\{[(R,R)\text{-mes-salcyan}]Al(\mu\text{-OH})\}_2$ (Figure 3.29). In the cases of $\{[(R,R)\text{-SiMe}_2Ph\text{-salcyan}]Al(\mu\text{-OH})\}_2$ (Figure 3.28) and $\{[(R,R)\text{-mes-salcyan}]Al(\mu\text{-OMe})\}_2$ (Figure 3.30) the 'open' and 'closed' cavities are not so obviously defined and appear 'open' on both sides.

(a)   **b)**
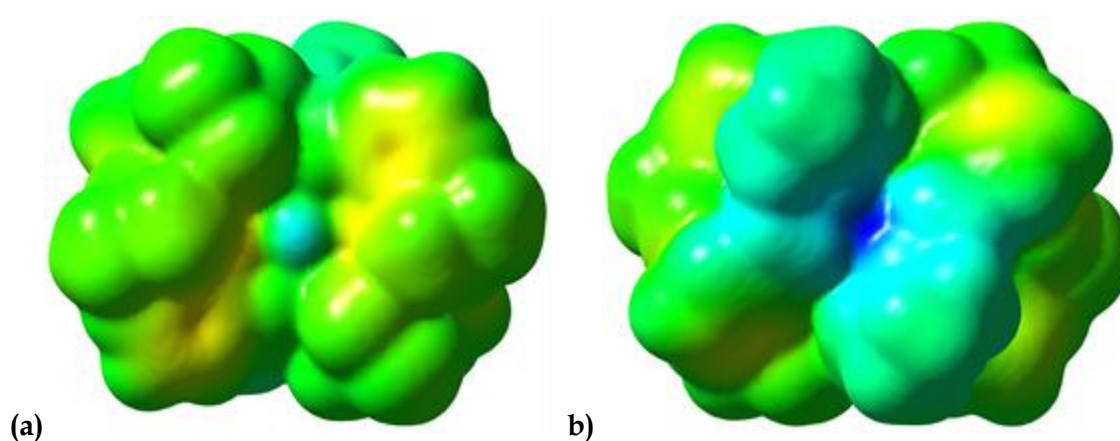
Figure 3. 26 GaussView representation of the electron density of $\{[(R,R)\text{-}^tBu\text{-salcyan}]Al(\mu\text{-OH})\}_2$, MO-260 (HOMO), on the 'open' face **(a)** and 'closed' face **(b)** of the complex.

(a)   **b)**
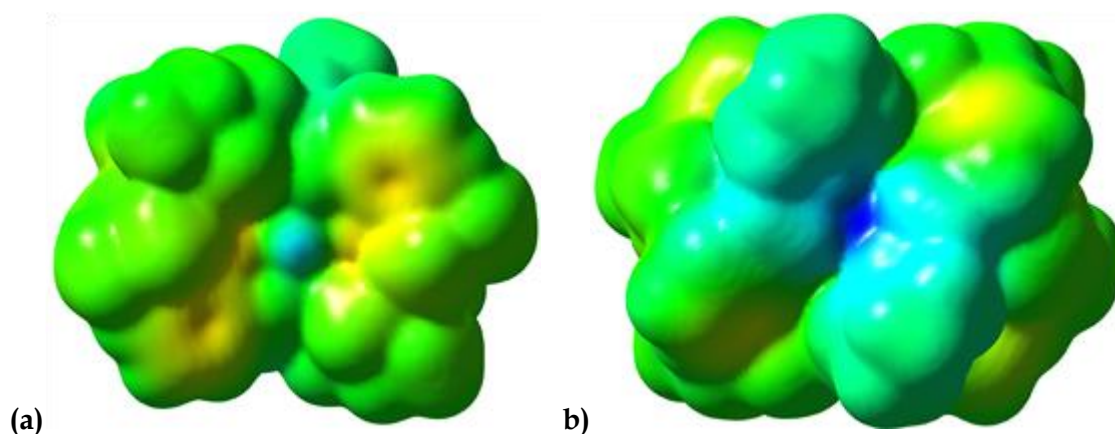
Figure 3.27 GaussView representation of the electron density of $\{[(R,R)\text{-tPn-salcyan}]Al(\mu\text{-OH})\}2$ MO-276 (HOMO), on the 'open' face (a) and 'closed' face (b) of the complex.
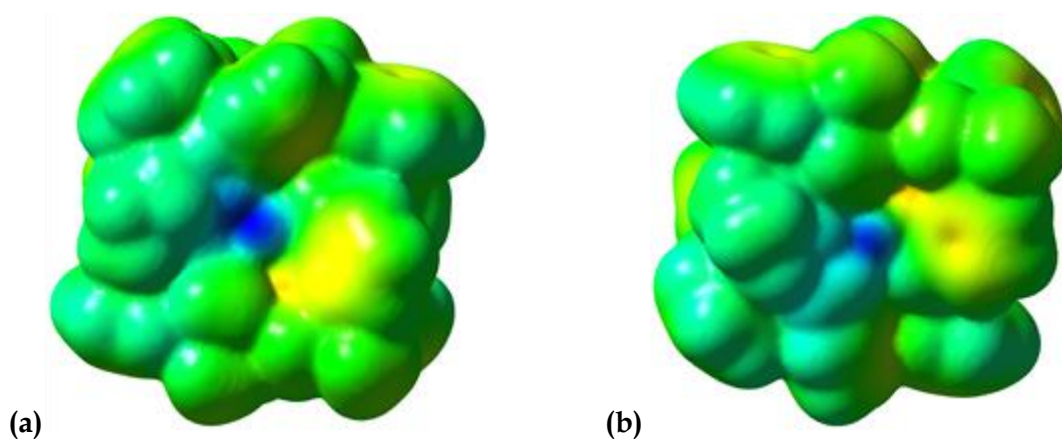
Figure 3.28 GaussView representation of the electron density of {[(R,R)-SiMe2Ph-salcyan]Al(μ-OH)}2, MO-340 (HOMO), on the 'open' face (a) and 'closed' face (b) of the complex.
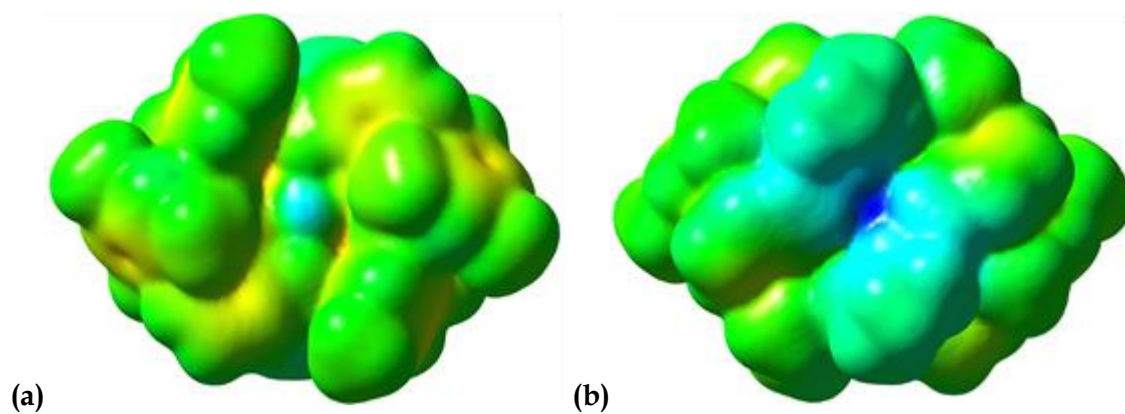
Figure 3.29 GaussView representation of the electron density of {[(R,R)-mes-salcyan]Al(μ-OH)}2, MO-324 (HOMO) on the 'open' face (a) and 'closed' face (b) of the complex.

(a)   (b)
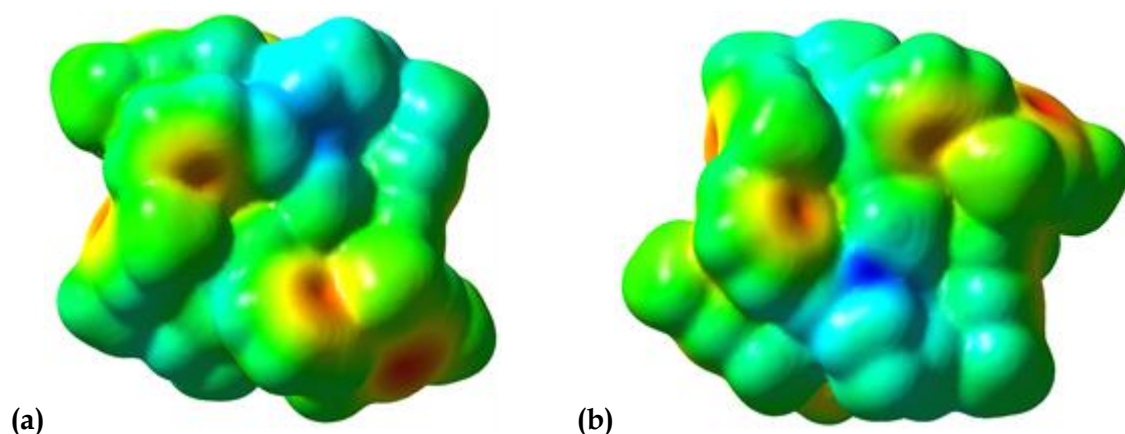
Figure 3.30 GaussView representation of the electron density of {[(R,R)-mes-salcyan]Al(μ-OMe)}2, MO-332 (HOMO) on the 'open' face (a) and 'closed' face (b) of the complex.

3.9 Conclusions of geometry optimised calculations

The geometry optimised calculations of five aluminium salcyan complexes have reaffirmed and answered some of the questions surrounding the mechanism of PA catalysis. Additional computational studies regarding the transition states of the proposed mechanism are being undertaken. Due to time restraints it was not possible for this work to be undertaken and presented in this thesis; however the questions that are envisaged to be answered are how the phosphate binds to the dimer cation? Why the carbonyl shown is not interacting with the metal centre? And how does the intermediate α-hydroxyphosphonate interact with the metal centre?

Now that there is a clearer picture with regards to the mechanism and how the structure of the aluminium salcyan complexes can affect the catalytic outcome with respect to the enantiomeric excess. The framework of the aluminium salcyan complexes can be used and built upon to create a more asymmetric open face, which could lead to the synthesis and catalytic testing of a complex that affords reasonable e.e.s (>85%) on most carbonyl substrates. It is envisaged that the important [P-C] bond forming step would occur at the intermediate phosphate complex and this would involve the open face.

Chapter 4 will present a more detailed discussion of the selected target molecules as catalysts with respect to a new aluminium salcyan system using the information gained from the computational and experimental studies.

3.10 References

[1]   J. B. Foresman, Æ. Frisch, *Exploring Chemistry with Electronic Structure Methods.*, 2nd *ed.*, Gaussian, Inc, **1996**.

[2]   A. G. Whittaker, A. R. Mount, M. R. Heal, *Instant Notes Physical Chemistry.*, 1st *ed.*, BIOS Scientific Publishers Limited, **2000**.

[3]   (a) J. J. P. Stewart, *J. Comput. Chem.*, **1989**, *10*, 209.

(b) J. J. P. Stewart, *J. Comput. Chem.*, **1989**, *10*, 221.

(c) J. J. P. Stewart, *J. Comput. Chem.*, **1991**, *12*, 320

(d) J. J. P. Stewart, *J. Molecular Modelling.*, **2004**, *10*, 155.

(e) J. J. P. Stewart, *Encyclopaedia of Computational Chemistry.*, Wiley, **1998**.

(f) R. O. Freire, G. B. Rocha, A. M. Simas, *Chem. Phys. Letts.*, **2006**, *425*, 138.

[4]   C. Cramer, *Essentials of Computational Chemistry Theories and Models*, 2nd *ed.*, John Wiley & Sons, Ltd, 2004.

[5]   C. Cramer, *Essentials of Computational Chemistry.*, John Wiley & Sons, Ltd, **2002**.

[6]   F. Jensen, *Introduction to Computational Chemistry.*, John Wiley & Sons, Ltd, **1999**.

[7]   J. C. Slater, *Phys. Rev.*, **1930**, *36*, 57.

[8]   E. Davidson, D. Feller, *Chem. Revs.*, **1986**, *86*, 681.

[9]   A. C. Gledhill, N. E. Cosgrove, T. D. Nixon, C. A. Kilner, J. Fisher, T. P. Kee, *Dalton Trans.*, **2010**, *39*, 9472.

[10]   HyperChem 7.0, Hypercube, Inc. Gainsville, FL, 32601, USA.

[11]   T. D. Nixon, PhD, University of Leeds, 2005.

[12]   M. J. Frisch M. J. Frisch, G.W. Trucks, H. B. Schlegel, G. E. Scuseria,M. A. Robb, J. R. Cheeseman, J. A. Montgomery Jr, T. Verven, K. N. Kudin, J. C. Burant, J.M.Millam, S. S. Iyengar, J. Tomasi, V. Barone, B. Mennucci, M. Cossi, G. Scalmani, N. Rega, G. A.

Petersson, T. Nakatsuji, M. Hada, M. Ehara, K. Toyota, R. Fukuda, J. Hasegawa, M. Ishida, T. Nakajima, Y. Honda, O. Kitao, H. Nakai,M. Klene, X. Li, J. E. Knox, H. P. Hratchian, J. B. Cross, C. Adamo, J. Jaramillo, R. Gomperts, R. E. Stratmann, O. Yazyev, A. J. Austin, R. Cammi, C. Pomelli, J. W. Ochterski, P. Y. Ayala, K. Morokuma, G. A. Voth, P. Salvador, J. J. Dannenberg, V. G. Zakrzewski, S. Dapprich, A. D. Daniels, M. C. Strain, O. Farkas, D. K. Malick, A. D. Rabuck, K. Raghavachari, J. B. Foresman, J. V. Ortiz, Q. Cui, A. G. Baboul, S. Clifford, J. Cioslowski, B. B. Stefanov, G. Liu, A. Liashenko, P. Piskorz, I. Komaromi, R. L. Martin, D. J. Fox, T. Keith, M. A. Al-Laham, C. Y. Peng, A. Nanayakkara, M. Challacombe, P. M. W. Gill, B. Johnson, W. Chen, M. W. Wong, C. Gonzalez, J. A. Pople, *Gaussian 03*, Revision C.02, Gaussian, Inc., Wallingford CT, 2004.

[13]   C. V. Ward, M. L. Jiang, T. P. Kee, *Tetrahedron Letts.*, **2000**, *41*, 6181.

[14]   A. C. Gledhill, *PhD.*, University of Leeds, **2009.**

[15]   J. Lewinskia, J. Zacharaa, I. Justyniakb, M. Dranka, *Coord. Chem. Rec*, **2005**, *249*, 1185.

Chapter 4

Multifunctional Ligands for PA Catalysis

ERWIN WITH HIS PSI CAN DO
CALCULATIONS QUITE A FEW.
BUT ONE THING HAS NOT BEEN SEEN
JUST WHAT DOES PSI REALLY MEAN.
    WALTER HUCKEL, TRANS. BY FELIX BLOCH

4. 1 Multifunctional ligands towards a PA catalyst

This chapter is divided into two parts. The first half will describe the work originally set out towards designing and synthesising a multifunctional aluminium salcyan complex for PA catalysis. In light of the results of the computational work described in Chapter 3 the project proceeded down a different route, of which this will be discussed further in the second half of the chapter.

4. 2 Bifunctional salcyen catalysts

Recent studies by the DiMauro and Kozlowski groups have shown that multifunctional ligands can possess the necessary properties needed for catalysis and asymmetric synthesis.[1], [2] More specifically DiMauro and Kozlowski detailed the catalytic applications of salcyen metal catalysts with a bifunctional design motif. These characteristics allow for a ligand to have one portion that will engage with a Lewis acid moiety to coordinate an electrophilic substrate, whilst another portion of the ligand is designed to interact with a nucleophilic species. Careful positioning of the catalyst and reactants, taking into account the proximity and geometry can facilitate reaction in a manner resembling enzymes (*e.g.* ligases). The very nature of having a bi-coordinating catalyst automatically enhances the electrophilic and nucleophilic portions of the ligand, Shibasaki and co-workers were one of the first to introduce such a motif, based on a hetero-bimetallic binaphthol framework (Figure 4.4) and exploit it in asymmetric catalysis. [3]

M^1 = La, Sm, Al
M^2 = Li, Na
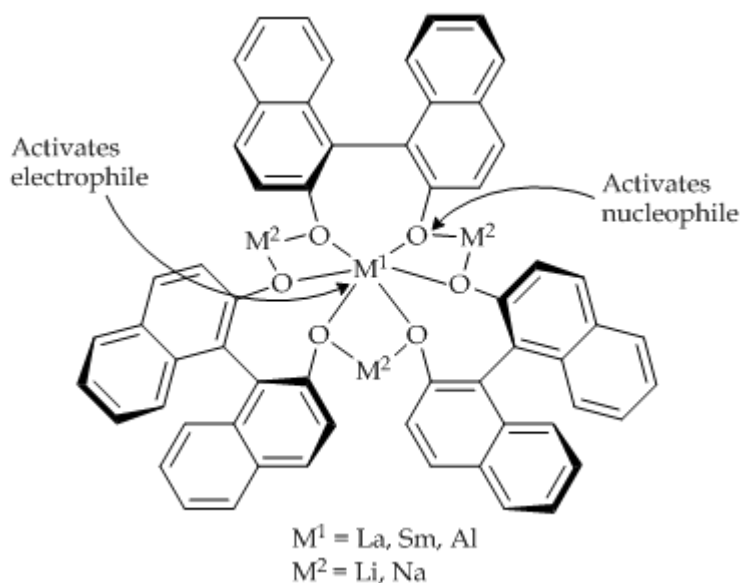
Figure 4.4 Shibasaki and co-workers heterobimetallic motif. [3], [4]

Very few examples of multifunctional catalysts exist. One of the earliest examples was developed by Hayaski and Ito, which catalysed the aldol reaction of isocyanoacetate and aldehydes. [5]
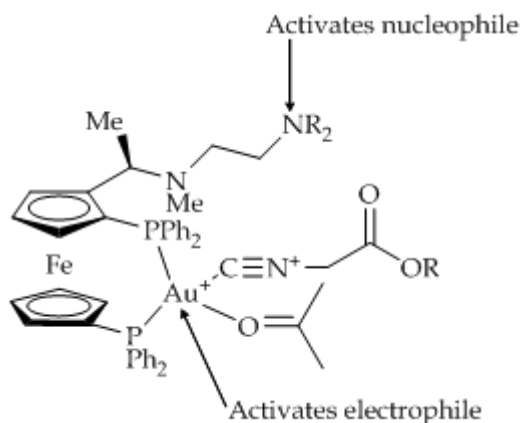
Figure 4.5 Bifunctional species developed by Hayashi and Ito. [4], [5]

The rigid structure of the salen ligand framework is attractive in the context of multifunctional catalysis as derivatisation is relatively straight-forward and various additional functionalities may be built into the scaffold.

4.3 Multimetallic salcyen complexes in phospho-aldol catalysis

Previous research within the Kee group has focused on introducing a Lewis basic functionality, such as a morpholine group, within a chiral salcyen ligand. Overall, the idea was to encourage carbonyl activation at a metal centre coordinated within a chiral salcyen/salcyan ligand field whilst a pendant Lewis basic (morpholine) group could act to deprotonate and hence activate the H-phosphonate reagent in PA catalysis. One key problem with this morpholine system was that upon deprotonation by morpholine, the subsequent phosphito group would be coordinated by only relatively weak hydrogen bonds and hence the catalyst may not have sufficient control over the delivery of the phosphorus reagent to one specific face of a bound carbonyl substrate (Figure 3.3).

Zinc forms part of the d-block metals of the periodic table with a valence configuration of $(n\text{-}1)d^{10}ns^2$, yet in its normal oxidation state of 2+, is effectively $d10$ and therefore not a transition metal. This has valuable implications for bifunctional catalysis as it means ligand field effects, so often observed with transition metals, are not a feature of the Zn^{2+} coordination chemistry. This in turn has a simplifying effect upon the coordination geometries observed.

Thus, if instead of the Lewis basic site within a chiral salcyen framework being based on an organic nitrogen moiety such as morpholine, one used an organometallic fragment based on the metal zinc, the same metal that is proposed for the Lewis acid site, some interesting possibilities emerge. The advantage of using zinc is the fact that it can form four and five-coordinate sites with relative ease, each of which may lend themselves to playing either the Lewis acidic or Lewis basic roles.
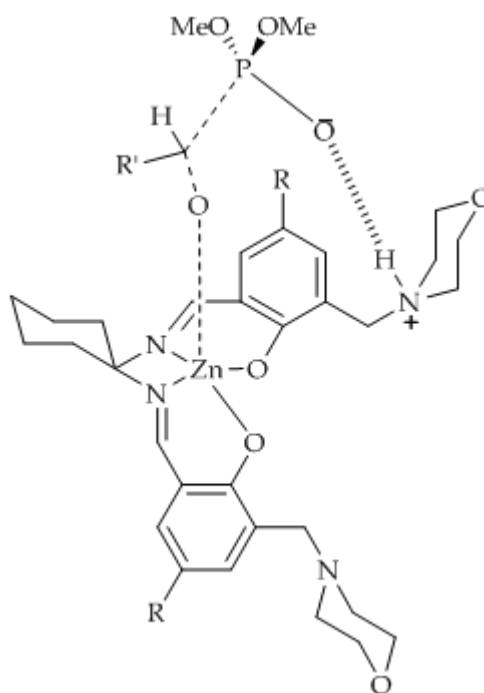
Figure 4.6 Proposed coordination of DMHP and benzaldehyde to salcyen complexes of zinc.

A new design strategy that introduced a homo-bimetallic function was envisaged, whereby the same metal may be introduced in a single step at two different sites; one with Lewis acidic and the other Lewis basic properties (Figure 3.4). The Lewis acid site would be a neutral, four coordinate zinc complex whilst the Lewis basic site would be a neutral, five coordinate cyclam ligand complexed to a zinc ethyl moiety. Initial studies focused on the cyclam being attached to the salicylaldehyde as shown in Figure 3.4, but previous molecular modelling studies showed that having the basic functions attached at the positions shown on the phenolic rings did not appear to encourage sufficient differentiation over delivery of the phosphito function to one specific face of a metal bound carbonyl. Consequently, the secondary Lewis basic cyclam moieties were modelled as positioned at the diaminocyclohexane nitrogen atoms as illustrated in Figure 3.5.
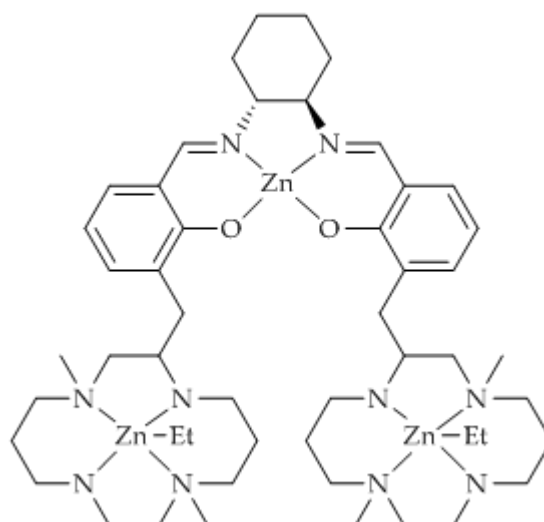
Figure 4.7 A possible zinc complex containing a zinc-cyclam function.
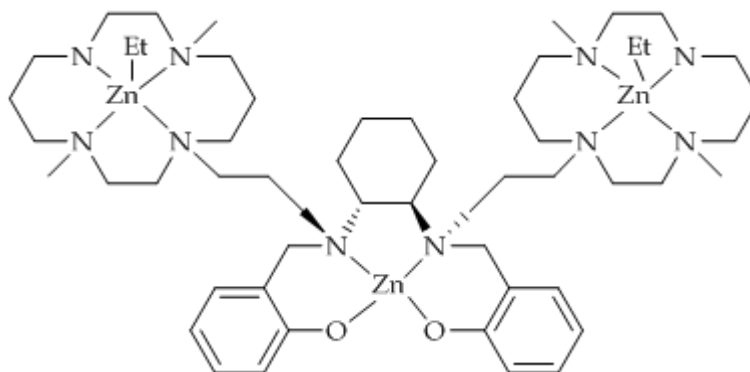
Figure 4.8 Attachment of the zinc-cyclam to the diamino framework.

Molecular modelling was performed on the system of Figure 3.5 at MM+ and PM3 levels (using the HyperChem 7.0 package) [6] to understand how the salcyan and cyclam segments may interact with each other and to explore the spatial arrangement of cyclam metal centres and their position relative to the salcyan metal centre (Figure 3.6).
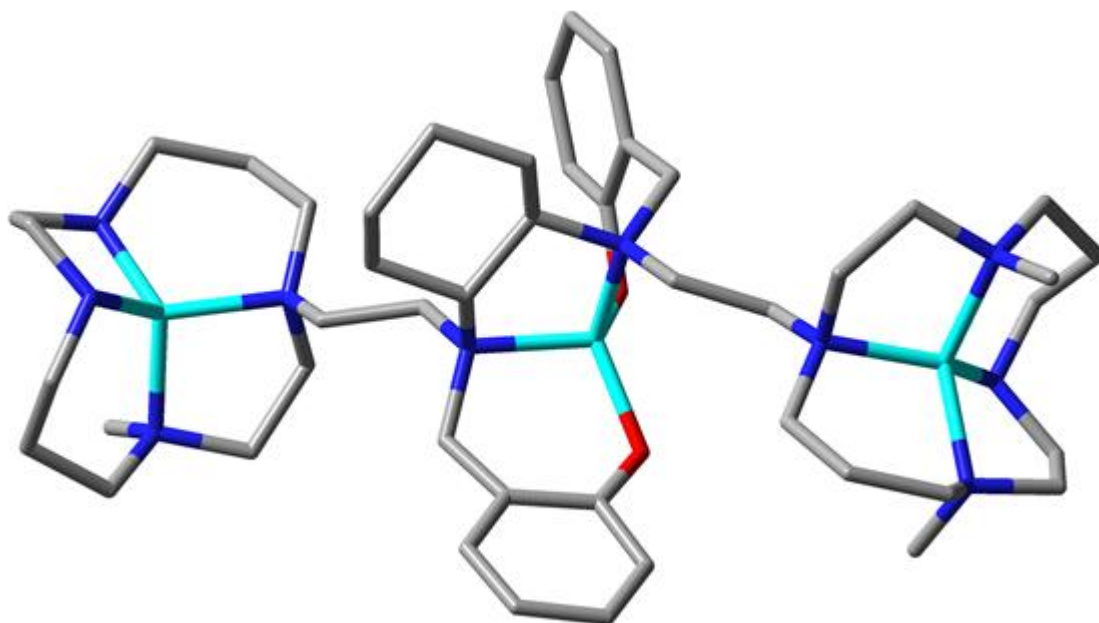
Figure 4.9 Zinc-coordinated salcyan at PM3 level with hydrogen's removed for clarity. (Red = oxygen, navy blue = nitrogen, pale blue = zinc, grey = carbon)

It was decided to model a complex containing a four-coordinate, Lewis acidic zinc atom coordinated at the salcyan portion of the complex, which subsequently would become five-coordinate upon binding of a carbonyl. Introducing the phosphonate group (dimethyl-H-phosphonate; DMHP) at one of the zinc-cyclam sites was envisaged to result in deprotonation of the DMHP by the Lewis basic, metal-bound ethyl group, producing a coordinated phosphite species (Figure 3.7) which subsequently is considered to react with the carbonyl substrate bound to the second, four-coordinate zinc metal within the salcyen pocket to afford a phosphonate with a new [P-C] bond. The resulting phosphonate is illustrated in Figure 3.8.
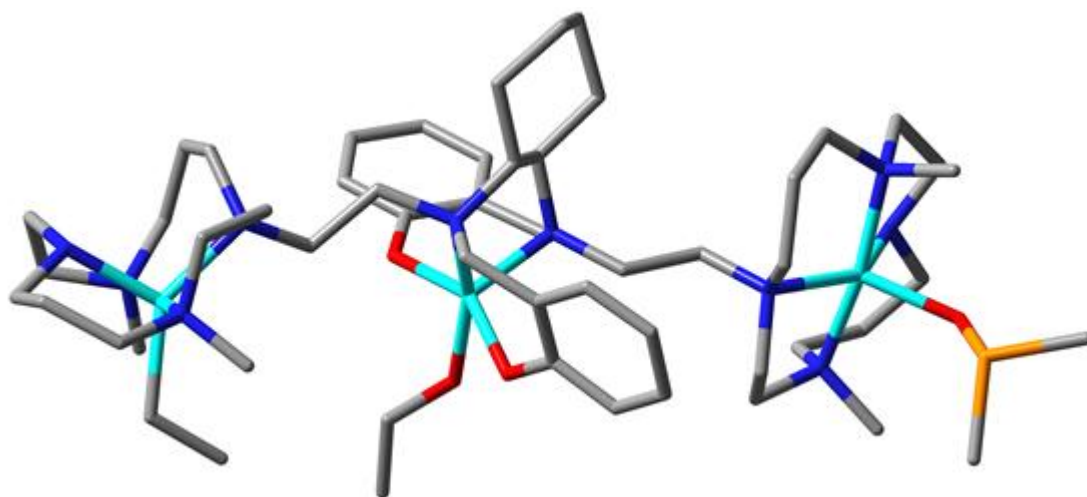
Figure 4.10 Zinc salcyan complex containing zinc-cyclam upon addition of acetaldehyde and DMHP. (Red = oxygen, navy blue = nitrogen, pale blue = zinc, yellow = phosphorus, grey = carbon)
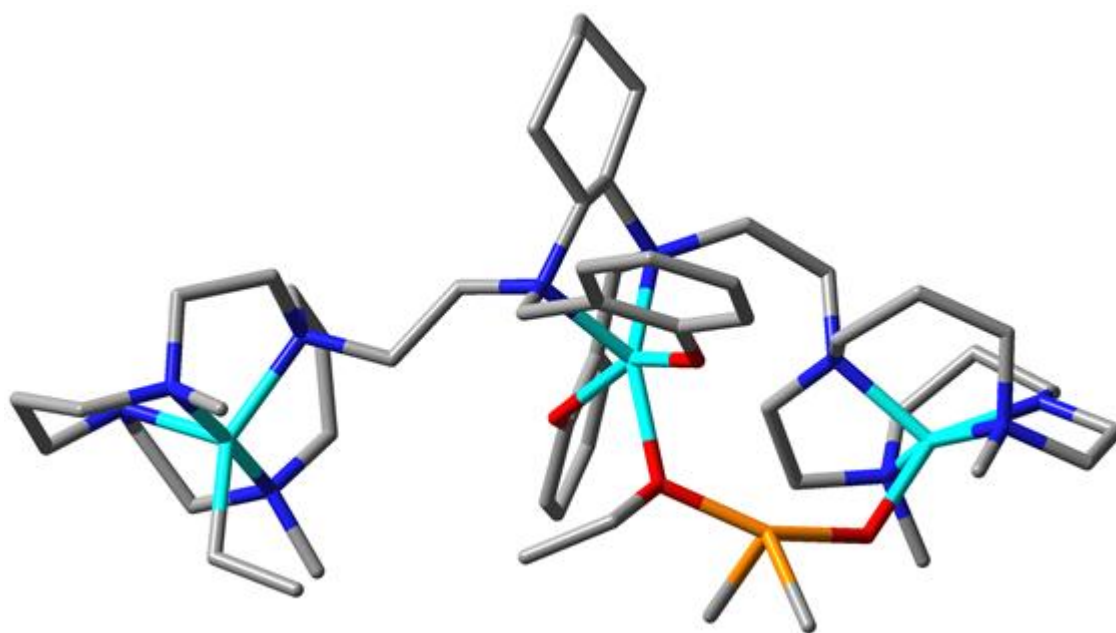
Figure 4.11 Zinc-coordinated salcyan attached to dimethyl-H-phosphonate with hydrogen atoms removed for clarity. (Red = oxygen, navy blue = nitrogen, pale blue = zinc, yellow = phosphorus, grey = carbon)

Upon visualisation of the models using HyperChem 7.0 they appeared theoretically favourable, with very little change in energy minimisations on addition of the substrates. The complex also appeared flexible enough to allow the conformational change that occurs when the P-C bond if formed.

Thus, the modelling allowed us to derive a certain level of confidence that our mechanistic strategy was not without merit; our target molecule along with some possible intermediates of the PA reaction may indeed proceed in such a way that we predict. The modelling also seems to suggest that not only could the complex bind the appropriate PA substrates but it could also maintain the conformational change brought about upon P-C formation.

4.4 Metal cyclams

Target molecules based upon the 1,4,8,11-tetraazacyclotetradecane (cyclam) framework have proved extremely useful in the fields of electrochemistry and catalysis.[7]   Synthetic modification of cyclams can easily take place as functionality can be incorporated during synthesis or substitution at the amine after isolation. The macrocyclic rings are capable of coordinating to a variety of metal centres forming stable charged or neutral species.[8], [9], [10]

Work carried out by Kochi and co-workers on the epoxidation of olefins revealed that nickel(II) complexes of cyclam-type ligands in conjunction with Schiff base and other ligand systems were capable of catalysing the conversion of iodosylbenzene to iodobenzene (Figure 3.9 and Scheme 4.1).[8]
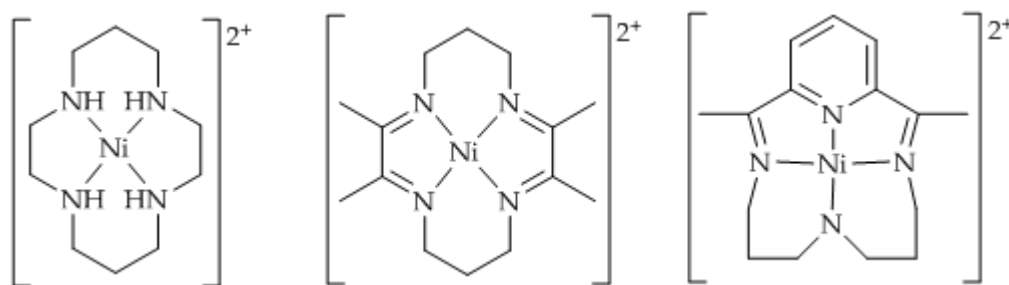
Figure 4.12 Nickel(II) complexes of cyclam-type compounds that catalyse the conversion of iodosylbenzene to iodobenzene.[8]
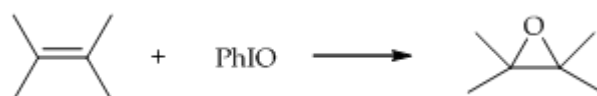
Scheme 4.1 Conversion of iodosylbenzene to iodobenzene.[8]

The relative ease with which cyclam systems can be modified at the nitrogen has led to these compounds being targets for bifunctional agents, whereby the backbone and additional 'arms' can be used to coordinate a metal atom.[2], [8]

It is envisaged that a controlled synthetic route to this class of compounds will allow a suitable mono-substituted cyclam to undergo a condensation reaction with (*R,R*)-diaminocyclohexane to afford a new Schiff base. Complexation with three equivalents of a suitable metal reagent could selectively afford mono-, di-, or tri-metallic compounds. It is worth emphasising that the target molecule is that shown in Figure 3.5.

4.5 Preparation of the cyclam 1,8-dimethyl-1,4,8,11-tetraazacyclotetradecane

4.5.1 Isolation of 1,8-dimethyl-1,4,8,11-tetraazacyclotetradecane (28)
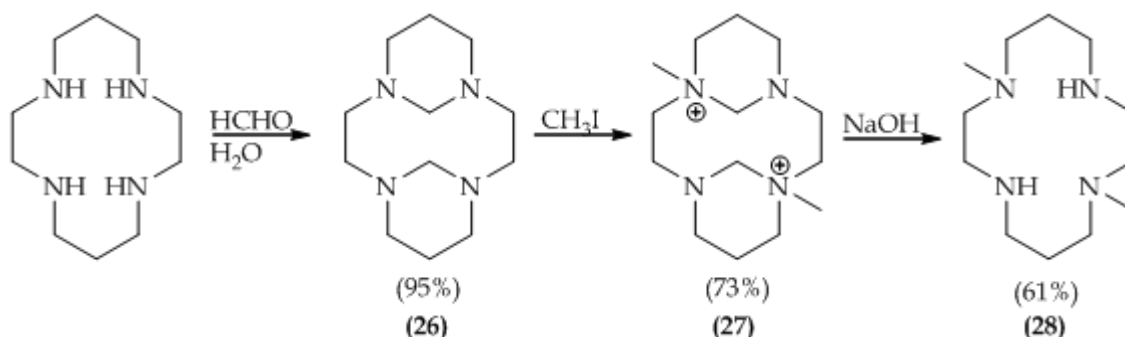
Scheme 4.2 Preparation of 1,8-dimethyl-1,4,8,11-tetraazacyclotetradecane **(28)**

Using information from Lecomte's 1998 European Journal of Organic Chemistry publication a procedure was devised by adding formaldehyde to a stirred solution of 1,4,8,11-tetraazacyclotetradecane in water at 0 °C. Upon stirring for 2 h a white precipitate formed which was removed by filtration, washed with water and dried under reduced pressure to afford 1,4,8,11-tetraazatricyclohexadecane **(26)** as a white solid (95%).[12]

Methyl iodide was added to a stirred solution of 1,4,8,11-tetraazatricyclohexadecane **(26)** dissolved in acetonitrile. After 5 min a white precipitate began to form and after 2 h the solid was removed by filtration, washed in acetonitrile and dried under reduced pressure. The product 1,8-dimethyl-4,11-diazoniatricyclohexadecane diiodide **(27)** was isolated as a white powder (73%).[12]

To a stirred solution of aqueous sodium hydroxide was added 1,8-dimethyl-4,11-diazoniatricyclohexdecane diiodide **(27)** The mixture was allowed to stir for 3 h before being extracted with DCM, dried over MgSO$_4$ and volatiles removed under reduced pressure. The colourless oil crystallised under reduced pressure or when stored under nitrogen at -18 °C. Characterisation by ^{1}H and

^{13}C{^{1}H} NMR and microanalysis proved that the cyclam **(28)** (61%) crystallised as a mono-hydrate.[12]
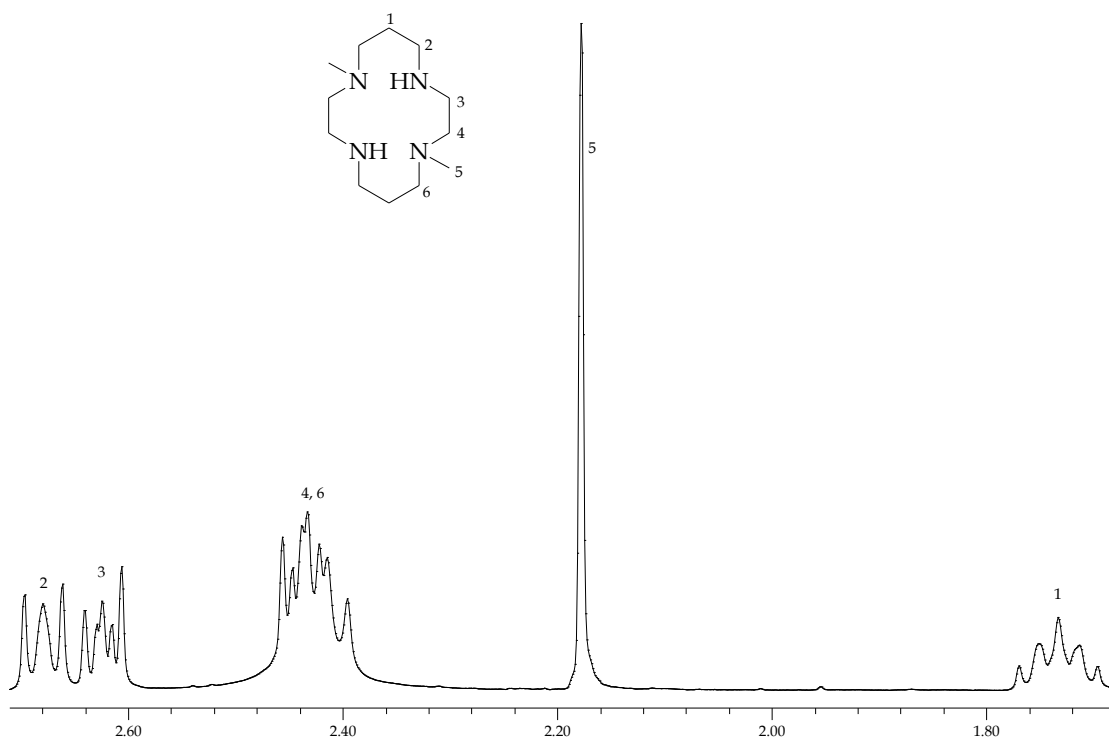
Figure 4.13 ^{1}H NMR of 1,8-dimethyl-1,4,8,11-tetraazacyclotetradecane **(28)** (330 MHz, CDCl$_3$, 298K).
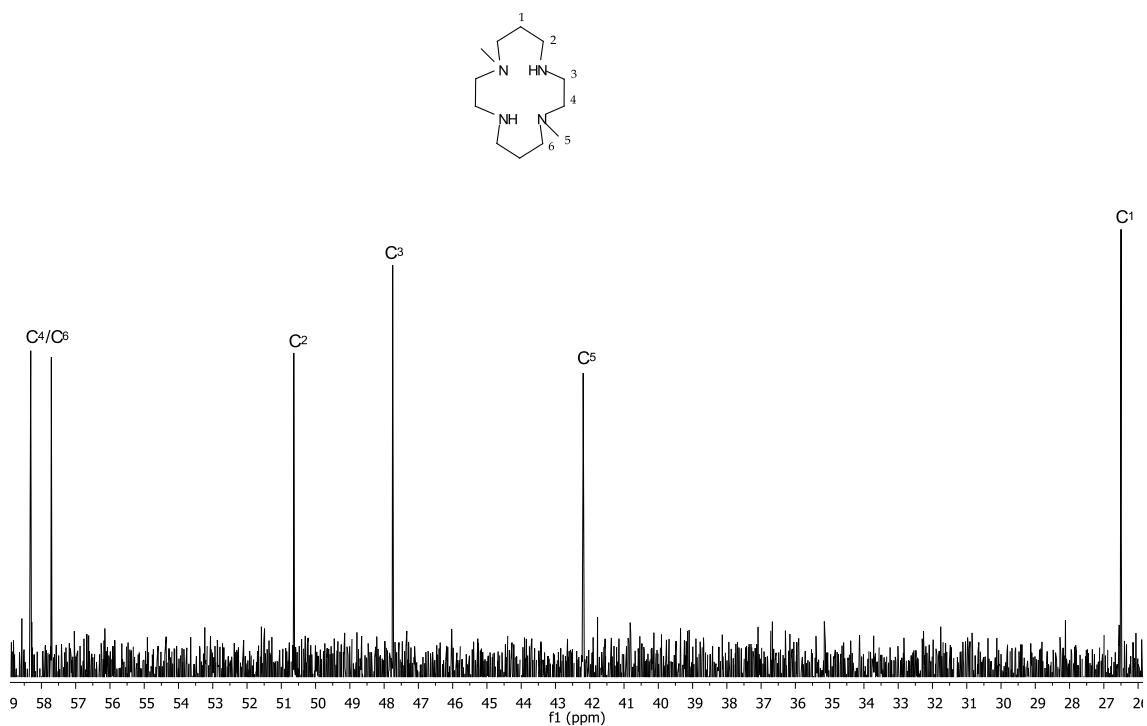
Figure 4.14 $^{13}C\{^1H\}$ NMR of 1,8-dimethyl-1,4,8,11-tetraazacyclotetradecane **(28)** (330 MHz, CDCl$_3$, 298K).

4.6 Synthesis of (R,R)-N,N′-bis-(2-hydroxy-3-tert-butylbenzyl)-1,2-diaminocyclohexane (30)

The general procedure for the production of compound **(30)** is outlined in Scheme 4.3 using protocols similar to those published by Jacobsen and Atwood. [13], [14]
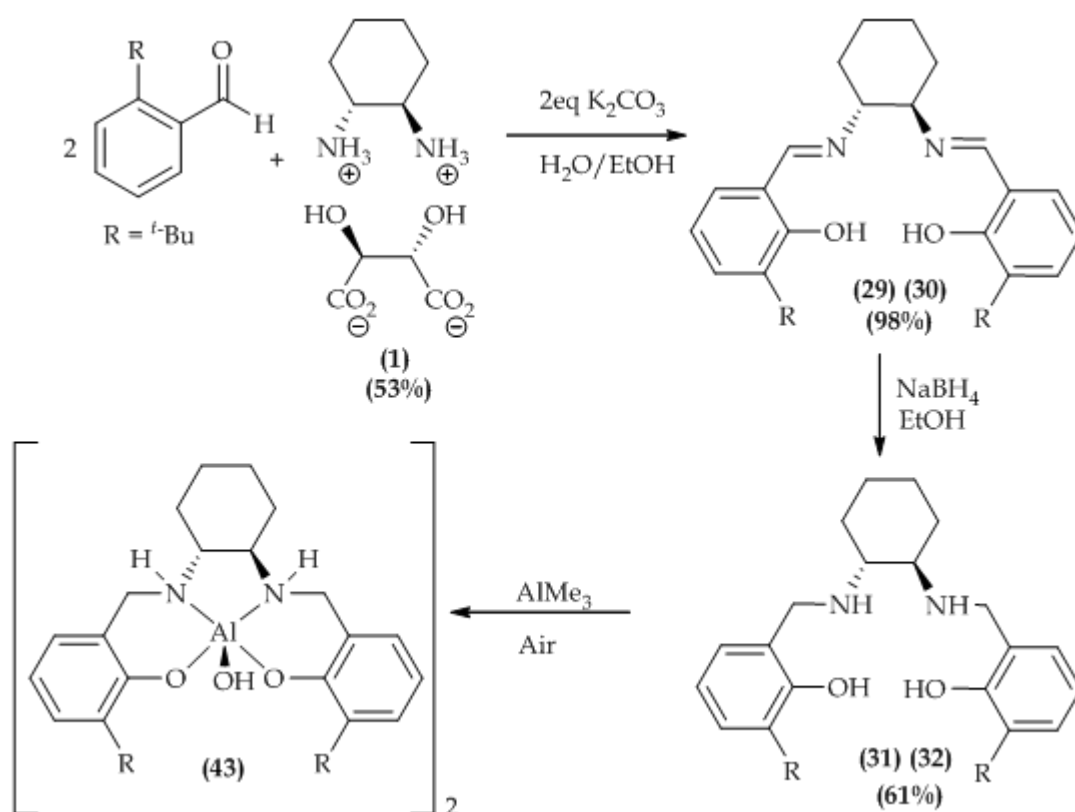
Scheme 4.3 General procedure for the synthesis of {(R,R)-[salcyan-3-(^{t}Bu)]Al(μ-OH)}$_2$ **(41)**.

The characterisation and modelling of phenolic N_2O_2 type salcyan ligands are well established and, given this laboratory's extensive use of such compounds in PA catalysis, are therefore obvious choices for use in bifunctional systems. The tert-butyl group has proven stereo-directing ability.

The chiral diamine salt undergoes a condensation reaction with the two equivalents of the 3-*tert*-butyl-2-hydroxybenzaldehyde along with two equivalents of base in the form of potassium carbonate in refluxing ethanol and water as shown in Scheme 4.3. The yellow product was recovered by filtration of the reaction slurry, any impurities washed out with water. The crude product was recrystallised from dichloromethane.
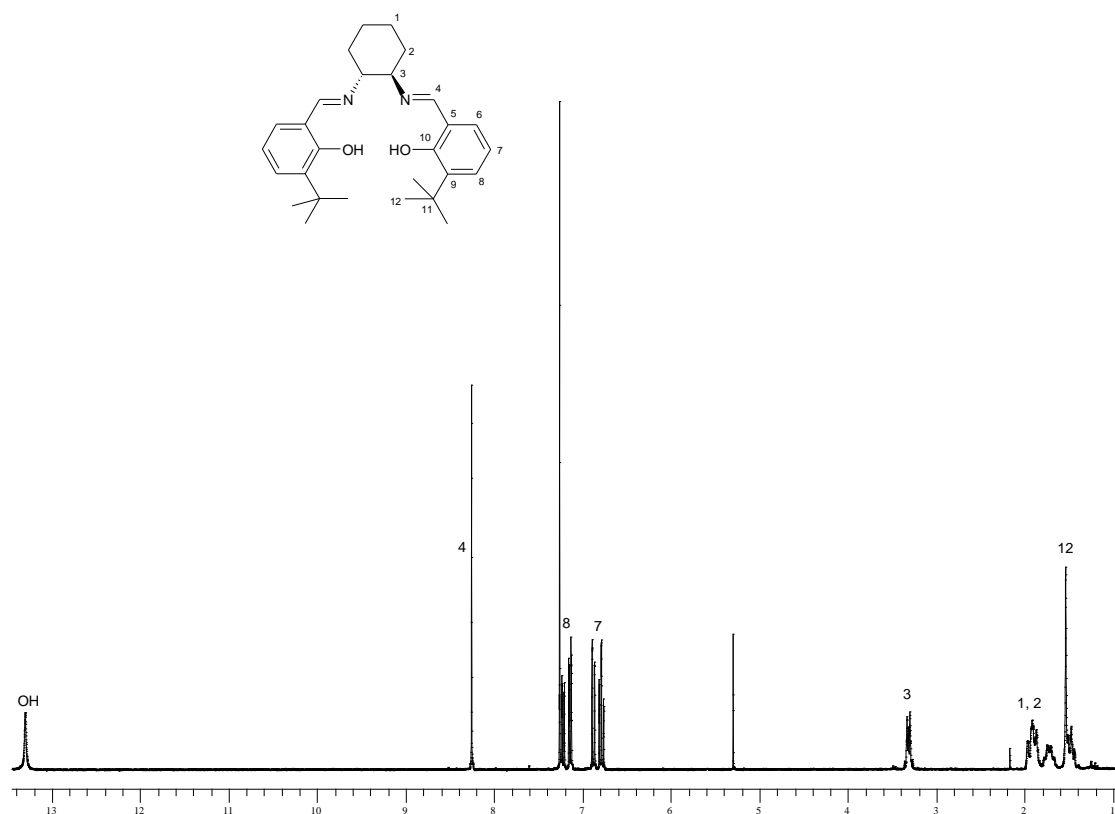
Figure 4.15 ^{1}H NMR of {(*R*,*R*)-[salcyen-3-(*t*Bu₂)]}**(30)** (CDCl₃, 300 MHz, 300 K)
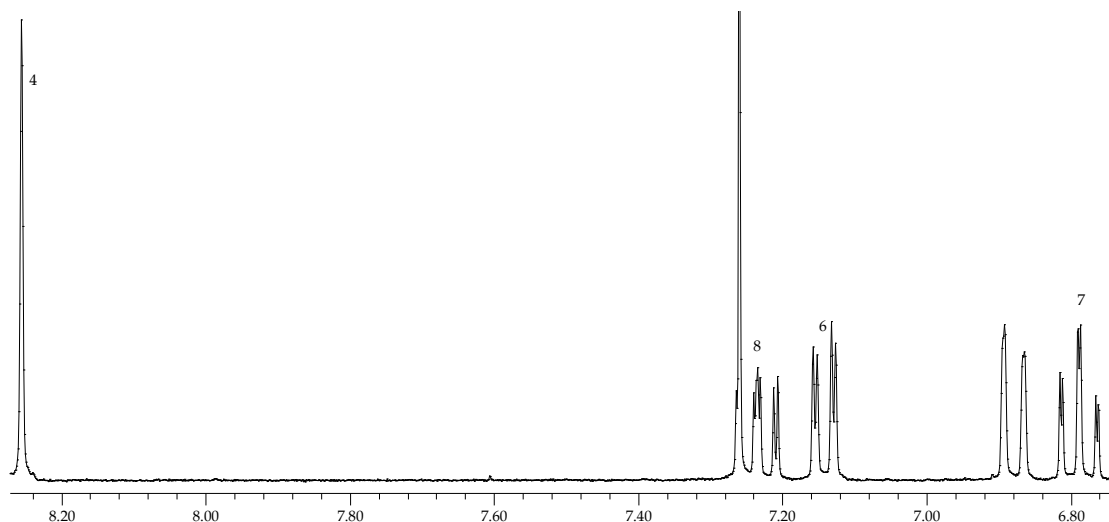
Figure 4.16 Expanded ^{1}H NMR of {(R,R)-[salcyen-3-(^{t}Bu$_2$)]}**(30)** (CDCl$_3$, 300 MHz, 300 K).

Expansion of the aromatic region of the ^{1}H NMR spectrum, Figure 3.13 shows the three inequivalent sp^2 hybridised aromatic protons. The splitting of the aromatic resonances due to coupling for C$_6$H and C$_8$H are as expected, a doublet of doublets at chemical shifts of δ^1H 7.30 and 7.28 ppm respectively. The resonance at δ^1H 6.85 ppm of C$_7$H is predicted to be split into a triplet of doublets as it has one proton either side within an interactive distance, instead three single resonances are observed, with a three bond coupling constant of 8.2 Hz. Also observed in the expansion spectrum is the high chemical shift singlet resonance at δ^1H 8.32 ppm of the imine function, C$_4$H, corresponding to sp^2 hybridisation and the connection to an electron-withdrawing nitrogen.
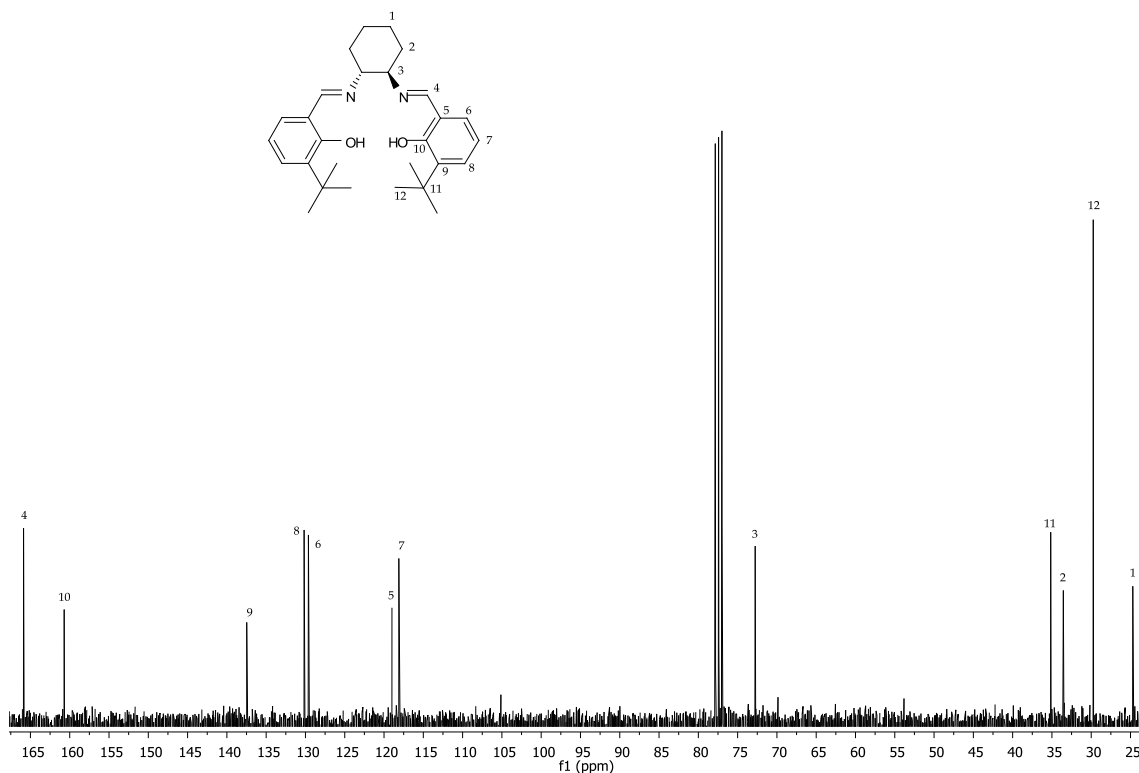
Figure 4.17 ^{13}C {^{1}H} NMR of {(R,R)-[salcyen-3-(^{t}Bu$_2$)]}**(30)** (CDCl$_3$, 300 MHz, 300 K).

The ^{13}C {^{1}H} NMR spectrum (Figure 4.14), as predicted shows only half of the possible peaks due to C_2 symmetry and also shows the five sp^3 hybridised alkyl groups, one sp^2 hybridised alkyl group and six sp^2 hybridised aromatic groups.

Reduction of the salcyen imine bond of **(30)** with an excess sodium borohydride in ethanol at reflux produced the salcyan compound **(31)** as a white solid. Compound **(31)** was collected after the addition of water and cooling *via* reduced pressure filtration and finally recrystallised from pentane.
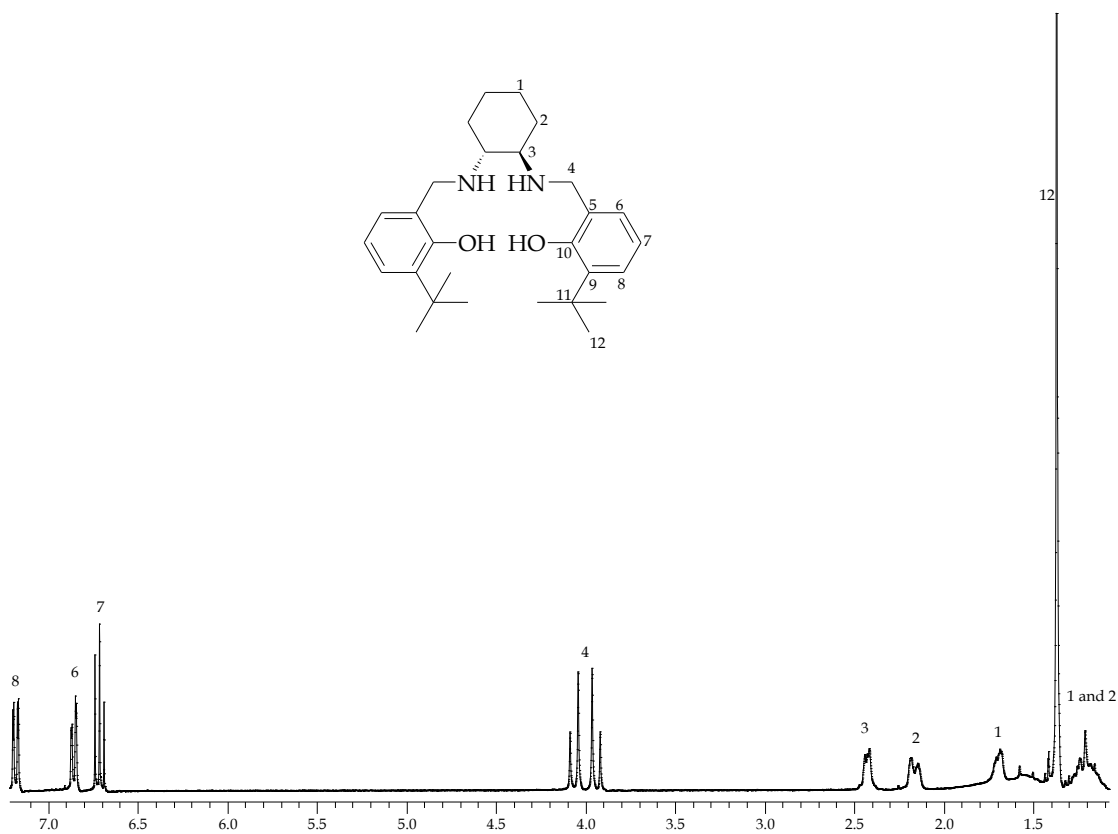
Figure 4.18 ¹H NMR of {(*R*,*R*)-[salcyan-3-(*t*Bu₂)]**(31)** (CDCl₃, 300 MHz, 300 K).

As with their salcyen cousins, the salcyan compounds retain their C_2 symmetry. The ¹H NMR of {(*R*,*R*)-[salcyan-3-(*t*Bu)]**(31)** does not differ greatly from that seen in Figure 3.12. The main differences occur around the lower frequency chemical shifts of C_3H and C_4H. Reduction of the imine bond does not appear to affect the chemical environment of the alkyl phenolic ring substituents.
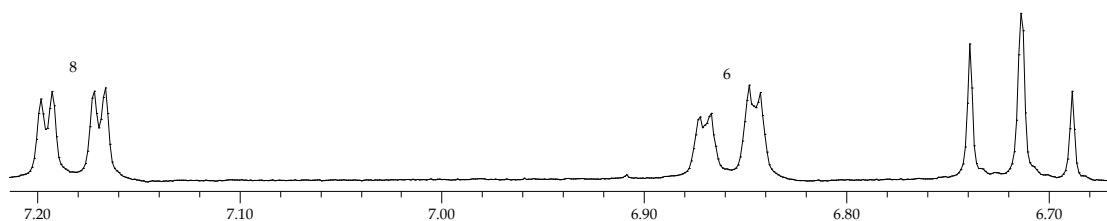
Figure 4.19 Expanded ¹H NMR of aromatic region of {(*R*,*R*)-[salcyan-3-(*t*Bu₂)]**(31)** (CDCl₃, 300 MHz, 300 K).

136

As expected the aromatic region of compound **(31)** is not highly different from that already seen for compound **(30)**. The same splitting patterns and similar chemical shifts are observed, with the most distinctive resonances being those of C_7H at δ^1H 6.71 ppm.

Evidence for the hydrogenation of the imine bond is apparent from the AB system produced by the diastereotopic protons of the methylene unit. The two protons are in different environments giving the observed chemical shifts of C_4H at δ^1H 4.08 and 3.96 ppm with a germinal coupling constant of 13.6 Hz. The lower resonance value is due to the loss of conjugation; however the coupling constant value is consistent with that of geminal coupling.
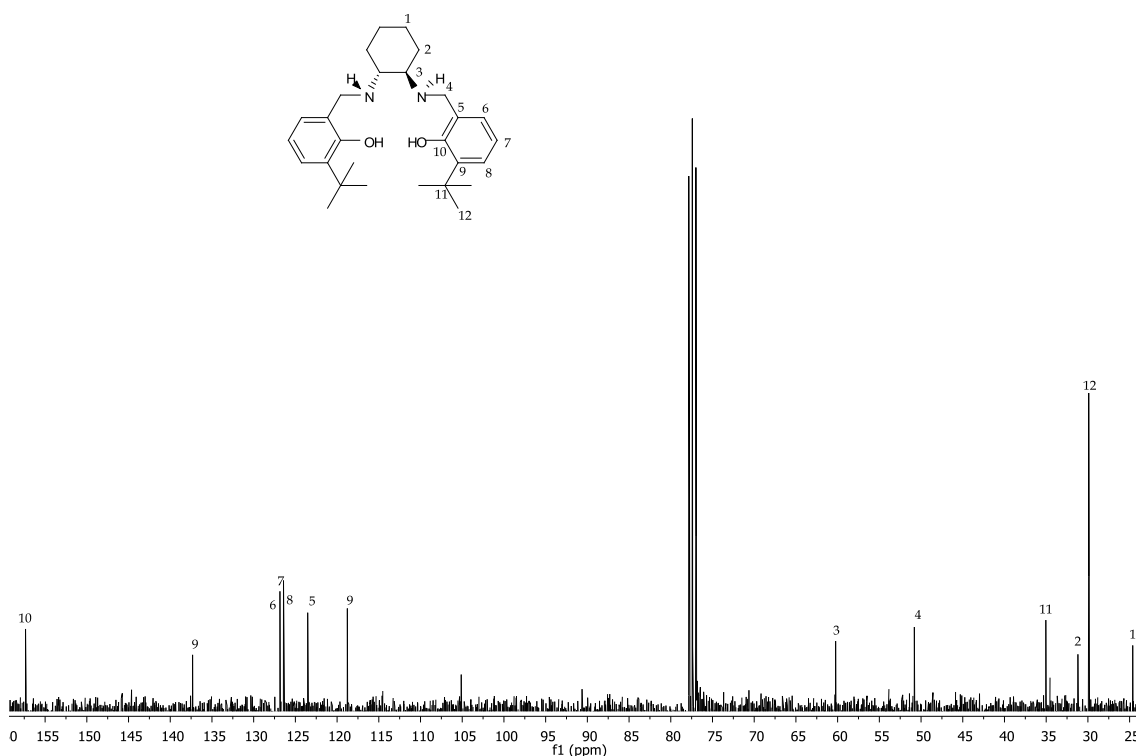
Figure 4.20 ^{13}C {^1H} NMR of {(*R,R*)-[salcyan-3-($^tBu_2$)]}**(31)** (CDCl$_3$, 300 MHz, 300 K).

The most obvious differences between the ^{13}C {^1H} NMR spectra of compounds **(30)** and **(31)** are the lowered values of chemical shift for C_3 at $\delta^{13}C$ {^1H} 60.2 ppm and C_4 at $\delta^{13}C$ {^1H} 50.8 ppm indicating a successful reduction of the imine bond.

4.7 Summary

Incorporating tetradentate macrocycles such as cyclams into the target molecule (Figure 3.15) was envisaged as developing a new, bifunctional class of molecule, comprising two distinct classes of metal centre, one electrophilic and one nucleophilic to activate and bring together both carbonyl and phosphonate substrates within a single catalytic entity. To date there has been success in preparing several key building blocks: 1,8-dimethyl-4,11-diazoniatricyclohexadecane **(28)** has been synthesised at a much lower cost and a higher purity than what is commercially available. The next stage of this project will involve linking the cyclam to the salcyan framework with the aid of a linker system. However, due to time restraints no such reactions were actually carried out with regards to a linker.

4.8 Phosphorus-Substituted Salcyan Complexes of Aluminium

In this chapter a brief summary of the conclusions drawn from earlier computational studies, as described in Chapter 3 are collected, along with an analysis of how these conclusions may help us to design and build a better molecular framework for developing a metal catalyst for the phospho-aldol reaction. A selection of target complexes and synthetic pathways and characterisation data are also discussed.

4.9 Introduction

One of the major issues associated with the current synthesis of new aluminium salcyan complexes within the Kee group, and others, is that it is heavily dependent upon linear, synthetic chemistry wherein each potential new catalyst needs to be prepared using standard covalent modifications to existing ligand systems. Such a strategy is both time consuming and no guarantee of success can be provided for a specific target complex. In principle a more satisfactory approach would be to construct a basic complex, which is capable of achieving a reasonable level of selectivity for a standard PA reaction and that then may be able to be modified *via* simple addition of suitable co-factors tuned to a specific substrate. This approach would open up the possibility of parallel processing and analysis thus allowing rapid screening of co-factors against a given substrate. A specific development in this direction towards the design and synthesis of new aluminium-containing salcyan complexes involves using organophosphorus-substituted salcyan complexes. They have a potential to influence the stereochemistry of phospho-aldol reactions through both their steric and electronic properties. These types of compound offer a range of sterically demanding groups close to the metal centre, which could then be manipulated by co-factor addition to alter both steric and electronic properties through, for example binding to metal atoms, H-bonding and other dative covalent complex formation. The ease with which these compounds may be synthesised is yet uncertain, however as they show close resemblance to previously synthesised silyl compounds, we anticipate that several will prove synthetically accessible. The use of a salcyan-substituted phosphorus ligand framework also opens the potential for using ^{31}P-NMR spectroscopy in monitoring reactions and also possibly mechanistic investigations.

4.10 Selection of target molecules as possible catalysts for the PA reaction

Complexes $\{(R,R)$-[salcyan(R)$_2$]Al(μ-OH)$\}_2$, where R = :PPh$_2$ and P(=O)Ph$_2$ were selected as target molecules to be synthesised. These target molecules have been selected due to the shape of the open faces as shown in Figure 4.21 and Figure 4.22.
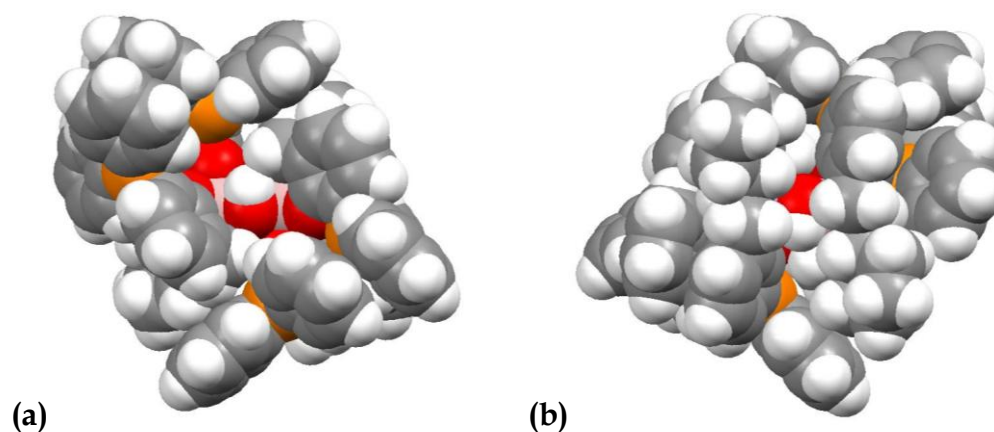
Figure 4.21 Space filling graphics of $\{(R,R)\text{-[salcyan(:PPh}_2)_2]\text{Al}(\mu\text{-OH})\}_2$ showing open **(a)** and closed **(b)** face obtained from HyperChem molecular modelling at Mm+.
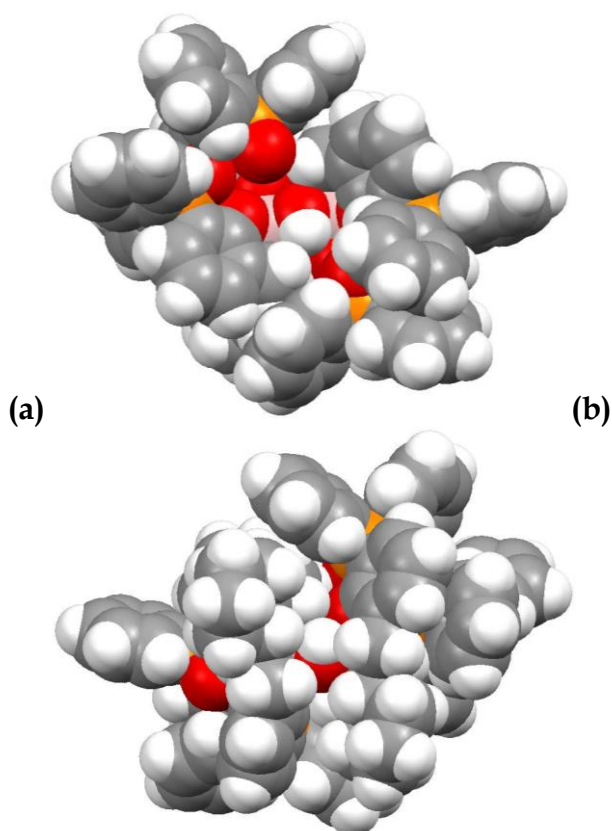
Figure 4.22 Space filling graphics of $\{(R,R)\text{-[salcyan(P(=O)Ph}_2)_2]\text{Al}(\mu\text{-OH})\}_2$ showing open **(a)** and closed **(b)** face obtained from HyperChem molecular modelling at Mm+.

Extensive studies, both synthetic and catalytic have been carried out on the basic salcyan N_2O_2 framework with reasonable e.e.s achieved. Continuing to use these basic frameworks is an added advantage as by introducing a

phosphine oxide or phosphine substitute it can provide a path to new complexes, which could potentially be modified by the addition of additives (co-factors) to optimise the performance for a given substrate, without the need to fully synthesise a new library of aluminium complexes.

4.11 Synthetic pathway towards phosphinyl and phosphine oxide salcyan complexes

Outlined below are two synthetic routes to phosphorus-substituted salcyan aluminium complexes. The initial method **(1)** (Scheme 4.4) was based on simple chemical reactions, however difficulties arose at step 2 and so a new synthetic route method **(2)** (Scheme 4.4) was devised. Part of the synthetic work has been approached as part of this thesis but unfortunately due to time constraints, a complete synthesis could not be achieved.
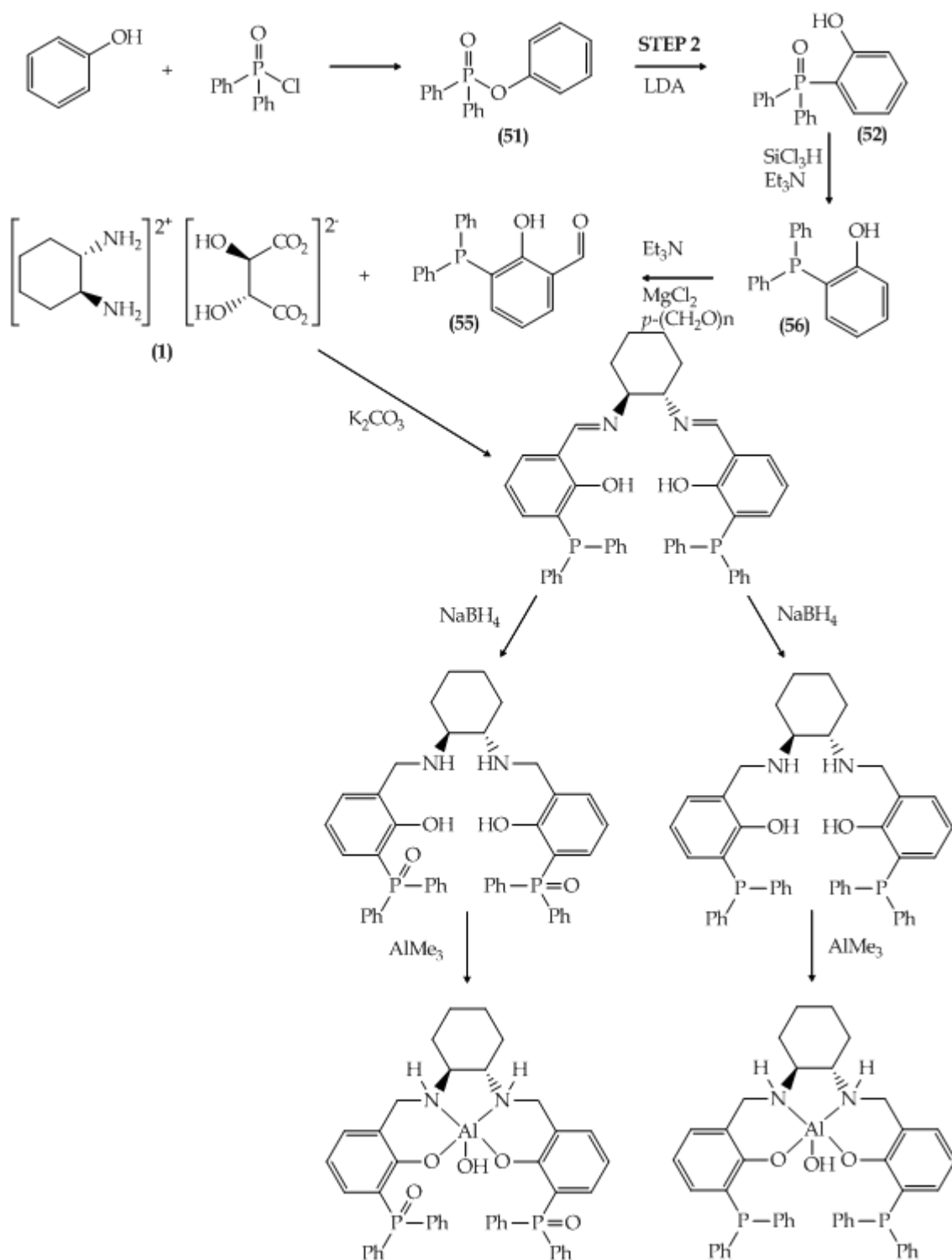
Scheme 4.4 Method 1 towards synthesising phosphorus substituted aluminium salcyan complex. All numbered steps have been synthesised or attempted. Further details are in Chapter 6.
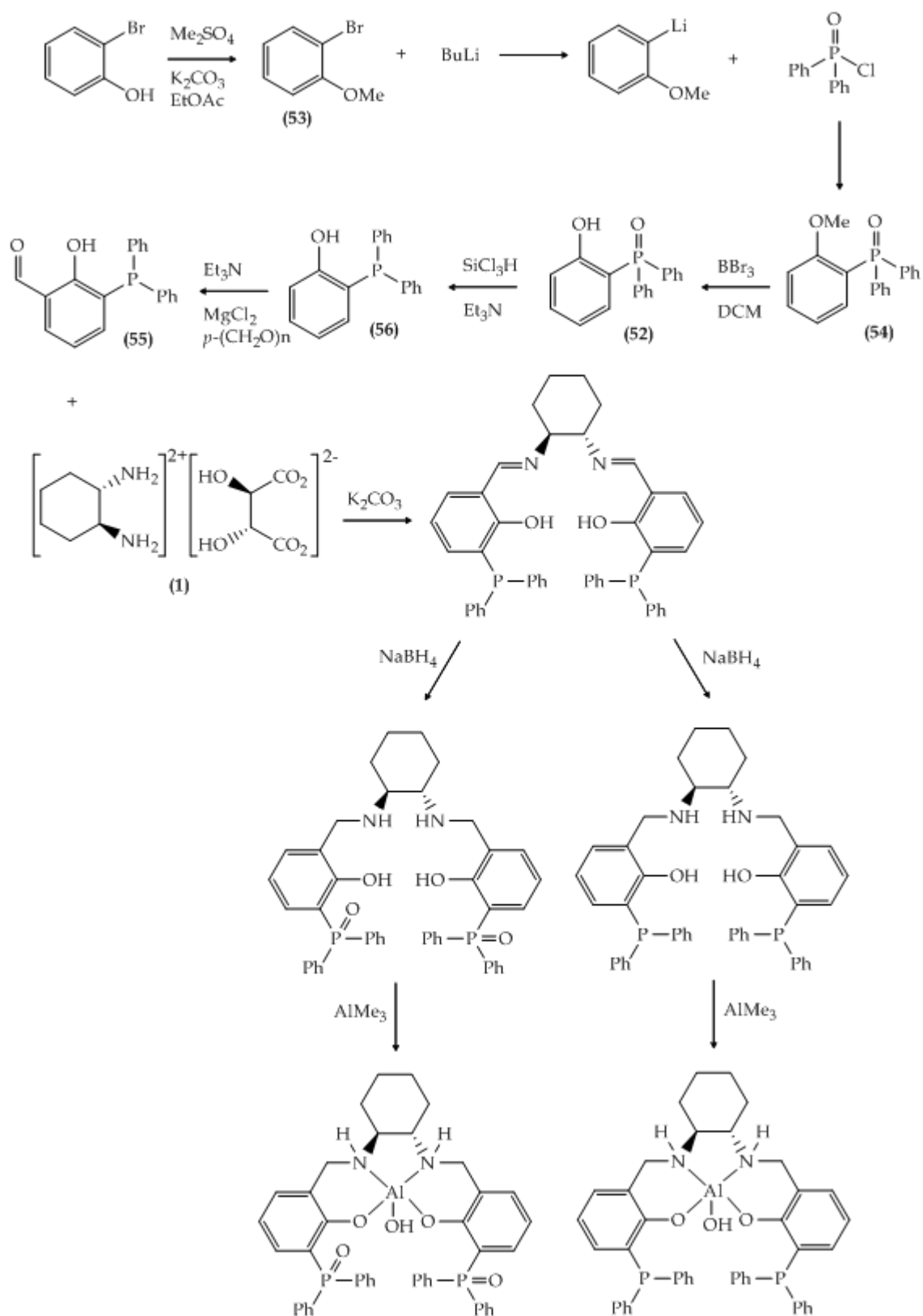
Scheme 4.5 Method 2 towards synthesising phosphorus substituted aluminium salcyan complex. All numbered steps have been synthesised or attempted. Further details are in Chapter 6.

The remainder of the chapter will describe the steps taken in method **(2)**, (Scheme 4.4) however all experimental data for method **(1)** (Scheme 4.4) can be seen in chapter 6.

4.12 Synthesis of 2-bromo anisole (53) [15], [16]
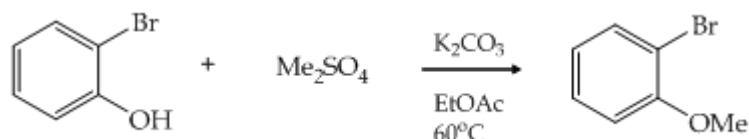
Scheme 4. 6 Synthesis of 2-bromo anisole **(53)**.

The 2-bromo anisole was synthesised by alkylating 2-bromo phenol with the addition of dimethyl sulphate *via* the S_N2 nucleophilic substitution method (Scheme 4.6).

Scheme 4.7 Reaction mechanism of S_N2 nucleophilic substitution. [17]

Potassium carbonate and 2-bromophenol in a 2:1 ratio were stirred together in ethyl acetate and 1.2 equivalents of dimethyl sulphate slowly added to the warmed solution. After 2 hours of stirring at room temperature the reaction mixture was quenched with water and the organics separated to afford the title compound as pale orange oil. Analysis *via* ^{1}H NMR spectroscopy was consistent with product formation (Figure 4.23), with characteristic peaks observed. A singlet resonance at δ^1H 3.88 ppm can be assigned to the methoxy group.

4.13 Synthesis of diphenylphosphinyl anisole (54)
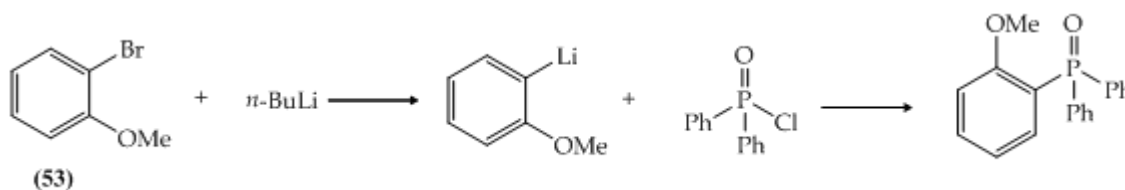
Scheme 4.8 Synthesis of diphenylphosphinyl anisole **(54).**

Several reaction methods were tested, which can be seen in detail in Chapter 6, prior to finding a successful synthetic procedure involving *n*-butyl lithium as a base for creating an organo-lithium intermediate. Procedures were taken from Orga and Baker and modified to suit the reaction conditions. [18], [19] The addition of diphenylphosphinyl chloride to the organo-lithium intermediate giving **(54)** as a white solid. As can be seen in Figure 4.23 and Figure 4.21, the aromatic region is rather complex and difficult to fully assign. The ^{31}P {^{1}H} NMR spectrum showed a resonance shift of δ ^{31}P {^{1}H} 28.4ppm indicating that the title compound had indeed been synthesised as this was compared to ^{31}P {^{1}H} data found in a literature search. [11]
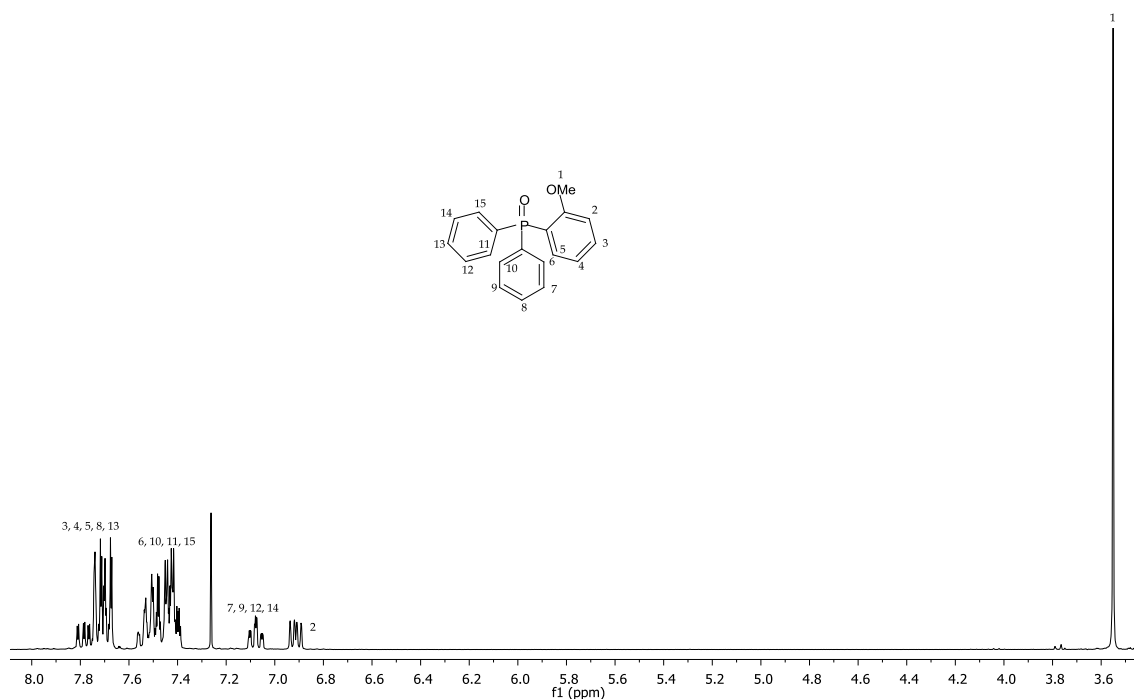
Figure 4.23 ^{1}H NMR of diphenylphosphinyl anisole **(54)** CDCl$_3$, 298K, 500 MHz.
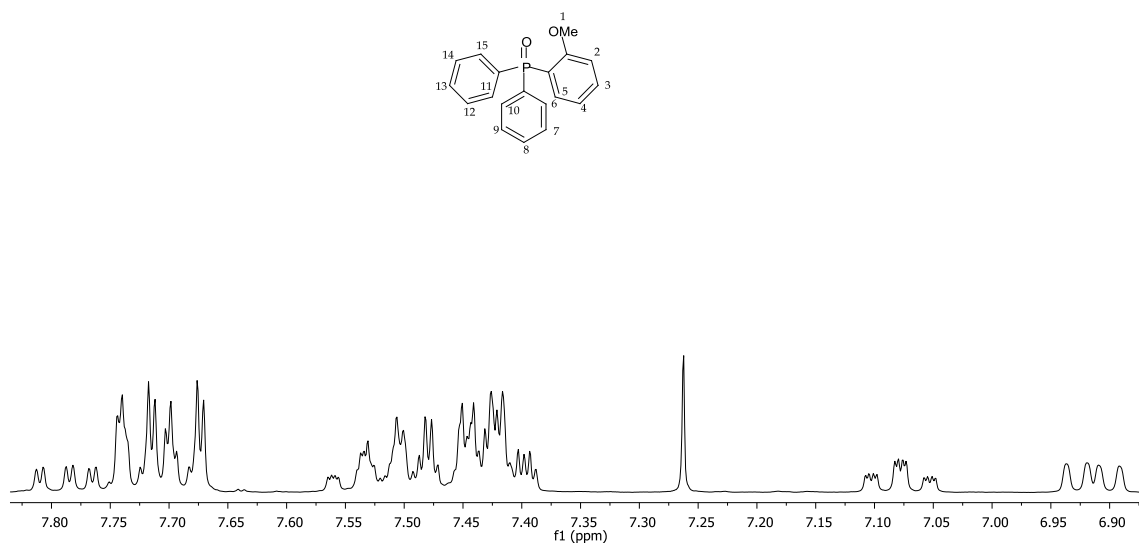
Figure 4.24 Expansion ^{1}H NMR of aromatic region of diphenylphosphinyl anisole **(54)** CDCl$_3$, 298K, 500 MHz.

4.14 Synthesis of diphenylphosphinyl phenol (52)
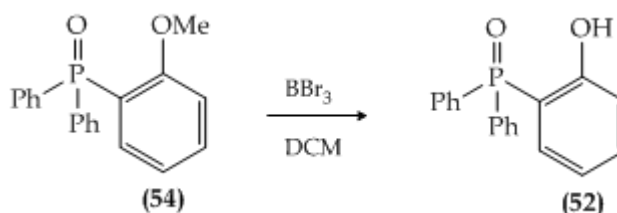
Scheme 4.9 Synthesis of diphenylphosphinyl phenol **(52)**.

The general procedure taken from McOmie's paper was used to synthesis the diphenylphosphinyl phenol. [20] Diphenylphosphinyl phenol was synthesised by the demethylation of diphenylphosphinyl anisole by treatment with boron tribromide (1M in DCM) at room temperature for 14h. The mixture was cooled to 0 °C, quenched with water and the organic product extracted into ethyl acetate, affording the crude product. Diphenylphosphinyl phenol was purified by column chromatography on silica with an eluent of dichloromethane: ethyl acetate (7:3 v/v) with 10% methanol however upon analysis by ^{31}P {^{1}H} NMR other impurities could be seen, indicating purification was not completely successful. It was decided that the impure title compound would be taken through to the next step in the hope that a better purification could take place.
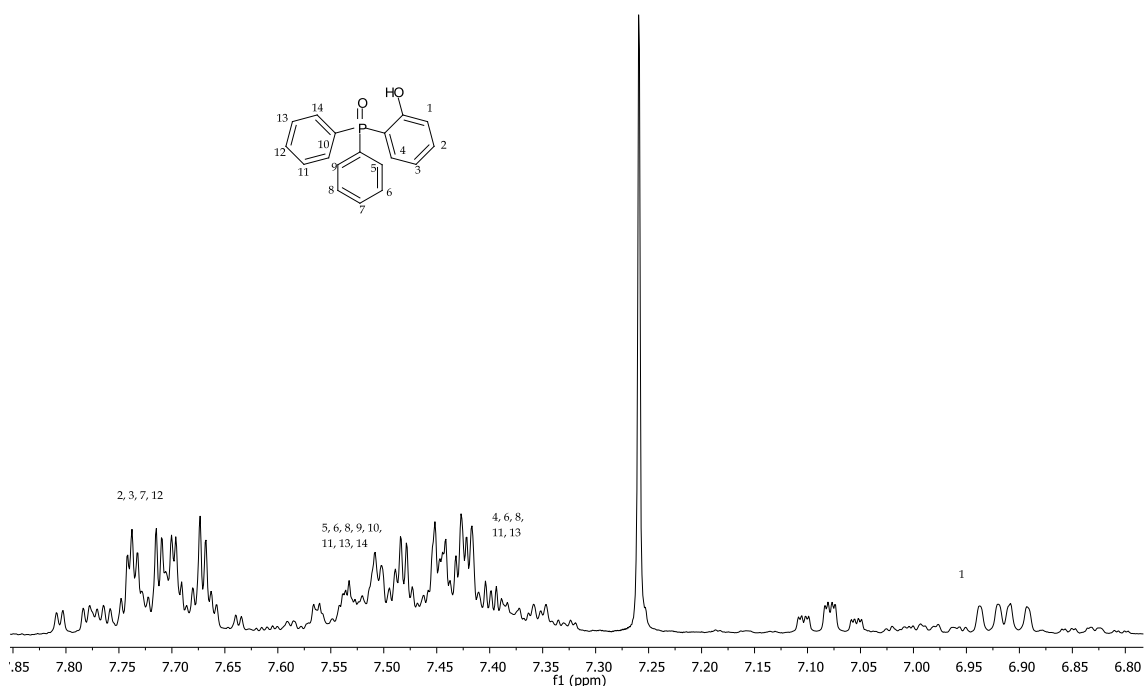
Figure 4.25 ^{1}H NMR of diphenylphosphinyl phenol **(52)** CDCl$_3$, 298K, 300 MHz.

The aromatic region is extremely complex making it difficult to fully characterise as well as the ^{31}P {^{1}H} NMR spectrum indicating the presence of impurities, however the chemical shift δ ^{31}P {^{1}H} of 40.1ppm was believed to belong to compound **(52)**.

4.15 Attempted synthesis of diphenylphosphinyl hydroxy-benzaldehyde (55)
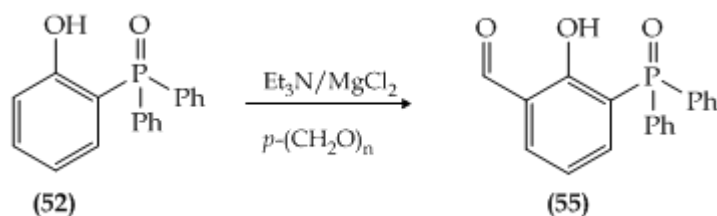
Scheme 4.10 Synthesis of diphenylphosphinyl hydroxy-benzaldehyde **(55)**.

Within the Kee group an *ortho*-formylation protocol using anhydrous magnesium(II) chloride in the presence of triethylamine was found to be highly successful and so was adopted for this procedure. [21] A mixture of 1 equivalent of phenol, 1.5 equivalents of magnesium(II) chloride, 3.65 equivalents of triethylamine and 6.76 equivalents of paraformaldehyde in acetonitrile at reflux did not give the desired selective *ortho*-formylation upon cooling and acidification. It is proposed that the oxygen on the phosphorus was preventing the selective *ortho*-formylation and so in order to continue it would be necessary to reduce the phosphine oxide to its phosphino form and attempt the selective formylation reaction again.

4.16 Attempted synthesis of diphenylphosphine phenol (56) and diphenylphosphine anisole (57)
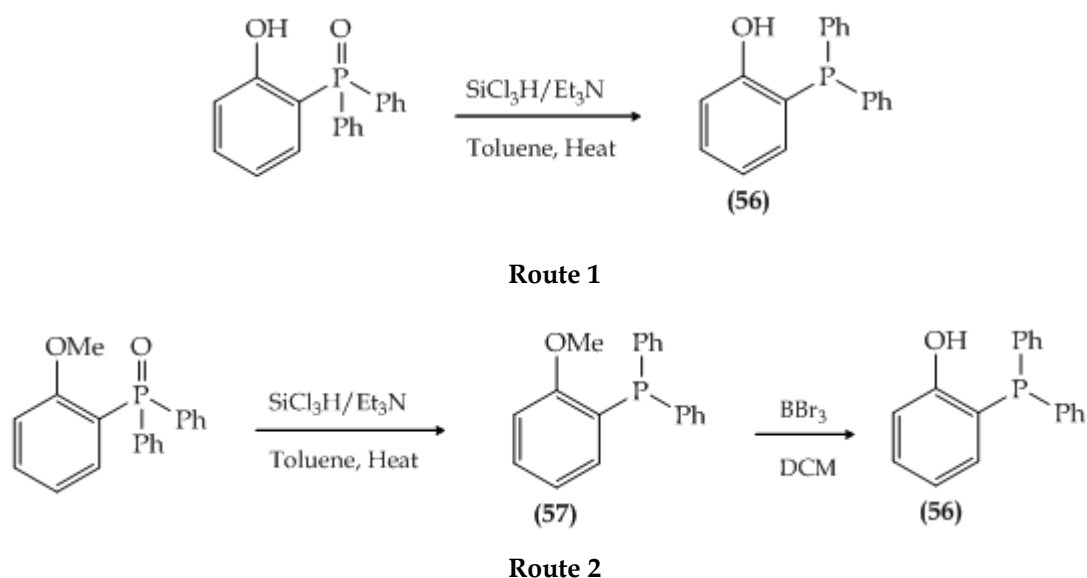
Route 1

Route 2

Scheme 4.11 Synthesis of diphenylphosphinyl hydroxy-benzaldehyde **(56)** *via* 2 routes.

Reduction of substituted phosphine oxide to its phosphine derivative was attempted *via* 2 routes, as shown in Scheme 4.10. Route 1 shows the reduction

of phenol substituted phosphine oxide to its phenol substituted phosphine cousin. [22] Route 2 shows a similar procedure however the starting substituted phosphine oxide is of the anisole form, rather than the phenol form. [20], [22] Substituted phosphine oxide could be reduced using trichlorosilane followed by deprotection of the methoxy group to its hydroxy form.

Both methods utilised the protocol from Baccolini and Todesco, which involved the use of trichlorosilane with triethylamine in toluene and heat. [22] Rather disappointingly these procedures were not successful for the diphenylphosphinyl compounds and due to time constraints the reaction was not pursued any further.

4.17 Conclusion

Although the synthetic work was not fully completed and a new phosphorus-substituted salcyan aluminium complex was not successfully created, some interesting results were uncovered. It has been possible to hypothesise a new synthetic pathway for the synthesis of phosphorus substituted aluminium salcyan complexes that would be worthy of future investigation.

In method 1, problems arose when trying to bring about the rearrangement of diphenylphosphinyl phenyl ester into diphenylphosphinyl phenol. The initial idea was to use the concept of a reverse Brook rearrangement, normally a reaction in which an organosilyl group switches position with a hydroxyl proton over a carbon to oxygen covalent bond, under the influence of a base. [23] We envisaged the reverse of this reaction, using a base such as LDA would result in synthesising the phenol from the ester, however this did not work and after several attempts using different reaction conditions (temperature) and solvents it was decided a new synthetic pathway would be needed.

Method 2 of the synthesis of phosphorus substituted aluminium salcyan complexes was also problematic. As a result of the failings in the rearrangement step of method 1 it was concluded that the new synthetic route would not need such a step. Due to the difficulty in making the diphenylphosphinyl phenol, using a protecting (methoxy) group on the starting hydroxyl reagent which could then be removed at a later stage, could be more successful and by doing so it would eliminate the need to make the phenyl ester.

The next obstacle occurred whilst attempting to synthesise the benzaldehyde derivative **(55)**. Within the Kee group there has been great success in using an *ortho*-formylation protocol employing anhydrous magnesium(II) chloride in the presence of triethylamine. [21] It is a simple, efficient and regioselective method for the preparation of substituted salicylaldehydes, however for our systems this reaction did not work. A possible reason could be the electron-withdrawing effect of the oxygen atom residing on phosphorus which impairs the rate of the reaction. This led us to pursue the synthesis of the phosphine derivatives; however initial results were not positive and due to time constraints it was not possible to continue it further.

4.18 References

[1]   E. F. DiMauro, M. C. Kozlowski, *Organic Letters*. **2001**, *3*, 3053.

[2]   E. F. DiMauro, M. C. Kozlowski, *J. Am. Chem. Soc.*, **2002**, *124*, 12668.

[3]   H. Sasai, T. Suzuki, N. Itoh, S. Arai, M. Shibasaki, *J. Am. Chem. Soc.*, **1993**, *115*, 10372.

[4]   E. F. DiMauro, M. C. Kozlowski,. Organic Letts. **2001**, *3*, 1641.

[5]   Y. Ito, M. Sawamura, T. Hayashi, *J. Am. Chem. Soc.*, **1986**, *108*, 6405.

[6]   HyperChem 7.0, Hypercube, Inc. Gainsville, FL, 32601, USA.

[7]   E. Y. Lee, D. Hong, H. W. Park, M. P. Suh, *Eur, J. Org. Chem.* **2003**, 3242.

[8]   J. D. Koola, J. K. Kochi, *J. Am. Chem. Soc.*, **1987**, *26*, 908.

[9]   N. Sengottuvelan, D. Saravanakumar, V. Narayanan, M. Kandaswamy, K. Chinnakali, G. Senthilkumar, *Bull. Chem. Soc. Jpn.* **2004**, *77*, 1153.

[10]   F. DeRosa, X. Bu, P. C. Ford, *Inorg. Chem.* **2003**, *42*, 4171.

[11]   W. Peng, J. M. Shreeve, *J. Flourine. Chem.* **2005**, *126*, 1054.

[12]   G. Royal, V. Dahaoui-Gindrey, S. Dahaoui, A. Tabard, R. Guilard, P. Pullumbi, C. Lecomte, *Eur. J. Org. Chem.* **1998**, 1971.

[13]   J. F. Larrow, E. N. Jacobsen, Y. Gao, Y. Hong, X. Nie, C. H. Zepp, *J. Org. Chem.* **1994**, *54*, 1939.

[14]   D. A. Atwood, *Coord. Chem. Rev.* **1997**, *165*, 267.

[15]   A. R. Massah, M. Mosharafian, A. R. Momeni, H. Aliyan, H. J. Naghash, *Synthetic Commun.*, **2007**, *37*, 1815.

[16]   H. F. Lewis, S. Shaffer, W. Trieschmann, H. Cogan, *Ind. Eng. Chem.*, **1930**, *22*, 34.

[17]   J. Clayden, N. Greeves, S. Warren, P. Wothers, *Organic Chemistry*, **2001**, *1st Ed*, p 689, Oxford.

[18]   M. G. Orga, M. Abdel-Hadi, S. Avola, N. Hadei, J. Nasielski, C. J. O'Brien, C. Valente, *Chemistry A European Journal,* **2007,** *13,* 150.

[19]   K. V. Baker, J. M. Brown, N. Hughes, A. J. Skarnulis, A. Sexton, *J. Org. Chem.*, **1991**, *56*, 698.

[20]   J. F. W. McOmie, M. L. Watts, D. E. West, *Tetrahedron*, **1968**, *24*, 2289.

[21]   T. V. Hansen, L. Skatteboel, D. Guthrie, D. P. Curran, *Org. Synth.*, **2005**, *82*, 64.

[22]   G. Baccolini, P. E. Todesco, *J. Org. Chem.*, **1975**, *40*, 2318.

[23]   A. G. Brook, *Acc. Chem. Res.*, **1974**, *7*, 77.

Chapter 5

Overall Conclusions and Future Proposal

VIRTUE IS LEARNED AT YOUR MOTHER'S KNEE,
VICES ARE PICKED UP AT SOME OTHER JOINT.

5.1 N_4 Salcyan Ligands and Complexes

It is clear to see in Chapter 1 that there has been a substantial amount of work carried out on the study towards new metal complexes for the catalysis of the PA reaction over the course of several decades. The search for new catalysts for the phospho-aldol reaction has indeed covered a wide variety of chemistry, from non-metallic to metal systems and as the search continues a new path is paved.

Within the Kee group the main focus of the PA reaction has been towards the salcyen and salcyen Schiff base complexes of aluminium (Figure 5. 1).
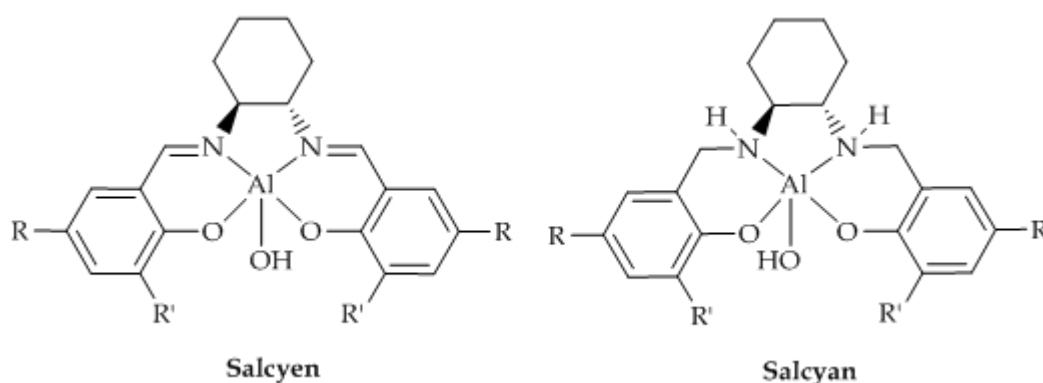
Figure 5. 1 Salcyan and salcyan Schiff base complexes, where R, R'=organo group

A substantial amount of work has been carried out in the Kee group with respect to synthesising new substituted aluminium salcyan complexes of which the vast majority have been catalytically tested. The main advantage of these systems is that they are not sensitive to air or moisture, they do not require heating or cooling and the catalyst loading is low (1-5 mol%).

However, thoughts soon turned to ways of improving the e.e. Molecular modelling had been carried out on potential complex structures to determine what structural factors could affect the catalytic outcome. It soon became apparent that substitution on the aromatic ring played a part in providing steric hindrance and by bringing it closer to the metal centre this could potentially cause stereo induction in the PA reaction. New salcyan ligands were developed containing *trans*-1,2-diaminocyclohexane backbones, with an N_4 binding motif instead of an N_2O_2 (Figure 5. 2).
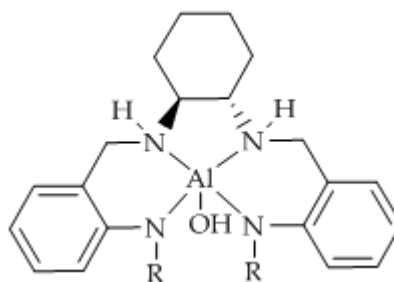
Figure 5. 2 General structure of an N_4 aluminium salcyan complex. R = organo group.

Synthesis of the ligands was extremely successful, in high yield and excellent purity, with new X-ray crystal structures also obtained. However creating the aluminium complex was not so successful. The standard procedure used to create aluminium complexes of the N_2O_2 motif uses trimethylaluminium in a dry dinitrogen atmosphere with heat. The alternative procedure also adopted in the Kee group is the addition of the ligand to aluminium isopropoxide in a dry dinitrogen atmosphere. Both procedures were attempted in trying to synthesise an N_4 aluminium salcyan complex, however neither were successful. A variety of bases were used in different proportions, however the reaction was still not successful. A possible solution could be that the added base (*e.g.* LDA) competes with the N_4 ligand for the trimethylaluminium as the lone pair of electrons of the N-R groups can also donate their electrons.

Complexation of the oxidised form of the N_4 salcyan, the N_4 salcyen has been successful in the Kee group. It would be interesting to see if it were possible to create an aluminium N_4 salcyen complex and then reduce the imine bond to form the aluminium N_4 salcyan complex.

5.2 Computational Studies Towards a Better Understanding of the PA Mechanism

Although creating new aluminium salcyan complexes is still of great interest to the Kee group, in order to better understand how new complexes can be developed it is important to understand just how the phospho-aldol reaction works and what role the aluminium salcyan complexes play. Currently there is no evidence towards the mechanism of the PA reaction, therefore a computational study was carried out on a selection of aluminium salcyan complexes of the structure $\{(R,R)\text{-}[salcyan(R)_2]Al(\mu\text{-}X)\}_2$

(X=OH or OMe, R=organo group). The initial computational study was to validate the use of our HyperChem 7.0 [10] system for molecular modelling studies done on potential aluminium salcyen and salcyan complexes. X-ray crystallographic data was used as a comparative tool and as an input tool for the Hartree-Fock, density functional theory and semi-empirical calculations. The main conclusion of the study is that the HyperChem semi-empirical calculations made a good comparison with the original X-ray data and could be used with a reasonable sense of confidence as a quick way of screening potential complexes as precursors in phospho-aldol catalysis. With this information in mind it was now possible to probe the mechanism of the PA reaction.

H/D exchange studies carried out in the Kee group demonstrated that deprotonation of DMHP was an important step of the reaction and the initial hypothesis was that it is the bridging OH that is responsible; however computational evidence shines a new light on this theory. [2]

Solid state (X-ray) and solution phase NMR studies also showed that the complexes remained in their dimeric forms. Further probing using 2D-diffusion ordered spectroscopy (DOSY) were carried out to see if any dissociation took place. The results showed that no form of dissociation took place. [2]

The solid state X-ray analyses of the crystal structures also gave some interesting results with regards to the shape around the metal centre. There appeared to be defined 'open' and 'closed' faces on some of the crystal structures, this was also apparent when looking at the electron density images of the DFT data. With this experimental evidence in mind it was now necessary to determine which site in the complex was the most basic and would act as a base in the mechanistic scheme. Computational calculations were carried out on the selection of complex structures and it was surprising to see that the most basic site of each of the complexes was not the bridging hydroxyl oxygen but it was in fact found on the salcyan phenoxy ring as shown by the HOMO and HOMO-1 data and corresponding images. Therefore in light of the experimental and computational evidence the picture for PA catalysis can be modified.
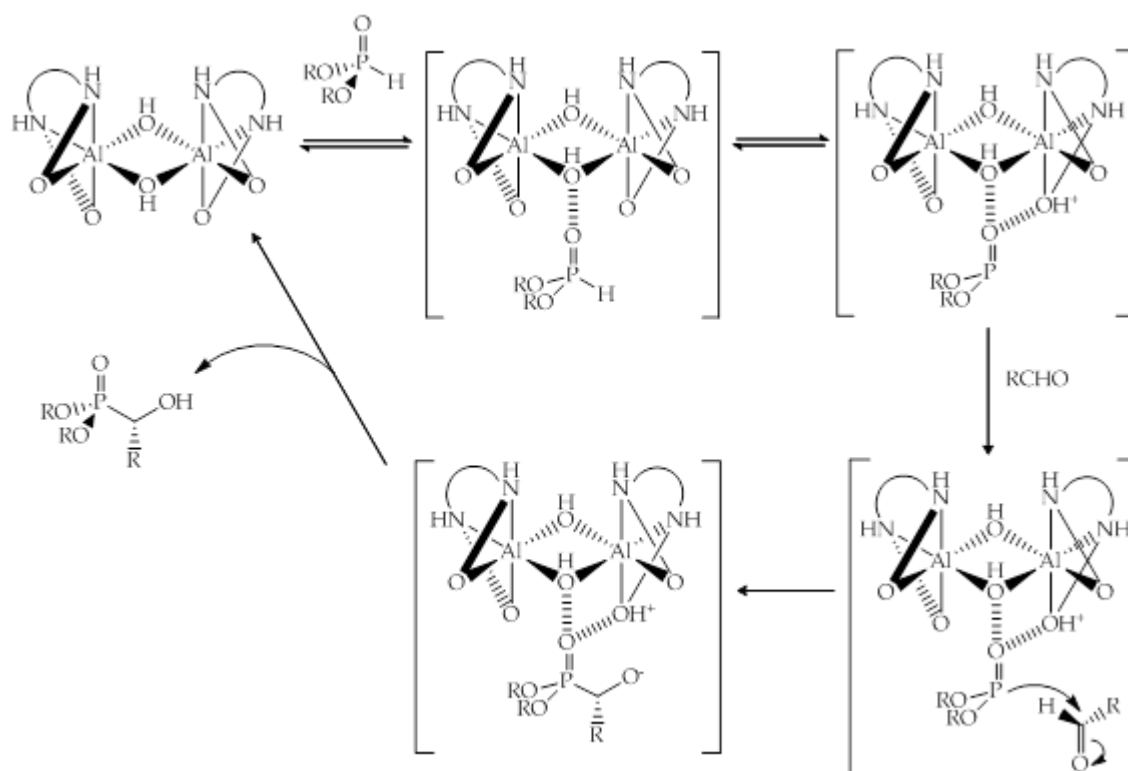
Scheme 5.1 Modified mechanistic outline for PA catalysis *via* dimeric aluminium salcyan complexes. [2]

Further computational calculations are being carried out to probe each transitional state of the proposed mechanism to see if indeed the new theories are correct. Without a complete and extensive computational study on the mechanism of the PA reaction it is not yet possible to say if the modified mechanistic outline (Scheme 5.1) is indeed the only possible mechanism.

5. 3 New Organophosphorus Substituted Salcyan Ligands

Now that there is a vast amount of experimental and computational data giving a clearer picture of the mechanism of the phospho-aldol reaction it was possible to tailor this information to help design and develop a better molecular framework. One of the major issues associated with the current synthesis of new aluminium salcyan complexes within the Kee group, and others, is that it is heavily dependent upon linear, synthetic chemistry wherein each potential new catalyst needs to be prepared using standard covalent modifications to existing ligand systems. This is both time

consuming and has no guarantee of success. A more satisfactory approach would be to construct a basic complex, capable of achieving a reasonable level of selectivity for a standard PA reaction, which could then be modified *via* simple addition of suitable co-factors tuned to a specific substrate. This approach would open up the possibility of parallel processing and analysis thus allowing rapid screening of co-factors against a given substrate. Using organophosphorus substituted salcyan complexes could potentially influence the stereochemistry of the PA reaction through steric and electronic effects. The ease with which these compounds could be synthesised was uncertain and the first synthetic pathway proved unsuccessful in its initial stages (Scheme 5.2).
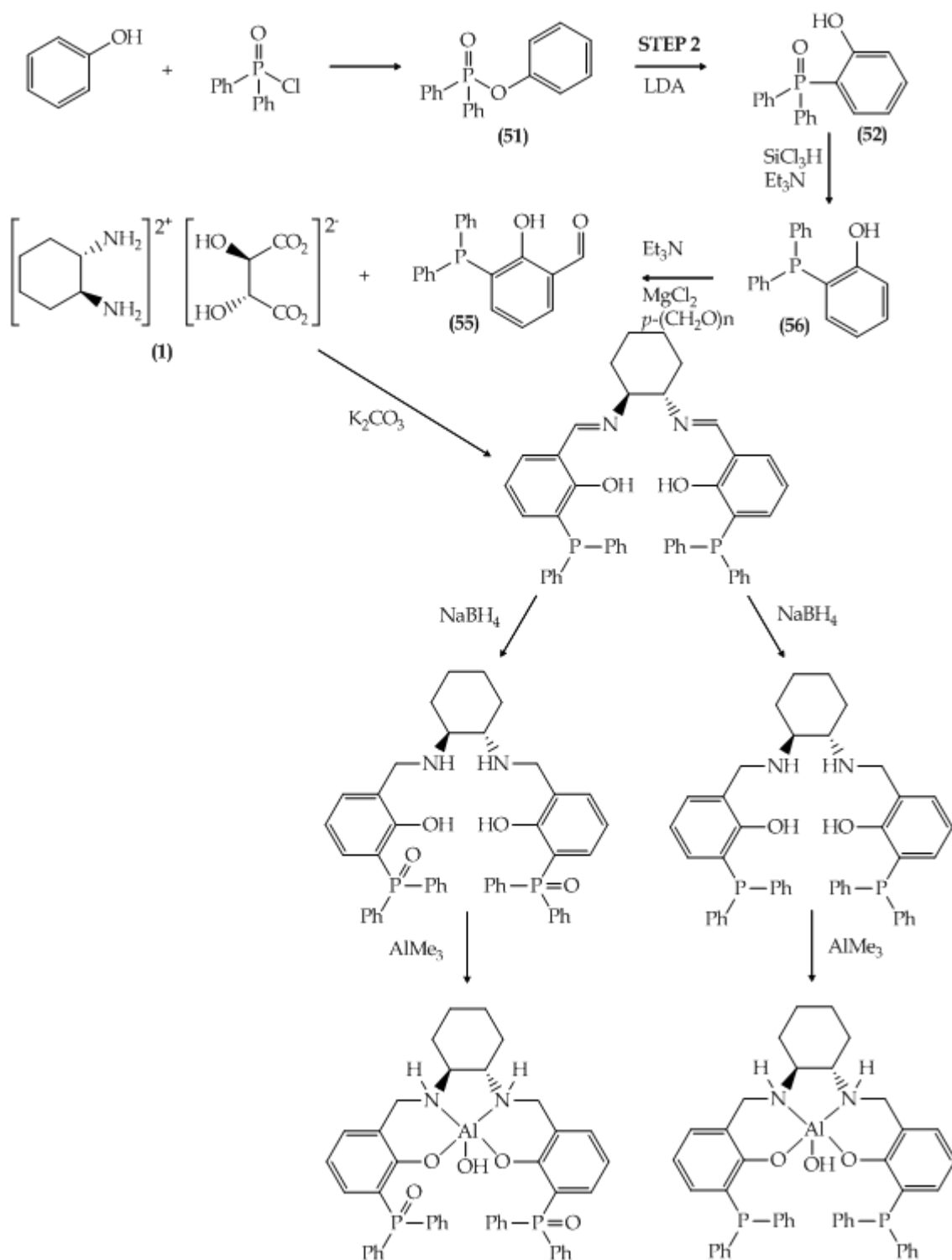
Scheme 5.2 Method 1 towards synthesising phosphorus substituted aluminium salcyan complex. All numbered steps have been synthesised or attempted.

The second synthetic pathway (Scheme 5.) was a little more rewarding and provided some interesting and new compounds, however this pathway was also challenging

and due to time constraints it was not possible to successfully synthesise a ligand precursor or complex.
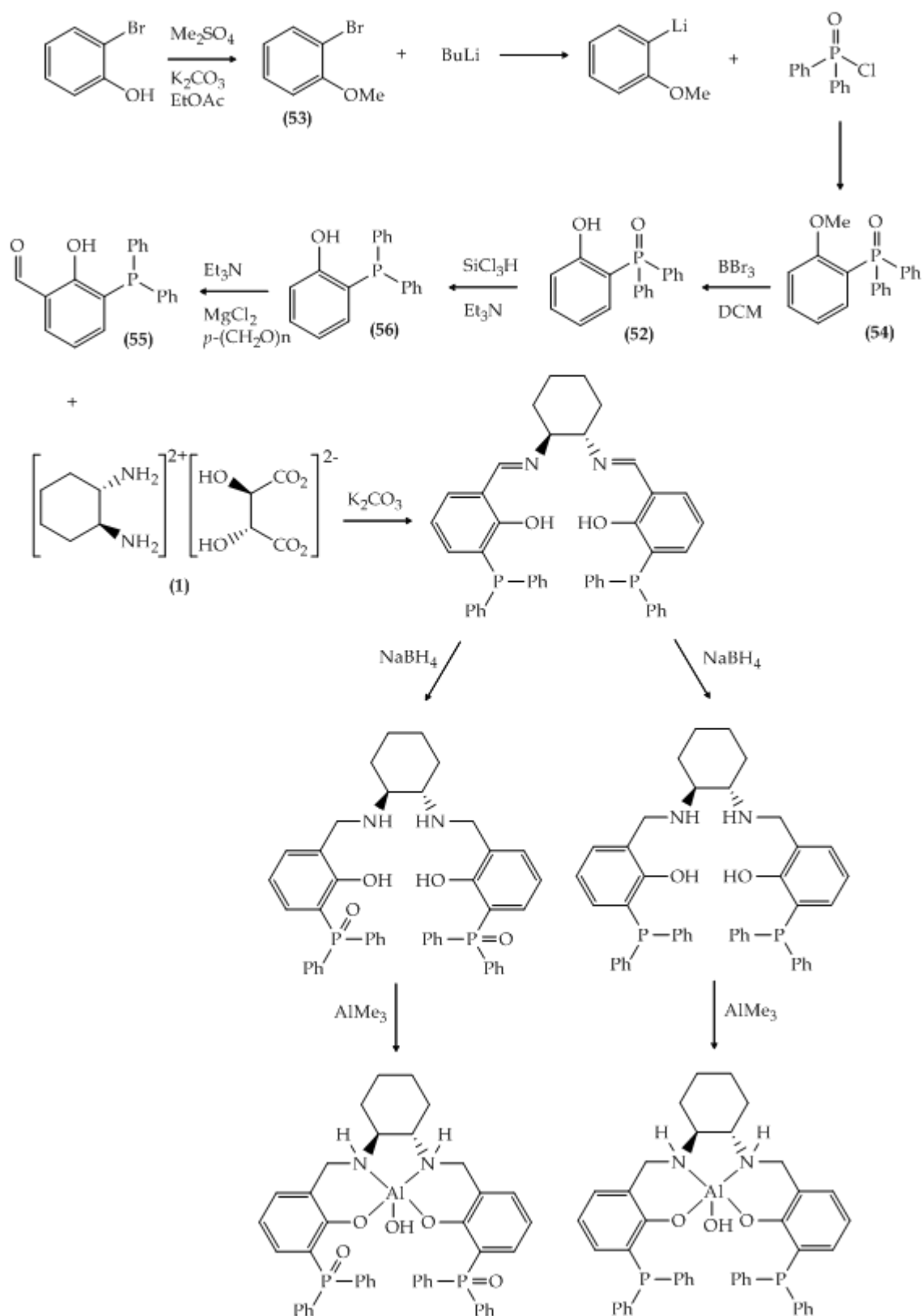
Scheme 5.3 Method 2 towards synthesising phosphorus substituted aluminium salcyan complex. All numbered steps have been synthesised or attempted.

5.4 Future Work Proposal

A new synthetic protocol is proposed in Scheme 5. for the synthesis of organophosphorus substituted salcyan aluminium complexes, one that would be worthy of further studying.
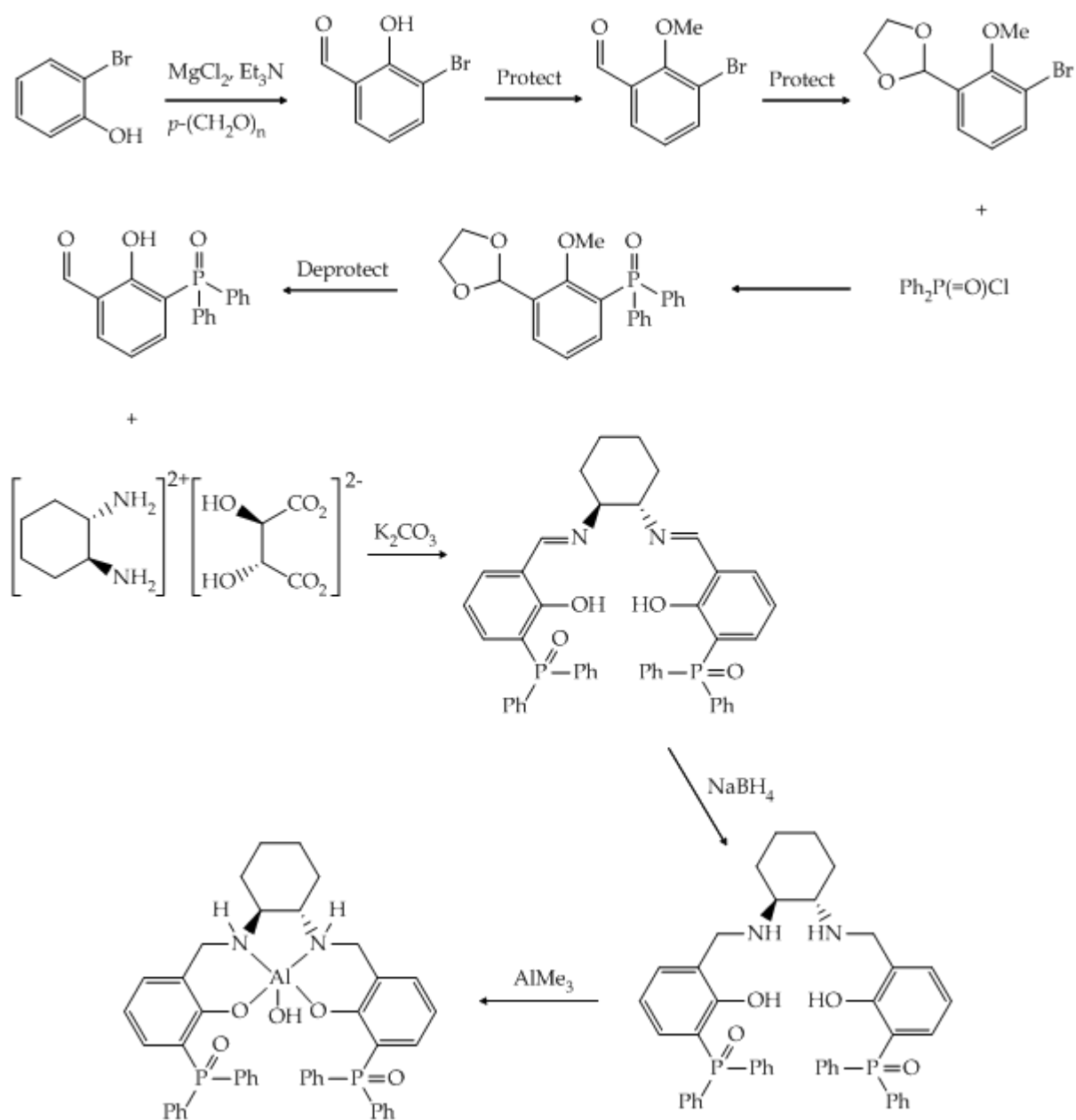
Scheme 5.4 Proposed new synthetic pathway towards the synthesis of a substituted phosphine oxide salcyan aluminium complex.

It is believed that by using two protecting steps, first a methoxy group, followed by a diol group would make creating the aromatic aldehyde much easier, this being the most challenging step of the synthetic route. There are no foreseeable difficulties in creating the diaminocyclohexane framework as the N_2O_2 motif has been synthesised extensively in the Kee group in high yield and purity.

5.5 References

[1]   HyperChem 7.0, Hypercube, Inc. Gainsville, FL, 32601, USA.

[2]   A. C. Gledhill, N. E. Cosgrove, T. D. Nixon, C. A. Kilner, J. Fisher, T. P. Kee, *Dalton Trans.*, **2010**, *39*, 9472.

Chapter 6

Experimental Details

THERE IS SOMETHING FASCINATING ABOUT SCIENCE.
ONE GETS SUCH WHOLESALE CONJECTURE OUT OF SUCH TRIFLING
INVESTMENTS.
MARK TWAIN

6.1 General considerations

All compounds were used as supplied or prepared as described herein. Solvents were pre-dried prior to use, THF, toluene and pentane were pre-dried over sodium wire and DCM was dried over calcium chloride. Subsequently, THF was distilled over sodium-metal and sodium-benzophenone ketyl, toluene over sodium metal, pentane over lithium aluminium hydride and DCM over calcium hydride. A twin drying column containing 4Å molecular sieves and potassium hydroxide was used to dry nitrogen gas prior to entry to the solvent stills.

^{1}H and ^{13}C {^{1}H} NMR spectra were recorded on a Bruker DPX300 spectrometer (operating frequency 300.1 MHz for ^{1}H and 75.48 MHz for ^{13}C) or a Bruker DRX 500 spectrometer (operating frequency 500.13 MHz for ^{1}H and 125 MHz for ^{13}C). All spectra were recorded at 300 K unless stated otherwise, chemical shifts (δ) are given in parts per million (ppm) downfield of tetramethylsilane (TMS) at zero ppm for ^{1}H resonances using $CHCl_3$ δ 7.24 ppm as an internal standard. ^{13}C {^{1}H} spectra were referenced to the centre triplet peak of deuterated chloroform (δ 77.2 ppm). Coupling constants J are given in Hertz (Hz). Multiplicities are reported as singlet (s), doublet (d), triplet (t), quartet (q) and sometimes a combination of broad singlet (bs) or multiplet (m) peaks. Spectroscopic assignments were performed where necessary by two-dimensional ^{1}H – ^{1}H and ^{13}C {^{1}H} – ^{1}H correlation techniques.

^{31}P {^{1}H} spectra were collected by Mr Simon Barrat on a Bruker DRX 500 spectrometer at operating frequency of 202.46 MHz at 300 K.

Mass spectra were recorded by Ms. Tanya Marinko-Covell on a Bruker Daltonics (Micro T.O.F) instrument operating in the electrospray mode in methanol or acetonitrile.

Elemental analyses were carried out by Mr Martin Huscroft at the University of Leeds Analytical Service.

Optical rotations were recorded at ambient temperature on an optical activity AA 10 polarimeter operating as 589.44 nm (sodium D-line) using a path-length of 0.5 dm and reported along with the solvent and concentration (C) in g /100 ml.

Melting points were recorded using a Bibby Stuart Scientific Melting point apparatus SMP3, recorded in degrees Celsius (°C) and are uncorrected.

Thin layer chromatography was carried out using silica gel (60 Å) TLC plates (flexible aluminium sheets, 200 μm thickness, 20 x 20 cm) as supplied by Fischer Scientific. They were visualised using a UVG-54 Mineralight short wave ultraviolet 254 nm lamp. Column chromatography was carried out using silica gel (35-70 μm particles), supplied by Fluorochem.

The intensity data for determination of the X-ray structures was collected at 150 (2) K using a Nonius Kappa CCD diffractometer or a Bruker-Ninius FR591/X8 Apex diffractometer both fitted with a charge-coupled device (CCD) area detector. Data collections were carried out at a temperature of 150 (2) K maintained by Oxford Cryostream apparatus providing a stream of dry nitrogen gas to the crystal. The structure data was collected by Mr C. A. Kilner and solved with SHELX-97 software.[1] Crystal structures were displayed and

manipulated using the X-seed program and colour pictures were rendered using POV-Ray.[2]   Graphics of molecular structures were also created using ORTEP3.[3]

Molecular modelling was carried out by inserting single crystal X-ray data into HyperChem 7.0 computational modelling software and energy minimised to Mm+ and semi-empirical PM3 level. [9]

Computational data was collected by inserting single crystal X-ray data into the graphical viewing software GaussView 4.1.2 and computational calculations carried out with Gaussian 03 program, revision C.02. Geometry optimisation calculations at RHF level with a 6-31 G* basis set and using a gradient-corrected hybrid density functional theory (DFT), B3LYP, with a 6-31 G* basis set. [10]

6.2 Synthesis of N_4 ligands based on aniline

6.2.1 Resolution of (R, R)-trans -1, 2-diaminocyclohexane (1) [6]
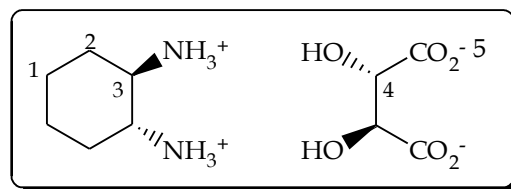
(1)

Procedure: In a 1l beaker, under ambient conditions, L-(+)-tartaric acid (150 g, 0.99 mol) was dissolved in distilled water (400 ml) and racemic-1, 2-diaminocyclohexane (223.44 g, 1.94 mol) added such that the reaction temperature reached *ca* 70 °C. Glacial acetic acid (100 ml, 1.75 mol) was added at a rate that the temperature reached *ca* 90 °C. The reaction mixture was allowed to cool to room temperature over a period of 2 hours and then to <5 °C for an additional 2 hours. The precipitate was collected by vacuum filtration, washed with ethanol and then dried under reduced pressure. Recrystallisation from distilled water afforded the title product as a white crystalline solid (117.5 g, 53%).

Melting point: 272.5 – 274.1 °C

Microanalysis %: ($C_{10}H_{20}N_2O_6$)

Found C: 45.6%, H: 7.7% and N: 10.5%. Requires C: 45.5%, H: 7.6% and N: 10.6%.

NMR spectroscopic data: ^{1}H NMR, (300 MHz, D_2O, 300K): δ = 4.69 (s, 12H, NH, OH), 4.30 (s, 2H, C_4H), 3.35 (m, 2H, C_3H), 2.14 (d, 2H, C_2H_{eq}), 1.77 (m, 2H, C_{1eq}), 1.76 (m, 2H, C_1H_{ax}), 1.31 (m, 2H, C_2H_{ax}).

^{13}C {^{1}H} NMR, (77MHz, D_2O 300K): δ = 178.7 (C_5), 74.2 (C_4), 52.6 (C_3), 29.7 (C_2), 23.2 (C_1)

Optical purity: $[\alpha]_D^{20}$ = +12.5 (c = 4 g/dl H_2O) (Literature value; $[\alpha]_D^{20}$ = +12.5)
[7]

6.2.2 Synthesis of 2-methylaminobenzaldehyde (13) [8]
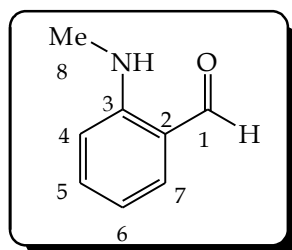
(13)

Procedure: In a 250ml two-neck flask equipped with a magnetic stirrer, to a slurry of anhydrous zinc chloride (14.30 g, 104.92 mmol) in dry tetrahydrofuran (100 ml) at 0°C, methyllithium (1.6 M solution in diethyl ether, 52.47ml, 83.95 mmol) was added. Upon warming to room temperature, a solution of anthranil (5.0 g, 41.97 mmol) in dry THF (10ml) followed by Ni(acac)$_2$ (0.54 g, 2.09 mmol) were added. After stirring for 2 h at room temperature the reaction was quenched with aqueous hydrochloric acid (6 M, 24 ml) then poured into water (100 ml) and the organics extracted into diethyl ether (2 × 100 ml), washed with water (50 ml) and the crude product concentrated *in vacuo*. The crude product was purified by flash column chromatography with eluent diethyl ether : hexane (1 : 3 v/v) to afford the title compound as a yellow oil (3.4 g, 59%).

Mass spectrum (EI): $[M – OH]^+$ = 106

Microanalysis %: (C_8H_9NO)

Found C: 71.2%, H: 6.6% and N: 10.2%. Requires C: 71.1%, H: 6.7% and N: 10.4%.

NMR spectroscopic data: ^{1}H NMR, (300 MHz, CDCl$_3$, 300K): δ = 9.86 (s, 1H, C$_1$H), 8.28 (bs, 1H, NH), 7.49 (dd, 1H, J^3 = 7.6 Hz, J^4 = 1.8 H,z C$_6$H), 7.37 (dd, 1H, J^3 = 6.9 Hz, J^4 = 1.4 Hz, C$_5$H), 6.75 (d, 1H, J^3 = 2.0 Hz, C$_4$H), 6.70 (d, 1H, J^3 = 3.4 Hz, C$_3$H), 2.92 (d, 3H, J^3 = 5.4 Hz, C$_8$H).

^{13}C {^{1}H} NMR, (77MHz, CDCl$_3$ 300K): δ = 194.3 (C$_7$), 152.0 (C$_2$), 136.9 (C$_6$), 136.2 (C$_5$), 119.0 (C$_1$), 115.1 (C$_4$), 110.8 (C$_3$), 29.5 (C$_8$).

6.2.3 Synthesis of 2-phenylamino benzaldehyde (14) [8]
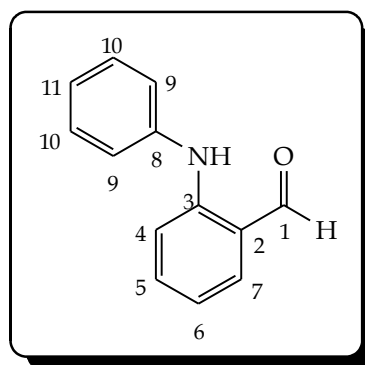
(14)

Procedure: 6.2.2 followed. Anhydrous zinc chloride (14.30 g, 104.92 mmol), phenyllithium (2.0M solution in –n-butyl ether, 41.98 ml, 83.95 mmol), anthranil (5.0 g, 41.97 mmol), Ni(acac)$_2$ (0.54 g, 2.09 mmol). The crude was purified by flash column chromatography with eluent diethyl ether: hexane (1:3 v/v) to afford title compound as a yellow solid. Recrystallisation from toluene afforded the title compound as large bright yellow needle crystals (6.1 g, 74%).

Melting point: 74.7 – 78.5 °C

Mass spectrum (ES): [M+H]$^+$ = 198

Microanalysis %: (C$_{13}$H$_{11}$NO)

Found C: 78.9%, H: 5.6 % and N: 7.2%. Requires C: 79.2%, H: 5.6% and N: 7.1%.

NMR spectroscopic data: ^{1}H NMR, (300 MHz, CDCl$_3$, 300K): δ = 10.05 (bs, 1H, NH), 9.91 (s, 1H, C$_1$H), 7.57 (dd, 1H, J^3 = 7.7 Hz, J^4 = 1.7 Hz, C$_3$H), 7.39 (m, 2H, C$_9$H), 7.33 (m, 1H, C$_4$H), 7.30 (m, 1H, C$_{10}$H), 7.28 (m, 1H, C$_5$H), 7.18 (m, 1H, C$_{11}$H), 6.89 (dd, 1H, J^4 = 1.0 Hz, C$_6$H).

^{13}C {^{1}H} NMR, (300MHz, CDCl$_3$ 300K): δ = 194.0 (C$_7$), 146.8 (C$_2$), 138.6 (C$_8$), 135.5 (C$_3$), 134.5 (C$_4$), 128.4 (C$_9$), 123.4 (C$_{11}$), 122.1 (C$_{10}$), 118.3 (C$_1$), 116.1 (C$_6$), 111.9 (C$_4$).

6.2.4 Synthesis of (*R,R*)-N,N′-bis-(2-methylamino-benzylidene)-trans-1,2-diaminocyclohexane (15) [6]
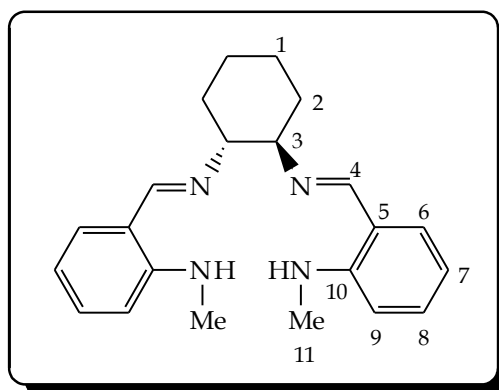
(15)

Procedure: In a 250 ml two-neck flask equipped with a magnetic stirrer, condenser and 100 ml addition funnel, methanol (50 ml) was added to tartrate salt **(1)** (0.977 g, 3.70 mmol) and anhydrous potassium carbonate (1.028 g, 7.44 mmol) dissolved in water (15 ml). The white slurry was heated to reflux and the solution of 2-methylaminobenzaldehyde **(13)** (1.005 g, 7.44 mmol) in methanol (30 ml) was added in a steady stream over 30 min. The solution was refluxed for a further 4 h, water (15 ml) was added and the solution allowed to cool to 0 °C overnight. The precipitate was collected by reduced pressure

filtration then extracted with dichloromethane (100 ml), washed with water (2 × 50 ml) and brine (1 × 30 ml), dried over magnesium sulphate and concentrated *in vacuo*, to yield a yellow powder. Recrystallisation from dichloromethane afforded compound **(17)** as yellow crystals (0.975 g, 76%).

Melting point: 120.9 – 123.6 °C

Mass spectrum (ESI): $[M+H]^+$ = 349.2

Microanalysis %: ($C_{22}H_{28}N_4$)

Found C: 75.8%, H: 8.3% and N: 16.0%. Requires C: 75.8%, H: 8.1% and N: 16.1%.

NMR spectroscopic data: ^1H NMR, (300 MHz, CDCl$_3$, 300K): δ = 8.90 (bs, 1H, NH), 8.29 (s, 2H, C_4H), 7.21 (ddd, 2H, J^3 = 7.8 Hz, J^4 = 1.5 Hz, C_7H), 7.12 (dd, 2H, J^3 = 7.5 Hz, J^4 = 1.5 Hz, C_6H), 6.73 (m, 2H, C_9H), 6.58 (m, 2H, C_8H), 3.27 (m, 2H, C_3H), 2.89 (d, 6H, $C_{11}H$), 1.89 (s, 2H, C_2H), 1.74 (s, 2H, C_1H), 1.56 (s, 2H, C_2H), 1.48 (s, 2H, C_1H).

^{13}C {^1H} NMR, (77MHz, CDCl$_3$ 300K): δ = 163.7 (C_4), 150.5 (C_{10}), 134.0 (C_6), 131.4 (C_7), 117.7 (C_5), 114.4 (C_8), 109.8 (C_9), 74.5 (C_3), 33.8 (C_2), 29.6 (C_{11}), 25.0 (C_1).

6.2.5 Synthesis of (*R*,*R*)-N,N'-bis-(2-phenylamino-benzylidene)-trans-1,2-diaminocyclohexane (16) [6]
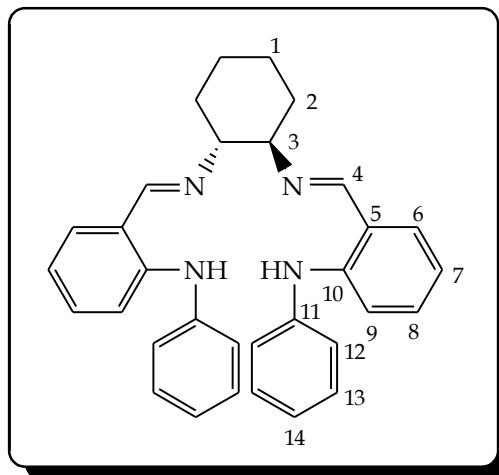
(16)

Procedure: **6.2.4** followed: potassium carbonate (0.703 g, 5.09 mmol), tartrate salt **(1)** (0.671 g, 2.54 mmol), ethanol (50 ml), 2-phenylamino-benzaldehyde **(14)** (1.000g, 5.07 mmol), ethanol (30 ml). Title compound was afforded as pale yellow crystals recrystallised from dichloromethane (0.9555 g, 80%).

Melting point: 59.8 – 64.7 °C

Mass spectrum (ES): $[M + H]^+$ = 473, $[M + 2H]^+$ = 474.

Microanalysis %: ($C_{32}H_{32}N_4$)

Found C: 81.4%, H: 6.9% and N: 11.8%. Requires C: 81.3%, H: 6.8% and N: 11.9%.

NMR spectroscopic data: ^{1}H NMR, (300 MHz, CDCl$_3$, 300K): δ = 11.2 (s, 2H, NH), 8.3 (s, 2H, C_4H), 7.3 (m, 4H, C_{13}H), 7.2 (m, 2H, C_9H), 7.1 (m, 4H, C_{12}H), 7.0 (m, 2H, C_7H), 6.9 (m, 2H, C_{14}H), 6.8 (dd, 2H, J^3 = 7.6 Hz, J^4 = 1.4 Hz, C_6H), 6.7 (ddd, 2H, J^4 = 1.0 Hz C_8H), 3.3 (m, 2H, C_3H), 1.9 (m, 2H, C_1H and C_2H), 1.7 (m, 2H, C_2H), 1.5 (m, 2H, C_1H).

^{13}C {^{1}H} NMR, (77MHz, CDCl$_3$ 300K): δ = 163.8 (C$_4$), 149.4 (C$_{10}$), 142.2 (C$_{11}$), 134.3 (C$_6$), 129.8 (C$_7$), 129.0 (C$_{13}$), 121.5 (C$_{12}$), 119.1 (C$_5$), 116.5 (C$_8$), 110.1 (C$_9$), 76.9 (C$_3$), 31.32 (C$_2$), 25.2 (C$_1$).

6.2.6 Synthesis of (*R,R*)-N,N′-bis-(2-methylamino-benzyl)-trans-1,2-diaminocyclohexane (17) [9]
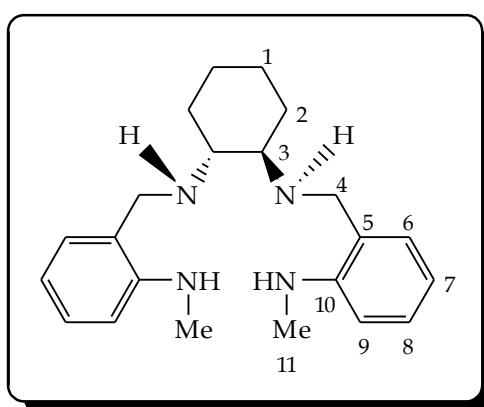
(17)

Procedure: In a 500 ml two-neck flask, equipped with a magnetic stirrer and a condenser, salcyen **(15)** (300 mg, 0.86 mmol) was dissolved in ethanol (15 ml) and heated at reflux for 30 min. Sodium borohydride (330 mg, 8.61 mmol) was added in small portions and the solution maintained at reflux until no yellow colouration remained. Water was added (15 ml) and the crude collected as a white solid by reduced pressure filtration. Recrystallisation from pentane afforded the title compound **(17)**, as a white crystalline solid (185 mg, 61%).

Melting point: 104 – 107 °C

Mass spectrum (ES): [M + H]$^+$ = 353, [M – C$_8$H$_8$N]$^+$ = 234

Microanalysis %: (C$_{22}$H$_{32}$N$_4$)

Found C: 74.3%, H: 9.1% and N: 15.8%.   Requires C: 74.9%, H: 9.1% and N: 15.8%.

NMR spectroscopic data: ^{1}H NMR, (300 MHz, CDCl$_3$, 300K): δ =7.29 (ddd, 2H, J^3 = 7.7 Hz, J^4 = 1.6 Hz, C$_7$H), 7.01 (dd, 2H, J^3 = 7.3 Hz, J^4 = 1.7 Hz, C$_6$H), 6.65 (ddd, 2H, J^3 = 87.4 Hz, J^4 = 1.1 Hz, C$_8$H), 6.56 (dd, 2H, J^3 = 7.6 Hz, J^4 = 0.7 Hz, C$_9$H), 5.30 (bs, 2H, NH), 3.89 (d, 2H, J^3 = 12.2 Hz, C$_4$H), 3.56 (d, 2H, J^3 = 11.9 Hz, C$_4$H), 2.65 (s, 2H, C$_{11}$H), 2.20 (m, 2H, C$_3$H), 1.77 (m, 2H, C$_2$H), 1.29 (m, 2H, C$_1$H).

^{13}C {^{1}H} NMR, (77MHz, CDCl$_3$ 300K): δ = 149.5 (C$_{10}$), 129.7 (C$_7$), 128.9 (C$_6$), 124.6 (C$_5$), 116.4 (C$_8$), 110.0 (C$_9$), 61.5 (C$_3$), 50.8 (C$_4$), 31.7 (C$_2$), 30.2 (C$_{11}$), 25.2 (C$_1$).

6.2.7 Synthesis of (*R*,*R*)-N,N′-bis-(2-phenylamino-benzyl)-trans-1,2-diaminocyclohexane (18) [9]
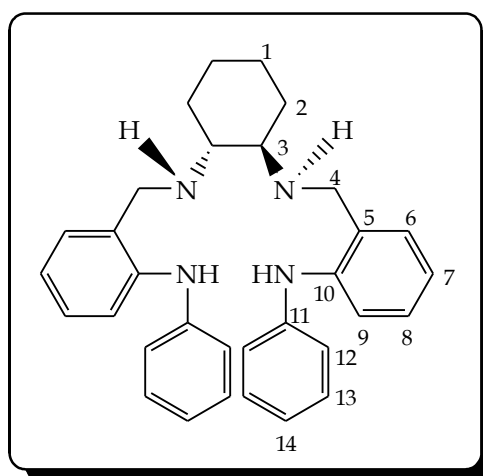
(18)

Procedure: 6.2.6 followed: salcyen **(16)** (955 mg, 2.02 mmol), ethanol (15 ml) and sodium borohydride (764 mg, 20.20 mmol). Title compound **(18)** was afforded as off-white crystals, (1.92 g, 78 %) recrystallised from dichloromethane.

Melting point: 59.5 – 62.2 °C

Mass spectrum (ES): $[M - H]^+ = 477$, $[M - C_{12}H_{12}N_2]^+ = 296$

Micro analysis %: $(C_{32}H_{36}N_4)$

Found C: 80.2%, H: 7.6% and N: 11.4%. Requires C: 80.6%, H: 7.6% and N: 11.8%.

NMR spectroscopic data: ^{1}H NMR, (300 MHz, CDCl$_3$, 300K): δ = 8.06 (bs, 2H, NH), 7.19 (ddd, 2H, J^3 = 7.6 Hz, J^4 = 1.7 Hz, C$_7$H), 7.14 (m, 2H, C$_{14}$H), 7.11 (dd, 2H, J^3 = 3.1 Hz, J^4 = 2.2 Hz, C$_6$H), 6.85 (m, 2H, C$_8$H), 6.82 (dd, 2H, J^3 = 3.1 Hz, J^4 = 1.1 Hz, C$_9$H), 6.79 (m, 4H, C$_{13}$H), 6.77 (m, 4H, C$_{12}$H), 4.00 (d, 2H, J^3 = 11.8 Hz, C$_4$H), 3.64 (d, 2H, J^3 = 11.8 Hz, C$_4$H), 2.35 (m, 2H, C$_3$H), 1.82 (m, 2H, C$_2$H), 1.38 (m, 2H, C$_1$H), 1.15 (m, 2H, C$_2$H), 0.93 (m, 2H, C$_1$H).

^{13}C {^{1}H} NMR, (77MHz, CDCl$_3$ 300K): δ =143.9 (C$_{10}$), 130.5 (C$_6$), 129.6 (C$_7$), 128.6 (C$_{13}$), 120.51 (C$_{14}$), 120.1 (C$_{12}$), 118.0 (C$_5$), 116.1 (C$_8$), 91.6 (C$_9$), 77.4 (C$_3$), 31.5 (C$_2$), 25.0 (C$_1$).

6.3 Synthesis of N$_4$ ligands based on pyrrole

6.3.1 Synthesis of pyrrylmagnesium bromide (19) [10]
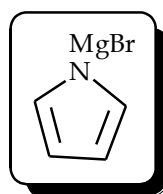
(19)

Procedure: All manipulations were carried out under a nitrogen atmosphere using oven dried apparatus due to the water sensitive nature of the Grignard reagent. Pyrrole (15 g, 0.22 mol) dissolved in THF (100 ml) was placed in a 250 ml 3-necked round bottomed flask. Methylmagnesium bromide (28.8 g, 0.24

mol) was added dropwise *via* a dropping funnel. The reaction mixture was stirred at room temperature until the gas evolution ceased after which it was refluxed for 2 hours at 65-67°C. The Grignard was then left to cool to room temperature to reveal a chocolate brown liquid (30.15 g, 80%). No analysis was performed on this liquid which was used as prepared directly in the next step.

6.3.2 Attempted synthesis of *tert*-butyl pyrrole (20) [10]
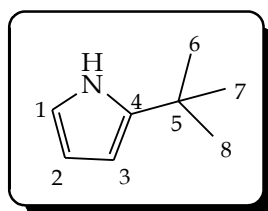
(20)

Procedure: *t*-Butyl chloride (37.46 g, 0.22 mol) was added to a refluxing solution of Grignard **(19)** (30.15 g, 0.22 mol) in dry tetrahydrofuran (100 ml) and refluxed for 3 h. Upon cooling to ambient temperature, water (100 ml) was added and the organics extracted into diethyl ether (2 × 50 ml). The crude product was dried over magnesium sulphate and concentrated *in vacuo*. Purification *via* flash column chromatography was unsuccessful with the following eluent systems (v/v): ethyl acetate (1): hexane (3): 10% methanol; dichloromethane (9): methanol (1). NMR analysis of the crude product revealed a mixture of products, however, signals which were consistent with the title compound **(20)** were observed although attempted purification proved unsuccessful.

NMR spectroscopic data: ^{1}H NMR, (300 MHz, CDCl$_3$, 300K): NMR analysis revealed the recovery of the starting materials as well as unknown impurities.

Purification was not clean. δ = 8.25 (bs, 1H, NH), 6.86 (s, 2H, C_1H – pyrrole), 6.30 (s, 2H, C_2H – pyrrole), 3.75 (m, alkyl – *t*-butyl), 3.49 (m, alkyl – *t*-butyl).

6.3.3 Attempted synthesis of pyrrole-carboxaldehyde (22)
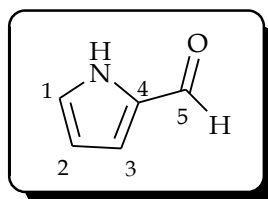
(22)

Procedure: Pyrrole (1.00 g, 14.90 mmol), triethylamine (5.50 g, 54.39 mmol), acetonitrile (50 ml) and paraformaldehyde (3.00 g, 100.00 mmol) and magnesium chloride (2.16 g, 22.76 mmol) were all placed in a 250 ml two-neck flask with a condenser and magnetic stirrer and refluxed for 4 h. The solution was cooled to room temperature and acidified with 5% aqueous hydrochloric acid (pH2). The organics were extracted into diethyl ether (3 × 40ml), dried over magnesium sulphate and concentrated *in vacuo* to leave muddy brown, treacle like liquid. NMR analysis of the crude product revealed a mass of impurities, with no distinctive peaks visible.

NMR spectroscopic data: ^{1}H NMR, (300 MHz, CDCl$_3$, 300K): NMR analysis revealed the recovery of the starting materials as well as unknown signals which did not appear to be consistent with the required product.

6.3.4 Attempted synthesis of 3,4-diethyl-2-methoxy methyl pyrrole carboxaldehyde (23) [11]
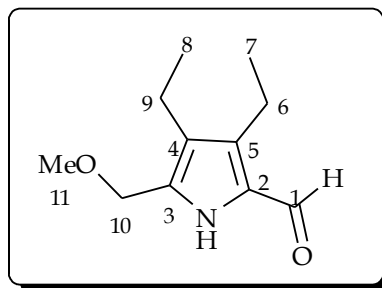
(23)

Procedure: To a stirred solution of 3-hexyne (1.14 ml, 10 mmol), and Ti(O-*i*Pr)$_4$ (3.70 ml, 12.5 mmol) in dry tetrahydrofuran (10 ml) was added *i*-PrMgCl (2.64 ml, 25 mmol) at -78°C under nitrogen. The yellow solution was warmed to -50°C over 30 minutes and left to stir for 3 h, α-methoxyacetonitrile (2.23 ml, 30 mmol) was introduced, resulting in a brown colouration, and left for a further 3 h to stir at -50°C. The solution was left to warm to room temperature overnight and the reaction terminated with aqueous hydrochloric acid (10 ml, 1 M) and vigorously stirred for 15 min. The organic products were extracted into diethyl ether (30 ml), washed with aqueous sodium hydrogen carbonate (15 ml), washed with water (50 ml), dried over sodium sulphate, filtered and the solvents concentrated *in vacuo*.

NMR spectroscopic data: ^{1}H NMR, (300 MHz, MeOH, 300K): NMR analysis revealed the recovery of the starting materials as well as signals which did not appear to be consistent with the required product.

6.3.5 Attempted synthesis of (*R*,*R*)-N,N′-bis-(1H-pyrrol-2-ylmethylene)-1,2-diaminocyclohexane (24) [6]
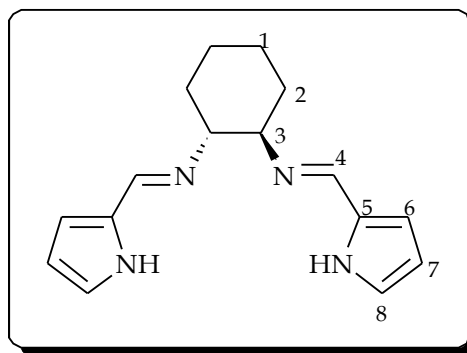
(24)

Procedure: In a 250ml two neck flask equipped with a condenser, magnetic stirrer and a 100ml addition funnel, tartrate (0.8 g, 7 mmol), potassium carbonate (1.93 g, 14 mmol) and water (20 ml) were added and stirred until fully dissolved. Ethanol (50 ml) was added and the solution brought to reflux. Pyrrole-2-carboxaldehyde (1.34 g, 14 mmol) was dissolved in ethanol (30 ml) and added in a steady stream over 30 min. No colour change occurred. The solution was refluxed for a further 5 h, water added (20 ml) and the mixture cooled to 5 °C overnight. A white precipitate was filtered off and extracted into DCM (30 ml), washed with brine (30 ml) and water (30 ml), the organics were separated off and dried over sodium sulphate and the solvents removed under reduced pressure to yield and colourless viscous oil. Analysis by NMR revealed only starting material and no indication of signals corresponding to pyrrole.

NMR spectroscopic data: ¹H NMR, (300 MHz, CDCl₃, 300K): NMR analysis revealed recovery of starting material.

6.3.6 Synthesis of (*R*,*R*)-N,N′-bis-(1H-pyrrol-2-ylmethylene)-1,2-diaminocyclohexane (25) [12]
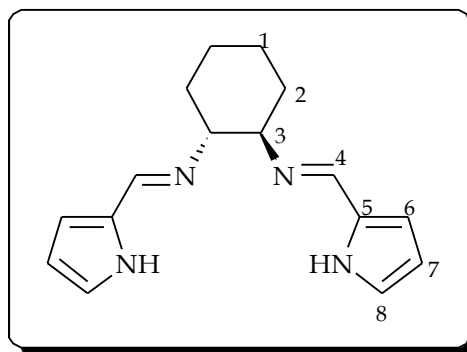
(25)

Procedure: *cis*/*trans*-diaminocyclohexane (239.8 mg, 0.26 ml, 2.1 mmol) and pyrrole-2-carboxaldehyde (400 mg, 4.2 mmol) were dissolved in ethanol (20 ml). The resulting mixture was stirred under a nitrogen atmosphere for 6 h. Solvent was removed under reduced pressure to yield a white precipitate in orange oil. The title compound was recrystallised from methanol.

Mass spectrum (ES): $[M + H]^+ = 269.2$

NMR spectroscopic data: ^{1}H NMR, (300 MHz, CDCl$_3$, 300K): $\delta = 7.88$ (s, 2H, C$_4$H), 6.90 (dd, 2H, C$_6$H), 6.47 (dd, 2H, C$_7$H), 6.27 (dd, 2H, C$_8$H), 5.53 (bs, 2H, NH), 2.82 (m, 2H, C$_3$H), 1.85 (m, 2H, C$_2$H), 1.76 (m, 2H, C$_1$H), 1.51 (m, 2H, C$_2$H), 1.26 (m, 2H, C$_1$H).

6.4 Cyclams

6.4.1 Synthesis of 1, 4, 8, 11-tetraazacyclohexadecane (26) [13]
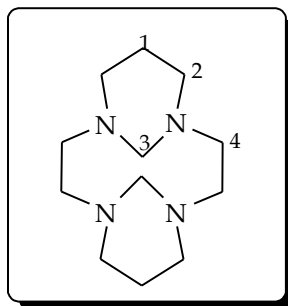
(26)

Procedure: In a 100ml round bottom flask 2 equivalents of formaldehyde (0.44 ml, 37 % H_2O) were rapidly added to a solution of 1, -4, -8, -11-tetraazacyclotetradecane (0.47 g, 2.35 mmol) in water (40 ml) at 0 °C (ice-bath used). The reaction mixture was stirred for 2 h upon which a white precipitate formed that was filtered off under reduced pressure, washed with water (20 ml) and dried under reduced pressure to yield the title compound as a white solid (499 mg, 95 %).

Mass spectrum (ES): $[M + H]^+$ = 225.2

Micro analysis %: ($C_{12}H_{24}N_4$)

Found C: 64.1%, H: 10.8% and N: 25.1%. Requires C: 64.2%, H: 10.8% and N: 25.0%.

NMR spectroscopic data: ^1H NMR, (300 MHz, $CDCl_3$, 300K): δ = 5.42 (dt, 2H, J^2 = 2.3 Hz, J^3 = 10.9 Hz, C_3H), 3.46 (dd, 2H, J^3 = 14.1 Hz, J^4 = 7.2 Hz, C_3H), 3.15 (dd, 4H, J^3 = 8.4 Hz, J^4 = 1.5 Hz, C_4H), 2.88 (d, 2H, J^3 = 10.9 Hz, C_3H), 2.84 (m, 4H, C_1H), 2.79 (m, 4H, C_1H), 2.66 (td, 4H, J^2 = 3.8 Hz, J^3 = 12.4 Hz, C_4H), 2.41 (dd, 2H, J^3 = 9.1 Hz, J^4 = 1.6 Hz, C_1H), 1.19 (m, 2H, C_1H).

^{13}C {^{1}H} **NMR, (77MHz, CDCl$_3$, 300K):** δ = 69.3 (C$_3$), 54.1 (C$_2$), 49.8 (C$_4$), 20.7 (C$_1$).

6.4.2 Synthesis of 1, 8-dimethyl-4, 11-diazoniatricyclo [9.3.1.1] hexadecane diiodide (27) [13]
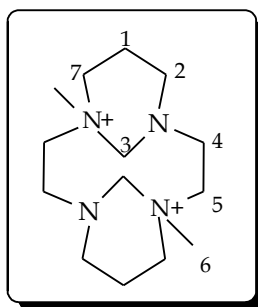
(27)

Procedure: 1, -4, -8, -11-Tetraazatricyclohexadecane (0.49 g, 2.23 mmol) was stirred in acetonitrile (15 ml) until dissolved. Methyl iodide (0.27 ml, 4.46 mmol) was rapidly added and the solution stirred at room temperature for 2 h. A white precipitate formed which was filtered off and washed with acetonitrile (10 ml), and dried under reduced pressure to yield the title compound as a white solid (1.08 g, 73 %).

Mass spectrum (ES): [M – I]$^+$ = 381.2, [M – (CH$_3$)$_2$ + I]$^+$ = 351.2

Micro analysis % : (C$_{14}$H$_{30}$N$_4$$^{2+}$)

Found C: 65.9%, H: 11.9% and N: 22.1%. Requires C: 66.1%, H: 11.9% and N: 22.0%.

NMR spectroscopic data: ^{1}H NMR, (300 MHz, CDCl$_3$, 300K): δ = 5.49 (dt, 2H, J^3 = 12.3 Hz, C$_3$H), 3.16 (m, 4H, C$_4$H), 2.95 (d, 2H, C$_3$H), 2.91 (m, 4H, C$_1$H), 2.66 (td, 4H, C$_4$H), 2.41 (m, 2H, C$_1$H), 1.64 (m, 2H, C$_1$H).

^{13}C {^{1}H} NMR, (77MHz, CDCl$_3$, 300K): δ = 69.3 (C$_3$), 54.1 (C$_2$), 49.8 (C$_4$), 20.7 (C$_1$).

6.4.3 Synthesis of 1, 8-dimethyl-1, 4, 8, 11-tetraazacyclotetradecane hexadecane diiodide (28) [13]
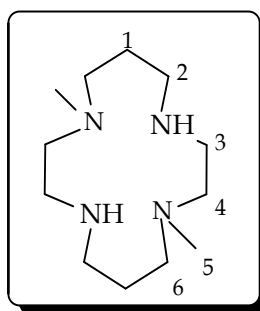
(28)

Procedure: 1, 8-Dimethyl-4, 11-diazoniatricyclo [9.3.1.1] hexadecane diiodide (300 mg, 0.59 mmol) was stirred in an aqueous solution of sodium hydroxide (3 M, 60 ml) for 3 h. The colourless solution was extracted with chloroform (5 x 30 ml) and the organic phases combined, dried over sodium sulphate and the solvents removed *via* reduced pressure to afford the product as a white solid (284.5 mg, 61 %).

Mass spectrum (ES): [M + H]$^+$ = 229.2, iodine's removed; [M – 2I] = 228.2.

Micro analysis % (C$_{14}$H$_{26}$N$_4$) very hygroscopic – evidence from MSDS from Aldrich

Found C: 60.7%, H: 11.8% and N: 22.7%. Requires C: 63.1%, H: 12.4% and N: 24.5%.

NMR spectroscopic data: ^{1}H NMR, (300 MHz, CDCl$_3$, 300K): δ = 2.68 (m, 4H, C$_2$H), 2.62 (m, 2H, C$_3$H), 2.42 (m, 8H, C$_4$H/C$_6$H), 2.18 (s, 6H, C$_5$H), 1.73 (m, 4H, C$_1$H).

^{13}C {^{1}H} NMR, (77MHz, CDCl$_3$, 300K): δ = 58.3 (C$_4$/C$_6$), 57.7 (C$_4$/C$_6$), 50.6 (C$_2$), 47.7 (C$_3$), 42.1 (C$_5$), 26.4 (C$_1$).

A: N$_2$O$_2$ systems based on phenol

6.4.4 Synthesis of (R, R)-N, N'-bis-(2-hydroxy-3-benzylidene)-1,2-diaminocyclohexane – (R, R)-[salcyen] (29) [6]
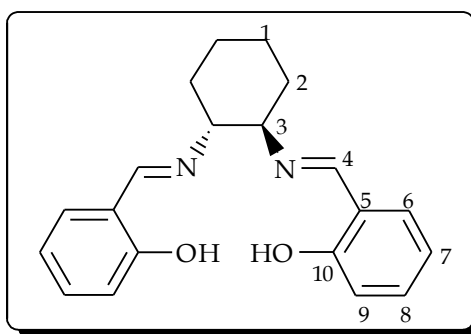
(29)

Procedure: In a 250 ml two neck flask equipped with a magnetic stirrer, condenser and 100 ml addition funnel, tartrate salt **(1)** (1.85 g, 7.0 mmol) and anhydrous potassium carbonate (1.93 g, 14.0 mmol) were added and dissolved in water (10 ml). Ethanol was added (40 ml) and the solution heated to reflux. Salicylaldehyde (1.49 ml, 14.0 mmol) dissolved in ethanol (17 ml) was gradually added to the refluxing mixture over a period of 30 min, resulting in a yellow solution and refluxed for a further 4 h. Water was added (15 ml) and the solution was allowed to cool to 5°C overnight. The yellow precipitate was

filtered off, extracted into dichloromethane (40 ml), washed with brine (15 ml) and water (15 ml). The organic layers were then dried over sodium sulphate, filtered and the solvents removed under reduced pressure to yield yellow crystals (2.25 g, 98 %).

Melting point: 62.6 – 64.7 °C

Mass spectrum (ES): $[M + H]^+$ = 323.2

Microanalysis %: ($C_{20}H_{22}N_2O_2$)

Found C: 73.5%, H: 6.8% and N: 8.5%. Requires C: 74.5%, H: 6.9% and N: 8.7%.

NMR spectroscopic data: ^{1}H NMR, (300 MHz, CDCl$_3$, 300K): δ = 13.30 (s, 2H, OH), 8.25 (s, 2H, C_4H), 7.23 (t, 2H, C_8H), 7.21 (dd, 2H, C_6H), 6.87 (dd, 2H, C_9H), 6.79 (t, 2H, C_7H), 3.31 (m, 2H, C_3H), 1.96 (m, 2H, C_2H), 1.86 (m, 2H, C_1H), 1.56 (m, 2H, C_2H), 1.44 (m, 2H, C_1H).

^{13}C {^{1}H} NMR, (77MHz, CDCl$_3$, 300K): δ = 163.7 (C_4), 159.9 (C_5), 131.1 (C_6), 130.4 (C_7), 117.6 (C_{10}), 115.7 (C_8), 89.1 (C_3), 32.1 (C_2), 23.2 (C_1).

6.4.5 Synthesis of (*R, R*)-N, N′-bis (2-hydroxy-3-tert-butyl-benzylidene)-1, 2-diaminocyclohexane – (*R,R*)-[salcyen-3-(^{t}Bu)$_2$] (30) [6]
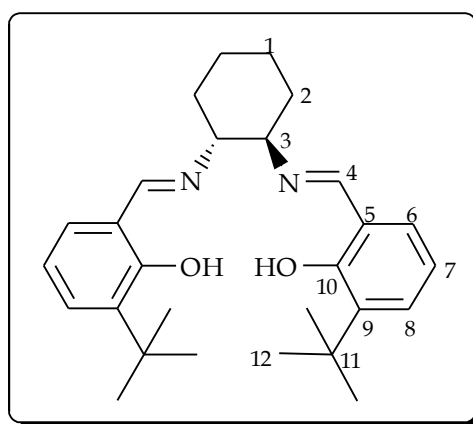
(30)

Procedure: 7.4.4 followed. Tartrate salt **(1)** (1.85 g, 7.0 mmol), potassium carbonate (1.93 g, 14.0 mmol), water (10 ml), ethanol (50 ml), 3-*tert*-butyl-2-hydroxybenzaldehyde (2.40 ml, 14.0 mmol), and ethanol (30 ml). Title compound (**30)** was isolated as yellow crystals recrystallised from dichloromethane (2.98 g, 98%).

Melting point: 81.3 °C

Mass spectrum (ES): $[M + H]^+$ = 435.30

Microanalysis %: ($C_{28}H_{38}N_2O_2$)

Found C: 76.9%, H: 8.8% and N: 6.0%. Requires C: 77.4%, H: 8.8% and N: 6.5%.

NMR spectroscopic data: ^{1}H NMR, (300 MHz, CDCl$_3$, 300K): δ = 13.37 (s, 2H, OH), 8.32 (s, 2H, C_4H), 7.30 (dd, 2H, J^4 = 1.7 Hz, C_6H) 7.28 (dd, 2H, J^4 = 1.6 Hz, C_8H), 6.85 (t, 2H, J^3 = 8.2 Hz, C_7H), 3.39 (m, 2H, C_3H), 1.99 (m, 2H, C_2H), 1.93 (m, 2H, C_1H), 1.60 (s, 9H, C_{12}H), 1.58 (m, 2H, C_2H), 1.54 (m, 2H, C_1H).

^{13}C {^{1}H} NMR, (77MHz, CDCl$_3$, 300K): δ = 167.4 (C_4), 162.2 (C_5), 138.9 (C_6), 131.6 (C_7), 131.1 (C_9), 120.5 (C_{10}), 119.6 (C_8), 74.3 (C_3), 36.6 (C_{11}), 35.0 (C_2), 31.2 (C_{12}), 26.2 (C_1).

6.4.6 Synthesis of (*R*,*R*)-[salcyan-3-(^{t}Bu)$_2$] (31) [9]
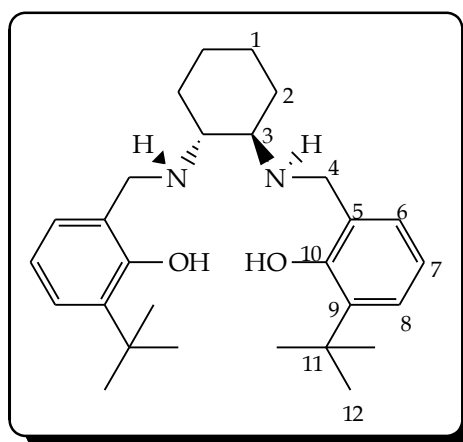
(31)

Procedure: 6.2.6 followed. Salcyen **(30)** (2.98 g, 6.86 mmol), ethanol (50 ml) and sodium borohydride (2.59 g, 68.6 mmol). Title compound **(31)** was obtained as off-white crystals, recrystallised from pentane (2.1 g, 61%).

Melting point: 109-110 °C

Micro analysis %: ($C_{28}H_{40}N_2O_2$)

Found C: 75.8%, H: 9.8% and N: 6.1 %. Requires C: 76.7%, H: 9.7% and N: 6.4%.

NMR spectroscopic data: ^{1}H NMR, (300 MHz, CDCl$_3$, 300K): δ = 10.9 (bs, 2H, NH), 7.17 (dd, 2H, J^3 = 8.0 Hz, J^4 = 1.6 Hz, C$_6$H), 6.85 (dd, 2H, J^3 = 7.1 Hz, J^4 = 1.7 Hz, C$_8$H), 6.71 (t, 2H, C$_7$H), 3.96 (dd, 2H, J^3 = 13.6 Hz, C$_4$H), 2.41 (m, 4H, C$_1$H, C$_2$H), 1.36)s, 9H, C$_{12}$H), 1.20 (m, 4H, C$_1$H, C$_2$H).

^{13}C {^{1}H} NMR, (77MHz, CDCl$_3$, 300K): δ = 157.3 (C$_5$) 137.3 (C$_6$), 126.8 (C$_9$), 126.4 (C$_7$), 123.5 (C$_{10}$), 118.7 (C$_8$), 60.2 (C$_3$), 50.8 (C$_4$), 35.0 (C$_{11}$), 31.2 (C$_2$), 29.9 (C$_{12}$), 24.6 (C$_1$).

B: Synthesis of ligands

6.5 Synthesis of Chiral Complexes Incorporating "Fluorous Ponytails"

6.5.1 Synthesis of 5-bromo-3-*tert*-butyl-2-hydroxybenzaldehyde (33) [14]
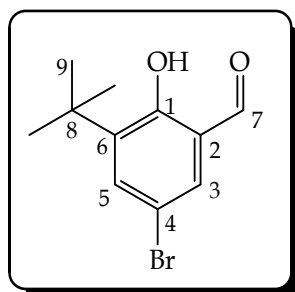
(33)

Procedure: a solution of bromine (0.77 ml, 15 mmol) in acetic acid (2.5 ml) was added drop wise at room temperature over 15 min to a solution of 3-*tert*-butyl-2-hydroxybenzaldehyde (2.5 g, 14 mmol) in acetic acid (5 ml). After 2 h the reaction was diluted with dichloromethane (30 ml), washed with water (10 ml), saturated sodium thiosulphate (10 ml), saturated aqueous sodium hydrogen carbonate (10 ml) and brine (10 ml), dried over magnesium sulphate and the solvents removed under reduced pressure to yield a yellow solid in the form of long needle crystals (3.60 g, 66%).

Melting point: 59.6 – 62.5 °C

Mass spectrum (ES): $[M]^+$ = 257.0, $[M – H]^+$ = 256.0, $[M + H]^+$ = 258.0.

Micro analysis %: ($C_{11}H_{13}O_2Br$)

Found C: 51.7%, H: 5.2%. Requires C: 51.4%, H: 5.1%.

NMR spectroscopic data: ^{1}H NMR, (300 MHz, CDCl$_3$, 300K): δ = 9.85 (s, 1H, C$_7$H), 7.61 (d, 1H, C$_3$H), 7.56 (d, 1H, C$_5$H), 1.44 (s, 9H, C$_9$H).

^{13}C {^{1}H} NMR, (77MHz, CDCl$_3$, 300K): δ = 196.4 (C$_7$), 160.6 (C$_2$), 138.0 (C$_3$), 137.4 (C$_6$), 134.0 (C$_4$), 122.0 (C$_1$), 111.5 (C$_8$), 29.4 (C$_9$).

6.5.2 Synthesis of 5-bromo-3-*tert*-butyl-2-methoxybenzaldehyde (34) [14]
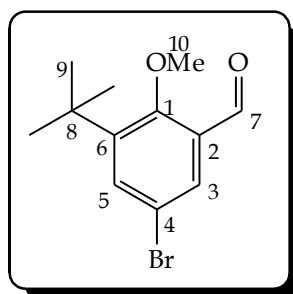
(34)

Procedure: dimethylsulphate (1.38 g, 1.04 ml, 10.97 mmol) was added to a mixture of 5-bromo-3-*tert*-butyl-2-hydroxybenzaldehyde **(33)** (2.35 g, 9.14 mmol) and solid potassium carbonate (2.53 g, 18.28 mmol) in acetone (30 ml). The mixture was stirred at room temperature overnight before being quenched with water (15 ml). The mixture was concentrated under reduced pressure to remove acetone and the residues extracted into DCM (30 ml). The organic layer was washed with brine (20 ml), dried over $MgSO_4$ and the solvents removed under reduced pressure to yield the title compound as a pale orange solid (2.45 g, 98%).

Melting point: 82.2 – 83.3 °C

Micro analysis %: ($C_{12}H_{15}O_2Br$)

Found C: 53.6%, H: 5.8%. Requires C: 53.2%, H: 5.6%.

NMR spectroscopic data: ^{1}H NMR, (300 MHz, CDCl$_3$, 300K): δ = 10.26 (s, 1H, C_7H), 7.80 (d, 1H, C_3H), 7.63 (d, 1H, J^2 = 2.6 Hz, C_5H), 3.94 (s, 3H, C_{10}H), 1.40 (s, 9H, C_9H).

^{13}C {^{1}H} NMR, (77MHz, CDCl$_3$, 300K): δ = 189.2 (C_7), 162.8 (C_3), 146.7 (C_2), 136.5 (C_4), 131.5 (C_2), 130.7 (C_6), 117.5 (C_5), 66.7 (C_{10}), 35.7 (C_8), 30.9 (C_9).

6.5.3 Synthesis of 2-(5-bromo-3-*tert*-butyl-2-methoxyphenyl)-1,3-dioxane (35) [14]
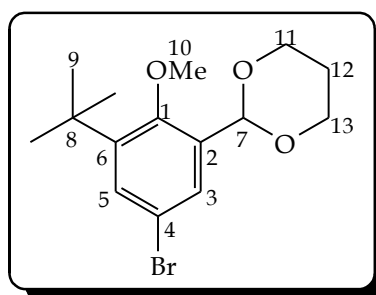
(35)

Procedure: Boron trifluoride diethyl ether (308.9 mg, 2.17 mmol) was added to a solution of compound **(34)** (2.47 g, 9.10 mmol) and 1,3-propandiol (3.46 mg, 3.3 ml, 45.5 mmol) in toluene (10 ml). The solution was refluxed for 4 h after which it was cooled to room temperature and diethyl ether (30 ml) added. The solution was washed with saturated aqueous $NaHCO_3$ (20 ml) and brine (20 ml), then dried over Mg SO_4 and volatiles removed under reduced pressure. The residues were purified by column chromatography (DCM: light petroleum ether, 1:1 v/v) to leave the title compound **(35)** as a red-orange oil (2.63 g, 88%).

Melting point: 68 °C

Micro analysis %: ($C_{15}H_{21}O_3Br$)

Found C: 54.5%, H: 6.5%. Requires C: 5.4.7%, H: 6.4%.

NMR spectroscopic data: ^{1}H NMR, (300 MHz, CDCl$_3$, 300K): δ = 7.74 (d, 1H, J^2 = 2.6 Hz, C_3H), 7.48 (d, 1H, J^2 = 2.6 Hz, C_5H). 5.82 (s, 1H, C_7H), 4.31 (m, 2H, $C_{11}H_{ax}$ $C_{13}H_{ax}$ or $C_{11}H_{eq}$ $C_{13}H_{eq}$), 3.99 (m, 2H, $C_{11}H_{ax}$ $C_{13}H_{ax}$ or $C_{11}H_{eq}$ $C_{13}H_{eq}$), 4.29 (s, 3H, $C_{10}H$), 1.43 (s, 9H, C_9H).

^{13}C {^{1}H} NMR, (300MHz, CDCl$_3$, 300K): δ = 157.0 (C_3), 145.4 (C_1), 138.2 (C_2), 131.4 (C_4), 129.6 (C_6), 117.4 (C_5), 97.8 (C_7), 68.1 (C_{11}/C_{13}), 64.1 (C_{10}), 35.7 (C_8), 31.3 (C_9), 26.1 (C_{12}).

6.5.4 Synthesis of 3-*tert*-butyl-5-formyl-4-methoxybenzene boronic acid (36) [14]
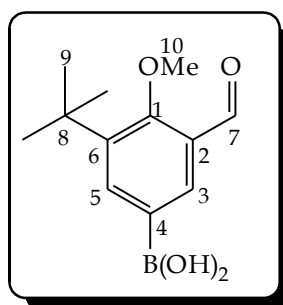
(36)

Procedure: A solution of **(35)** (2.63 g, 7.99 mmol) in THF (15 ml) was cooled to -78°C (using an acetone and dry ice bath) under nitrogen. Subsequently a solution of ^{n}BuLi (1.6 M in hexanes, 5.56 ml, 8.80 mmol) was added drop wise over 5 min. The solution was stirred at -78°C for 45 min before being quenched with a solution of $B(OCH_3)_3$ (2.91 ml, 26.2 mmol) in THF (5 ml). The resulting orange cloudy solution was stirred at -78°C for 2 h and then allowed to warm slowly to 0°C. After 4 h, water (10 ml) and diethyl ether (50 ml) were added. The organic layer was washed with HCl (10%, 3 x 20 ml) and brine (10 ml) and dried over $MgSO_4$. Volatiles were removed under reduced pressure yielding the title compound as orange viscous oil.

NMR spectroscopic data: ^{1}H NMR, (300 MHz, CDCl$_3$, 300K): δ = 10.39 (s, 1H, C$_7$H), 7.71 (d, 1H, C$_6$H), 7.61 (d, 1H, J^2 = 2.6 Hz, C$_4$H), 3.99 (s, 3H, C$_{10}$H), 1.41 (s, 9H, C$_9$H).

^{13}C {^{1}H} NMR, (77MHz, CDCl$_3$, 300K): δ = 189.4 (C$_7$), 142.8 (C$_1$), 136.7 (C$_4$), 129.9 (C$_6$), 62.6 (C$_{10}$), 34.2 (C$_8$), 29.9 (C$_9$).

6.5.5 Attempted synthesis of 3,5-bis-(perfluorooctyl)aniline (37) [15]
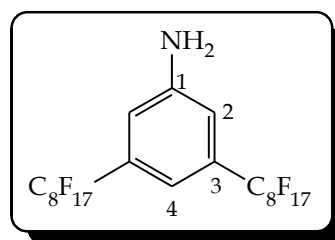
(37)

Procedure: A 100 ml flask equipped with a magnetic stirrer and a condenser was charged with 3,5-dibromoaniline (690 mg, 2 mmol), copper powder (640 mg, 10 mmol) and perfluorooctyliodide (2.4 g, 1.2 ml, 4.4 mmol) in anhydrous DMSO (6 ml). The brown muddy solution was stirred at 125°C for 16h under nitrogen. The solution was cooled, the copper filtered off and the crude product washed with ether (20 ml). Water (10 ml) was added to remove DMSO. A charcoal substance remained in solution and was removed via centrifugation and the volatiles removed under reduced pressure yielding the title compound **(37)** as a brown solid.

NMR spectroscopic data: ^{1}H NMR, (300 MHz, CDCl$_3$, 300K): NMR analysis revealed recovery of starting material as well as undefined products not consistent with the title compound.

6.5.6 Attempted synthesis of 3,5-bis-(perfluorooctyl)-benzene (38) [15]
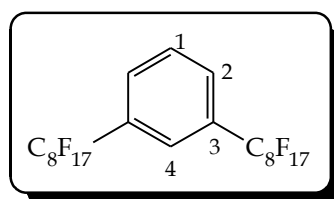
(38)

Procedure: A 50 ml Schlenk was charged with 3,5-diiodobenzene (659.8 mg, 2 mmol), copper powder (640 mg, 10 mmol) and perfluorooctyliodide (2.4 g, 1.2 ml, 4.4 mmol) in anhydrous DMSO (6 ml). The brown muddy solution was stirred at 125°C for 16h under nitrogen. The solution was cooled, the copper filtered off and the crude product washed with ether (20 ml). Water (10 ml) was added to remove DMSO. A green solution remained which darkened as time progressed.

NMR spectroscopic data: ^{1}H NMR, (300 MHz, CDCl₃, 300K): analysis indicated the recovery of starting material 3,5-diiodobenzene.

6.6 Synthesis of chiral aluminium complexes

6.6.1 Synthesis of (*R*,*R*)-[salcyan-3-(*t*Bu)$_2$] AlOH (41) [9], [16], [17]
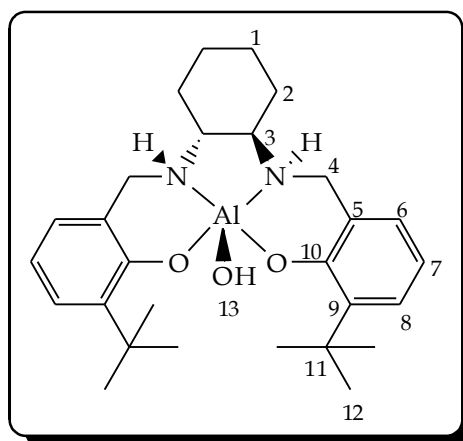
(41)

Procedure: Salcyan **(31)** (0.87 g, 1.98 mmol) was dissolved in pentane (100 ml) and trimethyl aluminium (1.0 ml, 1.98 mmol) was. Gas evolved and the solution turned cloudy. The reaction mixture was stirred for 5 h under nitrogen before being exposed to air yielding a white solid which was dissolved in THF, filtered to remove any insoluble material and the volatiles removed under reduced pressure to reveal a pale yellow solid which was dissolved in warm, dry THF and filtered to remove impurities. Recrystallisation was from chloroform producing the title compound as pale cream needle crystals.

Melting point: 284-286 °C

Micro analysis %: (C$_{28}$H$_{41}$N$_2$O$_3$)

Found C: 68.1%, H: 8.6%, N: 5.4%. Requires C: 69.9%, H: 8.6%, N: 5.8%.

NMR spectroscopic data: ^{1}H NMR, (300 MHz, CDCl$_3$, 300K): δ = 7.28 (dd, 2H, C$_8$H, ^{3}J$_{HH}$ 7.8 Hz), 7.09 (dd, 2H, C$_6$H, ^{3}J$_{HH}$ 7.8 Hz), 6.79 (dd, 2H, C$_8$H), 6.55 (dt, 2H, C$_7$H), 6.47 (dt, 2H, C$_7$H), 4.79 (d, 2H, C$_4$H), 4.62 (d, 2H, C$_4$H), 3.84 – 3.62 (m,

2H, C$_4$H), 2.58 (m, 2H, C$_3$H), 2.36 (m, 2H, C$_2$H), 2.19 (m, 2H, C$_3$H or C$_1$H), 1.75 (m, 2H, C$_2$H), 1.66 (m, 2H, C$_1$H), 1.58 (s, 9H, C$_{12}$H), 1.10 (m, 2H, C$_1$H), 0.92 (s, 9H, C$_{12}$H).

^{13}C {^{1}H} NMR, (77MHz, CDCl$_3$, 300K): δ = 163.1 (C$_{10}$), 139.5 (C$_9$) 128.7 (C$_6$), 128.1 (C$_8$), 127.4 (C$_6$), 126.8 (C$_8$), 125.0 (C$_5$), 123.3 (C$_5$), 116.2 (C$_7$), 59.6 (C$_3$), 57.0 (C$_3$), 50.9 (C$_4$), 49.4 (C$_4$), 35.6 (C$_{11}$), 34.8 (C$_{11}$), 31.7 (C$_{12}$), 30.4 (C$_2$), 29.9 (C$_{12}$), 29.7 (C$_2$) 24.9 (C$_1$), 24.8 (C$_1$).

6.6.2 Attempted synthesis of (*R*,*R*)-N,N'-bis-(2-methylamino-benzyl)-trans-1,2-diaminocyclohexane-aluminium methyl (42) [9], [16]
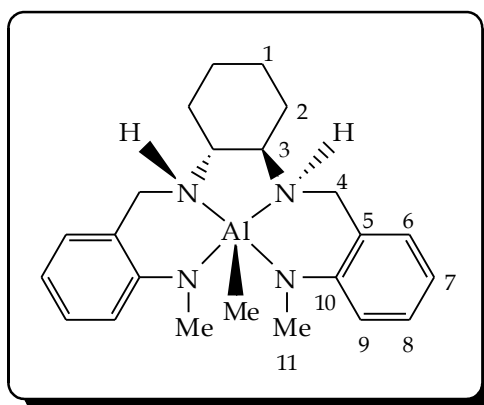
(42)

Procedure: (*R, R*)-N, N'-Bis-[salcyan (methylamino)$_2$] **(17)** (0.16 g, 0.47 mmol) was dissolved in dry toluene (5 ml) and trimethylaluminium (2.0 M solution in hexanes, 0.28 ml, 0.56 mmol) was added resulting in the colour changing from a pale yellow to a dark yellow. The mixture was heated to reflux for 24 h. On cooling to room temperature no precipitate formed, however when the crude product was exposed to air a creamy yellow solid formed.

Mass spectrum (ES): [M + H]$^+$ = 517.3, [M – Al]$^+$ = 489.3

NMR spectroscopic data: ^{1}H NMR, (300 MHz, CDCl$_3$, 300K): analysis shows free ligand with no aluminium attached. δ =7.29 (ddd, 2H, J^3 = 7.7 Hz, J^4 = 1.6 Hz, C$_7$H), 7.01 (dd, 2H, J^3 = 7.3 Hz, J^4 = 1.7 Hz, C$_6$H), 6.65 (ddd, 2H, J^3 = 87.4 Hz, J^4 = 1.1 Hz, C$_8$H), 6.56 (dd, 2H, J^3 = 7.6 Hz, J^4 = 0.7 Hz, C$_9$H), 5.30 (bs, 2H, NH), 3.89 (d, 2H, J^3 = 12.2 Hz, C$_4$H), 3.56 (d, 2H, J^3 = 11.9 Hz, C$_4$H), 2.65 (s, 2H, C$_{11}$H), 2.20 (m, 2H, C$_3$H), 1.77 (m, 2H, C$_2$H), 1.29 (m, 2H, C$_1$H).

^{13}C {^{1}H} NMR, (77MHz, CDCl$_3$ 300K): analysis shows free ligand with no aluminium attached. δ = 149.5 (C$_{10}$), 129.7 (C$_7$), 128.9 (C$_6$), 124.6 (C$_5$), 116.4 (C$_8$), 110.0 (C$_9$), 61.5 (C$_3$), 50.8 (C$_4$), 31.7 (C$_2$), 30.2 (C$_{11}$), 25.2 (C$_1$).

6.6.3 Attempted synthesis of (*R,R*)-N,N′-bis-(2-phenylamino-benzyl)-trans-1,2-diaminocyclohexane-aluminium methyl (43) [9], [16]
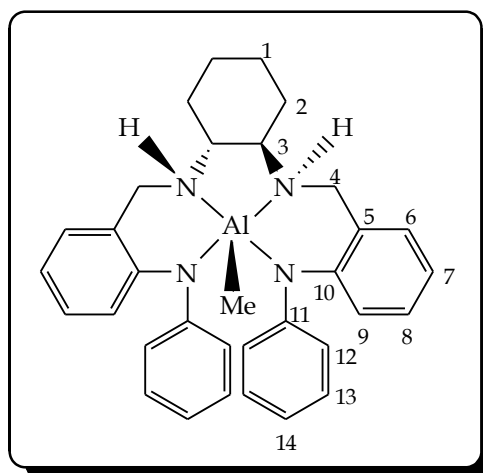
(43)

Procedure: (*R, R*)-N, N′-Bis-[salcyan (phenylamino)$_2$] **(18)** (0.14 g, 0.31 mmol) was dissolved in dry toluene (5 ml) and trimethylaluminium (2.0 M solution in hexanes, 0.19 ml, 0.38 mmol) was added resulting in the colour changing from a yellow to a dark orange. The mixture was heated to reflux for 24 h. On cooling

to room temperature only a small amount of precipitate formed around the edge of the flask, however when the crude product was exposed to air a creamy yellow solid formed.

NMR spectroscopic data: ^{1}H NMR, (300 MHz, CDCl$_3$, 300K): analysis showed the free ligand with no aluminium attached. δ = 8.06 (bs, 2H, NH), 7.19 (ddd, 2H, J^3 = 7.6 Hz, J^4 = 1.7 Hz, C$_7$H), 7.14 (m, 2H, C$_{14}$H), 7.11 (dd, 2H, J^3 = 3.1 Hz, J^4 = 2.2 Hz, C$_6$H), 6.85 (m, 2H, C$_8$H), 6.82 (dd, 2H, J^3 = 3.1 Hz, J^4 = 1.1 Hz, C$_9$H), 6.79 (m, 4H, C$_{13}$H), 6.77 (m, 4H, C$_{12}$H), 4.00 (d, 2H, J^3 = 11.8 Hz, C$_4$H), 3.64 (d, 2H, J^3 = 11.8 Hz, C$_4$H), 2.35 (m, 2H, C$_3$H), 1.82 (m, 2H, C$_2$H), 1.38 (m, 2H, C$_1$H), 1.15 (m, 2H, C$_2$H), 0.93 (m, 2H, C$_1$H).

^{13}C {^{1}H} NMR, (77MHz, CDCl$_3$, 300K): analysis showed the free ligand with no aluminium attached. δ =143.9 (C$_{10}$), 130.5 (C$_6$), 129.6 (C$_7$), 128.6 (C$_{13}$), 120.51 (C$_{14}$), 120.1 (C$_{12}$), 118.0 (C$_5$), 116.1 (C$_8$), 91.6 (C$_9$), 77.4 (C$_3$), 31.5 (C$_2$), 25.0 (C$_1$).

6.6.4 Attempted synthesis of (*R,R*)-[salcyan-3-(*^{t}Bu*)$_2$] diethyl methyl phosphonate (44) (I)
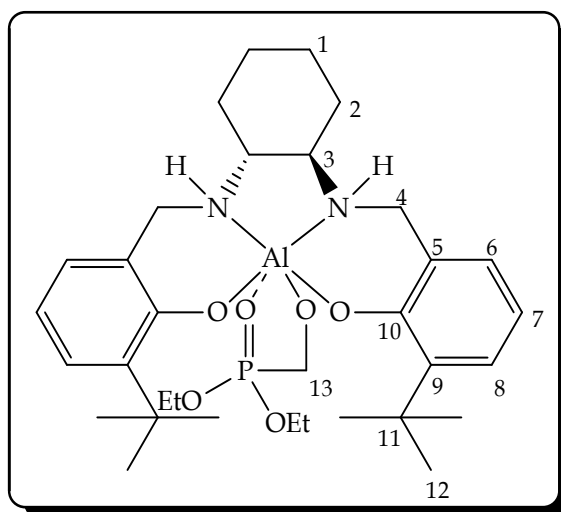
(44)

Procedure: In a Schlenk flask equipped with a magnetic stirrer and a nitrogen line, (*R, R*)-N, N′-bis-[salcyan-3-(^{t}Bu)$_2$]-Al(μOH) **(41)** (200 mg, 0.21 mmol) was dissolved in dry THF (20 ml). 2,6-Lutidine (0.69 ml, 0.63 mmol) was added and the reagents allowed to stir for 30 minutes. Diethyl iodomethylphosphonate (115.45 mg, 0.42 mmol) was added to the vessel. The reaction mixture was left to stir at room temperature overnight. A white precipitate was filtered off, leaving a pale yellow solution. Volatiles were removed under reduced pressure.

NMR spectroscopic data: ^{1}H NMR, (300 MHz, CDCl$_3$, 300K): analysis showed the presence of all starting material present in their original forms. The white precipitate was in fact compound **(41)**. δ = 7.28 (dd, 2H, C$_8$H, ^{3}J$_{HH}$ 7.8 Hz), 7.09 (dd, 2H, C$_6$H, ^{3}J$_{HH}$ 7.8 Hz), 6.79 (dd, 2H, C$_8$H), 6.55 (dt, 2H, C$_7$H), 6.47 (dt, 2H, C$_7$H), 4.79 (d, 2H, C$_4$H), 4.62 (d, 2H, C$_4$H), 3.84 – 3.62 (m, 2H, C$_4$H), 2.58 (m, 2H, C$_3$H), 2.36 (m, 2H, C$_2$H), 2.19 (m, 2H, C$_3$H or C$_1$H), 1.75 (m, 2H, C$_2$H), 1.66 (m, 2H, C$_1$H), 1.58 (s, 9H, C$_{12}$H), 1.10 (m, 2H, C$_1$H), 0.92 (s, 9H, C$_{12}$H).

6.6.5 Attempted synthesis of (*R,R*)-[salcyan-3-(^{t}Bu)$_2$] diethyl methyl phosphonate (44) (II)

Procedure: In a Schlenk flask equipped with a magnetic stirrer and a nitrogen line, (*R, R*)-N, N′-bis-[salcyan-3-(^{t}Bu)$_2$] Al(μOH) **(41)** (200 mg, 0.21 mmol) was dissolved in dry THF (10 ml). Molecular sieves and diethyl hydroxymethylphosphonate (69.81 mg, 0.42 mmol) were added to the vessel. The reaction mixture was left to stir at 100°C for 24 h. The solution went from colourless to pale brown slurry. The precipitate was filtered off leaving a pale yellow solution. Volatiles were removed under reduced pressure and the resulting mixture analysed by NMR spectroscopy.

NMR spectroscopic data: ^{1}H NMR, (300 MHz, CDCl$_3$, 300K): analysis showed the presence of all starting material present in their original forms. δ = 7.28 (dd, 2H, C$_8$H, ^{3}J$_{HH}$ 7.8 Hz), 7.09 (dd, 2H, C$_6$H, ^{3}J$_{HH}$ 7.8 Hz), 6.79 (dd, 2H, C$_8$H), 6.55 (dt, 2H, C$_7$H), 6.47 (dt, 2H, C$_7$H), 4.79 (d, 2H, C$_4$H), 4.62 (d, 2H, C$_4$H), 3.84 – 3.62 (m, 2H, C$_4$H), 2.58 (m, 2H, C$_3$H), 2.36 (m, 2H, C$_2$H), 2.19 (m, 2H, C$_3$H or C$_1$H), 1.75 (m, 2H, C$_2$H), 1.66 (m, 2H, C$_1$H), 1.58 (s, 9H, C$_{12}$H), 1.10 (m, 2H, C$_1$H), 0.92 (s, 9H, C$_{12}$H).

6.6.6 Attempted synthesis of (*R,R*)-[salcyan-3-(*t*Bu)$_2$] diethyl methyl phosphonate (44) (III)

Procedure: In a Schlenk flask equipped with a magnetic stirrer and a nitrogen line, (*R, R*)-N, N′-bis-[salcyan-3-(*t*Bu)$_2$] Al(μOH) **(41)** (200 mg, 0.21 mmol) and LDA (89.98 mg, 0.84 mmol) were dissolved in dry pentane (20 ml). Diethyl iodomethylphosphonate (115.45 mg, 0.42 mmol) was added to the vessel. The reaction mixture was left to stir at room temperature for 24 h. A white precipitate was filtered off and volatiles removed under reduced pressure leaving a colourless oil which was analysed by NMR spectroscopy.

NMR spectroscopic data: ^{1}H NMR, (300 MHz, CDCl$_3$, 300K): analysis showed the presence of all starting material present in their original forms. The white precipitate was in fact compound **(41)**. δ = 7.28 (dd, 2H, C$_8$H, ^{3}J$_{HH}$ 7.8 Hz), 7.09 (dd, 2H, C$_6$H, ^{3}J$_{HH}$ 7.8 Hz), 6.79 (dd, 2H, C$_8$H), 6.55 (dt, 2H, C$_7$H), 6.47 (dt, 2H, C$_7$H), 4.79 (d, 2H, C$_4$H), 4.62 (d, 2H, C$_4$H), 3.84 – 3.62 (m, 2H, C$_4$H), 2.58 (m, 2H, C$_3$H), 2.36 (m, 2H, C$_2$H), 2.19 (m, 2H, C$_3$H or C$_1$H), 1.75 (m, 2H, C$_2$H), 1.66 (m, 2H, C$_1$H), 1.58 (s, 9H, C$_{12}$H), 1.10 (m, 2H, C$_1$H), 0.92 (s, 9H, C$_{12}$H).

6.6.7 Attempted synthesis of (*R*,*R*)-[salcyan-3-(*^t*Bu)₂] diethyl methyl phosphonate (44) (IV)

6.6.7 Attempted synthesis of (*R*,*R*)-[salcyan-3-(tBu)₂] diethyl methyl phosphonate (44) (IV)

Procedure: In a Schlenk flask equipped with a magnetic stirrer and a nitrogen line, (*R*, *R*)-N, N′-bis-[salcyan-3-(tBu)₂] **(31)** (250 mg, 0.57 mmol)   and trimethylaluminium (2M, 27.32 µL, 0.57 mmol) and dry pentane (30 ml) were added. Diethyl hydroxymethylphosphonate (0.08 ml, 0.57 mmol) was added to the vessel. The reaction mixture was left to stir overnight at 50°C. A white cream solid resulted after volatiles were removed under reduced pressure.

NMR spectroscopic data: ^{1}H NMR, (300 MHz, CDCl₃, 300K): analysis indicated that the reaction had not taken place and all starting materials were recovered.

6.6.8 Attempted synthesis of (*R*,*R*)-[salcyan-3-(*^t*Bu)₂] diethyl methyl phosphonate (44) (V)

Procedure: In a Schlenk flask equipped with a magnetic stirrer and a nitrogen line, trimethylaluminium (2M, 0.29 ml, 0.58 mmol) and diethyl hydroxymethylphosphonate (95.83 mg, 0.57 mmol) in dry pentane (30 ml) were added at 0°C. Once all gas evolution had ceased (*R*, *R*)-N, N′-bis-[salcyan-3-(tBu)₂] **(31)** (250 mg, 0.57 mmol) dissolved in dry pentane (5 ml) was added and the reaction mixture left to stir at 50°C for 3 days. Once the salcyan had been added a white precipitate formed, this was filtered off and analysed by NMR spectroscopy.

NMR spectroscopic data: ^{1}H NMR, (300 MHz, CDCl₃, 300K): analysis indicated that the reaction had not taken place and all starting materials were recovered. The white precipitate was compound **(31)**. δ = 10.9 (bs, 2H, NH),

7.17 (dd, 2H, J^3 = 8.0 Hz, J^4 = 1.6 Hz, C_6H), 6.85 (dd, 2H, J^3 = 7.1 Hz, J^4 = 1.7 Hz, C_8H), 6.71 (t, 2H, C_7H), 3.96 (dd, 2H, J^3 = 13.6 Hz, C_4H), 2.41 (m, 4H, C_1H, C_2H), 1.36)s, 9H, $C_{12}H$), 1.20 (m, 4H, C_1H, C_2H).

6.6.9 Attempted synthesis of (R,R)-[salcyan-3-(^{t}Bu)$_2$] diethyl methyl phosphonate (44) (VI)

Procedure: In a Schlenk flask equipped with a magnetic stirrer and a nitrogen line, trimethylaluminium (2M, 0.29 ml, 0.58 mmol) and diethyl hydroxymethylphosphonate (0.08 ml, 0.57 mmol) in dry THF (20 ml) were added at 0°C. Once all gas evolution had ceased (R, R)-N, N′-bis-[salcyan-3-(^{t}Bu)$_2$] **(31)** (250 mg, 0.57 mmol) dissolved in dry THF (5 ml) was added and the reaction mixture left to stir at 70°C for 3 days. Once the salcyan had been added a white precipitate formed, this was filtered off and analysed.

NMR spectroscopic data: ^{1}H NMR, (300 MHz, CDCl$_3$, 300K): analysis indicated that the reaction had not taken place and all starting materials were recovered. The white precipitate was compound **(31)**. δ = 10.9 (bs, 2H, NH), 7.17 (dd, 2H, J^3 = 8.0 Hz, J^4 = 1.6 Hz, C_6H), 6.85 (dd, 2H, J^3 = 7.1 Hz, J^4 = 1.7 Hz, C_8H), 6.71 (t, 2H, C_7H), 3.96 (dd, 2H, J^3 = 13.6 Hz, C_4H), 2.41 (m, 4H, C_1H, C_2H), 1.36)s, 9H, $C_{12}H$), 1.20 (m, 4H, C_1H, C_2H).

6.6.10 Attempted synthesis of (R,R)-[salcyan-3-(^{t}Bu)$_2$] diethyl methyl phosphonate (44) (VII)

Procedure: In a Schlenk flask equipped with a magnetic stirrer and a nitrogen line, aluminium chloride (30.67 mg, 0.23 mmol) and diethyl

hydroxymethylphosphonate (0.03 ml, 0.23 mmol) in dry THF (10 ml) were added at 0°C. Once all gas evolution had ceased (*R, R*)-N, N′-bis-[salcyan-3-(*t*Bu)$_2$] **(31)** (100 mg, 0.23 mmol) dissolved in dry THF (5 ml) was added and the reaction mixture left to stir at 70°C for 3 days. Once the salcyan had been added a cream precipitate formed, this was filtered off and analysed.

NMR spectroscopic data: ^{1}H NMR, (300 MHz, CDCl$_3$, 300K): analysis indicated that the reaction had not taken place and all starting materials were recovered.

6.6.11 Attempted synthesis of (*R,R*)-[salcyan-3-(*t*Bu)$_2$] diethyl methyl phosphonate (44) (VIII)

Procedure: In a Schlenk flask equipped with a magnetic stirrer and a nitrogen line,

Diethyl hydroxymethylphosphonate (33.65 µL, 0.23 mmol) in dry toluene (10 ml) and aluminium isopropoxide (46.98 mg, 0.23 mmol) were added. This solution was left to stir for 2 h at 80°C. (*R, R*)-N, N′-bis-[salcyan-3-(*t*Bu)$_2$] **(31)** (100 mg, 0.23 mmol) dissolved in dry toluene (5 ml) was added and the mixture left to stir for 24 h. Volatiles were removed under reduced pressure leaving a pale cream oil.

NMR spectroscopic data: ^{1}H NMR, (300 MHz, CDCl$_3$, 300K): analysis indicated that the reaction had not taken place and all starting materials were recovered.

6.6.12 Attempted synthesis of (R,R)-[salcyan-3-(ᵗBu)₂] diethyl methyl phosphonate (44) (IX)

Procedure: In a Schlenk flask equipped with a magnetic stirrer and a nitrogen line. Diethyl hydroxymethylphosphonate (33.62 μL, 0.23 mmol) and ethylaluminium dichloride (38.99 μL, 0.23 mmol) in dry toluene (5 ml) were added. The solution was left to stir for 1 h at room temperature. (R, R)-N, N′-bis-[salcyan-3-(ᵗBu)₂] **(31)** (100 mg, 0.23 mmol) dissolved in dry toluene (5 ml) was added dropwise to the stirring solution and left to stir for 3 days. Volatiles were removed under reduced pressure, leaving a pale cream oil.

NMR spectroscopic data: ¹H NMR, (300 MHz, CDCl₃, 300K): analysis indicated that the reaction had not taken place and all starting materials were recovered.

6.6.13 Attempted synthesis of (R,R)-[salcyan-3-(ᵗBu)₂] AlCl (45) [9], [16]
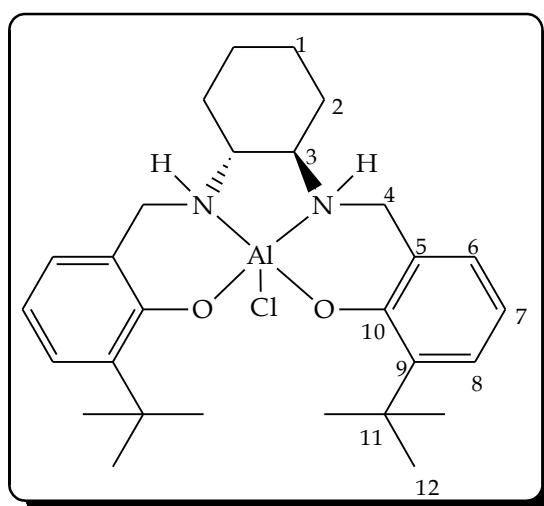
(45)

Procedure: In a Schlenk flask equipped with a magnetic stirrer and a nitrogen line, (*R, R*)-N, N′-bis-[salcyan-3-(ᵗBu)₂] **(31)** (200 mg, 0.46 mmol) was dissolved in dry toluene (10 ml). Dimethylaluminium chloride (60.16 µL, 0.46 mmol) was added in which a white gas evolved almost immediately. The reaction mixture was left to stir for 2 days at room temperature by which time the previously colourless solution had now turned pale yellow. The reaction was then left to stir for an additional 2 days at 80°C whereby the yellow colouration had intensified. Volatiles were removed under reduced pressure leaving yellow oil, which was analysed by NMR spectroscopy.

NMR spectroscopic data: ¹H NMR, (300 MHz, CDCl₃, 300K): δ = 7.32 (m, 2H, C₈H), 7.25 (m, 2H, C₆H), 6.88 (m, 2H, C₈H), 4.15 (d, 2H, C₄H), 4.03 (d, 2H, C₄H), 2.52 (m, 2H, C₃H), 2.27 (m, 2H, C₂H), 1.75 (m, 2H, C₂H), 1.55 (m, 2H, C₁H), 1.49 (s, 9H, C₁₂H), 1.08 (m, 2H, C₁H).

6.6.14 Attempted synthesis of (*R,R*)-N,N′-bis-(2-methylamino-benzyl)-trans-1,2-diaminocyclohexane-aluminium hydroxide (46) [17]
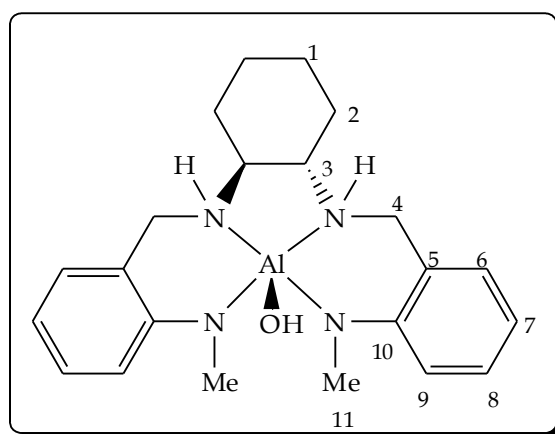
(46)

Procedure: In a Schlenk vessel (*R*,*R*)-[salcyan(methylamino)₂] **(17)** (200 mg, 0.57 mmol) and LDA (0.15 ml, 1.14 mmol) were added along with dry toluene (20 ml). The reaction mixture was left to stir for 30 minutes before aluminium isopropoxide (174.63 mg, 0.86 mmol) was added. The colour changed from colourless to a light brown. The solution was left to stir for 24 h under nitrogen at room temperature. Volatiles were removed under reduced pressure leaving a light brown solid, which was analysed by NMR spectroscopy.

NMR spectroscopic data: ¹H NMR, (300 MHz, CDCl₃, 300K): analysis showed the presence of starting material **(17)** among other impurities. Purification was not accomplished. δ =7.29 (ddd, 2H, J^3 = 7.7 Hz, J^4 = 1.6 Hz, C_7H), 7.01 (dd, 2H, J^3 = 7.3 Hz, J^4 = 1.7 Hz, C_6H), 6.65 (ddd, 2H, J^3 = 87.4 Hz, J^4 = 1.1 Hz, C_8H), 6.56 (dd, 2H, J^3 = 7.6 Hz, J^4 = 0.7 Hz, C_9H), 5.30 (bs, 2H, NH), 3.89 (d, 2H, J^3 = 12.2 Hz, C_4H), 3.56 (d, 2H, J^3 = 11.9 Hz, C_4H), 2.65 (s, 2H, $C_{11}H$), 2.20 (m, 2H, C_3H), 1.77 (m, 2H, C_2H), 1.29 (m, 2H, C_1H).

6.6.15 Attempted synthesis of (*R*,*R*)-N,N′-bis-(2-methylamino-benzyl)-trans-1,2-diaminocyclohexane-aluminium chloride(47) [9], [16]
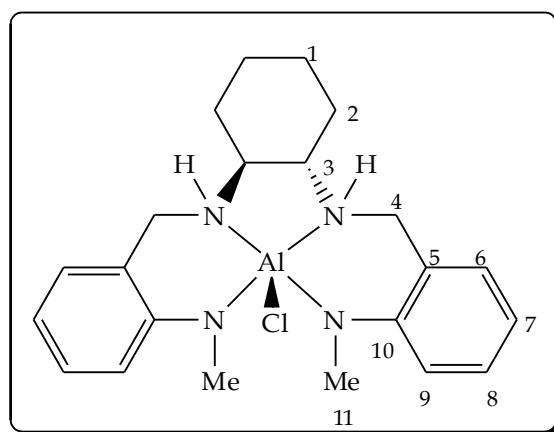
(47)

Procedure: In a Schlenk flask equipped with a magnetic stirrer and a nitrogen line, (*R,R*)-[salcyan(methylamino)$_2$] **(17)** (100 mg, 0.28 mmol) was dissolved in dry toluene (15 ml). Dimethylaluminium chloride (30.95 µL, 0.28 mmol) was added dropwise. A white gas evolved and the reaction mixture changed from pale yellow to deep orange. The reaction mixture was left to stir for 3 days at 80°C. Volatiles were removed under reduced pressure leaving a pale brown solid, which was analysed by NMR spectroscopy.

NMR spectroscopic data: ^{1}H NMR, (500 MHz, CD$_3$OD, 300K): analysis showed the presence of the ligand **(17)**, which was recovered. δ =7.29 (ddd, 2H, J^3 = 7.7 Hz, J^4 = 1.6 Hz, C$_7$H), 7.01 (dd, 2H, J^3 = 7.3 Hz, J^4 = 1.7 Hz, C$_6$H), 6.65 (ddd, 2H, J^3 = 87.4 Hz, J^4 = 1.1 Hz, C$_8$H), 6.56 (dd, 2H, J^3 = 7.6 Hz, J^4 = 0.7 Hz, C$_9$H), 5.30 (bs, 2H, NH), 3.89 (d, 2H, J^3 = 12.2 Hz, C$_4$H), 3.56 (d, 2H, J^3 = 11.9 Hz, C$_4$H), 2.65 (s, 2H, C$_{11}$H), 2.20 (m, 2H, C$_3$H), 1.77 (m, 2H, C$_2$H), 1.29 (m, 2H, C$_1$H).

6.6.16 Attempted synthesis of (*R,R*)-N,N′-bis-(2-methylamino-benzyl)-trans-1,2-diaminocyclohexane-aluminium chloride (48) [18]
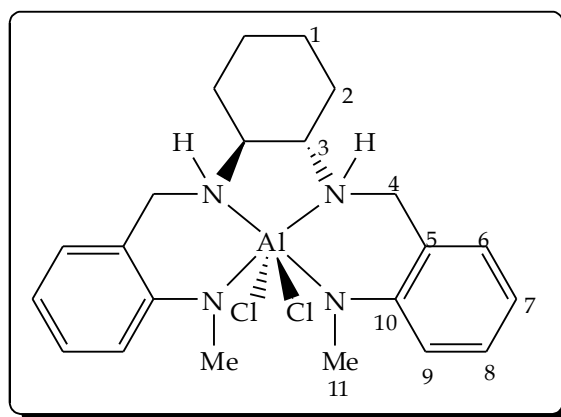
(48)

Procedure: In a Schlenk vessel equipped with a magnetic stirrer and nitrogen line, (*R, R*)-N, N′-bis-[salcyan (methylamino)$_2$] **(17)** (100 mg, 0.28 mmol) was added along with dry toluene (10 ml) and stirred until completely dissolved. Ethylaluminium dichloride (0.05 ml, 0.28 mmol) was added dropwise resulting in a white gas evolving and the reaction mixture changed from pale yellow to orange. The reaction mixture was left to stir for 3 days. Volatiles were removed under reduced pressure leaving an orange solid, which was analysed by NMR spectroscopy.

NMR spectroscopic data: ^{1}H NMR, (500 MHz, CD$_3$OD, 300K): analysis indicated the presence of ligand **(17)**, which was recovered. δ =7.29 (ddd, 2H, J^3 = 7.7 Hz, J^4 = 1.6 Hz, C$_7$H), 7.01 (dd, 2H, J^3 = 7.3 Hz, J^4 = 1.7 Hz, C$_6$H), 6.65 (ddd, 2H, J^3 = 87.4 Hz, J^4 = 1.1 Hz, C$_8$H), 6.56 (dd, 2H, J^3 = 7.6 Hz, J^4 = 0.7 Hz, C$_9$H), 5.30 (bs, 2H, NH), 3.89 (d, 2H, J^3 = 12.2 Hz, C$_4$H), 3.56 (d, 2H, J^3 = 11.9 Hz, C$_4$H), 2.65 (s, 2H, C$_{11}$H), 2.20 (m, 2H, C$_3$H), 1.77 (m, 2H, C$_2$H), 1.29 (m, 2H, C$_1$H).

^{13}C {^{1}H} NMR, (75 MHz, CD$_3$OD, 300K): analysis indicated the presence of ligand **(17)**, which was recovered. δ = 149.5 (C$_{10}$), 129.7 (C$_7$), 128.9 (C$_6$), 124.6 (C$_5$), 116.4 (C$_8$), 110.0 (C$_9$), 61.5 (C$_3$), 50.8 (C$_4$), 31.7 (C$_2$), 30.2 (C$_{11}$), 25.2 (C$_1$).

6.6.17 Attempted synthesis of (*R,R*)-N,N′-bis-(2-phenylamino-benzyl)-trans-1,2-diaminocyclohexane-aluminium chloride (49)
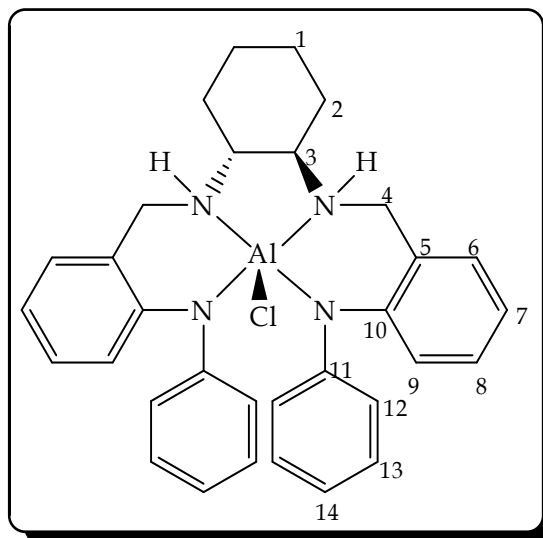
(49)

Procedure: In a Schlenk flask equipped with a magnetic stirrer and a nitrogen line, (*R, R*)-N, N′-bis-[salcyan (phenylamino)$_2$] **(18)** (100 mg, 0.21 mmol) was added along with triethylamine (0.12 ml, 0.84 mmol), aluminium chloride (27.97 mg, 0.21 mmol) and dry toluene (10 ml). The colour change was from a pale yellow to a deep orange. The reaction mixture was heated to reflux for 24 hrs. All volatiles were removed under reduced pressure and the mixture analysed by NMR spectroscopy.

NMR spectroscopic data: ^{1}H NMR, (500 MHz, CD$_3$OD, 300K): analysis indicated the presence of ligand **(18)**, which was recovered. δ = 8.06 (bs, 2H, NH), 7.19 (ddd, 2H, J^3 = 7.6 Hz, J^4 = 1.7 Hz, C$_7$H), 7.14 (m, 2H, C$_{14}$H), 7.11 (dd, 2H, J^3 = 3.1 Hz, J^4 = 2.2 Hz, C$_6$H), 6.85 (m, 2H, C$_8$H), 6.82 (dd, 2H, J^3 = 3.1 Hz, J^4 = 1.1 Hz, C$_9$H), 6.79 (m, 4H, C$_{13}$H), 6.77 (m, 4H, C$_{12}$H), 4.00 (d, 2H, J^3 = 11.8 Hz, C$_4$H), 3.64 (d, 2H, J^3 = 11.8 Hz, C$_4$H), 2.35 (m, 2H, C$_3$H), 1.82 (m, 2H, C$_2$H), 1.38 (m, 2H, C$_1$H), 1.15 (m, 2H, C$_2$H), 0.93 (m, 2H, C$_1$H).

6.6.18 Attempted synthesis of (*R,R*)-N,N′-bis-(2-phenylamino-benzyl)-trans-1,2-diaminocyclohexane-aluminium chloride (49) (I)

Procedure: In a Schlenk flask equipped with a magnetic stirrer and a nitrogen line, (*R, R*)-N, N′-bis-[salcyan (phenylamino)₂] **(18)** (100 mg, 0.21 mmol) was added along with *tert*-butyllithium (0.04 ml, 0.42 mmol) and dry toluene (10 ml). The solution was allowed to stir for a few minutes before aluminium chloride (27.97 mg, 0.21 mmol) was added. The reaction mixture was left to stir at room temperature overnight. The colour change was from a very pale yellow to a dark brown-black. All volatiles were removed under reduced pressure resulting in a dark brown solid.

NMR spectroscopic data: ¹H NMR, (500 MHz, CD₃OD, 300K): analysis and characterisation was extremely difficult due to the presence of multiple, unresolved peaks.

6.6.19 Attempted synthesis of (*R,R*)-N,N′-bis-(2-phenylamino-benzyl)-trans-1,2-diaminocyclohexane-aluminium chloride (49) (II) [18]

Procedure: In a Schlenk vessel equipped with a magnetic stirrer and nitrogen line, (*R, R*)-N, N′-bis-[salcyan (phenylamino)₂] **(18)** (200 mg, 0.42 mmol) was added along with dry toluene (10 ml). The salan solution was cooled to -78°C using a cardice and acetone bath. Dimethylaluminium chloride (0.06 ml, 0.42 mmol) was added dropwise. The reaction mixture was allowed to reach room temperature and left to stir for 24 hours under nitrogen. Volatiles were removed under reduced pressure leaving a pale cream solid, which was analysed by NMR spectroscopy.

NMR spectroscopic data: ^{1}H NMR, (300 MHz, CD$_3$OD, 300K): analysis indicated the presence of ligand **(18)**, which was recovered. δ = 8.06 (bs, 2H, NH), 7.19 (ddd, 2H, J^3 = 7.6 Hz, J^4 = 1.7 Hz, C$_7$H), 7.14 (m, 2H, C$_{14}$H), 7.11 (dd, 2H, J^3 = 3.1 Hz, J^4 = 2.2 Hz, C$_6$H), 6.85 (m, 2H, C$_8$H), 6.82 (dd, 2H, J^3 = 3.1 Hz, J^4 = 1.1 Hz, C$_9$H), 6.79 (m, 4H, C$_{13}$H), 6.77 (m, 4H, C$_{12}$H), 4.00 (d, 2H, J^3 = 11.8 Hz, C$_4$H), 3.64 (d, 2H, J^3 = 11.8 Hz, C$_4$H), 2.35 (m, 2H, C$_3$H), 1.82 (m, 2H, C$_2$H), 1.38 (m, 2H, C$_1$H), 1.15 (m, 2H, C$_2$H), 0.93 (m, 2H, C$_1$H).

6.6.20 Attempted synthesis of (R,R)-N,N′-bis-(2-phenylamino-benzyl)-trans-1,2-diaminocyclohexane-AlCl (49) (III) [18]

Procedure: In a Schlenk vessel equipped with a magnetic stirrer and nitrogen line, (R, R)-N, N′-bis-[salcyan (phenylamino)$_2$] **(18)** (100 mg, 0.21 mmol) was added along with dry toluene (10 ml) and stirred until completely dissolved. Dimethylaluminium chloride (0.03 ml, 0.21 mmol) was added dropwise resulting in a white gas evolving and the reaction mixture changed from colourless to a pale yellow. The reaction mixture was heated to 80°C and left to stir for 4 days. A cream precipitate was filtered off under reduced pressure and volatiles removed leaving a yellow solid. The crude product was recrystallised from methanol resulting in the formation of yellow needle crystals.

NMR spectroscopic data: ^{1}H NMR, (300 MHz, CD$_3$OD, 300K): δ =7.40 (m, 2H, C$_6$H), 7.15 (m, 2H, C$_{14}$H), 7.05 (m, 2H, C$_7$H), 7.01 (m, 2H, C$_8$H), 6.95 (m, 2H, C$_9$H), 6.75 (m, 4H, C$_{13}$H), 6.60 (m, 4H, C$_{12}$H), 3.75 (d, 2H, C$_4$H), 3.50 (d, 2H, C$_4$H), 2.10 (m, 2H, C$_3$H), 1.55 (m, 2H, C$_2$H), 1.10 (m, 2H, C$_2$H), 0.93 (m, 2H, C$_1$H).

6.6.21 Attempted synthesis of (*R,R*)-N,N′-bis-(2-phenylamino-benzyl)-trans-1,2-diaminocyclohexane-aluminium chloride (50) (I) [18]
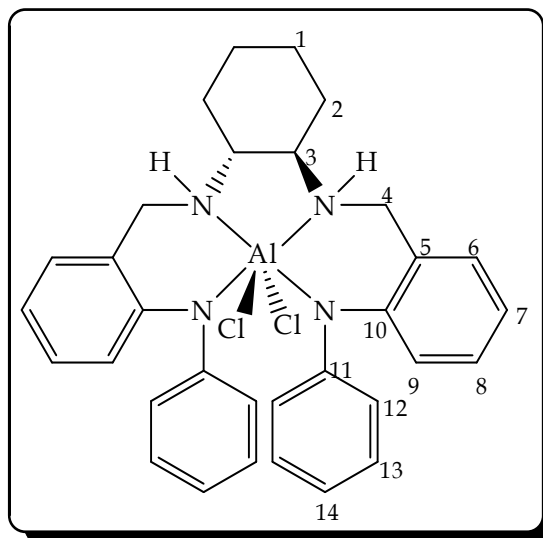
(50)

Procedure: In a Schlenk vessel equipped with a magnetic stirrer and nitrogen line, (*R, R*)-N, N′-bis-[salcyan (phenylamino)$_2$] **(18)** (100 mg, 0.21 mmol) was added along with dry toluene (10 ml) and stirred until completely dissolved. Ethylaluminium dichloride (25.32 mg, 35.61 µL) was added dropwise resulting in a white gas evolving and the reaction mixture changed from colourless to a deep yellow. The reaction mixture was left to stir for 3 days at room temperature. Volatiles were removed under reduced pressure leaving a yellow solid, which was examined by NMR spectroscopy.

NMR spectroscopic data: ^{1}H NMR, (300 MHz, CD$_3$OD, 300K): analysis indicated the presence of ligand **(18)**, which was recovered. δ = 8.06 (bs, 2H, NH), 7.19 (ddd, 2H, J^3 = 7.6 Hz, J^4 = 1.7 Hz, C$_7$H), 7.14 (m, 2H, C$_{14}$H), 7.11 (dd, 2H, J^3 = 3.1 Hz, J^4 = 2.2 Hz, C$_6$H), 6.85 (m, 2H, C$_8$H), 6.82 (dd, 2H, J^3 = 3.1 Hz, J^4 = 1.1 Hz, C$_9$H), 6.79 (m, 4H, C$_{13}$H), 6.77 (m, 4H, C$_{12}$H), 4.00 (d, 2H, J^3 = 11.8 Hz,

C_4H), 3.64 (d, 2H, J^3 = 11.8 Hz, C_4H), 2.35 (m, 2H, C_3H), 1.82 (m, 2H, C_2H), 1.38 (m, 2H, C_1H), 1.15 (m, 2H, C_2H), 0.93 (m, 2H, C_1H).

^{13}C {^1H} NMR, (77 MHz, CD$_3$OD, 300K): analysis indicated the presence of ligand **(18)**, which was recovered. δ =143.9 (C_{10}), 130.5 (C_6), 129.6 (C_7), 128.6 (C_{13}), 120.51 (C_{14}), 120.1 (C_{12}), 118.0 (C_5), 116.1 (C_8), 91.6 (C_9), 77.4 (C_3), 31.5 (C_2), 25.0 (C_1).

6.6.22 Attempted synthesis of (*R,R*)-N,N′-bis-(2-phenylamino-benzyl)-trans-1,2-diaminocyclohexane-AlCl$_2$ (50) (II) [18]

Procedure: In a Schlenk vessel equipped with a magnetic stirrer and nitrogen line, (*R, R*)-N, N′-bis-[salcyan (phenylamino)$_2$] **(18)** (100 mg, 0.21 mmol) was added along with dry toluene (10 ml) and stirred until completely dissolved. Ethylaluminium dichloride (25.32 mg, 35.61 µL) was added dropwise resulting in a white gas evolving and the reaction mixture changed from colourless to a deep orange. The reaction mixture was heated to reflux and left to stir for 4 days. A brown precipitate was filtered off under reduced pressure and volatiles removed leaving a yellow solid. The crude product was recrystallised from methanol and analysed by NMR spectroscopy.

NMR spectroscopic data: ^1H NMR, (500 MHz, CD$_3$OD, 300K): δ = 7.15 (m, 2H, C_6H, $C_{14}H$, C_7H), 7.05 (m, 2H, C_8H, C_9H), 6.90 (m, 2H, $C_{13}H$), 6.65 (m, 2H, $C_{12}H$), 3.85 (d, 2H, C_4H), 3.70 (d, 2H, C_4H), 2.30 (m, 2H, C_3H), 2.05 (m, 2H, C_2H, C_1H), 1.55 (m, 2H, C_1H), 1.00 (m, 2H, C_2H).

6.7 Towards the synthesis of phosphinyl ligands – Route 1

6.7.1 Synthesis of diphenylphosphinyl phenyl ester (51) [19], [20]
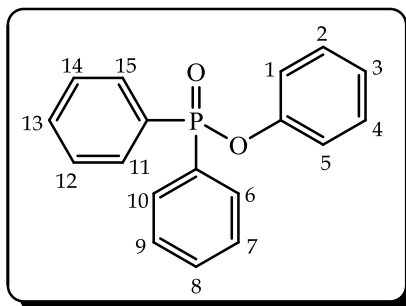
(51)

Procedure: In a clean, dry Schlenk equipped with a magnetic stirrer and nitrogen line was placed phenol (398.09 mg, 4.23 mmols), dry triethylamine (0.88 ml), diphenylphosphinic chloride (1 g, 4.23 mmols) and dry toluene (30 ml). A white gas evolved which died down after a few minutes. The reaction was left to stir at room temperature, under nitrogen for 4 hours. A white precipitate was observed and filtered off under reduced pressure, leaving a colourless solution. Volatiles were removed under reduced pressure leaving a pale cream solid.   Purification was achieved through silica column chromatography (DCM: ethyl acetate, 7:3 v/v). The title product was then recrystallised from DCM leaving white crystals (1.09g, 88%).

Melting point: 137.4 – 138.5 °C

Mass spectrum (ES): $[M]^+$ = 294.28, $[M + H]^+$ = 295.1

Micro analysis %: ($C_{18}H_{15}PO_2$)

Found C: 73.3%, H: 5.1%, P: 10.3%. Requires C: 73.5%, H: 5.2%, P: 10.5%.

NMR spectroscopic data: ^{1}H NMR, (300 MHz, CDCl$_3$, 300K): δ = 7.94 – 7.86 (m, 4H, C$_2$H, C$_4$H, C$_8$H, C$_{13}$H), 7.56 – 7.42 (m, 8H, C$_6$H, C$_7$H, C$_9$H, C$_{10}$H, C$_{11}$H, C$_{12}$H, C$_{14}$H, C$_{15}$H), 7.26 – 7.18 (m, 2H, C$_1$H, C$_5$H), 7.10 – 7.04 (m, 1H, C$_3$H).

^{31}P {^{1}H} NMR, (202 MHz, CDCl$_3$, 300K): δ = 30.99

6.7.2 Attempted synthesis of diphenylphosphinyl phenol (52) (I) [21]
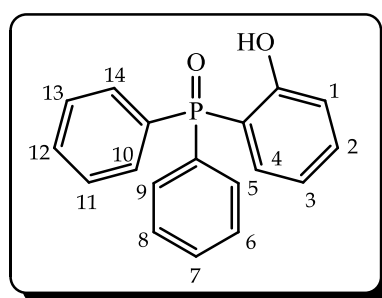
(52)

Procedure: In a two-necked flask equipped with a magnetic stirrer and nitrogen line, was placed diphenylphosphinyl phenyl ester **(51)** (200 mg, 0.68 mmols), diethyl ether (12.5 ml) and hexane (12.5 ml). The solution was stirred until all had dissolved. Lithium diisopropylamide (44.85 µL, 0.68 mmols) was added with stirring. The solution changed from colourless to pale brown upon stirring for 4 hours at room temperature. A small amount of precipitate was noted and filtered off under reduced pressure. Volatiles were removed, leaving beige solid, this was recrystallised from DCM to reveal pale orange needle crystals. The ^{31}P {^{1}H} NMR, ^{1}H NMR and melting point data are extremely similar to those of compound **(51)**. This suggests that the reaction had not been successful and further studies were needed.

Melting point: 136.5 – 140.3 °C

Mass spectrum (ES): [M + H]$^+$ = 295.1

NMR spectroscopic data: ^{1}H NMR, (300 MHz, CDCl$_3$, 300K): δ = 7.94 – 7.86 (m, 4H, C$_2$H, C$_4$H, C$_8$H, C$_{13}$H), 7.56 – 7.42 (m, 8H, C$_6$H, C$_7$H, C$_9$H, C$_{10}$H, C$_{11}$H, C$_{12}$H, C$_{14}$H, C$_{15}$H), 7.26 – 7.18 (m, 2H, C$_1$H, C$_5$H), 7.10 – 7.04 (m, 1H, C$_3$H).

^{31}P {^{1}H} NMR, (202 MHz, CDCl$_3$, 300K): δ = 31.01

6.7.3 Attempted synthesis of diphenylphosphinyl phenol (52) (II) [21]

Procedure: In an oven-dried two necked flask equipped with nitrogen line and a magnetic stirrer, was placed diphenylphosphinyl phenyl ester **(51)** (100 mg, 0.34 mmols) and dry THF (15 ml) and cooled to -78 °C (using a dry-ice and acetone bath). LDA (134.5 µL, 1.02 mmols) was added dropwise *via* a syringe. The reaction mixture was stirred at -78 °C for 30 minutes and quenched by the rapid addition of distilled water (5 ml). After warming to room temperature the organics were extracted into diethyl ether (30 ml) and washed with brine (20 ml), dried over MgSO$_4$, filtered and volatiles removed under reduced pressure, leaving a brown crystalline solid. A ^{31}P {^{1}H} NMR was taken of the crude product to see if the reaction had been successful.

NMR spectroscopic data: ^{31}P {^{1}H} NMR, (121 MHz, CDCl$_3$, 300K): analysis indicated the presence of only starting material, which was recovered, purified and reused.

6.7.4 Attempted synthesis of diphenylphosphinyl phenol (52) (III) [21]

Procedure: In an oven-dried two necked flask equipped with nitrogen line, condenser and magnetic stirrer, was placed diphenylphosphinyl phenyl ester **(51)** (100 mg, 0.34 mmols) and dry THF (15 ml). LDA (134.5 µL, 1.02 mmols)

was added dropwise *via* a syringe. The reaction was heated to 65-70 °C allowing the solution to gently reflux. The 4 hours the reaction was quenched with distilled water (4 ml), the organics extracted into diethyl ether (30 ml), dried over $MgSO_4$, filtered and volatiles removed under reduced pressure, leaving a pale yellow solid. A ^{31}P {^1H} NMR was taken of the crude product to see if the reaction had been successful.

NMR spectroscopic data: ^{31}P {^1H} NMR, (121 MHz, CDCl$_3$, 300K): analysis indicated the presence of only starting material, which was recovered as above.

6.7.5 Attempted synthesis of diphenylphosphinyl phenol (52) (IV) [21]

Procedure: In a Schlenk was placed diphenylphosphinyl phenyl ester **(51)** (100 mg, 0.34 mmols), toluene (15 ml) and a magnetic stirrer. Butyllithium (58 μL, 1.12 mmols) was gradually added to the solution which immediately changed the colour from colourless to a very dark brown. After stirring at room temperature for 1 hour the colour had changed to pale yellow. Distilled water (5 ml) was added, and reaction mixture dried over $MgSO_4$ with volatiles removed under reduced pressure. A TLC of the crude product was taken indicating the presence of another compound as well as starting material. Silica column chromatography (hexane: ethyl acetate, 6:4 v/v) was used to separate and purify the compounds. Among the starting material it was believed the other compounds could be either diphenyl phosphinyl or diphenyl phosphinic acid, however the ^{31}P {^1H} NMR and ^1H NMR data were inconclusive and starting material was the only fully identifiable compound.

NMR spectroscopic data: ^1H NMR, (300 MHz, CDCl$_3$, 300K): δ = 7.93 – 7.85 (m, 4H, C$_2$H, C$_4$H, C$_8$H, C$_{13}$H), 7.56 – 7.42 (m, 8H, C$_6$H, C$_7$H, C$_9$H, C$_{10}$H, C$_{11}$H, C$_{12}$H, C$_{14}$H, C$_{15}$H), 7.26 – 7.18 (m, 2H, C$_1$H, C$_5$H), 7.09 – 7.04 (m, 1H, C$_3$H).

^{31}P {^1H} NMR, (202 MHz, CDCl$_3$, 300K): δ = 31.08

6.8 Towards the synthesis of phosphinyl ligands – Route 2

6.8.1 Synthesis of 2-bromoanisole (53) [22]
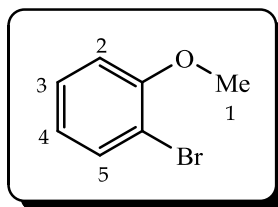
(53)

Procedure: In a flask equipped with a magnetic stirrer and condenser was placed potassium carbonate (23.84 g, 172.48 mmols) and ethyl acetate (150 ml), creating a white slurry. 2-Bromophenol (10 ml, 86.24 mmols) was added and the solution heated gently to 60 °C. Dimethyl sulphate (13.05 g, 103.49 mmols)) was gradually added, resulting in a temperature increase. Once all had been added the heat was removed and the solution left to stir for 2 hours at room temperature. After 2 hours the solution had thickened and was quenched with water (100 ml). The organics were separated and dried over $MgSO_4$, filtered and volatiles removed under reduced pressure, leaving an orange liquid (15.34 g, 95%).

Micro analysis %: (C_6H_7OBr)

Found C: 45.0%, H: 3.9%, Br: 42.4%. Requires C: 44.9%, H: 3.8%, Br: 42.7%.

NMR spectroscopic data: ^1H NMR, (300 MHz, $CDCl_3$, 300K): δ = 7.58 (dd, 1H, J = 7.8, 1.6 Hz C_5H), 7.29 (m, 1H, C_2H), 6.88 (m, 2H, C_3H, C_4H), 3.88 (s, 3H, C_1H)

6.8.2 Attempted synthesis of diphenylphosphinyl anisole (54) (I) [23], [24]
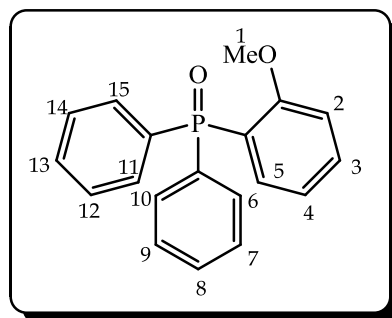
(54)

Procedure: In a Schlenk vessel was placed magnesium powder (129.98 mg, 5.35 mmols) and a magnetic stirrer. Under a nitrogen atmosphere the magnesium was left to stir for 2 days at room temperature. 2-Bromoanisole **(53)** (1.0 g, 5.35 mmols) was dissolved in dry THF (10 ml) and gradually added to the magnesium. The reaction mixture was left to stir at reflux for 1 hour. The reaction vessel was cooled to 0 °C (using an ice-bath). Diphenyl phosphinic chloride (0.71 ml, 3.75 mmols) was dissolved in dry THF (10 ml) and added to the Schlenk. The solution was left to reflux for a further 2 hours, producing a pale yellow solution. The reaction was quenched with water (5 ml) and extrated into DCM (20 ml), dried over $MgSO_4$, filtered and volatiles removed under reduced pressure leaving a pale orange oil. Analysis by ^{1}H NMR of the crude product showed the presence of the starting material. A further attempt using magnesium turnings was tested.

6.8.3 Attempted synthesis of diphenylphosphinyl anisole (54) (II) [23], [24]

Procedure: In a Schlenk vessel was placed magnesium turnings (129.98 mg, 5.35 mmols) and a magnetic stirrer. Under a nitrogen atmosphere the magnesium was left to stir for 24 hours at room temperature. 2-Bromoanisole **(53)** (1.0 g, 5.35 mmols) was dissolved in dry THF (10 ml) and gradually added to the activated magnesium. The reaction mixture was left to stir at reflux for 1 hour. The reaction vessel was cooled to 0 °C (using an ice-bath). Diphenyl phosphinic chloride (0.71 ml, 3.75 mmols) was dissolved in dry THF (10 ml) and added to the Schlenk. The solution was left to reflux for a further 2 hours, producing a pale yellow solution. The reaction was quenched with water (5 ml) and extrated into DCM (20 ml), dried over $MgSO_4$, filtered and volatiles removed under reduced pressure leaving a pale orange oil. Purification by silica gel column chromatography was carried out (ethyl acetate: DCM, 7:3 v/v). Four compounds were separated of which none corresponded to the title compound.

6.8.4 Attempted synthesis of diphenylphosphinyl anisole (54) (III) [23], [24]

Procedure: In a Schlenk vessel was placed magnesium turnings (156.07 mg, 6.42 mmols) and a magnetic stirrer. Under a nitrogen atmosphere the magnesium was left to stir for 24 hours at room temperature. An iodine crystal was added along with dry THF (3 ml) and 2-bromoanisole **(53)** (1.0 g, 5.35 mmols). The reaction mixture was left to stir at reflux for 1 hour. Diphenyl phosphinic chloride (1.21 ml, 4.12 was added to the Schlenk and the reaction left to stir for 24 hours at room temperature, upon which a white precipitate formed The reaction was quenched with water (15 ml) and extrated into DCM (30 ml), dried over $MgSO_4$, filtered and volatiles removed under reduced pressure leaving an

off-white paste (990 mg, 60%). Due to the mass of impurities present in the product a new strategy was devised.

6.8.5 Synthesis of diphenylphosphinyl anisole (54) (IV)

Procedure: In a round bottomed flask was placed a magnetic stirrer, nitrogen line and dry toluene (20 ml). 2-Bromoanisole (2.5 ml, 21.13 mmols) was added to the flask proceeded immediately by butyllithium (1.6M in hexanes, 13.21 ml, 21.13 mmols) producing a white precipitate. The reaction was left to stir for 1 hour at room temperature before diphenylphosphinyl chloride (5g, 21.13 mmols) was added and left to stir for 24 hours at room temperature. The solution was quenched with water (30 ml), resulting in an off-white precipitate crashing out, this was filtered and the organics extracted into DCM (50 ml), separated, dried over $MgSO_4$, filtered and volatiles removed under reduced pressure. Purification was achieved through leaving to stand in a small amount of DCM, producing white crystals (3.15g, 48%).

Micro analysis %: ($C_{19}H_{17}O_2P$)

Found C: 74.1%, H: 5.6%, P: 9.8%. Requires C: 74.0%, H: 5.6%, P: 10.0%.

Mass spectrum (ES): $[M + H]^+$ = 309.1

NMR spectroscopic data: ^{1}H NMR, (500 MHz, CDCl$_3$, 300K): δ = 7.79 – 7.69 (m, 5H, C_3H, C_4H, C_5H, C_8H, $C_{13}H$), 7.55 – 7.49 (m, 4H, C_6H, $C_{10}H$, $C_{11}H$, $C_{15}H$), 7.44 – 7.06 (m, 4H, C_7H, C_9H, $C_{12}H$, $C_{14}H$), 7.09 – 6.90 (m, 1H, C_2H), 3.55 (s, 3H, C_1H).

^{31}P {^{1}H} NMR, (202 MHz, CDCl$_3$, 300K): δ = 28.37

6.8.6 Synthesis of diphenylphosphinyl phenol (52) [25]
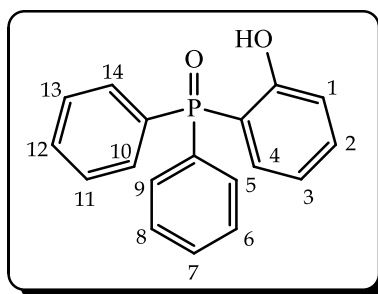
(52)

Procedure: A round bottomed flask equipped with a magnetic stirrer was purged with nitrogen before diphenylphosphinyl anisole **(54)** (2 g, 6.48 mmols) and DCM (50 ml) were added. This was then cooled to 0 °C and fresh, unopened boron tribromide (1M in DCM, 20 ml) was slowly added. The reaction mixture was allowed to reach room temperature and left to stir for a further 14 hours. The reaction mixture was cooled to 0 °C again and quenched with water (30 ml) and the organics extracted into ethyl acetate (15 ml) once the gas evolution had seised. Once separated they were then dried over Na_2SO_4, filtered and volatiles removed under reduced pressure. Purification was carried out using silica chromatography (DCM: ethyl acetate, 10% methanol 7:3 v/v) (0.76g, 40%). ^{31}P {^1H} NMR indicated the presence of another compound, closely related to the title compound and therefore proved too difficult to separate out. The impure title compound was taken through to the next stage.

Micro analysis %: ($C_{18}H_{15}O_2P$)

Found C: 69.4%, H: 5.4%, P: 10.5%. Requires C: 73.46%, H: 5.1%, P: 8.8%.

Mass spectrum (ESI): $[M + H]^+$ = 295.1.

NMR spectroscopic data: ^1H NMR, (300 MHz, CDCl$_3$, 300K): δ = 7.73 – 7.66 (m, 4H, C$_2$H, C$_3$H, C$_7$H, C$_{12}$H), 7.62 – 7.56 (m, 8H, C$_5$H, C$_6$H, C$_8$H, C$_9$H, C$_{10}$H, C$_{11}$H,

C$_{13}$H, C$_{14}$H), 7.44 – 7.38 (m, 5H, C$_4$H, C$_6$H, C$_8$H, C$_{11}$H, C$_{13}$H), 7.03 – 6.80 (m, 1H, C$_1$H).

^{31}P {^{1}H} NMR, (202 MHz, CDCl$_3$, 300K): δ = 40.11

6.8.7 Attempted synthesis of diphenylphosphinyl hydroxyl-benzaldehyde (55) [26]
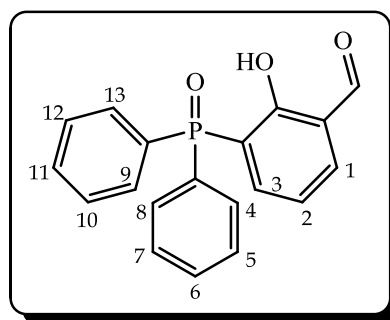
(55)

Procedure: In a two-neck flask equipped with a magnetic stirrer and condenser was placed diphenylphosphinyl phenol **(52)** (100 mg, 0.34 mmols), anhydrous magnesium chloride (48.54 mg, 0.51 mmols), dry triethylamine (125.58 mg, 1.24 mmols), acetonitrile (10 ml) and para-formaldehyde (68.92 μL, 2.30 mmols). The suspension was heated to reflux for 4 hours, cooled to room temperature and acidified with 5% aqueous HCl (pH 2). The organics were extracted into diethyl ether (3 x 20 ml), dried over MgSO$_4$, filtered and volatiles removed under reduced pressure, leaving a cream solid. ^{1}H NMR analysis indicated only the presence of the starting material and so reduction to the phosphine form before formylation could prove more successful.

6.8. 8 Attempted synthesis of diphenylphosphine phenol (56) [27]
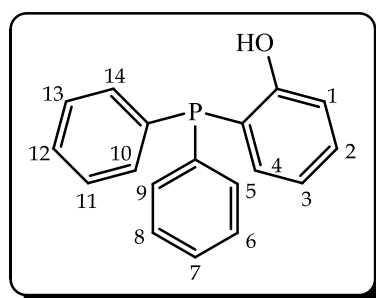
(56)

Procedure: To a three-neck flask equipped with a thermometer, condenser, magnetic stirrer and nitrogen line was placed triphenyl phosphinyl phenol **(52)** (300 mg, 1.02 mmols) and dry toluene (20 ml). To this was added dry triethylamine (0.09 ml, 0.61 mmols) and trichlorosilane (0.24 ml, 2.24 mmols). The temperature was increased to 90 °C and the reaction mixture refluxed for 6 hours. The reaction was quenched with water (5 ml), filtered and extracted into DCM (30 ml), dried over Na_2SO_4, filtered and volatiles removed under reduced pressure, leaving an off-white solid (180 mg, 63%). Analysis of the ^{31}P [^1H} NMR spectra indicated the presence of compounds **(52)** and **(54)** amongst a forest of unknown peaks. This data was supported by mass spectrometrical (ESI) analysis.

6.8.9 Attempted synthesis of diphenylphosphine anisole (57) [27]
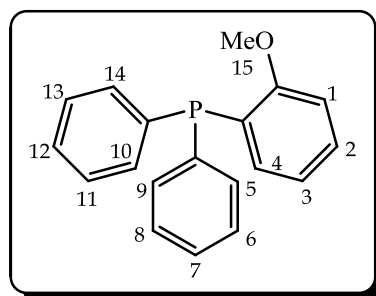
(57)

Procedure: To a three-neck flask equipped with a thermometer, condenser, magnetic stirrer and nitrogen line was placed diphenylphosphinyl anisole **(54)** (1 g, 3.24 mmols) and dry toluene (15 ml). To this was added dry triethylamine (0.27 ml, 1.94 mmols) and trichlorosilane (0.98 ml, 9.73 mmols). The temperature was increased to 90 °C and the reaction mixture refluxed for 6 hours. The reaction was quenched with water (10 ml), filtered and extracted into DCM (30 ml), dried over Na_2SO_4, filtered and volatiles removed under reduced pressure, leaving an off-white solid (0.76 g, 40%).

Mass spectrum (ESI): $[M + H]^+ = 293.1$

NMR spectroscopic data: ^{1}H NMR, (300 MHz, CDCl$_3$, 300K): extremely difficult to fully characterise due to a forest of peaks.

^{31}P {^{1}H} NMR, (121 MHz, CDCl$_3$, 300K): δ = -39.54

6.9 References

[1]   G. M. Sheldrick, *Acta. Cryst.*, **1990**, *A46*, 467.

[2]   C. J. Jason, *POV-Ray for Windows.*, V3.5, **2002**.

[3]   L. J. Farrugia, *J. Appl. Cryst.*, **1997**, *30*, 565.

[4]   HyperChem 7.0, Hypercube, Inc. Gainsville, FL, 32601, USA.

[5]   M. J. Frisch M. J. Frisch, G.W. Trucks, H. B. Schlegel, G. E. Scuseria,M. A. Robb, J. R. Cheeseman, J. A. Montgomery Jr, T. Verven, K. N. Kudin, J. C. Burant, J.M.Millam, S. S. Iyengar, J. Tomasi, V. Barone, B. Mennucci, M. Cossi, G. Scalmani, N. Rega, G. A. Petersson, T. Nakatsuji, M. Hada, M. Ehara, K. Toyota, R. Fukuda, J. Hasegawa, M. Ishida, T. Nakajima, Y. Honda, O. Kitao, H. Nakai,M. Klene, X. Li, J. E. Knox, H. P. Hratchian, J. B. Cross, C. Adamo, J. Jaramillo, R. Gomperts, R. E. Stratmann, O. Yazyev, A. J. Austin, R. Cammi, C. Pomelli, J. W. Ochterski, P. Y. Ayala, K. Morokuma, G. A. Voth, P. Salvador, J. J. Dannenberg, V. G. Zakrzewski, S. Dapprich, A. D. Daniels, M. C. Strain, O. Farkas, D. K. Malick, A. D. Rabuck, K. Raghavachari, J. B. Foresman, J. V. Ortiz, Q. Cui, A. G. Baboul, S. Clifford, J. Cioslowski, B. B. Stefanov, G. Liu, A. Liashenko, P. Piskorz, I. Komaromi, R. L. Martin, D. J. Fox, T. Keith, M. A. Al-Laham, C. Y. Peng, A. Nanayakkara, M. Challacombe, P. M. W. Gill, B. Johnson, W. Chen, M. W. Wong, C. Gonzalez, J. A. Pople, *Gaussian 03*, Revision C.02, Gaussian, Inc., Wallingford CT, 2004.

[6]   J. F. Larrow and E. N. Jacobsen, *J. Org. Chem.*, **1994**, *59*, 1939.

[7]   *Aldrich Handbook of Fine Chemicals.*, **2007-2008**, 836.

[8]   J. S. Baum, M. E. Condon, D. A. Shook, *J. Org. Chem.*, **1987**, *52*, 2983.

[9]   D. A. Atwood, *Coord. Chem. Revs.*, **1997**, *165*, 267

[10]   P. S. Skell and G. P. Bean, *J. Am. Chem. Soc.,* **1962**, *84*, 4655.

[11]   D. Suzuki, Y. Nobe, Y. Watai, R. Tanaka, Y. Takayama, F. Sato, H. Urabe, *J. Am. Chem. Soc.,* **2005**, *127*, 7474.

[12]   M. H. Fonseca, E. Eibler,, M. Zabel, B. König, *Inorg. Chim. Acta.*, **2005**, *352*, 136.

[13]   G. Royal, V. Dahaoui-Gindrey, S. Dahaoui, A. Tabard, R. Guilard, P. Pullumbi, C. Lecomte, *Eur. J. Org. Chem.*, **1998**, 1971.

[14]   M. Cavazzini, A. Manfredi, F. Montanari, S. Quici, G. Pozzi, *Chem. Commun.*, **2000**, 2171.

[15]   M. Cavazzini, A. Manfredi, F. Montanari, S. Quici, G. Pozzi, *Eur. J. Org. Chem.*, **2001**, 4639.

[16]   P. Wie, D. A. Atwood, *Polyhedron.*, **1999**, *18*, 641.

[17]   Z. Zhong, P. J. Dijkstra, F. Feijen, *Angew. Chem. Int. Ed.*, **2002**, *41*, 4150.

[18]   S. Gou, X. Zhou, J. Wang, X. Liu, X. Feng, *Tetrahedron.*, **2008**, *64*, 2864.

[19]   W. Peng, J. M. Shreeve, *J. Fluor. Chem.,* **2005,** 1054.

[20]   S. Hoz, E. J. Dunn, E. Puncel, *Phosphorus Sulfur 24.*, **1985**, 321.

[21]   R. J. Linderman, A. Ghannam, *JACS.*, **1990**, *6*, 2392.

[22]   A. R. Massah, M. Mosharafian, A. R. Momeni, H. Aliyan, H. J. Naghash, *Synthetic. Commun.*, **2007**, *37*, 1815.

[23]   M. G. Orga, M. Abdel-Hadi, S. Avola, N. Hadei, J. Nasielski, C. J. O'Brien, C. Valente, *Chemistry A European Journal.,* **2007,** *13,* 150.

[24]   K. V. Baker, J. M. Brown, N. Hughes, A. J. Skarnulis, A. Sexton, *J. Org. Chem.*, **1991**, *56*, 698.

[25]   J. F. W. McOmie, M. L. Watts, D. E. West, *Tetrahedron.*, **1968**, *24*, 2289.

[26]   T. V. Hansen, L. Skatteboel, D. Guthrie, D. P. Curran, *Org. Synth.*, **2005**, *82*, 64.

[27]   G. Baccolini, P. E. Todesco, *J. Org. Chem.*, **1975**, *40*, 2318.

Appendices

THERE ONCE WAS A GIRL NAMED IRENE,
WHO LIVED ON DISTILLED KEROSENE,
BUT SHE STARTED ABSORBIN'
A NEW HYDROCARBON,
AND SINCE THEN HAS NEVER BENZENE.

Appendix (i) Crystallographic data for 2-phenylamino benzaldehyde **(14)**
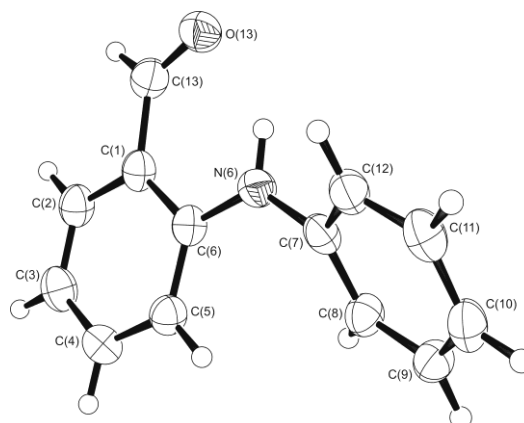
Formula	$C_{13}H_{11}NO$
Formula weight	197.23
Size	0.43 x 0.38 x 0.07 mm
Crystal morphology	Yellow plate
Temperature	150(2) K
Wavelength	0.71073 Å [Mo-K_α]
Crystal system	Orthorhombic
Space group	$Pca2_1$
Unit cell dimensions	a = 10.7960(3) Å α = 90°
	b = 9.5710(3) Å β = 90°
	c = 9.6460(4) Å γ = 90°
Volume	996.71(6) Å^3
Z	4
Density (calculated)	1.314 mg/m^3
Absorption coefficient	0.084 mm^{-1}
F(000)	416
Data collection range	$2.84 \leq \theta \leq 27.53°$
Index ranges	$-13 \leq h \leq 13, -12 \leq k \leq 12, -12 \leq l \leq 12$
Reflections collected	12149
Independent reflections	1215 [R(int) = 0.0957]
Observed reflections	968 [$I > 2\sigma(I)$]
Absorption correction	multi-scan
Max. and min. transmission	0.9942 and 0.4452
Refinement method	Full
Data / restraints / parameters	1215 / 1 / 137
Goodness of fit	1.034
Final R indices [$I > 2\delta(I)$]	R_1 = 0.0457, wR_2 = 0.1135
R indices (all data)	R_1 = 0.0638, wR_2 = 0.1260
Extinction parameter	0.045(9)
Largest diff. peak and hole	0.255 and -0.258e.Å^{-3}

Table 17 Atomic co-ordinates (x 10^4) and equivalent isotropic displacement parameters (Å^2 x 10^4) with standard uncertainties (s.u.s) in parentheses. U_{eq} is defined as $^1/_3$ of the trace of the orthogonalized U_{ij} tensor.

	x	y	z	U_{eq}
O(13)	-7270.8(18)	-3229.5(18)	-4223(2)	448(5)
N(6)	-9260(2)	-2820(2)	-2550(3)	381(6)
C(1)	-8247(2)	-5037(3)	-2893(3)	366(6)
C(2)	-8183(3)	-6474(3)	-2637(3)	401(7)
C(3)	-9047(3)	-7139(3)	-1836(3)	433(7)
C(4)	-10023(3)	-6367(3)	-1283(3)	404(6)
C(5)	-10094(3)	-4939(3)	-1487(3)	366(6)
C(6)	-9214(2)	-4232(2)	-2284(3)	348(6)
C(7)	-10133(2)	-1844(2)	-2047(3)	342(6)
C(8)	-10510(3)	-1803(3)	-670(3)	377(6)
C(9)	-11362(2)	-807(3)	-250(3)	392(7)
C(10)	-11821(3)	178(3)	-1166(3)	424(7)
C(11)	-11411(3)	164(3)	-2526(3)	413(7)
C(12)	-10597(3)	-852(3)	-2977(3)	384(7)
C(13)	-7322(3)	-4447(3)	-3820(3)	402(7)

Table 18 Anisotropic displacement parameters (Å^2 x 10^3). The anisotropic displacement factor exponent takes the form:

$$-2\pi^2[h^2a^{*2}U_{11} + \ldots + 2\,h\,k\,a^*\,b^*\,U_{12}]$$

	U_{11}	U_{22}	U_{33}	U_{23}	U_{13}	U_{12}
O(13)	391(12)	450(11)	504(13)	-15(10)	53(9)	-41(9)
N(6)	415(12)	299(10)	428(15)	9(10)	77(11)	4(9)
C(1)	360(14)	350(14)	388(15)	-60(12)	-49(11)	4(10)
C(2)	360(13)	374(14)	470(18)	-70(13)	-44(12)	47(10)
C(3)	458(16)	321(12)	520(19)	-9(13)	-83(14)	17(12)
C(4)	381(15)	386(13)	444(16)	27(13)	-13(13)	-37(11)
C(5)	340(13)	357(12)	400(16)	-29(12)	-7(11)	28(9)
C(6)	368(13)	327(13)	350(15)	-34(11)	-39(11)	8(10)
C(7)	289(12)	276(12)	459(17)	-2(11)	-1(11)	-39(9)
C(8)	425(15)	329(13)	378(16)	-2(12)	-2(12)	44(12)
C(9)	366(14)	392(14)	417(16)	-64(12)	37(12)	0(11)
C(10)	422(15)	302(13)	548(19)	-73(13)	-30(14)	20(11)
C(11)	402(14)	296(13)	540(18)	17(13)	-68(13)	-4(10)
C(12)	456(15)	314(13)	383(16)	-2(12)	-11(12)	-41(12)
C(13)	314(14)	450(14)	442(17)	-70(13)	6(11)	6(11)

Table 19 Hydrogen atom co-ordinates (x 10^3) and isotropic displacement parameters ($Å^2$ x 10^2) with s.u.s in parentheses.

	x	y	z	U_{eq}
H(6)	-8679.	-2486.	-3097.	46.
H(2)	-7524.	-7001.	-3028.	48.
H(3)	-8983.	-8113.	-1659.	52.
H(4)	-10647.	-6827.	-760.	48.
H(5)	-10754.	-4429.	-1076.	44.
H(8)	-10185.	-2453.	-21.	45.
H(9)	-11636.	-799.	686.	47.
H(10)	-12408.	853.	-867.	51.
H(11)	-11692.	860.	-3154.	50.
H(12)	-10350.	-876.	-3922.	46.
H(13)	-6697.	-5062.	-4147.	48.

Table 20 Interatomic distances (Å) with s.u.s in parentheses.

O(13)-C(13)	1.229(3)	N(6)-C(6)	1.377(3)
N(6)-C(7)	1.412(3)	C(1)-C(2)	1.400(3)
C(1)-C(6)	1.424(4)	C(1)-C(13)	1.455(4)
C(2)-C(3)	1.368(4)	C(3)-C(4)	1.393(4)
C(4)-C(5)	1.383(3)	C(5)-C(6)	1.396(4)
C(7)-C(8)	1.389(4)	C(7)-C(12)	1.399(4)
C(8)-C(9)	1.385(4)	C(9)-C(10)	1.384(4)
C(10)-C(11)	1.384(5)	C(11)-C(12)	1.381(4)

Table 21 Angles between interatomic vectors (°) with s.u.s in parentheses.

C(6)-N(6)-C(7)	127.5(2)	C(2)-C(1)-C(6)	119.7(3)
C(2)-C(1)-C(13)	117.1(2)	C(6)-C(1)-C(13)	123.2(2)
C(3)-C(2)-C(1)	121.5(3)	C(2)-C(3)-C(4)	119.0(3)
C(5)-C(4)-C(3)	120.8(3)	C(4)-C(5)-C(6)	121.3(3)
N(6)-C(6)-C(5)	123.6(2)	N(6)-C(6)-C(1)	118.7(2)
C(5)-C(6)-C(1)	117.6(2)	C(8)-C(7)-C(12)	119.2(2)
C(8)-C(7)-N(6)	122.9(2)	C(12)-C(7)-N(6)	117.8(3)
C(9)-C(8)-C(7)	119.6(3)	C(10)-C(9)-C(8)	121.3(3)
C(11)-C(10)-C(9)	119.0(3)	C(12)-C(11)-C(10)	120.6(3)
C(11)-C(12)-C(7)	120.2(3)	O(13)-C(13)-C(1)	126.4(3)

Table 22 Torsion angles (°) with s.u.s in parentheses.

C(6)-C(1)-C(2)-C(3)	1.5(4)	C(13)-C(1)-C(2)-C(3)	-176.7(3)
C(1)-C(2)-C(3)-C(4)	1.0(5)	C(2)-C(3)-C(4)-C(5)	-2.8(5)
C(3)-C(4)-C(5)-C(6)	1.9(4)	C(7)-N(6)-C(6)-C(5)	2.8(4)
C(7)-N(6)-C(6)-C(1)	-179.8(3)	C(4)-C(5)-C(6)-N(6)	178.2(3)
C(4)-C(5)-C(6)-C(1)	0.7(4)	C(2)-C(1)-C(6)-N(6)	-180.0(3)
C(13)-C(1)-C(6)-N(6)	-1.9(4)	C(2)-C(1)-C(6)-C(5)	-2.4(4)
C(13)-C(1)-C(6)-C(5)	175.7(3)	C(6)-N(6)-C(7)-C(8)	45.2(4)
C(6)-N(6)-C(7)-C(12)	-137.2(3)	C(12)-C(7)-C(8)-C(9)	1.8(4)
N(6)-C(7)-C(8)-C(9)	179.4(2)	C(7)-C(8)-C(9)-C(10)	-1.9(4)
C(8)-C(9)-C(10)-C(11)	-0.3(4)	C(9)-C(10)-C(11)-C(12)	2.7(4)
C(10)-C(11)-C(12)-C(7)	-2.8(4)	C(8)-C(7)-C(12)-C(11)	0.5(4)
N(6)-C(7)-C(12)-C(11)	-177.2(2)	C(2)-C(1)-C(13)-O(13)	175.9(3)
C(6)-C(1)-C(13)-O(13)	-2.2(5)		

Appendix (ii) Crystallographic data for (R,R)-N,N′-bis-(2-phenylamino-benzyl)-trans-1,2-diaminocyclohexane **(18)**
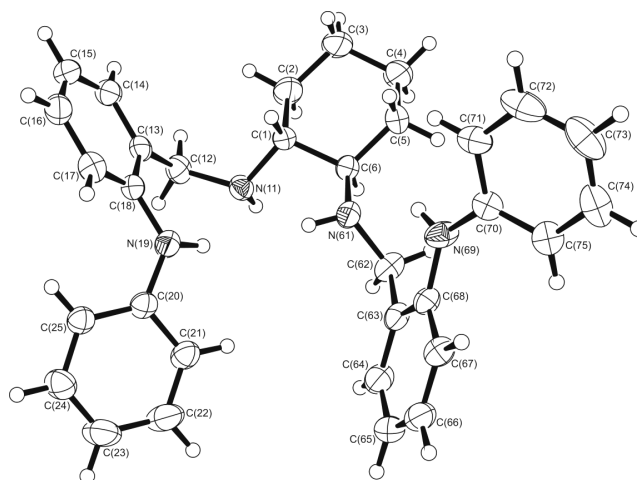
Formula	$C_{32}H_{36}N_4$	
Formula weight	476.65	
Size	0.37 x 0.24 x 0.22 mm	
Crystal morphology	Colourless fragment	
Temperature	150K	
Wavelength	0.71073 Å [Mo-K_a]	
Crystal system	Hexagonal	
Space group	$P6_1$	
Unit cell dimensions	a = 10.8060(2) Å	α = 90°
	b = 10.8060(2) Å	β = 90°
	c = 40.9239(12) Å	γ = 120°
Volume	4138.45(16) Å³	
Z	6	
Density (calculated)	1.148 Mg/m³	
Absorption coefficient	0.068 mm⁻¹	
F(000)	1536	
Data collection range	$2.18 \leq \theta \leq 28.11°$	
Index ranges	$-14 \leq h \leq 14$, $-14 \leq k \leq 14$, $-54 \leq l \leq 54$	
Reflections collected	52292	
Independent reflections	3413 [R(int) = 0.0327]	
Observed reflections	3164 [$I > 2\sigma(I)$]	
Absorption correction	multi-scan	
Max. and min. transmission	0.9843 and 0.9124	
Refinement method	Full	
Data / restraints / parameters	3413 / 1 / 332	
Goodness of fit	1.082	
Final R indices [$I > 2\square(I)$]	R_1 = 0.0363, wR_2 = 0.0900	
R indices (all data)	R_1 = 0.0405, wR_2 = 0.0926	
Largest diff. peak and hole	0.155 and -0.163e.Å⁻³	

Table 23 Atomic co-ordinates (x 10^4) and equivalent isotropic displacement parameters (Å^2 x 10^4) with standard uncertainties (s.u.s) in parentheses. U_{eq} is defined as $^1/_3$ of the trace of the orthogonalized U_{ij} tensor.

	x	y	z	U_{eq}
C(1)	8630.7(15)	8855.7(15)	497.4(4)	321(3)
C(2)	7762(2)	8610(2)	179.5(5)	549(5)
C(3)	6630(2)	9067(2)	209.8(7)	742(7)
C(4)	7302(2)	10622(2)	321.9(7)	729(7)
C(5)	8111(2)	10841.9(19)	644.2(6)	551(5)
C(6)	9270.1(16)	10421.7(15)	611.0(4)	336(3)
N(11)	9831.5(13)	8572.1(13)	459.9(3)	330(3)
C(12)	9459.0(17)	7123.0(17)	340.8(4)	388(3)
C(13)	8700.1(15)	5950.6(15)	595.5(3)	319(3)
C(14)	7433.2(17)	4701.7(17)	515.4(4)	411(3)
C(15)	6765.0(18)	3565.7(18)	734.4(5)	473(4)
C(16)	7361.6(18)	3686.0(18)	1042.1(5)	465(4)
C(17)	8612.0(18)	4926.5(18)	1131.0(4)	411(3)
C(18)	9308.5(16)	6060.5(15)	908.9(4)	335(3)
N(19)	10571.9(15)	7338.9(14)	987.5(4)	432(3)
C(20)	11849.9(16)	7473.4(16)	1108.8(3)	331(3)
C(21)	13049.7(18)	8868.0(18)	1116.1(4)	411(3)
C(22)	14381(2)	9093(2)	1211.2(5)	585(5)
C(23)	14548(2)	7937(2)	1307.1(5)	600(5)
C(24)	13368(2)	6577.8(19)	1312.0(4)	457(4)
C(25)	12023.4(16)	6332.2(16)	1213.7(3)	356(3)
N(61)	10071.5(13)	10707.6(13)	923.4(3)	333(3)
C(62)	11338.4(17)	12166.3(16)	928.7(4)	382(3)
C(63)	12122.1(15)	12538.8(14)	1253.1(3)	333(3)
C(64)	13549.6(17)	12898.6(17)	1272.8(4)	445(4)
C(65)	14317.1(18)	13339.5(19)	1565.3(5)	482(4)
C(66)	13630.8(17)	13428.7(16)	1843.9(4)	424(3)
C(67)	12192.7(16)	13067.0(16)	1834.1(3)	364(3)
C(68)	11418.7(15)	12610.4(15)	1539.7(3)	311(3)
N(69)	9960.9(14)	12173.1(16)	1511.0(3)	417(3)
C(70)	9118.1(16)	12481.0(16)	1720.5(3)	339(3)
C(71)	7659.0(17)	11482.4(19)	1743.7(4)	427(4)
C(72)	6771(2)	11780(2)	1940.9(5)	575(5)
C(73)	7340(2)	13062(3)	2115.0(4)	580(5)
C(74)	8786(2)	14037(2)	2092.8(4)	510(4)
C(75)	9678.3(18)	13770.0(17)	1896.0(3)	392(3)

Table 24 Anisotropic displacement parameters (Å^2 x 10^3). The anisotropic displacement factor exponent takes the form:

$$-2\pi^2[h^2a^{*2}U_{11} + \ldots + 2\,h\,k\,a^*\,b^*\,U_{12}]$$

	U_{11}	U_{22}	U_{33}	U_{23}	U_{13}	U_{12}
C(1)	28.2(7)	28.0(7)	39.7(7)	1.3(5)	-1.8(5)	13.7(6)
C(2)	52.8(10)	45.0(10)	65.4(11)	-10.4(8)	-28.9(9)	23.5(9)
C(3)	48.7(11)	46.8(11)	126(2)	-7.6(12)	-43.0(12)	23.4(9)
C(4)	50.5(11)	41.9(10)	130(2)	2.1(11)	-35.0(12)	25.8(9)
C(5)	44.5(10)	35.1(9)	92.5(15)	-5.8(9)	-7.9(9)	25.0(8)
C(6)	31.4(7)	26.8(7)	41.6(7)	3.1(6)	-0.4(6)	13.8(6)
N(11)	32.2(6)	33.6(6)	35.4(6)	1.3(5)	3.3(5)	18.0(5)
C(12)	43.6(8)	42.5(8)	36.5(7)	-5.5(6)	2.9(6)	26.3(7)
C(13)	32.7(7)	32.7(7)	37.0(7)	-6.8(6)	-0.9(6)	21.4(6)
C(14)	36.8(8)	40.0(8)	50.2(8)	-13.1(7)	-8.5(7)	22.1(7)
C(15)	29.8(8)	33.6(8)	76.2(11)	-9.1(8)	-3.1(8)	14.1(7)
C(16)	39.3(9)	36.4(9)	65.6(11)	7.1(7)	9.3(8)	20.2(7)
C(17)	44.0(9)	41.3(9)	43.3(8)	1.8(7)	-0.6(7)	25.2(7)
C(18)	31.5(7)	29.9(7)	42.3(7)	-6.4(6)	-3.3(6)	17.7(6)
N(19)	42.1(7)	30.0(7)	56.0(8)	-2.8(6)	-14.8(6)	16.9(6)
C(20)	36.6(8)	35.6(7)	25.4(6)	-6.0(5)	-5.8(5)	16.8(6)
C(21)	43.3(9)	35.7(8)	38.3(7)	-0.6(6)	-8.5(6)	15.3(7)
C(22)	41.6(10)	49.1(10)	62.9(11)	7.9(9)	-15.3(8)	6.2(8)
C(23)	40.1(9)	64.1(12)	67.5(12)	12.6(10)	-14.0(9)	19.9(9)
C(24)	46.4(9)	50.0(10)	42.6(8)	6.8(7)	-5.4(7)	25.5(8)
C(25)	38.0(8)	35.0(7)	32.1(7)	-2.9(6)	-4.4(6)	16.9(6)
N(61)	34.9(6)	28.0(6)	35.5(6)	-0.8(5)	1.5(5)	14.6(5)
C(62)	38.0(8)	35.8(8)	29.7(6)	-2.5(6)	7.6(6)	10.1(6)
C(63)	33.7(7)	26.1(7)	34.8(7)	-1.2(5)	5.1(6)	10.9(6)
C(64)	34.8(8)	39.7(8)	53.7(9)	-8.4(7)	9.1(7)	14.5(7)
C(65)	30.6(8)	41.8(9)	69.3(11)	-8.1(8)	-4.4(8)	15.9(7)
C(66)	40.6(8)	34.8(8)	45.0(8)	0.0(7)	-9.5(7)	13.6(7)
C(67)	37.3(8)	32.7(7)	31.5(7)	4.7(6)	3.1(6)	11.8(6)
C(68)	30.8(7)	25.7(7)	30.9(6)	2.0(5)	3.7(5)	9.8(6)
N(69)	30.7(7)	49.2(8)	35.9(6)	-14.3(6)	0.4(5)	13.0(6)
C(70)	35.4(7)	40.0(8)	26.8(6)	5.4(5)	3.6(5)	19.2(6)
C(71)	32.6(8)	49.7(9)	45.1(8)	7.2(7)	0.7(6)	20.0(7)
C(72)	37.9(9)	81.9(14)	56.8(10)	24.7(10)	12.4(8)	33.2(10)
C(73)	69.7(13)	91.5(16)	39.4(9)	15.9(9)	17.6(8)	60.3(13)
C(74)	76.2(13)	65.6(12)	33.0(7)	3.5(7)	3.4(8)	51.7(11)
C(75)	46.5(9)	44.1(8)	28.5(6)	4.6(6)	3.7(6)	23.7(7)

Table 25 Hydrogen atom co-ordinates (x 10^3) and isotropic displacement parameters (Å^2 x 10^2) with s.u.s in parentheses.

	x	y	z	U_{eq}
H(1)	797.4	821.3	67.1	39.
H(2a)	842.6	915.4	0.	66.
H(2b)	728.3	758.3	12.2	66.
H(3a)	615.9	895.5	-0.4	89.
H(3b)	589.	844.	36.9	89.

H(4a)	654.5	1087.4	35.2	88.
H(4b)	796.9	1126.	15.2	88.
H(5a)	742.8	1025.6	81.7	66.
H(5b)	856.	1185.7	71.	66.
H(6)	995.9	1104.7	44.	40.
H(12a)	1034.6	714.	27.2	47.
H(12b)	883.6	688.9	14.6	47.
H(14)	701.7	462.5	30.7	49.
H(15)	591.3	272.	67.4	57.
H(16)	691.4	291.7	119.3	56.
H(17)	899.6	500.5	134.4	49.
H(21)	1294.4	965.9	105.5	49.
H(22)	1518.3	1003.4	121.1	70.
H(23)	1546.2	808.7	136.8	72.
H(24)	1347.2	579.8	138.3	55.
H(25)	1122.5	539.	121.8	43.
H(62a)	1102.8	1286.9	88.2	46.
H(62b)	1200.5	1224.4	75.3	46.
H(64)	1401.7	1284.3	108.1	53.
H(65)	1528.9	1357.4	157.3	58.
H(66)	1414.4	1373.9	204.4	51.
H(67)	1173.8	1313.	202.7	44.
H(71)	726.9	1060.7	162.7	51.
H(72)	578.	1110.5	195.6	69.
H(73)	673.9	1326.2	224.7	70.
H(74)	917.6	1490.2	221.4	61.
H(75)	1066.6	1445.9	188.	47.
H(61)	1026.6	1000.	94.6	42.(5)
H(11)	1044.9	922.	30.2	33.(4)
H(19)	1076.9	815.2	86.9	51.(5)
H(69)	954.(2)	1159.(2)	135.8(5)	51.(5)

Table 26 Interatomic distances (Å) with s.u.s in parentheses.

C(1)-N(11)	1.4828(18)	C(1)-C(6)	1.5452(19)
C(1)-C(2)	1.548(2)	C(2)-C(3)	1.536(3)
C(3)-C(4)	1.530(3)	C(4)-C(5)	1.534(3)
C(5)-C(6)	1.537(2)	C(6)-N(61)	1.4874(19)
N(11)-C(12)	1.4905(19)	C(12)-C(13)	1.525(2)
C(13)-C(14)	1.398(2)	C(13)-C(18)	1.419(2)
C(14)-C(15)	1.395(3)	C(15)-C(16)	1.391(3)
C(16)-C(17)	1.394(2)	C(17)-C(18)	1.404(2)
C(18)-N(19)	1.4106(19)	N(19)-C(20)	1.405(2)
C(20)-C(25)	1.404(2)	C(20)-C(21)	1.414(2)
C(21)-C(22)	1.390(3)	C(22)-C(23)	1.405(3)
C(23)-C(24)	1.382(3)	C(24)-C(25)	1.399(2)
N(61)-C(62)	1.4837(19)	C(62)-C(63)	1.517(2)
C(63)-C(64)	1.392(2)	C(63)-C(68)	1.4207(19)
C(64)-C(65)	1.397(3)	C(65)-C(66)	1.390(3)

C(66)-C(67)	1.401(2)	C(67)-C(68)	1.408(2)
C(68)-N(69)	1.4050(19)	N(69)-C(70)	1.4065(19)
N(69)-H(69)	0.84(2)	C(70)-C(71)	1.399(2)
C(70)-C(75)	1.407(2)	C(71)-C(72)	1.408(3)
C(72)-C(73)	1.398(3)	C(73)-C(74)	1.383(3)
C(74)-C(75)	1.393(2)		

Appendix (iii) Crystallographic data of 5-bromo-3-*tert*-butyl-2-methoxybenzaldehyde **(34)**
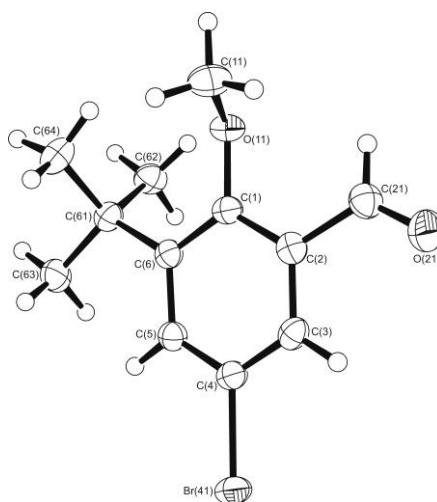
Formula	$C_{12}H_{15}BrO_2$
Formula weight	271.15
Size	0.3 x 0.25 x 0.24 mm
Crystal morphology	Colourless fragment
Temperature	150(2) K
Wavelength	0.71073 Å [Mo-K_α]
Crystal system	Monoclinic
Space group	$C2/c$
Unit cell dimensions	$a = 18.6838(4)$ Å $\quad$ $\sigma = 90°$
	$b = 8.6901(2)$ Å $\quad$ $\beta = 94.8420(10)°$
	$c = 14.3985(3)$ Å $\quad$ $\gamma = 90°$
Volume	2329.46(9) Å^3
Z	8
Density (calculated)	1.546 Mg/m^3
Absorption coefficient	3.507 mm^{-1}
$F(000)$	1104
Data collection range	$3.44 \leq \theta \leq 27.48°$
Index ranges	$-24 \leq h \leq 24$, $-11 \leq k \leq 11$, $-18 \leq l \leq 18$
Reflections collected	16054
Independent reflections	2668 [R(int) = 0.0448]
Observed reflections	2378 [$I > 2\sigma(I)$]
Absorption correction	multi-scan
Max. and min. transmission	0.433 and 0.3544
Refinement method	Full
Data / restraints / parameters	2668 / 0 / 141
Goodness of fit	1.032
Final R indices [$I > 2\sigma(I)$]	$R_1 = 0.0263$, $wR_2 = 0.0653$
R indices (all data)	$R_1 = 0.0312$, $wR_2 = 0.0676$
Extinction parameter	0.0060(3)
Largest diff. peak and hole	0.313 and -0.417e.Å^{-3}

Table 27 Atomic co-ordinates (x 10^4) and equivalent isotropic displacement parameters ($Å^2$ x 10^4) with standard uncertainties (s.u.s) in parentheses. U_{eq} is defined as $^1/_3$ of the trace of the orthogonalized U_{ij} tensor.

	x	y	z	U_{eq}
Br(41)	10708.98(10)	-2730.5(2)	6394.63(13)	332.5(10)
O(11)	8795.7(7)	2871.0(14)	6002.2(9)	295(3)
O(21)	10923.9(8)	3464.1(19)	5811.0(12)	463(4)
C(4)	10118.1(10)	-947(2)	6286.7(11)	265(4)
C(5)	9379.9(10)	-1129(2)	6269.0(11)	261(4)
C(2)	9970.6(10)	1749(2)	6073.1(12)	267(4)
C(21)	10289.1(11)	3242(2)	5825.4(13)	326(4)
C(6)	8910.2(9)	122(2)	6173.9(11)	246(4)
C(1)	9227.2(9)	1583(2)	6104.0(11)	248(4)
C(62)	7777.9(10)	380(2)	5123.8(14)	334(4)
C(61)	8090.0(10)	-128(2)	6098.2(13)	288(4)
C(3)	10423.9(10)	474(2)	6182.3(12)	275(4)
C(63)	7899.1(11)	-1826(2)	6221.8(15)	360(4)
C(64)	7732.3(11)	790(3)	6846.9(15)	406(5)
C(11)	8849.3(12)	3912(2)	6785.2(15)	406(5)

Table 28 Anisotropic displacement parameters ($Å^2$ x 10^3). The anisotropic displacement factor exponent takes the form:

$$-2\pi^2[h^2a^{*2}U_{11} + ... + 2\,h\,k\,a^*\,b^*\,U_{12}]$$

	U_{11}	U_{22}	U_{33}	U_{23}	U_{13}	U_{12}
Br(41)	319.3(14)	326.3(14)	349.4(14)	9.1(7)	14.3(8)	105.9(7)
O(11)	318(7)	247(7)	316(7)	-24(5)	5(5)	56(5)
O(21)	359(8)	399(9)	639(10)	-3(7)	92(7)	-89(7)
C(4)	275(9)	296(10)	226(8)	5(7)	23(7)	50(7)
C(5)	285(9)	266(9)	234(8)	7(7)	27(7)	10(7)
C(2)	293(9)	275(9)	233(8)	-15(7)	16(7)	-20(7)
C(21)	352(11)	301(10)	327(10)	-21(8)	32(8)	-35(8)
C(6)	261(9)	274(9)	204(8)	1(6)	21(6)	11(7)
C(1)	271(9)	263(9)	208(8)	-4(7)	10(6)	42(7)
C(62)	270(9)	350(11)	372(10)	16(8)	-36(8)	13(8)
C(61)	247(9)	298(10)	320(9)	2(7)	39(7)	4(7)
C(3)	238(9)	346(10)	241(8)	-5(7)	19(7)	11(7)
C(63)	274(10)	362(11)	445(11)	65(9)	26(8)	-37(8)
C(64)	303(10)	492(13)	438(12)	-57(10)	113(9)	25(9)
C(11)	450(12)	314(11)	450(12)	-117(9)	19(9)	64(9)

Table 29 Hydrogen atom co-ordinates (x 10^3) and isotropic displacement parameters ($Å^2$ x 10^2) with s.u.s in parentheses.

	x	y	z	U_{eq}
H(5)	9188.	-2135.	6323.	31.
H(21)	9972.	4075.	5668.	39.
H(62a)	7958.	-299.	4652.	50.
H(62b)	7924.	1441.	5010.	50.
H(62c)	7252.	321.	5088.	50.
H(3)	10930.	585.	6184.	33.
H(63a)	8084.	-2171.	6844.	54.
H(63b)	8116.	-2444.	5750.	54.
H(63c)	7376.	-1950.	6150.	54.
H(64a)	7222.	518.	6827.	61.
H(64b)	7780.	1894.	6727.	61.
H(64c)	7967.	542.	7463.	61.
H(11a)	8741.	3356.	7349.	61.
H(11b)	8506.	4756.	6668.	61.
H(11c)	9338.	4330.	6871.	61.

Table 30 Interatomic distances (Å) with s.u.s in parentheses.

Br(41)-C(4)	1.9019(18)	O(11)-C(1)	1.380(2)
O(11)-C(11)	1.442(2)	O(21)-C(21)	1.204(2)
C(4)-C(3)	1.374(3)	C(4)-C(5)	1.387(3)
C(5)-C(6)	1.397(2)	C(2)-C(3)	1.396(3)
C(2)-C(1)	1.401(3)	C(2)-C(21)	1.483(3)
C(6)-C(1)	1.408(3)	C(6)-C(61)	1.542(2)
C(62)-C(61)	1.538(3)	C(61)-C(63)	1.532(3)
C(61)-C(64)	1.539(3)		

Table 31 Angles between interatomic vectors (°) with s.u.s in parentheses.

C(1)-O(11)-C(11)	115.10(15)	C(3)-C(4)-C(5)	121.55(17)
C(3)-C(4)-Br(41)	119.82(13)	C(5)-C(4)-Br(41)	118.54(14)
C(4)-C(5)-C(6)	121.89(17)	C(3)-C(2)-C(1)	120.57(17)
C(3)-C(2)-C(21)	118.02(17)	C(1)-C(2)-C(21)	121.10(17)
O(21)-C(21)-C(2)	124.1(2)	C(5)-C(6)-C(1)	116.38(15)
C(5)-C(6)-C(61)	120.60(16)	C(1)-C(6)-C(61)	122.94(16)
O(11)-C(1)-C(2)	119.00(16)	O(11)-C(1)-C(6)	119.56(16)
C(2)-C(1)-C(6)	121.29(16)	C(63)-C(61)-C(62)	107.96(16)
C(63)-C(61)-C(64)	107.39(16)	C(62)-C(61)-C(64)	109.66(16)
C(63)-C(61)-C(6)	111.56(15)	C(62)-C(61)-C(6)	108.78(15)
C(64)-C(61)-C(6)	111.41(16)	C(4)-C(3)-C(2)	118.14(16)

Table 32 Torsion angles (°) with s.u.s in parentheses.

C(3)-C(4)-C(5)-C(6)	-2.1(3)	Br(41)-C(4)-C(5)-C(6)	-178.79(13)
C(3)-C(2)-C(21)-O(21)	-8.4(3)	C(1)-C(2)-C(21)-O(21)	177.99(19)
C(4)-C(5)-C(6)-C(1)	-0.5(2)	C(4)-C(5)-C(6)-C(61)	176.36(16)
C(11)-O(11)-C(1)-C(2)	-71.7(2)	C(11)-O(11)-C(1)-C(6)	112.54(19)
C(3)-C(2)-C(1)-O(11)	179.39(15)	C(21)-C(2)-C(1)-O(11)	-7.2(2)
C(3)-C(2)-C(1)-C(6)	-4.9(3)	C(21)-C(2)-C(1)-C(6)	168.56(16)
C(5)-C(6)-C(1)-O(11)	179.57(15)	C(61)-C(6)-C(1)-O(11)	2.8(2)
C(5)-C(6)-C(1)-C(2)	3.9(2)	C(61)-C(6)-C(1)-C(2)	-172.87(16)
C(5)-C(6)-C(61)-C(63)	4.6(2)	C(1)-C(6)-C(61)-C(63)	-178.74(16)
C(5)-C(6)-C(61)-C(62)	-114.34(18)	C(1)-C(6)-C(61)-C(62)	62.3(2)
C(5)-C(6)-C(61)-C(64)	124.66(18)	C(1)-C(6)-C(61)-C(64)	-58.7(2)
C(5)-C(4)-C(3)-C(2)	1.1(3)	Br(41)-C(4)-C(3)-C(2)	177.83(13)
C(1)-C(2)-C(3)-C(4)	2.3(3)	C(21)-C(2)-C(3)-C(4)	-171.38(16)

Appendix (iv) Crystallographic data of diphenylphosphinyl phenyl ester **(51)**
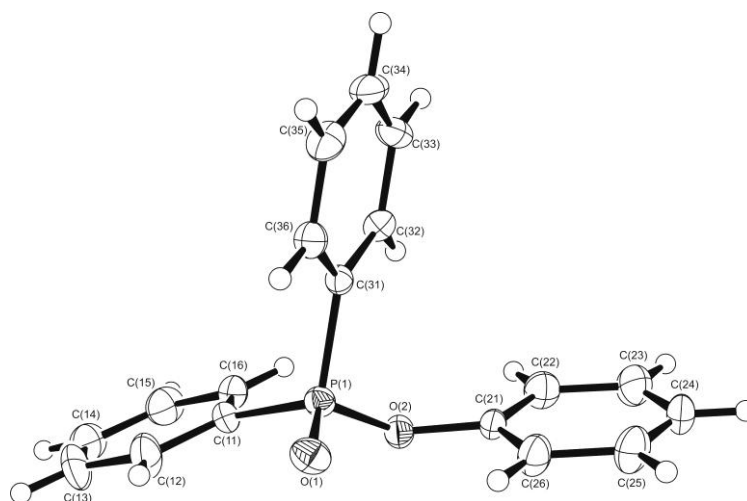
Formula	$C_{18}H_{15}O_2P$
Formula weight	294.27
Size	0.31 x 0.14 x 0.14 mm
Crystal morphology	Colourless fragment
Temperature	150K
Wavelength	0.71073 Å [Mo-K_α]
Crystal system	Monoclinic
Space group	$P2_1/n$
Unit cell dimensions	a = 9.3329(12) Å α = 90°
	b = 11.4890(14) Å β = 93.774(8)°
	c = 14.2455(18) Å γ = 90°
Volume	1524.2(3) Å³
Z	4
Density (calculated)	1.282 Mg/m³
Absorption coefficient	0.181 mm⁻¹
F(000)	616
Data collection range	2.28 ≤ θ ≤ 28.36°
Index ranges	-12 ≤ h ≤12, -14 ≤ k ≤ 15, -19 ≤ l ≤ 18
Reflections collected	29375
Independent reflections	3721 [R(int) = 0.0764]
Observed reflections	2619 [$I > 2\sigma(I)$]
Absorption correction	multi-scan
Max. and min. transmission	0.975 and 0.8772
Refinement method	Full
Data / restraints / parameters	3721 / 0 / 190
Goodness of fit	1.059
Final R indices [$I > 2\sigma(I)$]	R_1 = 0.0893, wR_2 = 0.3108
R indices (all data)	R_1 = 0.1172, wR_2 = 0.3275
Largest diff. peak and hole	1.399 and -0.585e.Å⁻³

Table 33 Atomic co-ordinates (x 10⁴) and equivalent isotropic displacement parameters (Å² x 10⁴) with standard uncertainties (s.u.s) in parentheses. U_{eq} is defined as $1/3$ of the trace of the orthogonalized U_{ij} tensor.

	x	y	z	U_{eq}
P(1)	2446.9(13)	776.8(11)	6990.8(8)	215(4)
O(1)	2061(4)	-445(3)	6713(3)	297(8)
O(2)	2312(3)	1120(3)	8085(2)	243(7)
C(11)	4345(5)	1105(4)	6910(3)	248(10)
C(12)	5167(6)	340(5)	6409(5)	390(13)
C(13)	6629(7)	565(6)	6322(5)	484(17)
C(14)	7265(6)	1532(6)	6740(5)	450(16)
C(15)	6449(6)	2303(6)	7251(4)	381(13)
C(16)	4981(5)	2096(5)	7329(4)	293(11)
C(21)	984(5)	1148(4)	8527(3)	222(9)
C(22)	759(6)	2107(5)	9090(4)	325(12)
C(23)	-493(7)	2153(6)	9585(4)	406(14)
C(24)	-1493(6)	1254(6)	9502(4)	382(13)
C(25)	-1250(6)	303(6)	8930(4)	399(14)
C(26)	-2(6)	236(5)	8431(4)	330(12)
C(31)	1336(5)	1828(4)	6324(3)	192(9)
C(32)	1104(5)	2966(4)	6639(3)	225(9)
C(33)	198(5)	3718(4)	6089(4)	280(11)
C(34)	-456(6)	3339(5)	5235(4)	321(12)
C(35)	-215(5)	2214(5)	4911(4)	305(11)
C(36)	685(5)	1452(4)	5456(3)	249(10)

Table 34 Anisotropic displacement parameters (Å² x 10³). The anisotropic displacement factor exponent takes the form:

$$-2\pi^2[h^2a^{*2}U_{11} + ... + 2\,h\,k\,a^*\,b^*\,U_{12}]$$

	U_{11}	U_{22}	U_{33}	U_{23}	U_{13}	U_{12}
P(1)	22.0(6)	19.2(6)	23.2(6)	-0.4(5)	1.9(4)	0.1(4)
O(1)	31.3(19)	20.8(17)	37(2)	-3.2(15)	-0.1(15)	-0.8(14)
O(2)	21.5(16)	28.8(18)	22.9(16)	0.0(14)	2.7(13)	0.6(13)
C(11)	20(2)	27(2)	28(2)	3.5(19)	6.8(18)	5.2(18)
C(12)	33(3)	35(3)	51(3)	-5(3)	19(3)	-2(2)
C(13)	31(3)	54(4)	63(4)	4(3)	25(3)	12(3)
C(14)	21(3)	61(4)	54(4)	22(3)	9(2)	5(3)
C(15)	28(3)	44(3)	41(3)	6(3)	0(2)	-6(2)
C(16)	25(2)	33(3)	31(3)	4(2)	7.4(19)	0(2)
C(21)	19(2)	28(2)	21(2)	4.1(18)	4.4(16)	1.2(18)
C(22)	34(3)	29(3)	35(3)	-1(2)	5(2)	-3(2)
C(23)	50(3)	39(3)	34(3)	-2(2)	16(3)	7(3)
C(24)	28(3)	52(4)	36(3)	10(3)	15(2)	6(2)

C(25)	30(3)	43(3)	48(3)	3(3)	11(2)	-13(2)
C(26)	34(3)	30(3)	36(3)	-2(2)	12(2)	-6(2)
C(31)	18(2)	19(2)	20(2)	0.3(16)	3.1(16)	-0.1(16)
C(32)	26(2)	21(2)	21(2)	-0.5(17)	1.3(17)	-3.0(18)
C(33)	25(2)	22(2)	37(3)	4(2)	0(2)	2.5(19)
C(34)	25(2)	40(3)	31(3)	14(2)	-2(2)	1(2)
C(35)	27(2)	41(3)	22(2)	0(2)	-4.2(19)	-6(2)
C(36)	25(2)	25(2)	24(2)	-2.8(19)	2.8(18)	-1.6(19)

Table 35 Hydrogen atom co-ordinates (x 10^3) and isotropic displacement parameters
(Å^2 x 10^2) with s.u.s in parentheses.

	x	y	z	U_{eq}
H(12)	4736.	-334.	6126.	47.
H(13)	7183.	47.	5973.	58.
H(14)	8257.	1678.	6683.	54.
H(15)	6891.	2965.	7545.	46.
H(16)	4422.	2625.	7663.	35.
H(22)	1440.	2721.	9141.	39.
H(23)	-658.	2801.	9978.	49.
H(24)	-2340.	1290.	9836.	46.
H(25)	-1936.	-309.	8876.	48.
H(26)	165.	-413.	8039.	40.
H(32)	1553.	3228.	7219.	27.
H(33)	32.	4487.	6301.	34.
H(34)	-1070.	3850.	4871.	39.
H(35)	-654.	1962.	4325.	37.
H(36)	852.	685.	5239.	30.

Table 36 Interatomic distances (Å) with s.u.s in parentheses.

P(1)-O(1)	1.497(4)	P(1)-O(2)	1.621(3)
P(1)-C(31)	1.818(5)	P(1)-C(11)	1.822(5)
O(2)-C(21)	1.427(5)	C(11)-C(12)	1.393(7)
C(11)-C(16)	1.399(7)	C(12)-C(13)	1.402(8)
C(13)-C(14)	1.377(10)	C(14)-C(15)	1.402(9)
C(15)-C(16)	1.402(7)	C(21)-C(22)	1.387(7)
C(21)-C(26)	1.396(7)	C(22)-C(23)	1.404(8)
C(23)-C(24)	1.392(9)	C(24)-C(25)	1.390(9)
C(25)-C(26)	1.406(7)	C(31)-C(32)	1.404(6)
C(31)-C(36)	1.409(6)	C(32)-C(33)	1.409(7)
C(33)-C(34)	1.394(8)	C(34)-C(35)	1.396(8)
C(35)-C(36)	1.410(7)		

Table 37 Angles between interatomic vectors (°) with s.u.s in parentheses.

O(1)-P(1)-O(2)	116.7(2)	O(1)-P(1)-C(31)	111.5(2)
O(2)-P(1)-C(31)	105.3(2)	O(1)-P(1)-C(11)	113.3(2)
O(2)-P(1)-C(11)	98.5(2)	C(31)-P(1)-C(11)	110.7(2)
C(21)-O(2)-P(1)	123.7(3)	C(12)-C(11)-C(16)	119.9(5)
C(12)-C(11)-P(1)	118.2(4)	C(16)-C(11)-P(1)	121.9(4)
C(11)-C(12)-C(13)	120.1(6)	C(14)-C(13)-C(12)	120.3(6)
C(13)-C(14)-C(15)	120.0(5)	C(16)-C(15)-C(14)	120.0(6)
C(11)-C(16)-C(15)	119.6(5)	C(22)-C(21)-C(26)	122.0(5)
C(22)-C(21)-O(2)	116.3(4)	C(26)-C(21)-O(2)	121.7(4)
C(21)-C(22)-C(23)	118.9(5)	C(24)-C(23)-C(22)	120.3(5)
C(25)-C(24)-C(23)	119.9(5)	C(24)-C(25)-C(26)	120.8(5)
C(21)-C(26)-C(25)	118.1(5)	C(32)-C(31)-C(36)	120.0(4)
C(32)-C(31)-P(1)	123.1(3)	C(36)-C(31)-P(1)	116.9(3)
C(31)-C(32)-C(33)	119.5(4)	C(34)-C(33)-C(32)	120.4(5)
C(33)-C(34)-C(35)	120.4(5)	C(34)-C(35)-C(36)	119.7(5)
C(31)-C(36)-C(35)	120.0(5)		

Appendix (v) Dalton Transaction journal publication accepted august 2010

# Asymmetric general base catalysis of the phospho-aldol reaction *via* dimeric aluminium hydroxides†

Alexandra C. Gledhill, Nichola E. Cosgrove, Tracy D. Nixon, Colin A. Kilner, Julie Fisher and Terence P. Kee*

Dimeric aluminium hydroxide complexes containing the (*R*,*R*)-*N*,*N*′-bis(2′-hydroxy-3′-organobenzyl)-*trans*-1,2-diaminocyclohexane ligand backbone effect catalysis of the phospho-aldol reaction under ambient, aerobic conditions at catalyst loadings of 0.5 mol% to afford enantioselectivities of *ca.* 65%.

The phospho-aldol (PA) reaction is one of the most versatile synthetic transformations for the construction of α-functionalised phosphonate esters, a class of molecule with considerable synthetic and medicinal application.[1] Catalysis of the PA reaction is achievable with control over the stereochemistry at the newly created stereogenic centre by the use of chiral metal complexes as mediators (Scheme 1); the most successful examples of which have been based on transition elements such as titanium,[2] aluminium[3] and lanthanides[4] whilst recent success has been obtained with chiral phosphonium salts.[5]
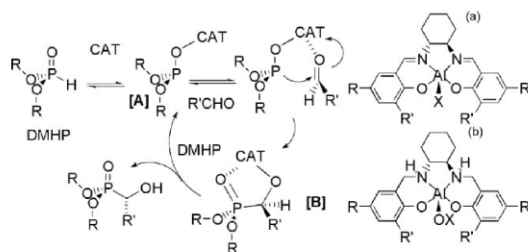
Scheme 1 A proposed working mechanism for the catalytic phospho-aldol reaction *via* chiral aluminium salen (a) [R = R′ = ¹Bu; R = R′ = H; X = Me, OSiR₃] & salan (b) [R = R′ = ¹Bu; X = H **1**; R = H; R′ = ¹Bu; X = H **2**; R = H; R′ = ¹Pn X = H **3**] complexes.

We have been exploring the potential of both chiral aluminium hydroxo[6] and more recently titanium oxo complexes[7] as asymmetric phospho-aldol catalysts and in the course of these studies informative structure–activity relationships (SAR) have emerged. The PA reaction between dimethyl-H-phosphonate (DMHP) and substituted benzaldehydes (RCHO) can be catalysed by [(*R*,*R*)-salcyen]AlX (Scheme 1a; X = Me, OSi¹BuMe₂) under aerobic conditions at 5mol% loadings. Enantioselectivities (e.e.'s) <50% were observed depending upon the nature of the

carbonyl substituent and the absolute configuration of the product (MeO)₂P(O)CHR(OH) was found to be *R*. Subsequently, we found that the closely related complex {[(*R*,*R*)-salcyan-¹Bu₄]Al(μ-OH)}₂ (**1** Scheme 1b) was also an active catalyst under aerobic conditions but at sub-1mol% catalyst loadings, affording e.e.'s <60% but now with an absolute product configuration of *S*; a change in e.e. (Δe.e.) of 110% compared to that of the salcyan system.[6] This observation led us subsequently to target a range of aluminium (*R*,*R*)-salcyan complexes in which the ligand framework was substituted with both isotropic and anisotropic groups (Scheme 1) through which we anticipated being able to more closely control the overall stereoselectivity of reaction. Analysis of the crystal structure of complex **1**, along with molecular modelling using the Hyperchem 7.0 package (Hypercube, Florida) suggests that the two *tert*-butyl substituents *para* to the phenoxy oxygen atoms (the *distal* substituents) should play no direct role in influencing stereochemical events at the catalytic centre; the two functionalities *ortho* to the phenoxy oxygen atoms (the *proximal* substituents) being important to stereodetermination. Thus removal of the *distal* substituents, as in complex **2**, was not expected to lead to significant differences in either complex structure or enantioselectivity in the PA reaction, a presumption which appears to be correct. Thus, employing a related synthetic protocol to that used to prepare complex **1** {[(*R*,*R*)-salcyan-¹Bu₄]Al(μ-OH)}₂;[6] condensation of AlMe₃ with [H₂-(*R*,*R*)-salcyan-¹Bu₂],[8] followed by exposure to aerobic moisture afforded **2** as colourless prisms in *ca.* 70% yield (see ESI for details†). Subsequently, the room temperature (298 K) PA addition of DMHP to benzaldehyde in the presence of 1 mol% **2** (based on aluminium), under fully aerobic conditions in THF, afforded a 95% conversion to *S*-configuration (MeO)₂P(O)CHPh(OH) after 4 h in 60% e.e. as determined by ³¹P-NMR using quinine as chiral solvating agent.[9] This compares favourably to the formation of the same stereochemistry product in 59% e.e. using **1** as PA catalyst (1 mol%; 298 K; THF; aerobic conditions).

We reasoned that increasing the steric influence of the *proximal* ligand substituents would lead to improved stereoselectivity and indeed, our preliminary results would appear to bear this out. Thus, reaction of (*R*,*R*)-*N*,*N*′-bis-[2′-hydroxy-3′-*tert*-pentylbenzyl]-*trans*-1,2-diaminocyclohexane[7] with aluminium tris-isopropoxide in toluene affords complex **3** in good yield‡ and subsequently we find this compound to be an excellent PA catalyst precursor. Phospho-aldol addition of DMHP to benzaldehyde in the presence of **3** under identical conditions to that of **2** above afforded 100% conversion to *S*-configuration (MeO)₂P(O)CHPh(OH) after 24 h in 66% e.e. (quinine CSA). Whilst this represents a rather modest increase on the stereoselectivity returned for **2**, we reasoned that such a 10% increase in selectivity upon changing a rather remote substituent hydrogen
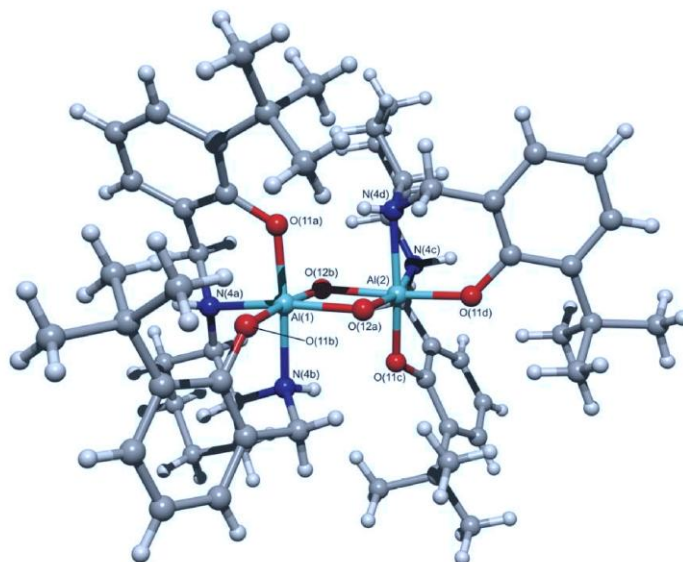
Fig. 1 Molecular structures of complexes **2** & **3**. Selected bond lengths (Å) and bond angles (°) for **2** (*one of the two independent molecules in the unit cell is shown above*): Al(1)–O(11b) 1.848(3), Al(1)–O(11a) 1.849(3), Al(1)–O(12a) 1.867(3), Al(1)–O(12b) 1.958(3), Al(1)–N(4a) 2.078(4), Al(1)–N(4b) 2.088(4), Al(2)–O(11d) 1.840(3), Al(2)–O(11c) 1.847(3), Al(2)–O(12a) 1.873(3), Al(2)–O(12b) 1.928(3), Al(2)–N(4d) 2.088(4), Al(2)–N(4c) 2.098(4). Al(1)–O(12a)–Al(2) 106.21(15), Al(2)–O(12b)–Al(1) 100.64(14). **3**: (*see ESI for graphic*†) Al(1)–O(69) 1.8491(16), Al(1)–O(19) 1.8744(16), Al(1)–O(1)1.8913(14), Al(1)–O(2) 1.9630(14), Al(1)–N(61) 2.1087(19), Al(1)–N(11) 2.1109(19), O(1)–Al(1)$^{(a)}$ 1.8913(14), O(2)–Al(1)$^{(a)}$ 1.9630(14), Al(1)$^{(a)}$–O(1)–Al(1) 105.71(10); Al(1)$^{(a)}$–O(2)–Al(1) 100.34(10). (*a*) x–y, –y, –z+1/3.

atom for a methyl group may be worthy of closer investigation. Subsequent single-crystal X-ray analysis of **2** and **3** reveal‡ that both are OH-bridged dimers, in which one bridging oxygen atom is *trans* to a phenoxy oxygen and the other *trans* to a nitrogen atom. Both **2** & **3** have the same basic molecular structure to the close relative **1** {[(*R*,*R*)-salcyan-^{t}Bu$_4$]Al(μ-OH)}$_2$, in which the fixed cyclohexyl carbon stereocentres possess *R* configurations (1° structure). These in turn induce *S* absolute configurations in stereocentres N4(a–d) (2° structure, Fig. 1 for a representative image of **2**). In addition, each octahedral aluminium centre possesses the same Λ configuration within a dimeric (3°) structure. Thus, the overall stereochemistry around each metal centre in all complexes **1**, **2** and **3** may be represented as (C$_R$,N$_S$,Al$_Λ$).

For both complexes **2** & **3**, it is clear that the Al$_2$O$_2$ bridge is distinctly asymmetric with one Al–O–Al hinge considerably more open [106.21(15)° and 105.71(10)°] than the other [100.64(14)° and 100.34(10)°] respectively which, together with the two metal coordination environments possessing the Λ configurations, results in these dimers having one bridge face significantly more open than the other as illustrated in the space-filling view of **2** in Fig. 2. The open face thus represents a rather shallow, C$_2$-symmetric cavity of approximate dimensions 13 × 10 Å for both **2** and **3**. There is, at present, circumstantial evidence that this differential cavity formation may play some role in the PA catalytic operation of complexes such as **2** & **3** as the X-ray analysis of **3** locates a disordered toluene molecule within the structure and this toluene molecule, with dimensions *ca.* 6 × 4 Å sits comfortably within the open cavity. A relatively close approach of the bridging
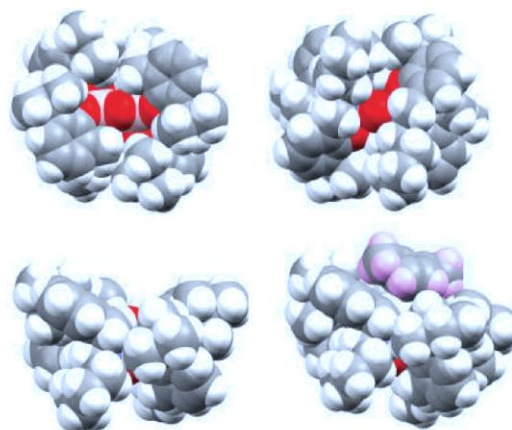
Fig. 2 Four space filling views emphasising the more open (*top left*) and closed (*top right*) cavities surrounding the Al$_2$O$_2$ bridge region of compound **2**. A side-view (*bottom left*) of **2** emphasises the rather shallow nature of the open cavity whilst a similar view of **3** (bottom right) reveals that this open cavity is capable of hosting small molecules, in this case a disordered toluene molecule (whose hydrogen atoms are outlined in light blue for emphasis).

oxygen atom to the toluene centroid of *ca.* 3.5 Å suggests that a non-covalent interaction may contribute to stabilising the toluene within the open cavity.

Our original working model for PA catalysis *via* these dimeric complexes involved initial dissociation to monomeric aluminium complexes in solution in the presence of DMHP, followed by deprotonation of DMHP to afford a metallophosphite complex which subsequently engaged in [P–C] bond formation with a bound carbonyl substrate prior to proton transfer from a second equivalent of DMHP and release of product α-hydroxyphosphonate from the metal coordination environment (Scheme 1). However, diffusion-ordered spectroscopy (DOSY) experiments[10] reveal that the diffusion coefficient of **3** in CDCl₃ solution at three different concentrations between 1.6–16 mg mL⁻¹ was more consistent with that of a dimer than a monomer (see ESI for full details†) suggesting that our original dissociative mechanism may need revision. Furthermore, crossover experiments employing equimolar amounts of complexes **2** and **3** revealed no indication for the formation of any crossover product, {[(*R*,*R*)-salcyan-ᵗBu₂]Al(μ-OH)₂Al{[(*R*,*R*)-salcyan-ⁱPn₂], within 3 days (298 K, THF-D₈, see ESI for details†). Moreover, isotope exchange studies suggested that dimeric salcyan complexes of aluminium such as **2** and **3** are capable of activating the H-phosphonate esters *via* deprotonation, supportive of their acting as general bases in PA catalysis. Thus, an 0.1 M solution of diethyl-H-phosphonate (selected as it is more stable than DMHP to hydrolysis) in ethanol-D₁ was treated with **3** (2.5 mol%) and monitored by ³¹P{¹H}-NMR spectroscopy over a period of 7 h at 300 K, during which time H/D exchange was observed in the DEHP with a pseudo first order rate constant of 1.15 s⁻¹ (a duplicate sample but without additional **3** did not reveal any H/D exchange under the same conditions; see ESI for further details†).

Geometry optimisation calculations on **2** at the DFT level, based on the X-ray structure, suggest that the HOMO and HOMO-1 for the system (separated by *ca.* 0.7 kcal mol⁻¹) are located principally on the salcyan phenoxy rings (Fig. 3) rather than on the bridging hydroxyl oxygen atoms (the latter contribute most to MO's some 35 kcal mol⁻¹ lower than the HOMO). Therefore, in the light of these new experimental and theoretical analyses we have modified our picture for PA catalysis *via* these dimeric aluminium hydroxides.
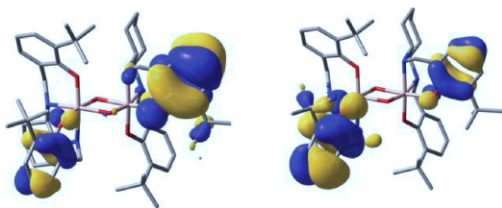

Fig. 3 HOMO (*left*) and HOMO-1 (*right*) for **2** (DFT).§

Initial approach of diorgano-H-phosphonate to the aluminium dimer in solution affords a H-bonded stabilised adduct at the open face of the dimer (Scheme 2). We envisage that benzaldehyde may act similarly towards H-bonding at this open face but such binding would be expected to be reversible. This adduct subsequently undergoes some degree of proton transfer at the open cavity of the aluminium dimer to afford, either a salt or strongly charge-separated complex, bound *via* H-bonding and/or electrostatic interactions within the cavity releasing significant electron density
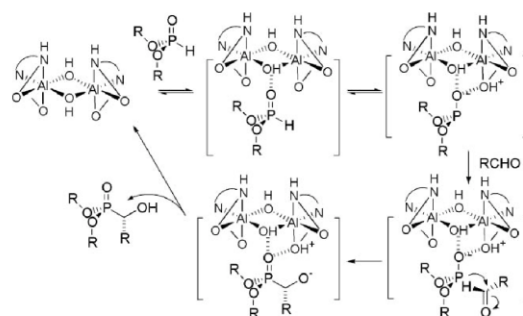
Scheme 2 Modified mechanistic outline for PA catalysis *via* dimeric aluminium salcyan complexes.

at the phosphorus centre.[11] Subsequent [P–C] bond formation followed by proton transfer and release of the phosphonate ester product completes the cycle. We have opted in this model to restrain the carbonyl from binding to the metal centre which we feel is reasonable on the grounds that, (i) the ¹H-NMR spectrum of **3** is unchanged in the presence of benzaldehyde (1 equivalent; THF-D₈) and (ii) enatioselectivity remained invariant from 65(±1)% through the benzaldehyde concentration range of 1, 2, 5 and 10 equivalents (with respect to DMHP; **3** as catalyst 1 mol% in THF, 298 K). Studies are currently underway to probe this mechanism in further detail and in particular devise ways of improving stereoselectivity.

Acknowledgements

Notes and references

‡ Crystallographic data for **2** (CCDC 749041): C₈₆H₁₀₂Al₂Cl₄N₄O₆, *M*ᵣ 2794.61, crystal size 0.27 × 0.18 × 0.09 mm, monoclinic, space group *P*2₁, *a* = 11.79800(10), *b* = 31.2880(2), *c* = 20.6198(2) Å, *α* = 90, *β* = 103.3000(3), *γ* = 90°, *V* = 7488.85(11) Å³, *Z* = 4, *D*c = 252 Mgm⁻³, *F*(000) = 3008, Mo-Kα radiation (*λ* = 0.71073 Å), *T* = 150(2) K, *μ* = 0.236 mm⁻¹. The 90149 reflections afforded 29189 independent reflection (*R*ᵢₙₜ = 0.0641) [*I* > 2*σ*(*I*)] *R*₁ = 0.0855, w*R*₂ = 0.2321, *R*₁ = 0.0986, w*R*₂ (all data) = 0.2457. There are four molecules of dichloromethane in the unit cell. Crystallographic data for **3** (CCDC 749040) C₆₇H₉₇Al₂N₄O *M*ᵣ 1109.45, crystal size 0.26 × 0 24 × 0 17 mm trigonal, space group *P*3₂21, *a* = 18.579(3), *b* = 18.579(3), *c* = 15.951(3) Å, *α*, *β* = 90; *γ* = 120° *V* = 4768.2(13) Å³, *Z* = 3, *D*c = 1.159 Mg m⁻³, *F*(000) = 1806 Mo-Kα, radiation (*λ* = 0.71073 Å), *T* = 150(2) K, *μ* = 0.098 mm⁻¹. The 69370 reflections measured on a Nonius Kappa CCD system afforded 3943 independent reflection (*R*ᵢₙₜ = 0.0457), [*I* > 2*σ*(*I*)] *R*₁ = 0.0377, w*R*₂ = 0.1066, *R*₁ = 0.0432, w*R*₂ (all data) = 0.1111.
§ Gradient-corrected hybrid density functional theory (DFT), B3LYP, along with the 6-31G* basis set was used in the computations reported herein. All calculations were carried out with the Gaussian 03 program, Revision C.02 (see ESI†).[12]

1 See for example B. Stowasser, K-H. Budt K-H, L. Jian-Qi, A. Peyman and D. Ruppert, *Tetrahedron Lett.*, 1992, **33**, 6625; T. Khushi, K. J. O'Toole and J. T. Sime, *Tetrahedron Lett.*, 1993, **34**, 2375; T. Yokomatsu, T. Yamagishi, K. Matsumoto and S. Shibuya, *Tetrahedron*, 1996, **52**, 11725; C. Meier, *Angew. Chem., Int. Ed. Engl.*, 1996, **35**, 70; Y-L. Zhang, Z-J. Yao, M. Sarmiento, L. Wu, T. R. Burke and Z-Y. Zhang, *J. Biol. Chem.*, 2000, **275**, 34205; T. D. Nixon and T. P. Kee, *Top. Curr. Chem.*, 2003, **223**, 45; H. W. He, T. Wang and J. L. Yuan, *J. Organomet. Chem.*, 2005, **690**, 2608; P. A. Badkar, N. P. Rath and C. D. Spilling, *Org.*

Lett., 2007, **9**, 3619; S. Bandyopadhyay, S. Dutta, C. D. Spilling, C. M. Dupureur and N. P. Rath, *J. Org. Chem.*, 2008, **73**, 8386; P. Merino, E. Marqués-Lopéz and R. P. Herrera, *Adv. Synth. Catal.*, 2008, **350**, 1195.

2 T. Yokomatsu, T. Yamagishi and S. Shibuya, *Tetrahedron: Asymmetry*, 1993, **4**, 1779; M. D. Groaning, B. J. Rowe and C. D. Spilling, *Tetrahedron Lett.*, 1998, **39**, 5485; B. J. Rowe and C. D. Spilling, *Tetrahedron: Asymmetry*, 2001, **12**, 1701; F. Yang, D. Zhao, J. Lan, P. Xi, L. Yang, S. Xiang and J. You, *Angew. Chem., Int. Ed.*, 2008, **47**, 5646.

3 T. Arai, M. Bougauchi, H. Sasai and M. Shibasaki, *J. Org. Chem.*, 1996, **61**, 2926; J. P. Duxbury, J. N. D. Warne, R. Mushtaq, C. V. Ward, M. Thornton-Pett, M. Jiang, R. Greatrex and T. P. Kee, *Organometallics*, 2000, **19**, 4445; B. Saito and T. Katsuki, *Angew. Chem., Int. Ed.*, 2005, **44**, 4600; B. Saito, H. Egami and T. Katsuki, *J. Am. Chem. Soc.*, 2007, **129**, 1978; K. Ito, H. Tsutsumi, M. Setoyama, B. Saito and T Katsuki, *Synlett*, 2007, (12), 1960; J. P. Abell and H. Yamamoto, *J. Am. Chem. Soc.*, 2008, **130**, 10521; K. Suyama, Y. Sakai, K. Matsumoto, B. Saito and T. Katsuki, *Angew. Chem., Int. Ed.*, 2010, **49**, 797.

4 E. M. Vogl, H. Groger and M. Shibasaki, *Angew. Chem., Int. Ed.*, 1999, **38**, 1570; H. Sasai, T. Arai, S. Watanabe and M. Shibasaki, *Catal. Today*, 2000, **62**, 17 and references therein.

5 D. Uraguchi, T. Ito and T. Ooi, *J. Am. Chem. Soc.*, 2009, **131**, 3836.

6 T. D. Nixon, S. Dalgarno, C. V. Ward, M. Jiang, M. A. Halcrow, C. A. Kilner, M. Thornton-Pett and T. P. Kee, *C. R. Chim.*, 2004, **7**, 809 and references therein.

7 A. Davis, C. A. Kilner and T. P. Kee, *Inorg. Chim. Acta*, 2004, **357**, 3493.

8 N. E. Cosgrove, S. A. Macgregor, T. D. Nixon, A. C. Gledhill, C. A. Kilner and T. P. Kee, manuscript in preparation.

9 E. Zymanczyk-Duda, M. Skwarczynski, P. Kofarski and B. Lejczak, *Tetrahedron: Asymmetry*, 1996, **7**, 1277.

10 V. V. Krishnan, *J. Magn. Reson.*, 1997, **124**, 468; M. S. Kaucher, Y-F. Lam, S. Pieraccini, G. Gottarelli and J. T. Davis, *Chem.–Eur. J.*, 2005, **11**, 164; L. Allouche, A. Marquis and J-M. Lehn, *Chem.–Eur. J.*, 2006, **12**, 7520.

11 J. Lewinskia, J. Zacharaa, I. Justyniakb and M. Dranka, *Coord. Chem. Rev.*, 2005, **249**, 1185.

12 M. J. Frisch, G. W. Trucks, H. B. Schlegel, G. E. Scuseria, M. A. Robb, J. R. Cheeseman, J. A. Montgomery Jr, T. Verven, K. N. Kudin, J. C. Burant, J. M. Millam, S. S. Iyengar, J. Tomasi, V. Barone, B. Mennucci, M. Cossi, G. Scalmani, N. Rega, G. A. Petersson, T. Nakatsuji, M. Hada, M. Ehara, K. Toyota, R. Fukuda, J. Hasegawa, M. Ishida, T. Nakajima, Y. Honda, O. Kitao, H. Nakai, M. Klene, X. Li, J. E. Knox, H. P. Hratchian, J. B. Cross, C. Adamo, J. Jaramillo, R. Gomperts, R. E. Stratmann, O. Yazyev, A. J. Austin, R. Cammi, C. Pomelli, J. W. Ochterski, P. Y. Ayala, K. Morokuma, G. A. Voth, P. Salvador, J. J. Dannenberg, V. G. Zakrzewski, S. Dapprich, A. D. Daniels, M. C. Strain, O. Farkas, D. K. Malick, A. D. Rabuck, K. Raghavachari, J. B. Foresman, J. V. Ortiz, Q. Cui, A. G. Baboul, S. Clifford, J. Cioslowski, B. B. Stefanov, G. Liu, A. Liashenko, P. Piskorz, I. Komaromi, R. L. Martin, D. J. Fox, T. Keith, M. A. Al-Laham, C. Y. Peng, A. Nanayakkara, M. Challacombe, P. M. W. Gill, B. Johnson, W. Chen, M. W. Wong, C. Gonzalez, J. A. Pople, *Gaussian 03*, Revision C.02, Gaussian, Inc., Wallingford CT, 2004.

248

Appendix (vi) Molecular orbital data for {[(*R*,*R*)-*t*Bu-salcyan]Al(*μ*-OH)}₂ collected from geometry optimisation calculations carried out to RHF level using 6-31G* as a basis set.

Molecular Orbital	Eigenvalue (a.u.)	Electron Volts (eV)	Energy (kcal mol⁻¹)	Difference (kcal mol⁻¹)	
261	0.03809	1.0365	23.902	-196.17	**LUMO**
260	-0.27452	-7.4702	-172.264	0.00	**HOMO**
259	-0.27593	-7.5086	-173.149	0.88	
258	-0.2801	-7.6221	-175.766	3.50	
257	-0.28269	-7.6926	-177.391	5.13	
256	-0.30669	-8.3456	-192.451	20.19	
255	-0.31084	-8.4586	-195.055	22.79	
254	-0.31268	-8.5086	-196.210	23.95	
253	-0.31403	-8.5454	-197.057	24.79	
252	-0.39392	-10.7194	-247.189	74.92	
251	-0.39646	-10.7885	-248.783	76.52	
250	-0.40047	-10.8976	-251.299	79.03	
249	-0.40437	-11.0037	-253.746	81.48	

Total energy: -3318.989837 a.u.

-90316.35145 eV

-2082699.313 kcal mol⁻¹

Appendix (vii) Molecular orbital data for {[(*R*,*R*)-*t*Pn-salcyan]Al(*μ*-OH)}₂ collected from geometry optimisation calculations carried out to RHF level using 6-31G* as a basis set.

Molecular Orbital	Eigenvalue (a.u.)	Electron Volts (eV)	Energy (kcal mol⁻¹)	Difference (kcal mol⁻¹)	
277	0.03911	1.064	24.542	-194.020	**LUMO**
276	-0.27008	-7.349	-169.478	0.000	**HOMO**
275	-0.27034	-7.356	-169.641	-0.163	
274	-0.27605	-7.512	-173.224	-3.746	
273	-0.27693	-7.536	-173.776	-4.298	
272	-0.30817	-8.386	-193.380	-23.902	
271	-0.30825	-8.388	-193.430	-23.952	
270	-0.31199	-8.490	-195.777	-26.299	
269	-0.31202	-8.491	-195.796	-26.318	
268	-0.39309	-10.697	-246.668	-77.190	
267	-0.39506	-10.750	-247.904	-78.426	
266	-0.39982	-10.880	-250.891	-81.413	
265	-0.40297	-10.966	-252.868	-83.390	

Total energy: -3474.97976619 a.u.

-94561.1494 eV

-2180584.553 kcal mol⁻¹

Appendix (viii) Molecular orbital data for $\{[(R,R)\text{-SiMe}_2\text{Ph-salcyan}]\text{Al}(\mu\text{-OH})\}_2$ collected from geometry optimisation calculations carried out to RHF level using 6-31G* as a basis set.

Molecular Orbital	Eigenvalue (a.u.)	Electron Volts (eV)	Energy (kcal mol^{-1})	Difference (kcal mol^{-1})	
341	0.04707	1.281	29.537	-200.326	**LUMO**
340	-0.27217	-7.406	-170.789	0.000	**HOMO**
339	-0.27409	-7.459	-171.994	-1.205	
338	-0.27695	-7.536	-173.789	-2.999	
337	-0.28417	-7.733	-178.320	-7.530	
336	-0.31186	-8.486	-195.695	-24.906	
335	-0.31590	-8.596	-198.230	-27.441	
334	-0.31669	-8.618	-198.726	-27.937	
333	-0.32336	-8.799	-202.912	-32.122	
332	-0.32474	-8.837	-203.778	-32.988	
331	-0.32513	-8.847	-204.022	-33.233	
330	-0.32585	-8.867	-204.474	-33.685	
329	-0.32858	-8.941	-206.187	-35.398	

Total energy:	-5085.148405	a.u.
	-138377.0584	eV
	-3190981.476	kcal mol^{-1}

Appendix (ix) Molecular orbital data for $\{[(R,R)\text{-mes-salcyan}]Al(\mu\text{-OH})\}_2$ collected from geometry optimisation calculations carried out to RHF level using 6-31G* as a basis set.

Molecular Orbital	Eigenvalue (a.u.)	Electron Volts (eV)	Energy (kcal mol^{-1})	Difference (kcal mol^{-1})	
325	0.03777	1.028	23.701	-196.712	**LUMO**
324	-0.27571	-7.503	-173.011	0.000	**HOMO**
323	-0.27616	-7.515	-173.293	-0.282	
322	-0.27764	-7.555	-174.222	-1.211	
321	-0.27837	-7.575	-174.680	-1.669	
320	-0.28841	-7.848	-180.980	-7.969	
319	-0.28851	-7.851	-181.043	-8.032	
318	-0.29753	-8.096	-186.703	-13.692	
317	-0.29765	-8.100	-186.778	-13.768	
316	-0.30127	-8.198	-189.050	-16.039	
315	-0.30136	-8.201	-189.106	-16.096	
314	-0.30649	-8.340	-192.326	-19.315	
313	-0.30662	-8.344	-192.407	-19.396	

Total energy: -4081.270753 a.u.
-111059.5397 eV
-2561038.210 kcal mol^{-1}

Appendix (x) Molecular orbital data for $\{[(R,R)\text{-mes-salcyan}]Al(\mu\text{-OMe})\}_2$ collected from geometry optimisation calculations carried out to RHF level using 6-31G* as a basis set.

Molecular Orbital	Eigenvalue (a.u.)	Electron Volts (eV)	Energy (kcal mol^{-1})	Difference (kcal mol^{-1})	
333	0.04968	1.352	31.175	-198.017	**LUMO**
332	-0.26588	-7.235	-166.842	0.000	**HOMO**
331	-0.26985	-7.343	-169.334	-2.491	
330	-0.27368	-7.447	-171.737	-4.895	
329	-0.27768	-7.556	-174.247	-7.405	
328	-0.28943	-7.876	-181.620	-14.778	
327	-0.29030	-7.900	-182.166	-15.324	
326	-0.29213	-7.949	-183.314	-16.472	
325	-0.29751	-8.096	-186.691	-19.848	
324	-0.29934	-8.146	-187.839	-20.996	
323	-0.30036	-8.173	-188.479	-21.637	
322	-0.30851	-8.395	-193.593	-26.751	
321	-0.30916	-8.413	-194.001	-27.159	

Total energy: -4158.896991 a.u.
-113171.9049 eV
-2609749.451 kcal mol^{-1}